Investigating the Role of ADAM17 in Human Cytomegalovirus Infection

A thesis submitted in candidature for the degree of

Doctor of Philosophy (PhD)

Anzelika Trinca

January 2023

Division of Infection and Immunity

School of Medicine

Cardiff University

Acknowledgments

I would like to thank my supervisor Prof Eddie Wang for the incredible opportunity that this PhD project has been. Thank you for believing in me (even when I did not believe in myself), for supporting and encouraging me both professionally and personally, for being so optimistic and guiding me through the last four years, especially when things were not going to plan. I would also like to express a special thank you to my secondary supervisor Prof Richard Stanton for all his help. Thank you for being so patient, always finding the time to help in your very busy schedule, for your support and expertise.

Thank you to Prof Gavin Wilkinson, Dr Ceri Fielding and Dr Simon Kollnberger, who always showed interest in my research and provided valuable insights and ideas, which I found incredibly helpful. I would like to acknowledge our collaborator Prof Michael Weekes from the University of Cambridge for the proteomics work. Thank you to Martin Potts and Dr Katie Nightingale for their help with the secretome and PMP datasets.

I was incredibly lucky to have the most amazing friends and colleagues supporting me throughout this journey, which I am deeply grateful for. A special thank you to Dr Lauren Kerr, Dawn Roberts, Nia Cwyfan Hughes, Lauren Jones, Dr Pragati Amratia and Dr Evelina Davies for their friendship, kindness, encouragement, and incredible support throughout.

To my husband Matthew, who married me in the final, most stressful, year of my PhD – are you crazy?! I cannot thank you enough for being on this insane journey with me. I could not have done it without you. Thank you to my in-laws for being so loving, supportive and understanding.

Моя дорогая мама, я посвящаю эту диссертацию тебе. Ты мой самый главный мотиватор и мои достижения это, в первую очередь, твоя заслуга. Спасибо за всё что ты для меня делаешь. Моя любимая бабушка, спасибо за твою веру в меня и постоянную поддержку. Спасибо что ты так сильно мной гордишься. И, конечно же, мой родной дедушка, я знаю ты присматривал за мной всё это время сверху и помогал мне в этом непростом деле. Я знаю ты всегда рядом, спасибо тебе за это.

Summary

Human cytomegalovirus (HCMV) is one of the most widespread, highly successful herpesviruses, establishing a life-long viral infection in humans. HCMV has been described as a paradigm of immune evasion able to manipulate many immune functions in the host. One of the host manipulation strategies employed by HCMV is the downregulation of a disintegrin and metalloproteinase 17 (ADAM17) – an important ectodomain shedding protease responsible for cleaving over a 100 substrates including many immunoregulatory molecules, such as receptors, cytokines, chemokines and adhesion molecules. Synergistic action of viral UL148 and UL148D result in a rapid ADAM17 downregulation from the surface of HCMV-infected cells.

This thesis explores the mechanism and consequences of ADAM17 impairment by HCMV genes UL148 and UL148D, demonstrating the significance of ADAM17 downregulation in HCMV infection. UL148 and UL148D were shown to interfere with ADAM17 maturation, resulting in expression of only the intracellular immature precursor, and absence of mature ADAM17 on the surface of wildtype HCMV-infected cells. The mechanism of ADAM17 impairment was shown to be complex, suggesting that UL148 and UL148D act to downregulate ADAM17 via distinct mechanisms, with a possibility of a third viral gene involved in the process. The global consequences of ADAM17 downregulation by HCMV were analysed using proteomics and validated using biochemical and flow cytometric techniques, revealing that this virus manipulation impacted multiple cell surface and secreted host proteins. This included stabilisation of Vasorin, Jagged1, Nectin1 and Endothelial protein C receptor (EPCR), as well as a number of viral proteins. Other known ADAM17 targets were not stabilised, suggesting specific control by HCMV. The functional consequences of these changes to the levels of secreted and soluble proteins were tested and revealed the importance of ADAM17 impairment in regulatory T cell and NK cell function; however with so many ADAM17 substrates stabilised on cell surface as a result of HCMV infection, many other pathways are likely also affected.

Table of contents

X

List of Tables

List of Figures

Abbreviations

AC	Assembly compartment
ACE2	Angiotensin converting enzyme 2
AD	Alzheimer's disease
ADAM17	A Disintegrin And Metalloproteinase 17
ADAMs	A Disintegrin And Metalloproteinases
ADCC	Antibody-dependent cellular cytotoxicity
AIDS	Acquired immunodeficiency syndrome
APCs	Professional antigen presenting cells
APP	β-amyloid precursor protein
BAC	Bacterial artificial chromosome
BTLA	B and T lymphocyte attenuator
CANDIS	Conserved ADAM seventeeN Dynamic Interaction Sequence
CAR	Coxsackie adenovirus receptor
cCMV	Congenital HCMV
CDK1	Cyclin-dependent kinase
CID	Cytomegalic inclusion disease
CNS	central nervous system
ConA	Concanavalin A
CPE	Cytopathic effect
CRKL	Crk-like protein
DC	Dendritic cell
DMEM	Dulbecco's Modified Eagles Medium
DMSO	Dimethyl sulfoxide
DNAM-1	DNAX accessory molecule-1
dsDNA	Double-stranded DNA
DTT	Dithiothreitol
EBV	Epstein-Barr virus
EerI	Eeyarestatin I
EGFR	Epidermal growth factor receptor
EndoH	Endoglycosidase H

EPCR	Endothelial protein C receptor
ER	Endoplasmic reticulum
ERAD	ER-associated protein degradation
ERLAD	ER-to-lysosome-associated degradation
FACS	Fluorescence-activated cell sorting
FBS	Foetal bovine serum
FCAR	Immunoglobulin alpha Fc receptor
FcRs	Fc receptors
FoxP3	Forkhead box protein P3
FRMD8	FERM domain-containing protein 8
gB	Glycoprotein B
gH	Glycoprotein H
gL	Glycoprotein L
gM	Glycoprotein M
gN	Glycoprotein N
gO	Glycoprotein O
HAART	Highly active antiretroviral therapy
HCMV	Human Cytomegalovirus
HFFF	Human foetal foreskin fibroblast
HHV-5	Human herpesvirus-5
hiPSC	Human induced pluripotent stem cell
HLA	Human leukocyte antigen
hpi	Hours *post* infection
HSCT	Hematopoietic stem cell transplantation
HSPGs	Heparan sulphate proteoglycans
HSV-1; HSV-2	Herpes simplex virus-1 and -2
hTERT	Human telomerase reverse transcriptase
HUVECs	Human umbilical vein endothelial cells
IE, E, EL, L	Immediate-early, Early, Early-late, Late
IFN	Interferon
IL-6R	IL-6 receptor
IP	Immunoprecipitation
IRF3	IFN regulatory factor 3

iRhom1 and 2	Inactive rhomboid protein 1 and 2
Kif	Kifunensine
KIRs	killer immunoglobulin like receptors
KSHV	Kaposi's sarcoma-associated herpesvirus
LPS	Lipopolysaccharide
mAb	Monoclonal antibody
MACS	Magnetic activated cell sorting
MEM	Minimal essential media
MHC-I and -II	Major histocompatibility complex class I and II
MICA/B	MHC-I related protein A/B
MIEP	Major immediate-early promoter
MMP	Matrix metalloproteinase
MOI	Multiplicity of infection
MPD	Membrane proximal domain
mwt	Molecular weight
NEC	Nuclear egress complex
NIEPs	Non-infectious enveloped particles
NK cells	Natural killer cells
NKG2D	Natural-killer group 2, member D
NRG2	Neuregulin-2
Nrp2	Neuropilin-2
OD600	Optical density
ORF	Open reading frame
PACS1 and 2	Phosphofurin acidic cluster sorting protein 1 and 2
PAMPs	Pathogen-associated molecular patterns
PBMCs	Peripheral blood mononuclear cells
PBS	Phosphate-Buffered Saline
PCR	Polymerase Chain Reaction
PDGFRα	Platelet-derived growth factor receptor alpha
PFU	Plaque forming units
PKC	Protein kinase C
PKR	Protein kinase R
PLCG2	Phospholipase C gamma 2

PM	Plasma membrane
PMNLs	Polymorphonuclear lymphocytes
PMP	Plasma membrane profiling
PNGaseF	Peptide:N-glycosidase F
PRPs	Pattern recognition receptors
PVR/CD155	Poliovirus receptor
QTV	Quantitative temporal viromics
RA	Rheumatoid arthritis
RAd	Replication-deficient recombinant adenovirus
RHBDD1	Rhomboid domain containing 1
RPMI	Roswell Park Memorial Institute 1640 Medium
RT	Room temperature
sACE2	Soluble ACE2
SARS-CoV-2	Severe acute respiratory syndrome coronavirus 2
SEL1L	Suppressor/Enhancer of Lin-12-like
SFi	Skin fibroblasts
SGV	Salivary gland virus
sIL-6R	Soluble IL-6R
SILAC	Stable isotope labelling by amino acids in cell culture
SNHL	Sensorineural hearing loss
SOT	Solid organ transplant
sTNFα	Soluble TNFα
TACE	TNFα converting enzyme
TAE	Tris-acetate-EDTA
TGFα	Transforming growth factor alpha
TGFβ	Transforming growth factor beta
TGFβRIII	Transforming growth factor-beta receptor type 3
TGS	Tris-Glycine-SDS
Th17 cells	T helper 17 cells
THBD	Thrombomodulin
TIGIT	T cell immunoglobulin and ITIM domain
TLRs	Toll-like receptors
TMT	Tandem mass tag

tmTNFα	Transmembrane TNFα
TNFR1 and 2	TNF Receptors I and II
TNFα	Tumour necrosis factor alpha
TRAIL-R1; R2	TNF-related apoptosis inducing ligand receptors 1 and 2
Tregs	Regulatory T cells
UPR	Unfolded protein response
VZV	Varicella-zoster virus
WB	Western Blot
WCL	Whole cell lysate
WT	Wildtype
β2m	β2 microglobulin

1   Introduction

1.1   Human Cytomegalovirus

1.1.1   Herpesviridae Family

Human cytomegalovirus (HCMV), also known as Human herpesvirus-5 (HHV-5), is a member of the *Herpesviridae* family of large DNA viruses (also known as herpesviruses). Nine herpesviruses are known to infect humans, however overall, there are over 100 different herpesviruses that infect a wide range of various species, such as birds, reptiles, fish, invertebrates, primates and other mammals (Weir 1998; Davison et al. 2009; Sharma et al. 2016). Herpesviruses persist in the host for life by establishing a state of latency, described as the ability of the virus to enter (and exit) a state in which the genome is maintained, but no new virions are produced (Grinde 2013; Cohen 2020). Herpesvirus seroprevalence is high worldwide, with approximately 90% of the population having antibodies specific against at least one of the nine human herpesviruses (Lan and Luo 2017). Characteristically, herpesviruses have a unique four-layer structure comprising of a core, capsid, tegument and envelope. The core contains a linear double-stranded (ds) DNA molecule enclosed within the capsid, surrounded by an amorphous protein matrix called the tegument. The phospholipid envelope encases the tegument and contains viral glycoproteins involved in cell attachment and viral entry, and is formed as the virion buds through cellular membranes (Liu and Zhou 2007).

Based on their genetic organisation, growth characteristics and cell tropism, herpesviruses are divided into alpha (α), beta (β) and gamma (γ) subfamilies (Whitley 1996; Muller et al. 2021). There are three α-herpesviruses known to infect humans: varicella-zoster virus (VZV), herpes simplex virus (HSV)-1 and -2; all of which have been shown to have similar characteristics, such as broad tropism, a short replication cycle and the ability to establish latency in neurons of sensory ganglia (Whitley 1996; Pellet and Roizman 2013; Cohen 2020). In contrast, β-herpesviruses have a much longer replication cycle, limited host

range, and the ability to establish latency in multiple cell types (Whitley 1996). HCMV is one of the members of the β-herpesvirus subfamily together with HHV-6A, HHV-6B and HHV-7 (Mocarski 2007; Pellet and Roizman 2013). Kaposi's sarcoma-associated herpesvirus (KSHV or HHV-8) and Epstein-Barr virus (EBV) are two known human γ-herpesviruses, characterised by limited tropism and an ability to establish latent infection in lymphoid cells (Whitley 1996; Pellet and Roizman 2013; Cohen 2020). Herpesvirus subfamily groupings reflect the diversity of genetic organisation and gene content of herpesviruses. The α-herpesviruses have the smallest genomes, whereas β-herpesviruses are some of the largest human infecting viruses (Davison and Bhella 2007).

1.1.2 HCMV Genome

Out of all nine human herpesviruses HCMV has the largest genome being twice the size of the VZV genome and over 50% larger than the HSV-1 genome (Davison and Bhella 2007). Indeed, HCMV is the largest virus known to infect humans, with dsDNA genome of 235 ±1.9 kbp in length, although that is strain dependent (Murphy and Shenk 2008). HCMV has a complex E-type genome in which two unique regions (long U_L and short U_S) are flanked by inverted repeats at terminal ends and internal U_L/U_S intersection (TR and IR, respectively) (Murphy and Shenk 2008; Van Damme and Van Loock 2014). The TR_L region consists of *a* and *b*, whereas the TR_S region consists of *c* and *a* sequences. The IR_L to IR_S region consists of inverted *b'a'c'* sequences, resulting in an *ab*-U_L-*b'a'c'*-U_S-*ca* E-type genome (**Figure 1.1**) (Murphy and Shenk 2008; Stanton et al. 2010; Sijmons et al. 2014).

There are 15 gene families within the HCMV genome containing between 2 to 14 members, including those named after the RL11, UL14, UL18, UL25, UL82, UL120, US6, US7, US12, and US22 genes (**Table 1.1**) (Nichols 2018; Ye et al. 2020). HCMV has the largest number of gene families of any human herpesvirus (Davison and Bhella 2007). HCMV gene families are separated based on their homology and are involved in a variety of functions ranging from cell tropism and entry, viral replication, and virion assembly (Davison and Bhella 2007). In fact, together, HCMV gene families encompass 70 genes,

which is over half of the number of non-core genes in the HCMV genome (Davison 2011). There is some debate over the number of protein-coding genes in the HCMV genome. By 2019, 305 full-length distinct complete HCMV genomes have been published from multiple HCMV strains, including low- and high-passage strains demonstrating significant inter-strain variability in HCMV genetic composition (Martí-Carreras and Maes 2019). However, a general understanding is that clinical HCMV encodes over 170 protein-coding genes, at least 16 pre-miRNAs, 26 mature miRNAs as well as four major long non-coding RNAs (Davison et al. 2003; Dunn et al. 2003b; Dolan et al. 2004; Zhang et al. 2007).
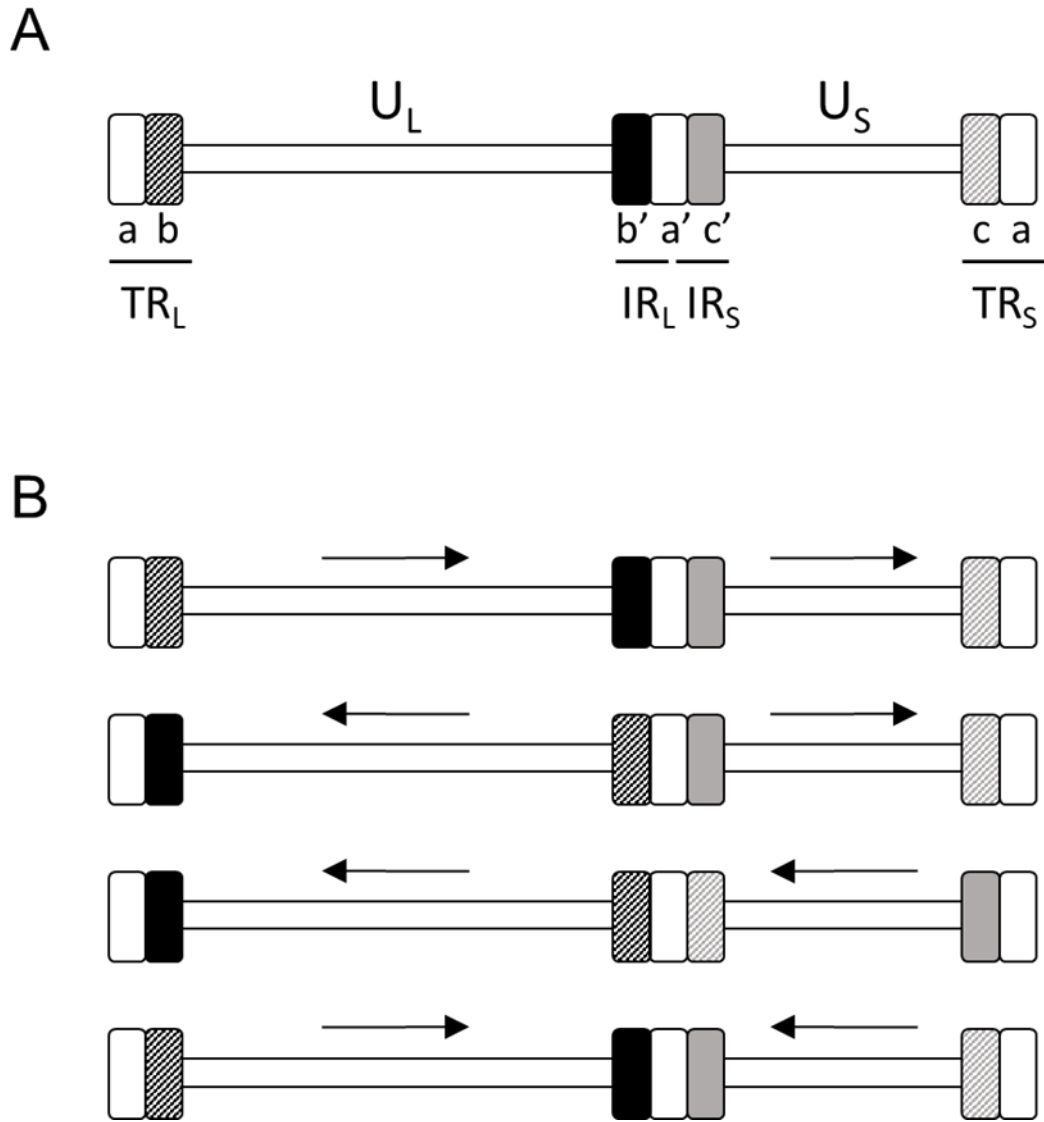
Figure 1.1: HCMV genome structure (A) and its alternative isomeric forms (B). (A) The HCMV genome is an E-type genome containing a unique long (U_L) and a unique short (U_S) region, flanked by inverted repeats at terminal ends (TR_L/TR_S) and internal U_L/U_S intersection, resulting in TR_L-U_L-IR_L-IR_S-U_S-TR_S genome organisation. Sequence a/a' (white) is shared by both U_L and U_S regions. Sequence b/b' (solid/striped black) is unique to the long region, whereas c/c' (solid/striped grey) is unique to the short. **(B)** Four HCMV genome isomeric forms generated as a result of homologous recombination between repetitive regions, changing the orientation of unique domains. Adapted from (Martí-Carreras and Maes 2019).

Table 1.1: HCMV gene families, their members and functions.

HCMV Gene Family	*HCMV Gene members*	*Description/Function*	*References*
RL1	RL1, UL145	Both RL1 and UL145 have been shown to be involved in degradation of host anti-viral factors impairing innate immune responses.	(Gatherer et al. 2011; Nightingale et al. 2018; Le-Trilling et al. 2020; Nightingale et al. 2022)
RL11	RL5A, RL6, RL11, RL12, RL13, UL1, UL4, UL5, UL6, UL7, UL8, UL9, UL10, UL11	Most are membrane glycoproteins with immunomodulatory roles (UL10, UL11, UL7) or act as viral Fcγ receptors (RL11, RL12, RL13).	(Lilley et al. 2001; Davison and Bhella 2007; Shikhagaie et al. 2012; Bruno et al. 2016; Zischke et al. 2017)
UL14	UL14, UL141	Membrane glycoproteins involved in NK cell evasion (UL141) and impairing cell adhesion (UL14).	(Tomasec et al. 2005; Davison and Bhella 2007; Wilkinson et al. 2008; Prod'homme et al. 2010)
UL18	UL18, UL142	MHC-I associated membrane glycoproteins that play an important role in NK cell evasion.	(Davison and Bhella 2007; Prod'homme et al. 2007; Wilkinson et al. 2008; Ashiru et al. 2009)
UL25	UL25, UL35	Tegument proteins potentially involved in virion packaging (UL25) and type I Interferon Response (UL35).	(Baldick and Shenk 1996; Battista et al. 1999; Davison and Bhella 2007; Fabits et al. 2020)

UL30	UL30, UL30A	Functions remain unknown.	(Salsman et al. 2008)
DURP (or UL82)	UL31, UL72, UL82, UL83, UL84	Tegument proteins involved in cell cycle regulation, gene expression, antiviral signalling (UL82, UL83) and DNA replication and transcriptional activation (UL84).	(Xu et al. 2002; Browne and Shenk 2003; Cantrell and Bresnahan 2006; Davison and Bhella 2007; Fu et al. 2017)
UL120	UL120, UL121, possibly UL119	Membrane glycoproteins with unknown functions.	(Davison and Bhella 2007)
UL146	UL146, UL147	Both UL146 and UL147 encode proteins with sequence characteristics of CXC chemokines, however only UL146 has been functionally validated as a viral homologue of CXCL1.	(Penfold et al. 1999; Saederup and Mocarski 2002; Sparer et al. 2004; Lurain et al. 2006)
US1	US1, US31, US32	Functions remain unknown.	(Davison and Bhella 2007)
US2	US2, US3	Membrane glycoproteins involved in the blocking of antigen presentation by degrading or retaining MHC-I.	(Jones et al. 1995; Jones et al. 1996; Johnson and Hegde 2002; Davison and Bhella 2007; Han et al. 2013)
US6	US6, US7, US8, US9, US10, US11	Membrane glycoproteins involved in the blocking of antigen presentation by impairing MHC-I processing, whereas US7	(Lehner et al. 1997; Furman et al. 2002; Huber et al. 2002; Tirabassi and

		and US8 has been shown to target TLR-signalling pathways.	Ploegh 2002; Tirosh et al. 2005; Lin et al. 2007; Park et al. 2019)
US12	US12, US13, US14, US15, US16, US17, US18, US19, US20, US21	Regulate the levels of cellular immune ligands, often via degradation, with US16, US18 and US20 involved in tropism and US12, US14, US18 and US20 having NK evasion functions.	(Bronzini et al. 2012; Fielding et al. 2014; Cavaletto et al. 2015; Fielding et al. 2017)
US22	UL23, UL24, UL26, UL28, UL29, UL36, UL43, US22, US23, US24, US26, IRS1, TRS1	Tegument proteins with involvement in immune evasion. UL36 inhibits Caspase-8-induced apoptosis, whereas TRS1 and IRS1 dysregulate antiviral protein kinase R (PKR).	(Colberg-Poley 1996; Skaletskaya et al. 2001; Adair et al. 2002; Davison and Bhella 2007)
GPCR	UL33, UL78, US27, US28	Chemokine receptor-like homologues with US28 being the most characterised protein able to bind multiple ligands from distinct chemokine classes and regulate multiple signalling pathways.	(Chee et al. 1990; Davison and Bhella 2007; Vomaske et al. 2009)

1.1.3 HCMV Strains

The debate surrounding HCMV genome composition has been partially driven by the use of different laboratory-adapted HCMV strains, known to have distinct *in vitro* acquired mutations. The first complete DNA sequence of HCMV was published in 1990 using a high-passage strain AD169, describing 208 designated open reading frames (ORFs) (Chee et al. 1990). However, subsequent sequencing of high- and low-passaged strains demonstrated major deletions in the U_L/b' region, as well as other mutations outside the U_L/b' region, in high-passage strains such as AD169 and Towne (Cha et al. 1996). Strains AD169 and Towne lack 15 and 13 kbp DNA segments, respectively, compared to strain Toledo, identifying at least 19 previously missed ORFs (Cha et al. 1996). Identification of novel HCMV genes and their incorporation into the existing HCMV gene nomenclature system, resulted in some unrelated genes having similar names, including UL148, UL148A, UL148B, UL148C and UL148D. Previously unidentified protein-coding regions have been named by adding a letter in logical order to a name of a known gene in a similar location (Davison et al. 2003). Hence, despite the similarity in their names, UL148 and UL148D genes are genetically unrelated and exhibit no overt homology to each other or any other HCMV gene (Dolan et al. 2004) (**Figure 1.2**).

It is well established that long-term passaging of clinical HCMV isolates *in vitro* results in recombination and excision events within the HCMV genome, not only changing the genetic makeup of the strain, but the levels of virulence and cell tropism of the virus (Cha et al. 1996; Wilkinson et al. 2015). As a result of numerous mutations acquired through long *in vitro* culturing, high-passage strains AD169 and Towne became easier and quicker to grow in the laboratory compared to clinical strains, however they lost the ability to infect several cell types, including epithelial and endothelial cells (Ryckman et al. 2006). In fact, reduced virulence of high-passaged attenuated strains is evident by their limited pathogenicity when introduced to seronegative individuals during vaccine trials (Just et al. 1975; Neff et al. 1979; Quinnan et al. 1984). In contrast, HCMV strains such as Merlin do not have major genome re-arrangements, their genetic organisation is therefore highly similar to clinical

isolates. As a result, low-passage HCMV strains can facilitate clinically relevant research (Sijmons et al. 2014; Wilkinson et al. 2015). HCMV strain Merlin was the first low passage HCMV strain to be sequenced that had a genome accurately representing a 'wildtype' (WT) genome (**Figure 1.2**) (Dolan et al. 2004). Merlin was isolated from a urine sample of a congenitally infected infant in Cardiff and sequenced following three passages in human fibroblast cells, revealing *in vitro* acquired mutations in just a single gene, UL128 (within the UL128 locus (UL128L), consisting of genes UL128, UL130 and UL131A). Subsequent sequencing also identified a mutation in RL13 gene (Dolan et al. 2004; Stanton et al. 2010). Mutations in RL13 and UL128L are known to be selected during *in vitro* propagation (Murrell et al. 2013). The Merlin genome was therefore cloned into a bacterial artificial chromosome (BAC), enabling these mutations to be repaired to match the sequence of the original clinical isolate (Stanton et al. 2010). The restored Merlin BAC demonstrated dramatically reduced replication *in vitro*, which led to the reselection of *de novo* mutations in both genes. This problem was solved by rendering RL13 and UL128L expression 'repressible' in a particular cell line. This enabled the propagation of a wildtype HCMV Merlin in cell culture without risk of mutation (Stanton et al. 2010). HCMV strain Merlin is now accepted by the WHO as the reference genome for HCMV (Wilkinson et al. 2015).

Table 1.2: Common HCMV laboratory strains, including their passage status, genetic mutations and isolation method.

HCMV Strain	*Passage*	*Details*	*Reference*
Merlin	Low passage	Isolated from the urine of congenitally infected child and passaged 3 times in fibroblasts before the genome was sequenced. Has point mutations in RL13 and UL128. Was subsequently BAC cloned and repaired to wildtype.	(Dolan et al. 2004; Wilkinson 2008; Stanton et al. 2010; Wilkinson et al. 2015)
AD169	High passage	Isolated from adenoids of a child and passaged over 50 times in HFs. Acquired a 15 kb deletion in the U_L/b' region (UL133-UL151), mutations in RL5A, RL13, UL36, UL131A, and duplications of RL11, RL12, and part of RL13.	(Rowe et al. 1956; Elek and Stern 1974; Bradley et al. 2009; Sijmons et al. 2014)
Toledo	Low passage	Isolated from the urine of congenitally infected child and passaged several times in fibroblasts. Has mutations in RL13, UL9 and UL128, as well as partial inversion of the U_L/b' region.	(Quinnan et al. 1984; Cha et al. 1996; Dolan et al. 2004)
Towne	High passage	Isolated from the urine of infected infant and passaged 125 times in WI-38 fibroblasts. Has a 13 kb deletion in the U_L/b' region and mutations in RL13, UL1, UL40, UL130, US1, and US9.	(Plotkin et al. 1975; Dolan et al. 2004; Bradley et al. 2009; Sijmons et al. 2014)
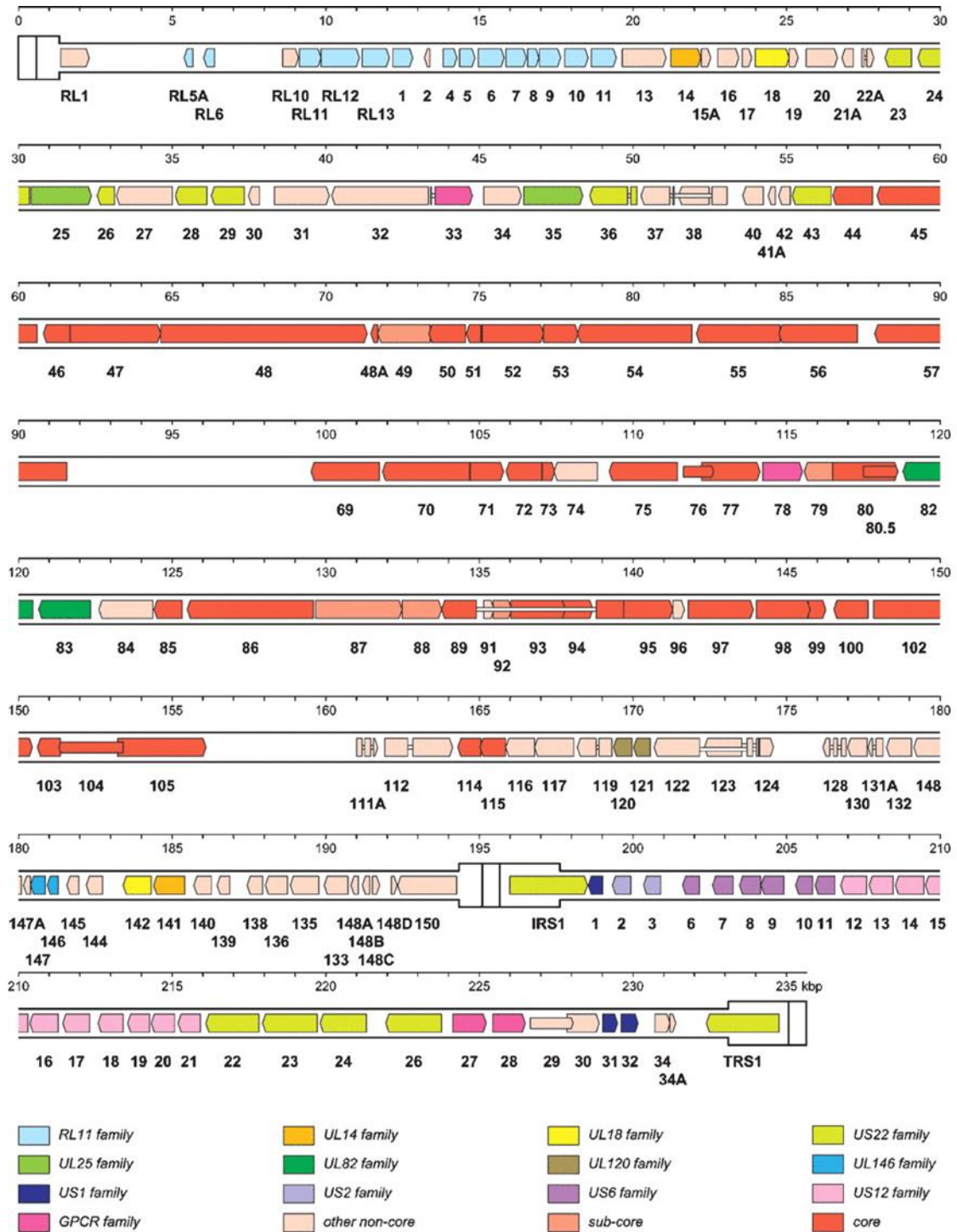
Figure 1.2: Schematic of consensus WT HCMV genome based on the strain Merlin, shown from 5' to 3'. Coloured arrows indicate protein coding regions, whereas narrow white bars represent introns. Different colours differentiate between genes based on conservation across the α-, β- and γ-herpesviruses (core genes in red) or between the β- and γ-herpesviruses (sub-core genes in pink), with subsets of the remaining non-core genes grouped into gene families. Taken from (Dolan et al. 2004).

1.1.4 Discovery and Isolation

First reports of HCMV date back to 1881, when Hugo Ribbert observed large cytomegalic cells with intranuclear inclusions in the kidneys of a stillborn with syphilis (Ribbert 1904). Within the next few decades, in the 19th century, more reports of nuclear and cytoplasmic inclusions in various organs of stillborn and living infants were recorded (Ho 2008). In 1950 a term cytomegalic inclusion disease (CID) was used for the first time, suggesting a common cause for previously reported cases of observed cytomegaly (Wyatt and Saxton 1950). The viral origin of the disease was confirmed 3 years later in 1953 by Minder WH, who observed 199 nm particles in the pancreatic cells of a tissue specimen from a child with CID (Minder 1953). The first HCMV isolation was in 1955-1956 by Margaret Smith from a kidney of a one-month-old infant dying from CID, as well as a salivary gland from a dead infant (Smith 1956). She referred to the virus as salivary gland virus (SGV), with Wallace Rowe publishing back-to-back papers describing the isolation of a cytopathogenic agent resembling SGV from the adenoid tissue of a CID patient (Rowe et al. 1956). The virus isolated by Wallace Rowe became the pioneering laboratory HCMV strain AD169 used for decades to study HCMV biology and pathogenesis (Wilkinson et al. 2015).

1.1.5 Virus Structure

HCMV has a characteristic herpesvirus virion structure and is approximately 200 to 230 nm in diameter (Mocarski et al. 2007). The dsDNA molecule is enclosed within the capsid, surrounded by the tegument layer containing viral proteins, as well as over 70 cellular host proteins (**Figure 1.3**) (Varnum et al. 2004; Kalejta 2008). Over half of virion proteins appear to be present in the tegument with the other half appearing in the capsid or the envelope in HCMV strain AD169 (Varnum et al. 2004). Some of the main tegument viral proteins include pp65, pp150, pp71, pp28, pUL47 and pUL48 (Kalejta 2008). Phosphoprotein 65 (pp65, UL83 gene product) is the major component of the HCMV tegument and is believed to serve an important function during the viral life cycle, as suggested by its rapid entry into the nucleus of infected cells, as well as strong humoral and cellular responses by the host in response to pp65

(Jahn et al. 1987; Revello et al. 1992; McLaughlin-Taylor et al. 1994; Wills et al. 1996; Kern et al. 2002; Varnum et al. 2004). Its main function is the modulation of host immune responses, including both innate and adaptive arms of the immunity, as demonstrated by its ability to disrupt the interferon (IFN) response and block the presentation of viral peptides to the major histocompatibility complex class I (MHC-I) molecules (Abate et al. 2004; Kalejta 2008; Tomtishen 2012). The second most abundant viral protein in the tegument is the highly immunogenic pp150 (UL32 gene product), shown to interact with the capsid and be crucial for HCMV replication (Jahn et al. 1987; Baxter and Gibson 2001; Dunn et al. 2003b). Another viral protein known to be important for efficient HCMV replication is pp71 (UL82 gene product) which facilitates immediate early gene activation (Bresnahan and Shenk 2000). Tegument protein pp28 (UL99 gene product) is involved in the final packaging and envelopment of the virion, as demonstrated by Δpp28 HCMV unable to make infectious virions despite no defects being present in viral DNA replication or gene expression (Silva et al. 2003). Finally, pUL47 and pUL48 are also present in the tegument at high levels and are involved in transporting the nucleocapsid into the host nucleus, with pUL48 also possibly inhibiting proteasomal degradation of viral proteins upon virion entry into cells, and pUL47 stabilising pUL48 (Bechtel and Shenk 2002; Wang et al. 2006).

The lipid bilayer envelope surrounding the tegument contains at least 20 virus-encoded glycoproteins that are essential for a variety of viral functions, such as cell attachment, virus entry, virion maturation and cell-to-cell spread (Chee et al. 1990). These include glycoproteins B (gB, UL55 gene product), gH (UL75 gene product), gL (UL115 gene product), gM (UL100 gene product), gN (UL73 gene product), and gO (UL74 gene product) – all of which have been shown to be essential for efficient viral growth, as HCMV deletion mutants lacking these proteins have growth defects, or are unable to grow altogether (Dunn et al. 2003b; Varnum et al. 2004).

In addition to infectious virions, HCMV produces two additional particles referred to as non-infectious enveloped particles (NIEPs) and dense bodies (Irmiere and Gibson 1983). NIEPs structurally resemble infectious virions, but lack viral genomes within the capsid, whereas dense bodies lack the capsid,

and thus the genome, entirely (Liu and Zhou 2007; Gibson 2008). The function of these additional viral particles poorly understood, however there is some evidence suggesting that they play a role in immune evasion by redirecting the attention of immune cells and effector molecules away from infectious particles, facilitating entry of the latter into the cells (Liu and Zhou 2007; Gibson 2008).
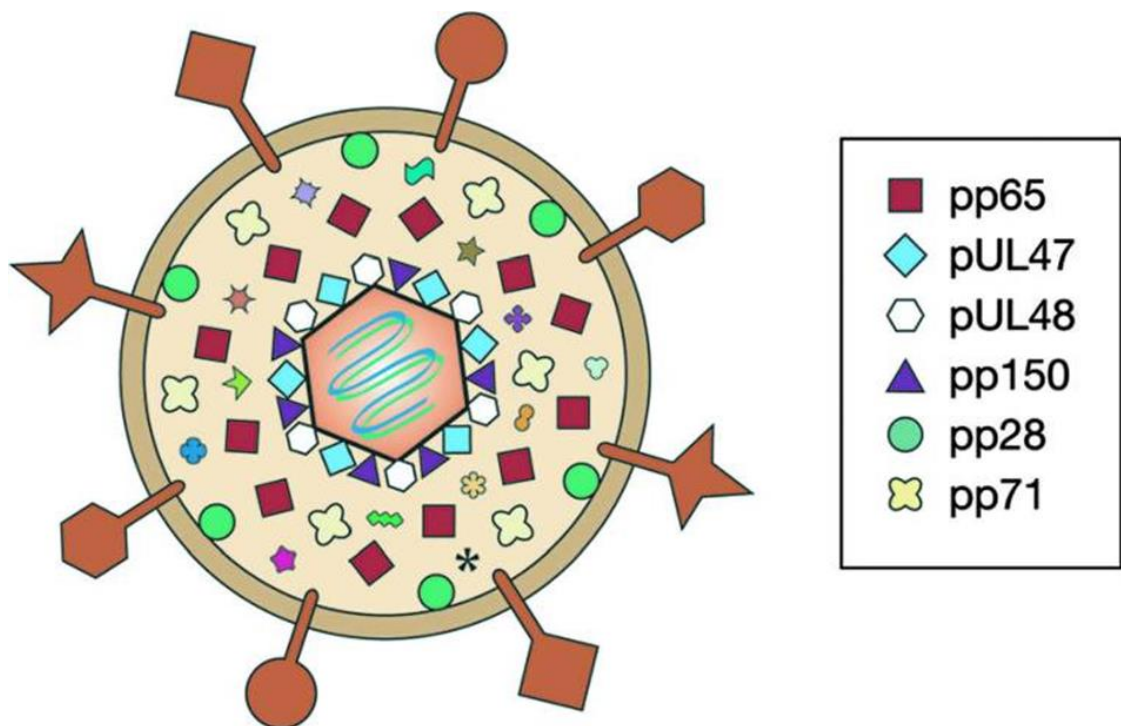
Figure 1.3: A schematic of the HCMV virion. A standard infectious HCMV virion contains dsDNA genome enclosed within the capsid, which is surrounded by tegument and lipid bilayer envelope. Most abundant tegument proteins are presented, with the shapes on the envelope representing various glycoproteins. Figure adapted from (Kalejta 2008).

1.1.6 HCMV Life Cycle

Typical of a herpesvirus, the HCMV life cycle consists of lytic and latent infections (Grinde 2013; Cohen 2020). During lytic infection, HCMV gene transcription, DNA replication and protein translation are actively ongoing, resulting in formation and release of infectious viral progeny. However, due to the host immune system targeting viral replication, HCMV may also avoid host immune surveillance by staying dormant in the host in a 'latent' state (Grinde 2013; Cohen 2020). During latent infection, viral DNA is censored by being packaged into certain histones, however latent HCMV can reactivate and restart lytic replication, producing infectious virions. External events such as immune suppression, exposure to environmental stimuli or extreme stress trigger this (Ioudinkova et al. 2006; Ong et al. 2017; Cohen 2020). Overall, both lytic and latent life cycle stages are essential for successful HCMV survival, replication and spread.

1.1.6.1 Cell Entry

The first step in the replication cycle of HCMV is host cell entry, facilitated by the envelope glycoproteins on the surface of the virion, as well as a number of cellular receptors. Like most herpesviruses, HCMV enters cells via direct fusion of the viral envelope with the plasma membrane, or by receptor-mediated endocytosis, resulting in release of the nucleocapsid to the cytoplasm (Isaacson et al. 2008; Jean Beltran and Cristea 2014). The importance of viral glycoproteins in cell entry has been well established in HCMV and has been shown to be dependent on cell type and pH (Compton et al. 1992; Ryckman et al. 2006). The ability of HCMV to infect a variety of cell types is related to different combinations of envelope proteins present on the viral envelope. There are three complexes termed glycoprotein complex I, II, and III (gC-I, gC-II, and gC-III) present on the HCMV envelope (Nguyen and Kamil 2018; Wang and Zhao 2020).

gC-I is comprised of gB homotrimers linked by disulphide bonds and is involved in envelope-membrane fusion during viral entry (Britt and Auger 1986). A number of host proteins have been reported to interact with gB and facilitate fusion of the membranes, such as the platelet-derived growth factor

receptor α (PDGFRα), epidermal growth factor receptor (EGFR) and β1-integrin (Wang et al. 2003; Feire et al. 2004; Soroceanu et al. 2008; Feire et al. 2010). A disulphide-linked heterodimer of gM and gN represents the second glycoprotein complex gC-II, which is also the most abundant glycoprotein complex on the virion (Mach et al. 2000; Varnum et al. 2004; Mach et al. 2005; Kropff et al. 2012). gM/gN play essential roles in virion attachment to the cell membrane mediated by their binding to heparan sulphate proteoglycans (HSPGs) on the cell surface (Kari and Gehrz 1992). gC-III is comprised of gH, gL and gO, and is commonly referred to as the "trimer" or "gH/gL/gO". It is a heterotrimeric complex where gH and gL are disulphide-linked to a heavily N-glycosylated gO shown to bind PDGFRα, transforming growth factor-beta receptor type 3 (TGFβRIII) and neuregulin-2 (NRG2) (Huber and Compton 1997,1998; Ciferri et al. 2015; Ye et al. 2020). Viral gH/gL, together with gB, are considered to be the core membrane fusion proteins that facilitate virion entry into multiple cell types (Nguyen and Kamil 2018; Wang and Zhao 2020; Ye et al. 2020), whereas the role of gO in the context of gH/gL/gO trimer has been associated with cell-free viral spread in all cell types and cell-cell entry specifically into fibroblasts (Jiang et al. 2008; Wille et al. 2010; Zhou et al. 2015; Ye et al. 2020). Viral gH/gL also forms another complex with small glycoproteins encoded by the UL128L locus forming a 'pentamer' also known as 'gH/gL/UL128-131A' (Wang and Shenk 2005; Ryckman et al. 2008; Ciferri et al. 2015; Nguyen and Kamil 2018). The pentamer has been shown to be essential to facilitate endocytosis-mediated entry into endothelial, epithelial and myeloid cells via binding to neuropilin-2 (Nrp2), as well as a number of other host proteins on the surface such as CD147 and potentially CD46, thrombomodulin (THBD) and immunoglobulin alpha Fc receptor (FCAR) (Ryckman et al. 2008; Martinez-Martin et al. 2018; Nguyen and Kamil 2018).

1.1.6.2   Viral Gene Expression

After the virion enters a cell, the viral nucleocapsid is transported to the nucleus via dynein-microtubule machinery of the host, mediated by viral UL47 and UL48 tegument proteins, where viral transcription and replication begins (Ogawa-Goto et al. 2003; Liu and Zhou 2007). During productive HCMV infection, host RNA polymerase II and a number of other host and viral proteins

facilitate genome transcription allowing for a coordinated viral gene expression cascade (Rozman et al. 2022). Traditionally, four main gene expression cascades were described during lytic HCMV infection based on their regulation and kinetics – immediate-early (IE), early (E), early-late (EL) and late (L) (Mocarski et al. 2007; Reeves 2011; Weekes et al. 2014). The use of viral DNA replication inhibitors that act at various stages of DNA replication helped to classify and define HCMV gene expression cascades (Chambers et al. 1999; Reeves 2011). IE gene expression starts at 1 hr *post* infection (hpi) and peaks at 4-8 hpi. It is independent of the *de novo* expression of any other viral genes, and encodes genes that inhibit initial innate immune responses and activate expression of E and EL genes (Wilkinson et al. 1984; Reeves 2011). E and EL gene expression is triggered 8-12 hpi and is necessary to initiate and facilitate viral DNA replication and synthesis, as well as enhance the production of L gene products required for the assembly, maturation, and release of viral progeny. L gene expression occurs mostly during and *post* DNA replication and is highest at 72-96 hpi, associated with the activation of genes involved in virion maturation and egress (Mocarski et al. 2007; Isomura and Stinski 2013; Weekes et al. 2014; Wang and Zhao 2020).

Recent advances in proteomics techniques facilitated an in-depth quantitative temporal viromics (QTV) study, identifying five distinct cascades of HCMV gene expression classified as temporal classes Tp1, Tp2, Tp3, Tp4 and Tp5 based on their temporal profiles (**Figure 1.4**) (Weekes et al. 2014), complementary to and mostly consistent with the classical IE, E, EL, L nomenclature defined by the use of metabolic inhibitors, with most IE and L genes demonstrating Tp1 and Tp5 temporal profiles, respectively (Mocarski et al. 2007; Weekes et al. 2014). Mapping changes in HCMV gene expression using QTV method further demonstrated the complexity of DNA regulation and replication strategies used by HCMV to ensure successful viral replication in the host.
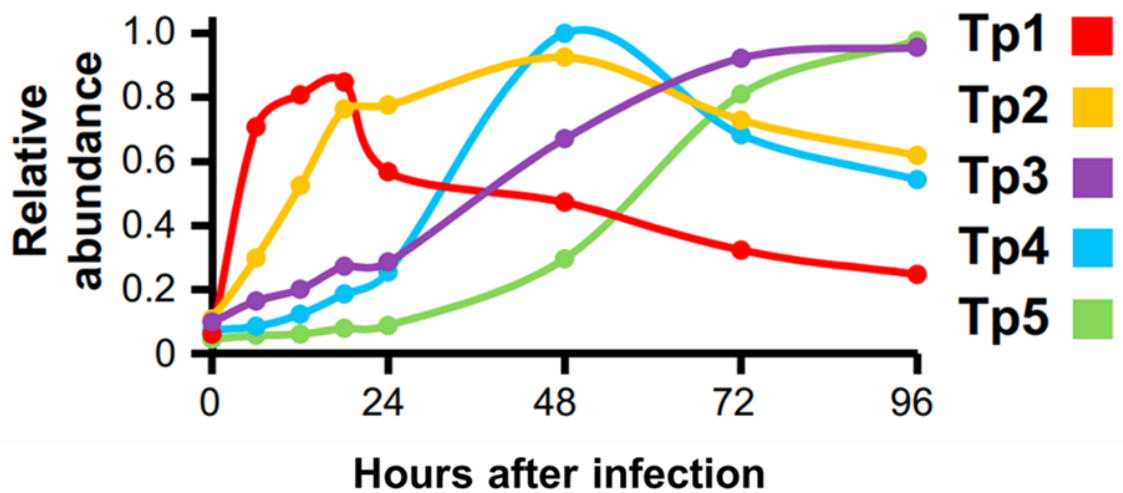
Figure 1.4: Five temporal classes of HCMV gene expression based on their gene expression patterns and timings described by Weekes et al., 2014. The figure was adapted from Weekes et al., 2014.

1.1.6.3   DNA Replication and Egress

HCMV DNA replication takes place at the origin for DNA replication, termed *ori*Lyt found in the U$_L$ region upstream of UL57 (Chee et al. 1990; Anders et al. 1992). The pUL84-pUL122 (IE2) complex is required for the activation of *ori*Lyt-dependent DNA replication in lytically infected cells (Xu et al. 2002), along with six core proteins, pUL44 (DNA processivity factor), pUL54 (DNA polymerase), pUL70 (primase), pUL105 (helicase), pUL102 (primase-associated factor) and pUL57 (single-stranded DNA-binding protein) (Pari 2008). Together these proteins begin the cascade of coordinated gene expression to facilitate viral DNA amplification which occurs after the expression of early genes and before late gene expression (Mocarski et al. 2007).

Once the genome is replicated, viral DNA is enclosed into a nucleocapsid, which is then released into the cytoplasm. Nucleocapsid formation is mediated by a number of viral proteins, including pUL80, pUL77, pUL93 and an enzyme complex called terminase, consisting of pUL51, pUL52, pUL56, pUL77,

pUL89, and pUL93 (Ye et al. 2020). Viral pUL77 and pUL93 stabilise DNA packaging (Köppen-Rung et al. 2016), whilst maturational protease pUL80 helps to assemble the four core nucleocapsid components together – major capsid protein (MCP/UL86), minor capsid binding protein (TRI1/UL46), minor capsid protein (TRI2/UL85), and smallest capsid protein (SCP/UL48A) (Gibson 2008; Tandon and Mocarski 2012). The terminase enzyme complex cleaves concatemeric viral DNA into individual sections ready for packaging into the nucleocapsid (Ligat et al. 2018; Ye et al. 2020). In brief, the nuclear virus maturation step can be summarised by capsid assembly, DNA encapsidation, initial tegumentation and nuclear egress (Tandon and Mocarski 2012). After maturation, nucleocapsids enter the nuclear egress complex (NEC) comprising of two core proteins pUL50 and pUL53, as well as a number of other viral and cellular kinases, such as pUL97, protein kinase C (PKC) and Cyclin-dependent kinase (CDK1) (Marschall et al. 2020). NEC facilitates egress of the nucleocapsids into the assembly compartment (AC), as well as acting as a quality control checkpoint where the preference to egress is given to the capsids that are most mature (Tandon and Mocarski 2012; Tandon et al. 2015). Following nuclear egress through NEC, nucleocapsids travel to the AC – a highly vacuolated part of the cytoplasm containing multiple cellular organelles hijacked and reorganised by viral proteins and microRNAs (Das et al. 2014; Hook et al. 2014). Cis- and trans-Golgi network, endoplasmic reticulum (ER) and endosomes become rearranged into concentric cylindrical layers forming the AC, surrounded by the kidney bean shaped nucleus (Das et al. 2007; Alwine 2012; Das et al. 2014). Viral pUL47, pUL48, pUL94 and pUL103 are known to contribute to AC biogenesis, amongst other HCMV proteins (Das et al. 2014). The AC is crucial in facilitating additional tegumentation to the nucleocapsid, virion assembly and secretion (Das et al. 2007; Alwine 2012; Hook et al. 2014). When virions leave the AC, they acquire a host-derived envelope enriched with HCMV proteins as they bud out of the Golgi and into the trans-Golgi vesicles. The vesicles then transport mature virions to the cell membrane where they are released by direct membrane fusion or exocytosis as infectious viral progeny (Das et al. 2007; Kalejta 2008; Alwine 2012; Ye et al. 2020).

1.1.6.4   Latent Infection and Reactivation

Following lytic infection, HCMV, as all herpesviruses, establishes lifelong persistence in the host in the form of latency. Viral latency is characterised as the ability of a virus to enter a dormant state in the host, in which it remains undetected by the immune system by supressing its viral gene expression to a minimum and halting the production of viral progeny (Elder and Sinclair 2019; Forte et al. 2020). HCMV DNA replication machinery is inhibited by gene silencing, histone and chromatin modifications, as well as the suppression of the viral major immediate-early promoter (MIEP) (Sinclair and Sissons 2006; Mocarski et al. 2007). HCMV is able to reactivate throughout the lifetime of its host and is generally not associated with disease in healthy individuals, however reactivation is a major cause of morbidity and mortality in immunocompromised and immunosuppressed individuals (Forte et al. 2020).

HCMV infects hematopoietic progenitor cells in the bone marrow, however it only establishes latency in the myeloid lineage (Forte et al. 2020). Indeed, viral DNA can be detected in pluripotent CD34+ stem cells, however after progenitor cells differentiate into monocytes, B-, T-cells and polymorphonuclear lymphocytes (PMNLs), viral genomes can only be detected in CD14+ monocytes (Taylor-Wiedeman et al. 1991; Sinclair and Sissons 2006). The frequency of monocytes carrying latent HCMV genome in the blood of seropositive individuals is estimated to be 1 in 10,000 cells (Slobedman and Mocarski 1999).

HCMV reactivation is poorly understood, however it appears to be triggered by inflammation, in particularly increased levels of the inflammatory cytokine tumour necrosis factor alpha (TNFα). In order to reactivate and enter lytic infection, HCMV requires monocytes to differentiate into dendritic cells (DCs) and macrophages (Reeves and Sinclair 2013; Poole et al. 2015). IE gene expression has previously been detected in mature DCs following differentiation and was associated with reactivation of the viral MIEP as a result of differentiation-mediated chromatin remodelling (Reeves et al. 2005). TNFα signalling has also been shown to activate MIEP, as well as NFκB, which

has multiple binding sites in the MIEP, creating an amplifying loop of virus reactivation mediated by inflammatory responses (Forte et al. 2020).

1.1.7 HCMV Tropism

Despite establishing latency in very specific cell types such as CD34+ progenitor cells and peripheral blood monocytes, HCMV is able to lytically infect virtually any cell type *in vivo*, apart from lymphocytes and PMNLs (Grefte et al. 1994; Sinzger et al. 1995; Sinzger et al. 2008). Endothelial and epithelial cells, fibroblasts, smooth muscle cells and highly differentiated myeloid cells are considered to be the main sites for lytic HCMV infection (Sinzger et al. 1995; Gerna et al. 2019). Indeed, such broad cellular tropism allows HCMV to establish infection in almost every organ, with the liver, lungs, gastrointestinal tract, retina and brain being the predominant sites for HCMV infections in immunocompromised individuals (Plachter et al. 1996; Sinzger et al. 2008). Interestingly, despite such broad tropism and ability to infect multiple tissues and organs, HCMV specificity at the host level is highly restricted to humans (Sinzger et al. 2008). As a result, there are no animal models available to study HCMV infection, with researchers relying on patient and autopsy samples for *in vivo* studies, as well as *in vitro* cell work.

A number of HCMV susceptible cell lines are used to study various stages of the viral cycle *in vitro*. Both primary and immortalised cell culture models are available and include skin and lung fibroblasts, retinal pigmented and kidney epithelial cells, hepatocytes, monocyte-derived macrophages and dendritic cells, as well as vascular endothelial cells, to name a few (Sinzger et al. 2008; Gerna et al. 2019). Peripheral blood monocytes and CD34+ hematopoietic progenitor cells derived from umbilical cord blood are commonly used to study HCMV latency, whilst skin and lung fibroblasts, as well as human umbilical vein endothelial cells (HUVECs) are used for long-term propagation of clinical HCMV isolates and to study HCMV lytic cycle (Sinzger et al. 2008). In fact, it has been shown that the choice of a cell line for HCMV propagation *in vitro* is associated with the changes in the tropism of the passaged virus. HCMV propagation in endothelial cells retains a relatively broad cell tropism of the original clinical isolate (Waldman et al. 1991), in contrast to propagation in

fibroblasts, which results in the selection of multiple genetic mutations in the viral genome, which limit infection to fibroblasts (Sinzger et al. 1999; Scrivano et al. 2011). As well as eliminating tropism for other cell types, mutations selected in fibroblasts that include the U$_L$/b' region, RL13 and UL128L, result in enhanced growth in fibroblasts (Dargan et al. 2010; Stanton et al. 2010). Nevertheless, as a result of the high titres and their ready infectability, fibroblasts became a standard cell line for the growth and generation of HCMV stocks for *in vitro* work (Mocarski et al. 2007).

1.2 Clinical Significance

1.2.1 Epidemiology

HCMV has a very high seroprevalence worldwide with some parts of the world demonstrating seroprevalence rates of over 90%. Geographic and socioeconomic backgrounds, as well as age, ethnicity and sex, have all been associated with HCMV acquisition patterns (Boppana and Fowler 2007; Cannon et al. 2010; Fowler et al. 2022). In developing regions such as South America, Sub-Saharan Africa, East Asia, and India, the vast majority of pre-school children (>90%) test positive for HCMV specific antibodies, in contrast to children of similar age in developed countries, where seroprevalence is below 20% (Boppana and Fowler 2007). Nevertheless, multiple studies have shown that HCMV seroprevalence generally increases with age with most studies reporting seroprevalence of 60% or over for individuals over 50 years old in developed countries (Cannon et al. 2010). For example, a study performed in the United States reported HCMV seroprevalence of 36.3% in children versus 90.8% in those aged over 80 years old (Staras et al. 2006). A number of systematic literature reviews also consistently found increased incidence of HCMV specific antibodies in ethnic minorities compared to Caucasian individuals, as well as in women of reproductive age compared to men (Staras et al. 2006; Cannon et al. 2010; Fowler et al. 2022). It is generally believed that childcare is the factor contributing to increased HCMV seroprevalence in women (van Rijckevorsel et al. 2012; Wujcicka et al. 2014). It is most likely linked to the way HCMV transmits, which is usually through

direct contact with body fluids from an infected person, including blood, breast milk, saliva and urine (Boppana and Fowler 2007).

Despite such high seroprevalence rates worldwide, HCMV infection is mostly asymptomatic for the vast majority of people and does not result in severe disease. However, it can be life-threatening for immunodeficient, immunocompromised or immune naïve individuals. Indeed, HCMV is considered a common opportunistic infection in the foetus, allograft recipients, bone marrow transplant and acquired immunodeficiency syndrome (AIDS) patients (Griffiths et al. 2015).

1.2.2   Transplant Recipients and AIDS Patients

In the transplant setting, HCMV infection frequently results in serious complications, with various degrees of disease depending on the serostatus of donor/recipient, organ and transplant type, as well as the level of immune suppression (Houldcroft et al. 2020; Griffiths and Reeves 2021).

Solid organ transplant (SOT) patients suffer from HCMV reinfection or reactivation, with 60-75% of patients demonstrating some evidence of active HCMV infection in the first year following transplant (Pereyra and Rubin 2004; Houldcroft et al. 2020). A primary HCMV infection occurs when a seronegative recipient receives an organ from a seropositive donor (D+/R-). This combination of HCMV donor/recipient serostatus is associated with the highest risk of HCMV viremia in SOT due to the recipient being immunologically HCMV-naïve, as well as receiving a high level of immunosuppressive agents to avoid graft rejection (Atabani et al. 2012). Immunosuppression is also associated with the reactivation of endogenous latent virus in seropositive recipients, however the incidence of symptomatic infection in those instances is lower compared to the D+/R- donor/recipient pair, 15-20% to 50-65%, respectively (Pereyra and Rubin 2004). In the instance where both the donor and the recipient are HCMV seropositive, a superinfection may develop if reactivating virus is of donor origin, with 30% of cases developing symptomatic HCMV disease (Pereyra and Rubin 2004).

In the hematopoietic stem cell transplantation (HSCT) setting the highest incidence of HCMV-associated complications occurs when a seropositive recipient receives a graft from a seronegative donor (D-/R+), which is in contrast to SOT. The D-/R+ combination in HSCT is the most serious because the recipient originated latent HCMV reactivates due to proinflammatory responses occurring in the recipient as a result of surgery, immunosuppressive therapy and the lack of HCMV-specific memory responses from the seronegative donor (Boeckh and Nichols 2004). Whereas, in the D+/R- scenario, the recipient receives a very low proportion of latently-infected stem cells in the donated graft (estimated <0.01%), this D+ graft also transfers HCMV cell-mediated immunity to the recipient, which is able to keep the virus under control (Grob et al. 1987; Griffiths and Reeves 2021).

In both HSCT and SOT, HCMV disease can result in graft rejection, increased risk of other opportunistic infections, pneumonia, gastrointestinal disease, hepatitis, retinitis, as well as invasive disease in other organs (e.g., nephritis, myocarditis, pancreatitis), to name a few (Azevedo et al. 2015). Combined with the effects of immunosuppressive treatments, HCMV disease can be life-threating for those receiving an organ transplant.

Individuals with AIDS are also considered to be vulnerable to the opportunistic HCMV infections. Before the introduction of highly active antiretroviral therapy (HAART), AIDS patients were extremely affected by HCMV disease with up to 25% of patients with AIDS experiencing life- or sight-threatening infections due to the virus (Drew 1988; Shafer and Vuitton 1999; Springer and Weinberg 2004). Retinitis was the most common complication accounting for 75%–85% of HCMV disease in these patients, incidence rates of which went down substantially (~80%) with the use of HAART (Kempen et al. 2003; Griffiths and Reeves 2021). Although nowadays HCMV-associated retinitis in AIDS patients has virtually disappeared, some cases still occur in patients who have not taken antiretroviral therapy either by choice or due to financial and socioeconomic reasons (Griffiths et al. 2015).

1.2.3 Congenital HCMV

In addition to HCMV transmission via direct contact with body fluids from an infected person, as well as in the transplant setting, it can vertically transmit from a pregnant mother with primary or secondary infection, or reactivation, to her unborn child, resulting in a congenital HCMV (cCMV) infection (Bristow et al. 2011; Dietrich and Schieffelin 2019). Primary cCMV infection occurs when a previously seronegative pregnant mother contracts a HCMV infection during her pregnancy, transmitting the virus to the foetus, whereas secondary cCMV infection occurs when latent HCMV in a seropositive mother reactivates or if the mother contracts a new strain of HCMV (Bristow et al. 2011; Pass and Anderson 2014).

A meta-analysis of 34 articles assessing all live-born infants for HCMV infection determined that birth prevalence of cCMV was 0.64%, with some parts of the world, such as Latin America, Africa and Asia reporting higher rates of cCMV infections of 1-2% (Kenneson and Cannon 2007; Fowler et al. 2017). Although the majority of cCMV+ infants will be asymptomatic and will not develop any complications following infection, approximately half of infants with symptomatic cCMV will manifest permanent long-term health problems (Fowler et al. 2017). Sensorineural hearing loss (SNHL) is the most common complication of cCMV (Grosse et al. 2008), however other conditions include mental retardation, cerebral palsy and impaired vision (Bristow et al. 2011; Dietrich and Schieffelin 2019). In fact, disabilities caused by cCMV infection are more common in children than other more recognized disabling diseases such as Down's syndrome or spina bifida (Cannon 2009).

1.2.4 Treatments and Therapeutics

Despite the clear need for a vaccine against HCMV, no vaccine is currently licensed for use, however a number of approved drugs against HCMV are routinely used (Arvin et al. 2004; Perera et al. 2021; Scarpini et al. 2021). Ganciclovir is considered to be the gold standard for treating active HCMV infection. It is a nucleoside analogue that, when phosphorylated by viral kinase UL97, inhibits the viral DNA polymerase UL54 (Lischka and Zimmermann

2008; Krishna et al. 2019). Ganciclovir is used as pre-emptive therapy in transplant patients, and to treat symptomatic cCMV disease, as well as HCMV retinitis in AIDS patients (Scarpini et al. 2021). Valganciclovir is a derivative of ganciclovir – a ganciclovir prodrug with oral bioavailability, routinely given to SOT recipients as a prophylaxis to delay the onset of HCMV disease and reduce disease-associated complications (Paya et al. 2004; Lischka and Zimmermann 2008). Foscarnet and cidofovir are administered as second-line drugs to address resistance to ganciclovir. Foscarnet acts as a reversible product inhibitor, interfering with viral DNA polymerase UL54 function, whereas cidofovir is a structural analogue of cytosine monophosphate interfering with DNA elongation step during viral replication (Lischka and Zimmermann 2008; Perera et al. 2021). Letermovir is another antiviral drug that acts by suppressing the HCMV-terminase complex involved in HCMV replication (Marty et al. 2017). There are other drugs currently available to treat active HCMV infection, however, all of the currently licensed and prescribed drugs have serious side effects associated with their use. Neutropenia is the main side effect from ganciclovir treatment in cCMV infants, with instances of it causing thrombocytopenia and hepatotoxicity, as well as temporary and permanent infertility in animal studies (Lischka and Zimmermann 2008; Scarpini et al. 2021). Foscarnet has been shown to cause electrolyte imbalance in transplant patients, cidofovir has been associated with renal toxicity, whereas letermovir was reported to cause adverse gastrointestinal effects (Perera et al. 2021; Scarpini et al. 2021). Overall, the cytotoxicity associated with the use of anti-viral therapies, as well as the emergence of drug-resistant HCMV strains, results in limits to treatment options for those suffering from HCMV-related diseases, highlighting the need for novel HCMV treatments and vaccine developments.

1.3   HCMV Immunity

HCMV infection induces a very broad spectrum of immune responses, facilitated by both innate and adaptive arms of the immune system. This includes the induction of innate mechanisms at the early stages of infection, such as inflammatory cytokine production and activation of natural killer (NK)

cells, which in turn drives adaptive immune responses, such as production of antibodies and CD4+/CD8+ T cell responses against HCMV (Jackson et al. 2011). The responses to HCMV are so robust, that the percentage of HCMV-specific peripheral blood T lymphocytes in seropositive individuals is among the highest recorded in any viral infection (Gillespie et al. 2000). Due to such robust and strong immune responses against the virus, HCMV infection in immunocompetent individuals is well controlled and generally asymptomatic. However, over the course of 200 million years of co-evolution, HCMV has developed numerous immune evasion strategies, allowing the virus to establish persistence in the host even in the face of such powerful immunity and reactivate when the immune system is compromised (McGeoch et al. 1995; Jackson et al. 2011).

1.3.1 Innate Immune Responses

Innate immune responses serve as a first line of defence against HCMV infection, with the induction of pro-inflammatory interferons and activation and recruitment of NK cells, neutrophils, as well as professional antigen presenting cells (APCs), such as DCs and macrophages (Chaplin 2010; Jackson et al. 2011). Upon cell entry, HCMV is sensed by pattern recognition receptors (PRRs), such as toll-like receptors (TLRs), which recognise virus-derived pathogen-associated molecular patterns (PAMPs). Activation of TLRs by PAMPs results in inflammatory cytokine secretion, and, in most cases, type I IFN production creating a hostile environment for viral replication and spread (Takeuchi and Akira 2001; Rossini et al. 2012). Viral gB and gH have been shown to trigger TLR2 at the very early stages of HCMV infection, activating NF-κB signalling, and subsequently resulting in the release of pro-inflammatory cytokines and chemokines, recruitment of professional APCs, phagocytes and NK cells (Compton et al. 2003; Boehme et al. 2006). Other TLRs have also been implicated in immune responses against HCMV, such as TLR3, TLR4, TLR7, TLR8, and TLR9 – shown to be involved in viral detection by recognising viral nucleic acids, as well as the inhibition of viral replication through IFN-β-dependent mechanisms. HCMV also activates IFN regulatory factor 3 (IRF3) through TLR-independent DNA sensing

mechanisms, further upregulating type I IFN signalling (Rossini et al. 2012; Ye et al. 2020).

In response to the initial pro-inflammatory signalling, professional APCs become activated and begin the processing and presentation of viral antigens to adaptive immune cells – B cells, as well as CD8+ and CD4+ T cells. Macrophages have been shown to recognise viral particles just hours after infection and contribute to inflammation by secreting pro-inflammatory cytokines, such as IFN I, IFNγ and TNFα, aimed to contain viral infection (Baasch et al. 2020). DCs, upon recognition of PAMPs, undergo maturation and migrate to the lymphoid tissues to stimulate differentiation of naïve T cells (Patente et al. 2018).

NK cells rapidly accumulate in several organs during viral infection to prevent severe disease by directly eliminating virally infected cells by cytotoxicity and recruiting other cell types by secreting cytokines and chemokines, including IFNγ and TNFα (La Rosa and Diamond 2012; Rossini et al. 2012; Biron and Tarrio 2015). It has been suggested that activated NK cells create a favourable cytokine microenvironment that supports and drives maturation and activation of adaptive immunity, T cells in particular (Moretta et al. 2008; La Rosa and Diamond 2012). Indeed, the role of NK cells in facilitating anti-HCMV responses is well documented. Individuals lacking NK cells have been shown to be at a higher risk of developing severe HCMV disease, highlighting the importance of NK cells in protection against HCMV (Biron et al. 1989; Hu et al. 2022). Furthermore, patients with rare genetic disorders involving overexpression of an inhibitory killer immunoglobulin like receptors (iKIRs) on NK cells have severe recurrent episodes of HCMV disease (Gazit et al. 2004). Killer immunoglobulin like receptors (KIRs) represent just one family of activating and inhibitory NK cell receptors, with NK cells exhibiting a whole plethora of receptors on their surface that regulate NK cell responses by balancing activating and inhibitory signals (Pegram et al. 2011). During HCMV infection, activating NK cell receptors, such as activating KIRs and Natural-killer group 2, member D (NKG2D), can potentially recognise either virus-derived molecules on infected cells, or self-proteins that are upregulated on "stressed", i.e. infected, cells, inducing NK cell killing (Rossini et al. 2012). By

working through these receptors, NK cells have the capacity to kill virally infected cells via the perforin/granzyme pathway. NK cells can also be activated through antibody-dependent cellular cytotoxicity (ADCC) (Aicheler et al. 2013). In ADCC, NK cells activate via an interaction between Fc receptors (FcRs) on the NK cell surface, in particular CD16, and Fc portion of an antibody bound to a target cell. *In vivo* HCMV infection has been associated with huge expansions of NKG2C+ FcεR1γ- NK cells, known to have enhanced ADCC responses and are believed to provide protection from HCMV disease (Foley et al. 2012; Ataya et al. 2020).

1.3.2   HCMV Evasion of Innate Immunity

Even at the very early stages of infection, HCMV is able to interfere with cellular signalling and dampen immune responses. Tegument proteins UL82 and UL83 reduce type I IFN signalling by dysregulating IRF3 phosphorylation and inhibiting its nuclear localisation, with UL83 also inhibiting NF-κB signalling (Ye et al. 2020; Cox et al. 2021). HCMV UL31 inhibits DNA sensing mechanisms, IE1 and IE2 interfere with IFN signal transduction, whilst US7 and US8 target TLR-mediated signalling by degrading TLR3 and TLR4 (Park et al. 2019; Ye et al. 2020). The US2 gene family has also been shown to interfere with antigen presentation by professional APCs to T cells by downregulating MHC-I and interfering with peptide loading on to MHC (Hanley and Bollard 2014; Cox et al. 2021). Interestingly, MHC-I downregulation makes HCMV-infected cells more susceptible to NK cell-mediated killing since inhibitory NK cell signals depend on the presence of MHC-I molecules. However, HCMV has developed numerous strategies to target NK cell activation in order to overcome the negative effects associated with MHC-I downregulation (**Figure 1.5**) (Wilkinson et al. 2008).

Some of these immune-evasins are able to promote inhibitory NK cell signals. UL18 is a viral homologue of host MHC-I that binds the inhibitory NK cell receptor, LILRB1 (LIR-1), inhibiting the activation of LILRB1+ NK cells, whereas UL40 upregulates nonclassical MHC-I molecule HLA-E (human leukocyte antigen E), known to inhibits NK cell-mediated lysis by interacting with CD94/NKG2A receptors (Tomasec et al. 2000; Wang et al. 2002;

Prod'homme et al. 2007; Jackson et al. 2011). Most NK cell evasion genes identified to date, however, target activating NK cell signals. Viral UL141 intracellularly retains at least four host proteins involved in NK cell signalling (Patel et al. 2018). Activating NK cell ligands poliovirus receptor (PVR/CD155) and Nectin2 (CD112) are targeted for degradation by UL141, preventing them from binding to NK cells via receptors DNAX accessory molecule-1 (DNAM-1/CD226) and CD96, thus preventing NK cell-mediated activation and target lysis (Tomasec et al. 2005; Prod'homme et al. 2010). Furthermore, UL141 retains TNF-related apoptosis inducing ligand receptors 1 and 2 (TRAIL-R1 and R2) in the ER inhibiting NK cell-mediated apoptosis (Nemčovičová et al. 2013; Smith et al. 2013). Multiple HCMV proteins have been shown to target MHC-I related protein A (MICA) – one of the ligands for the activating receptor NKG2D (Patel et al. 2018). UL148A, US18, and US20 all have been shown to traffic MICA to the lysosome for degradation, with US9 and UL147A targeting MICA for proteasomal degradation and UL142 retaining it in the cis-Golgi (Chalupny et al. 2006; Ashiru et al. 2009; Fielding et al. 2014; Seidel et al. 2015; Seidel et al. 2021). Indeed, NK cell activation via NKG2D is a pathway that is heavily targeted by HCMV. Apart from MICA, NKG2D has many other ligands, including MHC-I related protein B (MICB), ULBP1-3, RAET1E (ULBP4), RAET1G (ULBP5) and RAET1L (ULBP6) (Jackson et al. 2011). Viral UL16 has been shown to retain MICB, as well as ULBP1, ULBP2 and ULBP6 inside the cell preventing their surface expression, and thus their ability to interact with NKG2D (Cosman et al. 2001; Eagle et al. 2009). MICB expression is further reduced by miRNA-UL112, which binds MICB RNA preventing its translation, consequently resulting in lower surface MICB levels (Stern-Ginossar et al. 2008).

NK-mediated ADCC responses are also targeted by multiple HCMV genes. RL11 and UL119-UL118 bind the Fc portion of IgG, preventing interaction with FcγRs on NK cells and dampening ADCC responses, whereas UL148 impairs CD58 (LFA-3) surface expression inhibiting NK cell-mediated ADCC (Corrales-Aguilar et al. 2014; Wang et al. 2018). The impressive arsenal of HCMV genes targeting NK cell functions demonstrates the importance of NK

cells in controlling the disease, as well as the extent to which HCMV encodes for evasion strategies designed to avoid detection and killing by NK cells.
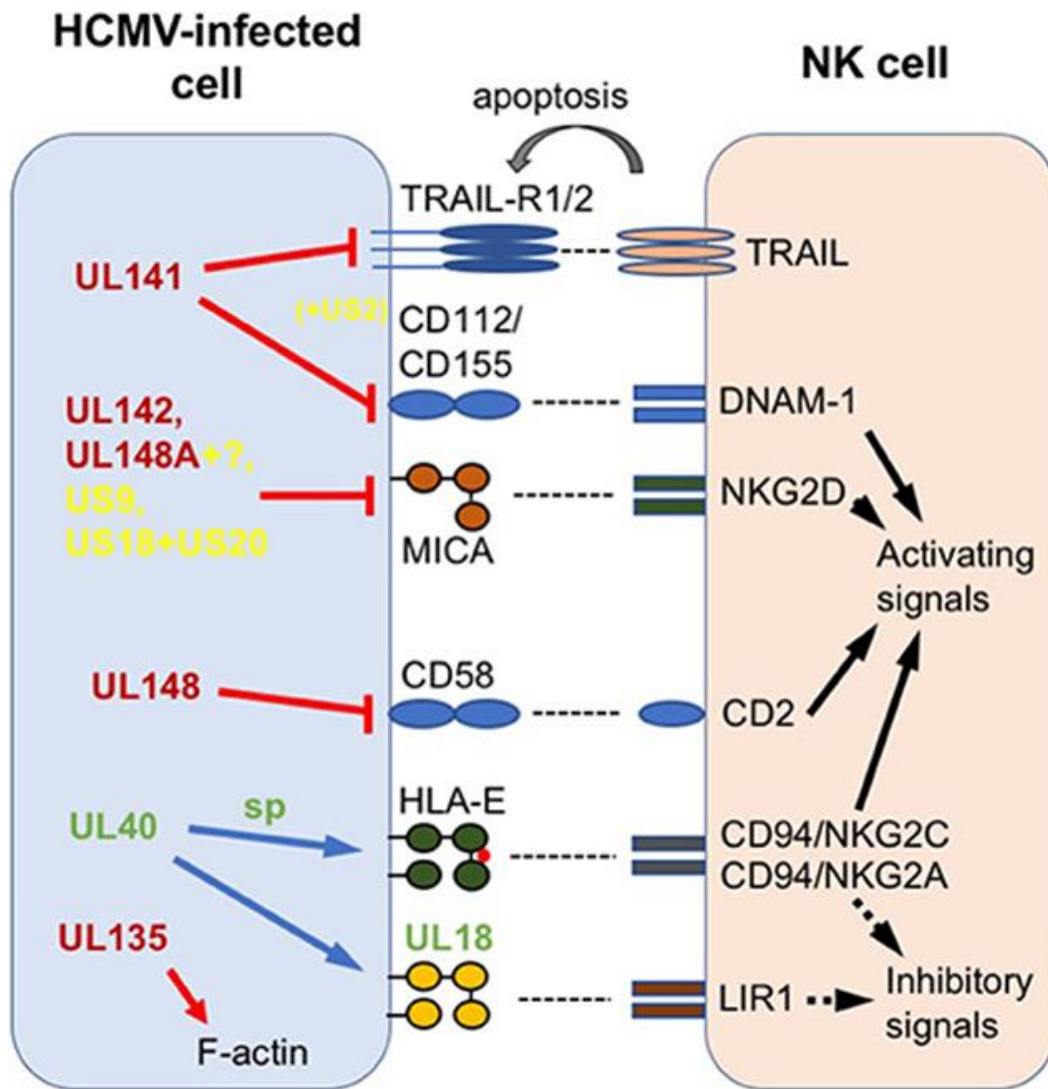
Figure 1.5: Summary of some known HCMV-encoded NK modulators. HCMV proteins are represented by red, green and yellow colours, whereas host proteins are in black. Solid black arrow = intracellular NK activation signal; dotted black arrow = intracellular NK inhibition signal; gray arrow = extracellular signal to target; red line = impairs surface expression; red arrow = disrupts intracellular expression; blue arrow = increases surface expression; sp = signal peptide. Figure taken from (Patel et al. 2018).

1.3.3   Adaptive Immune Responses

Adaptive immunity plays a crucial role in controlling primary HCMV infection as well as keeping the virus under control in its latent stage (**Figure 1.6**). Both cellular and humoral mechanisms mediated by B and T lymphocytes are responsible for protecting the host from HCMV disease (Jackson et al. 2011). A comparative study by Fowler et al. (1992) demonstrated that maternal adaptive, in particular humoral, immunity plays a protective role against severe cCMV disease. Infants born to mothers with pre-existing HCMV immunity showed reduced risk of symptomatic cCMV disease and long-term complications associated with the infection, compared to the mothers who suffered primary HCMV infection during pregnancy (Fowler et al. 1992). In cases where the mother is able to provide transplacental IgG antibodies against HCMV to the foetus, the severity of cCMV disease has been shown to be reduced (Schleiss 2013). The main targets of the neutralizing antibody responses in HCMV are viral antigens involved in the early stages of the viral infection, such as envelope glycoproteins gB, gM/gN, trimer gH/gL/gO, pentamer gH/gL/UL128-131A, tegument protein pp65 (UL83 gene product) and non-structural IE1 protein involved in transcription (Hanley and Bollard 2014; Hu et al. 2022).

However, perhaps the most striking aspect of the adaptive immune responses against HCMV are the HCMV-specific T cell responses. HCMV infection results in huge expansions of CD8+ T cells, and lesser expansions of CD4+ T cells, with seropositive individuals demonstrating higher frequencies of HCMV-specific T cells than those observed with other human viruses. It is estimated that at least 10% of the total T cell repertoire is directed towards HCMV in seropositive individuals, dominating T cell memory compartments in those people (Sylwester et al. 2005; Marchi et al. 2019; Hu et al. 2022). The role of both CD8+ and CD4+ T cells in HCMV infection is well documented in HSCT and SOT patients, in particular kidney, lung and heart transplant recipients (Hanley and Bollard 2014). Cytotoxic CD8+ T cells respond to HCMV peptides presented on professional APCs via MHC-I, activating their killing functions, whilst CD4+ T helper cells recognise viral peptides presented via MHC-II,

enhancing CD8+ T cell and B cell functions (Cox et al. 2021). HCMV-specific T cells are known to target multiple HCMV antigens, however the immunodominant targets are the tegument protein pp65 and IE1 (La Rosa and Diamond 2012; Hanley and Bollard 2014). T cells in over 50% of seropositive individuals are able to recognise viral pp65 and IE1, with other ORFs including UL48, UL55, UL122, UL32, UL123, UL99 and UL82 also demonstrating recognition potential for both CD4+ and CD8+ T cell responses (Sylwester et al. 2005).

In addition to the established role of αβ T cells, such as CD4+ helper and CD8+ cytotoxic T cells, other T cell subsets are also known to play a role in HCMV infection, such as γδ T cells and regulatory T cells (Tregs) – a specialised subset of CD4+ T cells (Jackson et al. 2011). Although γδ T cells are considered as innate immune cells, they have previously been shown to develop memory-like adaptive responses and play a vital role in protection against influenza (Sabbaghi et al. 2020). There is evidence from SOT and HSCT recipient studies that a subset of γδ T cells (Vδ2-) is expanded following HCMV reactivation, with healthy seropositive individuals also demonstrating increased numbers of Vδ2- γδ T cells compared to seronegative individuals (Knight et al. 2010). Immunosuppressive Tregs have also been implicated in HCMV infection, with one study demonstrating enhanced T cell immune responses to HCMV when Tregs were depleted from peripheral blood mononuclear cells (PBMCs) (Aandahl et al. 2004).

1.3.4   HCMV Evasion of Adaptive Immunity

Similar to the plethora of immune evasion strategies employed by HCMV to escape innate immune responses, the virus has also evolved to counteract host adaptive immunity. In fact, dampening of the CD8+ T cell adaptive immune responses happens very early on in infection when the HCMV US2 gene family heavily downregulates surface MHC-I on APCs and interferes with peptide loading. Meanwhile, miR-US4-1 and miR-UL112-5p further inhibit CD8+ T cell response by targeting aminopeptidase ERAP1, which is known to facilitate trimming of viral peptides into mature epitopes for presentation on the MHC-I molecule (Kim et al. 2011; Romania et al. 2017). HCMV also

downregulates CD4+ T cell responses by inhibiting MHC-II presentation mediated by viral US2 (Miller et al. 2001). In addition to its NK inhibitory function, UL148 also inhibits CD8+ T cell responses by retaining the host adhesion protein CD58 inside the cell (Wang et al. 2018). Furthermore, the virus expresses transcripts from the UL111A region which encode two homologues of an immunosuppressive cytokine IL-10, shown to inhibit PBMC proliferation, synthesis of IFNγ and decrease surface expression of both MHC class I and II molecules on monocytes (Spencer et al. 2002; Jenkins et al. 2008). UL11 is another immunomodulatory protein shown to bind the receptor tyrosine phosphatase CD45 and impair TCR signalling, resulting in impaired T cell activation and proliferation (Gabaev et al. 2011). In general, HCMV targets adaptive immune responses mostly by interfering with antigen presentation on APCs, however it employs additional mechanisms to escape T cell-mediated functions and reduce pro-inflammatory signalling, allowing the virus to establish lifelong latency and persistency.
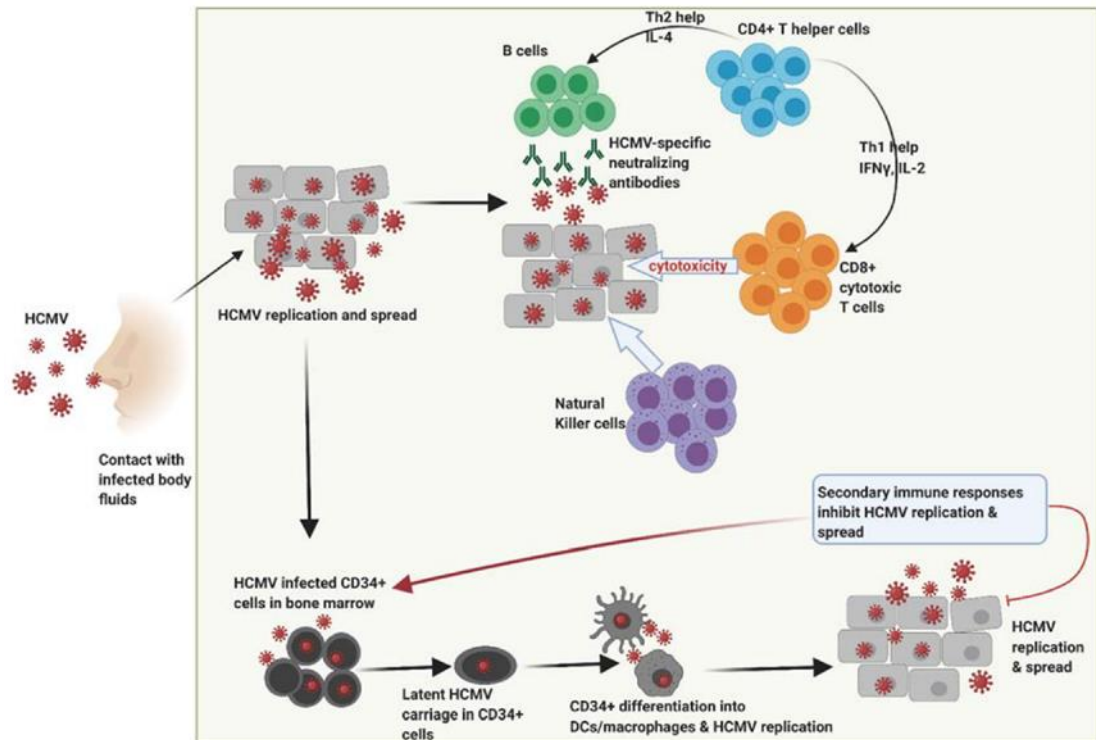
Figure 1.6: A summary of immune responses against HCMV. HCMV enters the host through direct contact with infected bodily fluids. It replicates within host cells, resulting in robust immune responses against the virus that includes generation of HCMV-specific neutralizing antibodies, recruitment of NK cells and high frequencies of CD4+ helper and CD8+ cytotoxic T cells. Despite such robust immune responses, HCMV establishes latency in CD34+ myeloid cells in the bone marrow. During reactivation memory responses keep viral replication under control. Figure taken from (Cox et al. 2021).

1.4   A disintegrin and metalloprotease 17

The ADAMs (A Disintegrin And Metalloproteinases) are a family of multifunctional, type 1 transmembrane proteins that facilitate ectodomain proteolysis, also known as shedding, of a diverse array of cell surface proteins. ADAM-mediated ectodomain shedding facilitates the release of the extracellular portion of a wide range of cell surface receptors and ligands, leaving the membrane-retained portion of the protein on the cell surface (Edwards et al. 2008; Ager 2012). Typical substrates of ADAM proteases include adhesion and differentiation factors, growth factors, cytokines, chemokines and their receptors (Weber and Saftig 2012). By regulating the levels of their substrates, ADAMs influence a broad range of signalling pathways and biological processes involved in immunity and inflammation, cancer progression, cell development and differentiation, cell migration, and axon guidance (Duffy et al. 2009; Ager 2012). To date, 21 functional ADAMs have been characterised in humans, with 13 being proteolytically active (Edwards et al. 2008; Ager 2012; Mullooly et al. 2016). One of these proteolytically active ADAMs is ADAM17.

ADAM17, also known as TNFα converting enzyme TACE, is perhaps the most widely studied ADAM. It is a protein of 824 amino acids (accession number NM_003183), encoded by *ADAM17* located on chromosome 2p25 (Gooz 2010). It was originally discovered as an enzyme that cleaves transmembrane TNFα (tmTNFα) from the cell surface, releasing its soluble form (sTNFα) (Black et al. 1997; Moss et al. 1997). However, subsequently it was shown to facilitate shedding of other ligands from the cell surface, with about 100 ADAM17-dependent substates identified to date (Moss and Minond 2017; Zunke and Rose-John 2017; Calligaris et al. 2021). Examples of ADAM17 substrates include cytokines TNFα, RANKL and IL-8, signalling receptors such as TNF Receptors I and II (TNFR1 and 2), cell adhesion molecules L-selectin and ALCAM, however the list of known ADAM17 targets is much more extensive, demonstrating ADAM17's massive capacity to regulate a wide range of biological functions (**Table 1.3**) (Moss and Minond 2017; Zunke and Rose-John 2017; Calligaris et al. 2021). By cleaving its substrates, ADAM17

facilitates downstream signalling, which can be achieved by multiple mechanisms. Released soluble molecules can bind to their receptors on the same cell, neighbouring cells or more distant cells in the same tissue, and even enter the bloodstream (Gooz 2010). ADAM17 is a widely expressed metalloprotease, found in various tissues including the brain, heart, placenta, kidneys, small intestine, ovaries, testis, thymus and skeletal muscle (Peschon et al. 1998; Ebsen et al. 2013). With such a large substrate profile and expression pattern, ADAM17 has been implicated in a broad range of physiological and pathological processes.

Table 1.3: A table of known ADAM17 targets. Table was adapted from (Calligaris et al. 2021) and contains most known ADAM17 targets.

Cytokines	*Cell-to-Cell Communication*	*Signalling-Receptors*	*Cell Adhesion*	*Cellular Transport*	*Enzymes*	*Others*
TNFα	Amphiregulin	Axl	ALCAM	SCRB1	ACE-2	APP
CSF-1	HB-EGF	CD16	CD44	LRP-1	Carbonic Hydrolase 9	APLP-2
KL-1	TGFα	CD163	L-selectin	LDL-R	Klotho	Prion protein
KL-2	Epigen	CD30 (TNFRSF8)	Collagen XVII	SORCS-1	NPR1	Vasorin
Lymphotoxin α	Epiregulin	CD40 (TNFRSF5)	Desmoglein-2	SORCS-3		PMEL-17
RANKL	NRG-1	CD89	EpCam	SORL-1		Sydecan-1
Cx3cl1	Jagged	EPCR	GP-1ba	SORT-1		Sydecan-4
IL-8	DLL-1	ErbB-4	GP-5	TREM-2		Pre-adypocyte factor
	PD-L1	GHRH receptor	GP-6	IGF-2R		Collagen IV *
	ICOS-L	M-CSFR	ICAM-1			PCPE-1 *

Cytokines	Cell-to-Cell Communication	Signalling-Receptors	Cell Adhesion	Cellular Transport	Enzymes	Others
	IL-1R2	NRP-1	L1-CAM			Cystatin C *
	IL-6R	PTK7	LYPD3			Ebola virus Glycoprotein **
	LAG-3	PTPRZ	MUC-1			
	MIC-A	PTPRF	NCAM			
	MIC-B	SEMA-4D	Nectin-4			
	TIM-1	TNF-R1	SynCAM-1			
	TIM-3	TNF-R2	VACM-1			
	TIM-4	NTRK1	Thrombospondin-4			
	IL-15R	VEGF-R2	JAM-A			
		Notch-1				

* Secreted proteins identified as substrates of soluble ADAM17.

** A virus-encoded protein that is released by ADAM17 after viral infection.

1.4.1   ADAM17 Biology

1.4.1.1   Structure of ADAM17 Protein

The metalloprotease ADAM17 consists of six domains – a pro-domain, a metalloproteinase domain, a disintegrin domain, a cysteine-rich membrane proximal domain (MPD), conserved ADAM seventeen dynamic interaction sequence (CANDIS), and a single transmembrane/cytoplasmic domain (**Figure 1.7**) (Black et al. 1997; Moss et al. 1997; Zunke and Rose-John 2017). The N-terminal pro-domain of ADAM17 contains the classical Zn^{2+} chelating sequence HEXXHXXGXXH which inhibits its catalytic activity and is important in ADAM17 maturation, whereas the metalloproteinase, also known as catalytic, domain, facilitates ADAM17 shedding function (Maskos et al. 1998; Zunke and Rose-John 2017). The functions of the disintegrin domain and CANDIS are poorly understood, however they are suggested to be involved in potential substrate recognition and sheddase activation (Zunke and Rose-John 2017). The MPD has been shown to be subject to complex regulatory control involving switching of conformation, which either restricts or facilitates its interaction with substrates (Düsterhöft et al. 2013; Sommer et al. 2016).

In terms of interaction with its substrates, ADAM17-mediated cleavage typically occurs in *cis*, i.e. within the same cell membrane harbouring both proteinase and substrate. However, there is some evidence of ADAM17 working in *trans*, i.e. cleaving substrates from neighbouring or interacting cells (Janes et al. 2005; Grötzinger et al. 2017). Cleavage of α5β1-integrin by ADAM17 has been reported in both *cis* and *trans* fashion, with some preliminary evidence suggesting that the cleavage of SARS-CoV-2 (severe acute respiratory syndrome coronavirus 2) spike protein S may occur in cis and trans by both ADAM10 and ADAM17 (Grötzinger et al. 2017; Jocher et al. 2022). Indeed, ADAM10, a close relative of ADAM17, has also been shown to cleave Ephrin-A5 in *trans* from the surface of opposing cells, further supporting *trans*-mediated cleaving of substrates by ADAMs (Janes et al. 2005).
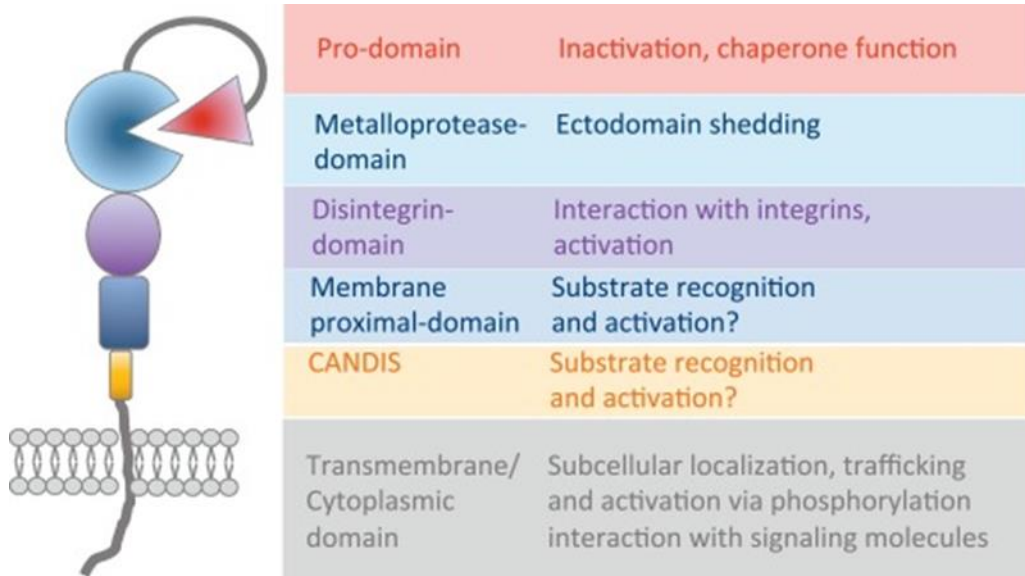
Figure 1.7: Structure of ADAM17 and functions associated with individual protein domains. Figure taken from (Zunke and Rose-John 2017).

1.4.1.2 ADAM17 Regulation

ADAM17 is synthesised in the ER as an immature proform/zymogen, with its function restricted by the presence of the pro-domain (Lorenzen et al. 2016). Proteolytically inactive members of the rhomboid family iRhom1 and 2 are involved in the maturation and trafficking of immature ADAM17 from the ER to the plasma membrane through the Golgi (Adrain et al. 2012; Lee et al. 2016). iRhom1/2 knockout results in a lack of ER to Golgi trafficking of ADAM17 and consequent lack of ADAM17 maturation and loss of shedding capacity (Christova et al. 2013). FERM domain-containing protein 8 (FRMD8) stabilises the iRhom/ADAM17 complex, as demonstrated by reduced ADAM17 and iRhom2 protein levels in tissues of FRMD8-deficent mice (Künzel et al. 2018). The maturation of ADAM17 takes place in the Golgi, where the pro-domain is cleaved off by a proteolytic enzyme Furin (Endres et al. 2003; Peiretti et al. 2003). Furin is also regulated by a phosphofurin acidic cluster sorting protein 1 (PACS1), which transports Furin into the trans-Golgi network where it can facilitate ADAM17 maturation (Wan et al. 1998). With the help of iRhoms, mature ADAM17 is trafficked onto the cell membrane where it can perform its shedding function (Lorenzen et al. 2016). Once mature ADAM17 reaches the cell surface, it exists in a 'closed/inactive' and 'open/active' protein confirmation (Takeda et al. 2006). The conformation change into 'open/active' state upon stimulation is thought to be facilitated by the MPD domain, allowing the shedding activity to begin (Düsterhöft et al. 2013; Sommer et al. 2016). Under unstimulated conditions, ADAM17 undergoes phosphofurin acidic cluster sorting protein 2 (PACS2)-dependent endocytic recycling (Dombernowsky et al. 2015). PACS2 co-localizes with ADAM17 in early endosomes and diverts it away from degradation pathways, as demonstrated by decreased recycling and stability of internalized ADAM17 in PACS2 knockout cells (Dombernowsky et al. 2015). The ADAM17 regulation steps are summarised in **Figure 1.8**. Such tight regulation of ADAM17 maturation and localisation further implies the important role that ADAM17 plays in signalling of many pathways and processes.
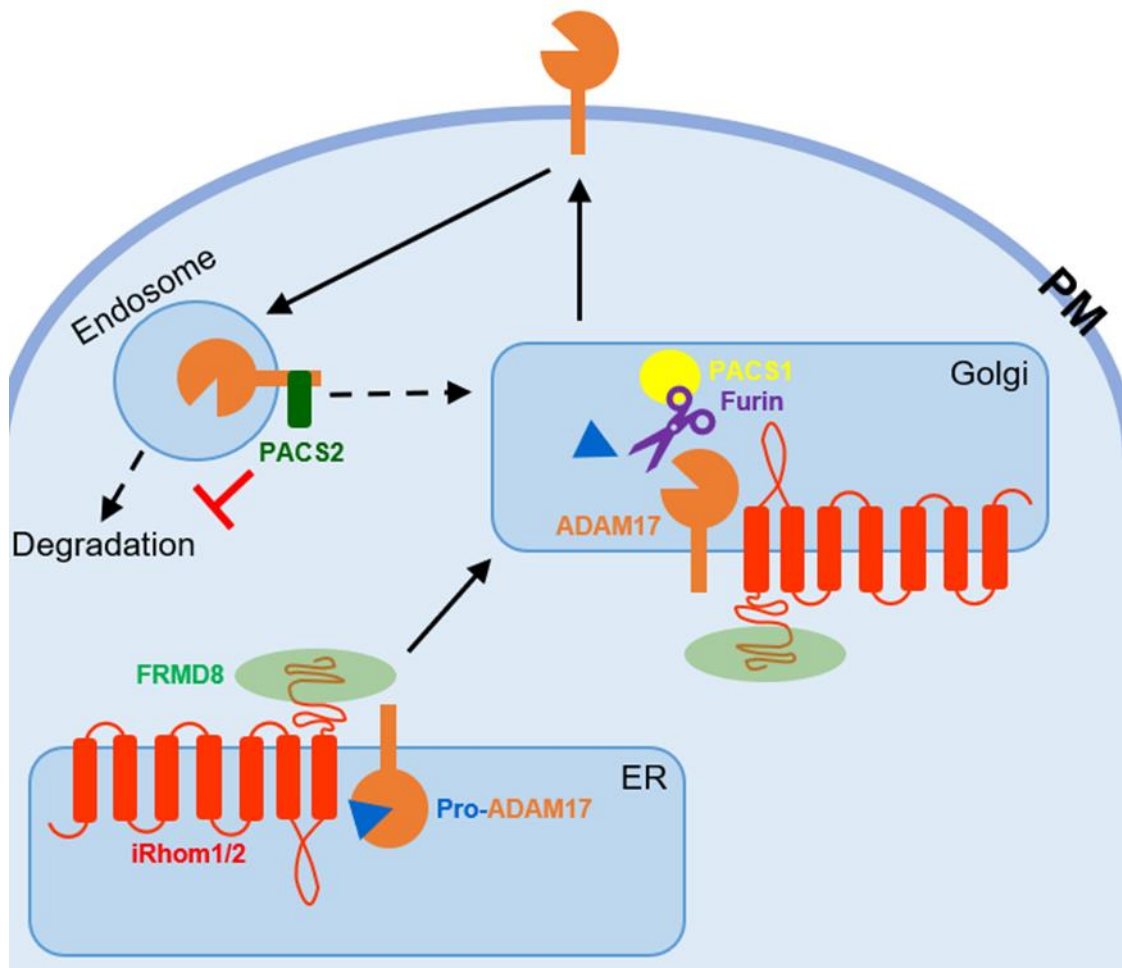
Figure 1.8: Schematic diagram of ADAM17 regulation and maturation.
ADAM17 is synthesised in the ER as an immature precursor (pro-ADAM17).
It is transported by iRhom1/2 to the Golgi for maturation. iRhom1/2 complex is
stabilised by FRMD8. In the Golgi ADAM17 pro-domain is cleaved by Furin
resulting in mature form of ADAM17. Furin activity is regulated by PACS1.
Mature ADAM17 is transported to the cell surface where it can perform its
function as an ectodomain shedding protease. PACS2 regulates ADAM17 cell
surface levels by diverting endocytosed ADAM17 away from degradation
pathways (Wan et al. 1998; Dombernowsky et al. 2015; Künzel et al. 2018).
PM = Plasma membrane; dotted line represents two different fates of
endocytosed ADAM17 depending on situational signalling, which is either
degradation or recycling of the protein.

1.4.2 Functional Significance of ADAM17

1.4.2.1 Role in Development

The first insight into the role of ADAM17 in development came from a study by Peschon et al. (1998), where ADAM17 knockout mice were non-viable and had severe epithelial abnormalities. Specifically, ADAM17 shedding activity was linked to this lethal phenotype, as ADAM17$^{\Delta Zn/\Delta Zn}$ mice lacking the Zn^{2+}−binding site of the metalloenzyme catalytic domain demonstrated perinatal lethality between embryonic day 17.5 and birth (Peschon et al. 1998). Since then many conditional ADAM17 knockout mice models have been developed facilitating ADAM17 knockout in specific cell types and tissues in a temporal fashion (Zunke and Rose-John 2017). Although the viability of mice and observed phenotypes differ between different ADAM17 knockout mice models, most models report improved survival of mice when ADAM17 knockout is tissue restricted compared to ubiquitous ADAM17 deficiency. Some of the phenotypes reported in viable ADAM17 knockout mice include hair defects, open eyes at birth, epithelial abnormalities, heart defects and higher susceptibility to atherosclerosis (Zunke and Rose-John 2017).

There have been a handful of reported cases of mutations in *ADAM17* gene in humans. Blaydon et al. (2011) identified a loss-of-function mutation in *ADAM17* (603–606delCAGA) in two siblings with both children presenting the same clinical features involving the skin, hair, and gut. In both individuals, the skin lesions were observed on the second day of life, which developed into a rash and erythrodermic psoriasis, contributing to frequent *Staphylococcus aureus* infections. They also suffered from candida and pseudomonas infections of the skin, and experienced frequent diarrhoea, with the girl developing chronic diarrhoea and intercurrent gastrointestinal infections by the age of 4 months. The girl died at the age of 12 years from fulminant parvovirus B19–associated myocarditis, whereas the affected boy was found to have left ventricular dilatation, however, was otherwise relatively healthy (Blaydon et al. 2011). Bandsma et al (2015) presented a similar case where a girl with a homozygous frameshift mutation in *ADAM17* (NM_003183.4:c.308dupA) presented with severe diarrhoea, skin rash, and recurrent sepsis, eventually

leading to her death at the age of 10 months because of refractory hypoxia (Bandsma et al. 2015). Although the presented cases clearly demonstrate the devastating effects of lack of ADAM17 in humans, they also suggest that in some cases (the boy in the Blaydon study) there may be mechanisms that compensate for the lack of ADAM17. Indeed, a study by Hartl et al. (2018) identified a rare single-nucleotide variation in *ADAM17* (rs142946965 [p.R215I]) associated with late-onset Alzheimer's disease (AD) within one studied family. They demonstrated that the mutation resulted in *ADAM17* loss of function and, as a result, upregulation of ADAM17-dependent β-amyloid precursor protein (APP) gene expression and elevated amyloid β peptides formation *in vitro*, known to contribute to AD progression (Hartl et al. 2018). However no other symptoms were reported in the study, in contrast to the two studies previously discussed. These observations are consistent with the results generated using ADAM17 deficient mouse models, which demonstrated varied severity of pathology depending on the mouse genotype (Zunke and Rose-John 2017).

1.4.2.2   Role in Disease

ADAM17 dysregulation has also been implicated in multiple diseases and pathologies. In cancer, high levels of ADAM17 are generally associated with poor cancer prognosis (Calligaris et al. 2021). ADAM17 activity has been associated with the progression of several malignancies, including colon and breast cancer linked to its ability to trigger the EGFR pathway by shedding EGFR ligands, such as transforming growth factor alpha (TGFα) (Rossello et al. 2016). ADAM17-mediated EGFR signalling also activates pathological airway remodelling contributing to lung diseases, including asthma, chronic obstructive pulmonary disease and cystic fibrosis (Shiomi et al. 2011). Another ADAM17-mediated pathway implicated in disease is TNFα signalling, which has been associated with many chronic inflammatory diseases, such as rheumatoid arthritis (RA) (Calligaris et al. 2021). Anti-TNFα inhibitors are established treatment of RA and other inflammatory diseases, with preclinical studies demonstrating that ADAM17 blocking protects against RA to a similar extent as the inhibition of TNFα signalling (Issuree et al. 2013). Increased levels of tmTNFα and its receptor TNFR2, as a result of reduced ADAM17-

mediated shedding, have been implicated in atherosclerosis, promoting the recruitment and proliferation of macrophages to the lesions and consequently cholesterol accumulation and atherosclerotic plaque formation (Nicolaou et al. 2017). Furthermore, IL-6 trans-signalling, driven by ADAM17-mediated shedding of the IL-6 receptor (IL-6R), was suggested to play a role in inflammatory bowel disease (Gooz 2010). Upregulated levels of ADAM17 have been observed in intestinal epithelial cells during the active phase of Crohn's disease (Cesaro et al. 2009).

In addition to the conditions mentioned, the role of ADAM17-mediated signalling has been implicated in kidney and heart disease, diabetes and neurological diseases, such as multiple sclerosis and AD (Gooz 2010; Calligaris et al. 2021). Such broad ADAM17 involvement in so many biological processes and pathologies can be explained by the impressive repertoire of substrates that this metalloprotease regulates.

1.4.2.3 ADAM17 in Immunity

It is well established that ADAM17 plays an essential role in immunity and inflammation. The vast majority of its substrates have some immunoregulatory functions (**Table 1.3**), dysregulation of which drives disease, as described above. TNFα signalling is one of the key immune pathways regulated by ADAM17. In a mouse model of human disease multiple sclerosis, tmTNFα was shown to be anti-inflammatory, whereas ADAM17-mediated shedding of surface TNFα into its soluble form rendered it pro-inflammatory (Alexopoulou et al. 2006; Scheller et al. 2011). TNFα signalling is mediated by two receptors TNFR1 and TNFR2, with sTNFα having stronger affinity to TNFR1, whereas tmTNFα preferentially binds TNFR2 (Horiuchi et al. 2010). TNFR1-mediated signalling is, indeed, associated with inflammatory immune responses, cytotoxic and pro-apoptotic functions, whereas TNFR2 signalling appears to have both overlapping (i.e. pro-inflammatory) and opposing (i.e. immunosuppressive) effects to TNFR1-mediated signalling (Qu et al. 2017). In the tumour microenvironment, tmTNFα and TNFR2 interaction has been associated with both – progression of cancer by recruiting immunosuppressive cells and enhancing the survival, metastasis, and apoptosis resistance of

tumour cells, as well as tmTNFα/TNFR2-mediated cytotoxicity and cell death (Qu et al. 2017). Overall, the TNFα pathway is incredibly complex and context-dependent, with ADAM17 shedding activity playing an important role in regulating the levels of soluble and transmembrane TNFα, as well as both TNFα receptors TNFR1 and TNFR2 (Scheller et al. 2011).

ADAM17 is also the main sheddase for adhesion glycoprotein L-selectin (CD62L), known to play a crucial role in leucocyte recruitment to lymph nodes and inflamed tissues to survey APCs for peptide-MHC complexes (Ivetic et al. 2019). ADAM17-mediated shedding of L-selectin in mouse and human T cells has been shown to be essential for proliferation and activation of peptide-MHC activated CD8+ T cells (Mohammed et al. 2019). Mohammed et al. (2019) engineered mice expressing T cells with cleavable or non-cleavable L-selectin, demonstrating huge clonal expansions of cytotoxic T cells in mice with cleavable L-selectin in response to vaccinia infection. In contrast, mice with shedding-resistant L-selectin showed delayed T cell proliferation, resulting in 8-fold lower CD8+ T cell expansions (Mohammed et al. 2019). The study confirmed that the observed phenotype was indeed ADAM17-dependent and not attributed to closely related ADAM10 or a number of other metalloproteinases. Hence, ADAM17 plays an important role in T cell immune responses by regulating T cell recruitment through L-selectin shedding, with the lack of shedding suggesting reduced T cell proliferation in response to infection (Mohammed et al. 2016; Mohammed et al. 2019).

Indeed, ADAM17 has been shown to influence various aspects of T cell biology. ADAM17-mediated shedding of IL-6R influences the differentiation of naïve and memory CD4+ T cells into either Treg or T helper (Th)17 cells (Wing and Sakaguchi 2010). IL-6 trans-signalling mediated by ADAM17-cleaved soluble IL-6R (sIL-6R), together with TGFβ signalling, induces the differentiation of pro-inflammatory Th17 cells, whereas TGFβ signalling on its own facilitates differentiation of immunosuppressive Tregs (Dominitzki et al. 2007; Jones et al. 2010). The role of ADAM17 in this process is further supported by the fact that ADAM17 regulates TGFβ signalling by cleaving Vasorin – a known inhibitor of TGFβ activity. In fact, only the ADAM17-cleaved

soluble form of Vasorin has been shown to inhibit TGFβ pathway (Ikeda et al. 2004; Malapeira et al. 2011).

Finally, ADAM17 activity has also been implicated in the function of other immune cell types, such as NK cells and DCs. ADAM17 shedding of MICA/B – ligands of the NK cell receptor NKG2D, leads to NK cell-mediated lysis of target cells (virally-infected or tumour cells) and cytokine secretion, thus playing a central role in immune system activation (Boutet et al. 2009). Activated NK cells are also associated with increased shedding of ADCC receptor CD16 and L-selectin by ADAM17, correlated with increased IFNγ production and levels of the activation marker CD107a (Romee et al. 2013), further highlighting the role of ADAM17 in NK cell function. ADAM17 is also involved in DC function, in particular DC podosome regulation. The podosome is an actin-rich structure on the surface of DCs which is dissociated before DCs can migrate to the lymph nodes to stimulate T cells. ADAM17 has been shown to facilitate podosome dissociation, restoring migratory capacity of DCs lost during acute antigen sampling (West et al. 2008). Although the exact mechanism between ADAM17 and podosome dissociation remains unknown, it is clear that ADAM17 is involved in the early phase of DC activation and thus in the early phase of the immune response (Scheller et al. 2011).

1.4.2.4   Role in Infection

With the ability to regulate such an abundance of substrates involved in immunity and inflammation, ADAM17 has also been implemented in controlling bacterial and viral infections. In mice, *Klebsiella pneumoniae* infection of the lungs has been shown to be cleared by neutrophils activated by ADAM17-dependent L-selectin shedding (Cappenberg et al. 2019). In contrast, in SARS-CoV-2 infection in humans, ADAM17 activation has been associated with increased shedding of the SARS-CoV-2 entry receptor – the angiotensin converting enzyme 2 (ACE2), preventing viral entry and diminishing infection in human organoids (Monteil et al. 2020; Calligaris et al. 2021).

Despite some evidence suggesting a protective role of ADAM17 in infection, high levels of soluble ACE2 (sACE2) and sTNFα, possibly explained by the

activation of ADAM17 in response to SARS-CoV-2, have been associated with increased severity of SARS-CoV-2 disease COVID-19, suggesting a detrimental role for the protease in development of COVID-19 (Jose and Manuel 2020; Saheb Sharif-Askari et al. 2020; Calligaris et al. 2021). Bacterial *Listeria monocytogenes* infection of mice with ADAM17-deficient T cells, developed regular listeria-specific T cell responses regardless of their ADAM17 status, suggesting that ADAM17 is not required for control of listeria infection (Link et al. 2017).

Interestingly, *Lactobacillus gasseri* has been shown to downregulate the expression of ADAM17 in THP1-derived *Helicobacter pylori*-infected macrophages at both the transcriptional and protein levels (Gebremariam et al. 2019). *H. pylori* is a human-adapted bacterial pathogen that colonises the stomach and promotes gastric disorders. Supplemented with probiotics, strains of *Lactobacillus*, have been shown to improve the outcome of *H. pylori*-associated disease. ADAM17 downregulation by *L. gasseri* has been demonstrated to block the production of the pro-inflammatory cytokines TNFα and IL-6, promoting an anti-inflammatory environment and interfering with *H. pylori* virulence mechanisms (Gebremariam et al. 2019). Hence, there is some evidence in the literature of microorganisms manipulating ADAM17 expression to impact downstream ADAM17-dependent signalling.

1.4.2.5   ADAM17 and HCMV Infection

In contrast to *L. gasseri,* HCMV infection was originally shown to have no effect on ADAM17 levels when HCMV strain AD169 was used (Esteso et al. 2014). However, recently a previous PhD student in the lab Dr Mihil Patel demonstrated that infection of human fibroblasts with a 'wildtype' HCMV strain Merlin results in significant downregulation of surface ADAM17 levels (**Figure 1.9**). Dr Mihil Patel was studying the levels of TNFR2 following HCMV infection and discovered that strains such as Merlin and Toledo, result in surface TNFR2 upregulation, in contrast to high-passaged strains, such as AD169 and Towne. He later attributed these differences to the lack of the U$_L$/*b'* region in the high passage strains and performed an U$_L$/*b'* single gene deletion screen, identifying two viral HCMV proteins involved in surface TNFR2 upregulation –

UL148 and UL148D. To study the mechanism of UL148- and UL148D-driven TNFR2 regulation, Dr Mihil Patel performed mass spectrometry (MS) proteomics experiment using ΔUL148 and ΔUL148D HCMV mutants, identifying ADAM17 as a potential mechanistic explanation for increased surface TNFR2 levels in HCMV infection, since TNFR2 is a known ADAM17 target. Consequently, Dr Mihil Patel confirmed that UL148 and UL148D synergistically targeted ADAM17 early in HCMV infection, by potentially interfering with protease maturation, resulting in increased surface TNFR2 and reduced soluble TNFR2 levels . This is a novel and important finding, since it is the first example of microbial gene products targeting a member of the ADAM family of metalloproteases.
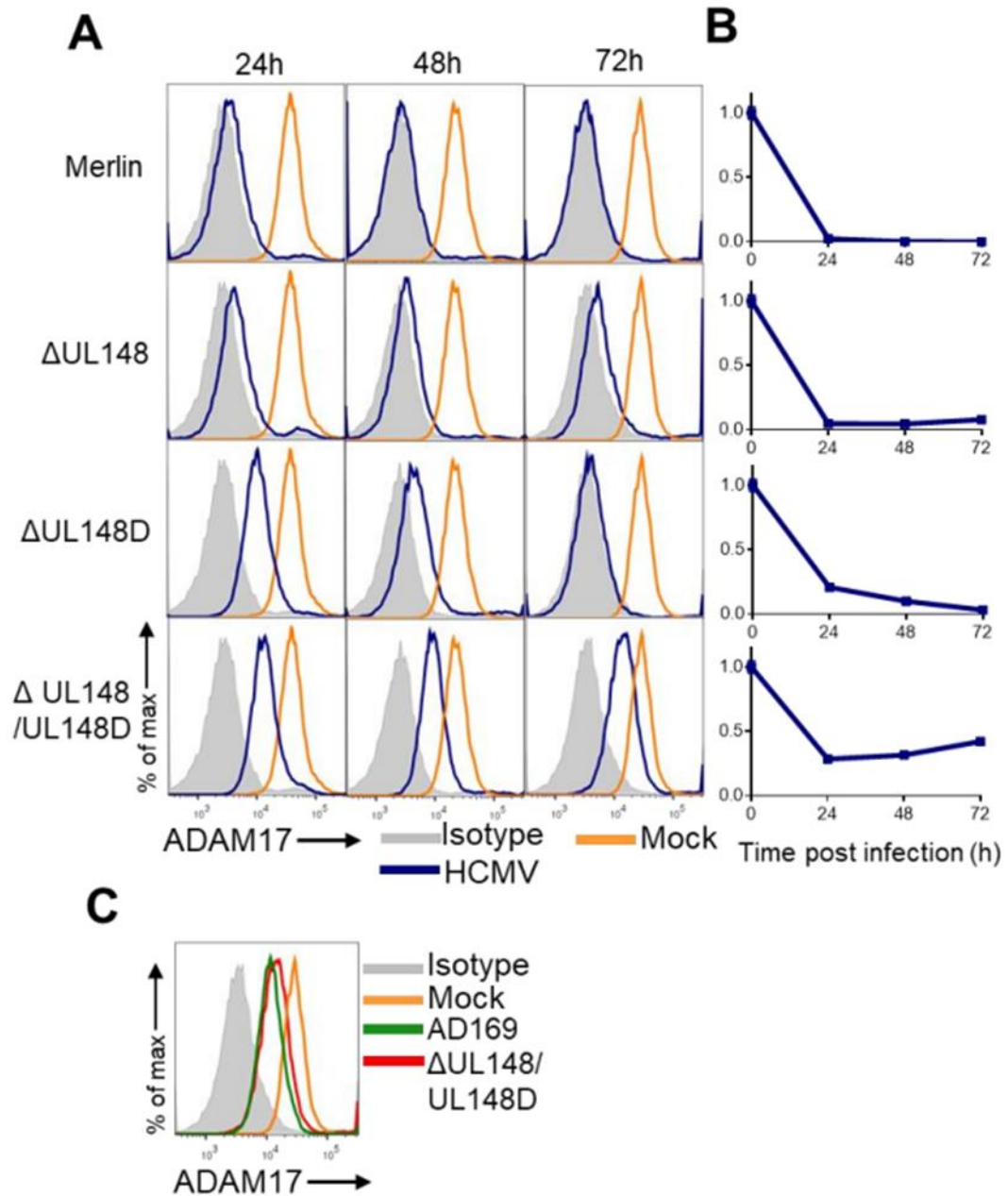
Figure 1.9: Timecourse of ADAM17 expression during HCMV infection taken from Patel (2018) PhD thesis. "HF-TERT cells were infected with HCMV variants or mock infected. At 24h intervals cells were stained for ADAM17. **(A)** Representative flow cytometry histograms comparing HCMV to mock infected cells. **(B)** Relative fluorescence of ADAM17 for HCMV mutants. Each point shows mean relative ADAM17 ±SEM of triplicate infections. ADAM17 MFI of mock infected cells was set at 1.0 with other values plotted as a relative value **(C)** Comparison between AD169 and ΔUL148/UL148D infected cells at 72hpi." (Patel 2018).

1.5 Aims and Objectives

The overarching hypothesis of this PhD thesis is that ADAM17 impairment by HCMV UL148 and UL148D represents an immunomodulatory strategy developed by the virus to manipulate the levels of multiple surface and soluble proteins, thereby interfering with their downstream signalling in a way that benefits HCMV.

This thesis aims to:

1. Characterise the global changes in the levels of surface and soluble proteins in HCMV-infected cells as a result of ADAM17 impairment by UL148 and UL148D.
2. Identify the mechanism of UL148- and UL148D-driven ADAM17 downregulation.
3. Investigate the functional consequences of ADAM17 impairment on multiple host immune processes, to determine their benefit to the virus.

2   Materials and Methods

2.1   Reagents

2.1.1   Tissue Culture Media

Table 2.1: Media and reagents used for tissue culture.

Media/reagent	*Components*
2% Avicel	20g of Avicel (RC-591 NF) mixed in 1 L ddH$_2$O, autoclaved
DMEM	Dulbecco's Modified Eagles Medium (DMEM) (4.5 ml/L glucose) (Sigma, D5796; Gibco, 11574486)
DMEM-10	DMEM with 10% (v/v) foetal bovine serum (FBS) (Sigma, F9665)
DMEM X2	50% (v/v) sterile ddH$_2$O, 20% (v/v) 10x Minimal essential media (MEM) (Gibco, 21430), 20% (v/v) FBS, 6% (v/v) sodium bicarbonate (Gibco, 25080), 4% (v/v) penicillin/streptomycin (Gibco, 15070063), 2% (v/v) L-glutamine (Gibco, 25030024)
Freezing media	90% (v/v) FBS mixed with 10% (v/v) dimethyl sulfoxide (DMSO) (Sigma, D2650)
Heavy-SILAC-DMEM-0	SILAC DMEM Flex Media (ThermoFisher, A2493901) with L-Lysine:2HCl and L-Arginine:HCl (0.25 units each/500 ml of media)

	(CK GAS PRODUCTS LTD), 250 µg/ml L-Proline (Sigma, P5607), 1% (v/v) L-glutamine, 1% (v/v) D-glucose (ThermoFisher, A2494001)
Heavy-SILAC-DMEM-10	SILAC DMEM Flex Media with 10% dialysed FBS (ThermoFisher, 26400044), L-Lysine:2HCl and L-Arginine:HCl (0.25 units each/500 mL of media), 250 µg/ml L-Proline, 1% (v/v) L-glutamine, 1% (v/v) D-glucose
McCoy's 5A media	McCoy's 5A media (Gibco, 16600082) with 10% (v/v) FBS and 1% (v/v) L-glutamine
NK cell media	RPMI-10 with 5% (v/v) human AB serum (Welsh Blood Service), 100 U/ml rhIL-2 (Proleukin, Chiron), and 10 ng/ml IL-15 (PeproTech, 200-15)
RPMI	Roswell Park Memorial Institute 1640 Medium (RPMI) (Sigma, R0883) with 1% (v/v) L-glutamine
RPMI-10	RPMI with 10% (v/v) FBS
2x Treg media	RPMI-10 with 1% (v/v) human AB serum (Welsh Blood Service), 10 ng/ml TGFβ (BioRad, PHP143B) and 200 U/ml rhIL-2
TrypLE	1x Express TrypLE Express (Gibco, 12605-010)
Trypsin	1X Trypsin-EDTA solution (Sigma, T3924)

2.1.2   Buffers and Solutions

Table 2.2: Buffers and solutions used in this thesis.

Buffer/solution	*Components*
0.7% Agarose Gel	1x Tris-acetate-EDTA (TAE) buffer (National Diagnostics, B9-0030), 0.7% (w/v) agarose (Geneflow, A4-0700), 1:2000 Midori Green (Nippon Genetics, MG04)
Ampicillin	100 mg/ml ampicillin sodium (Duchefa Biochemie, A0104.0025) in dH_2O
Chloramphenicol	12.5 mg/ml chloramphenicol (Boehringer, 634433) in 100% ethanol
ConA elution buffer	25% (v/v) 4x NuPAGE LDS buffer (Invitrogen, NP0008), 5% (v/v) 1 M dithiothreitol (DTT) (Invitrogen, Y00147), 30% (v/v) sucrose (50% solution in ddH_2O) (Fisher Scientific, S/8600153), 40% (v/v) ddH_2O
ConA lysis buffer	1% (v/v) NP-40 (Calbiochem, 492016), 10 mM 1,10-phenanthroline (Sigma Aldrich, 131377), 50 mM Tris-HCL (Fisher Scientific, BP153-1), 300 mM NaCl (Fisher Scientific, S/3160/65), 5 mM EDTA (Sigma Aldrich, ED2SC), 1 mM MgCl2 (Acros, 413415000), 1 mM CaCl2 (Sigma Aldrich, C1016), 1% (v/v) proteinase inhibitor cocktail (Sigma Aldrich, P8340) in ddH_2O

DABCO	2.5 g 1,4-diazabicyclo[2.2.2]octane (DABCO) (Sigma Aldrich, D2,780-2), 90 ml glycerol (Fisher Chemical, G/0650/17), 10 ml PBS
EndoH/PNGaseF ConA elution buffer	25% (v/v) 4x NuPAGE LDS buffer, 5% (v/v) DTT, 30% (v/v) sucrose (50% solution in ddH$_2$O), 30% (v/v) ddH$_2$O, 10% 10x Glycoprotein Denaturing buffer (New England BioLabs, B0701S)
FACS buffer	PBS with 1% (v/v) FBS
Fixing solution	10% (v/v) formaldehyde (Sigma Aldrich, 252549) and 90% (v/v) PBS
10% Glycerol	10% (v/v) glycerol in ddH$_2$O
Kanamycin	15 mg/ml kanamycin (Melford Biolaboratories, K22000-10.0) in ddH$_2$O
L-Arabinose	L-Arabinose powder (Sigma, A3256)
LB agar	1 L LB broth with 7.5 g Agar powder (VWR, 20767.232)
LB broth	1 L ddH$_2$O with 20 g LB broth low salt (Duchefa Biochemie, L1703.0500)
0.5% NP-40	250 µl NP-40 in 50 ml PBS
NuPAGE lysis buffer	25% (v/v) 4x NuPAGE LDS buffer with 10% DTT and 65% ddH$_2$O
PBS	Dulbecco's Phosphate-Buffered Saline (PBS) (Sigma, D8537)

PBST   PBS with 0.1% Tween20 (Merck, 822184)

Pierce IP lysis   Pierce IP lysis buffer (ThermoFisher, 87788) with 1% (v/v) proteinase inhibitor cocktail, 2 mM Sodium Fluoride (NaF) (Sigma Aldrich, 56521), 2 mM Sodium Orthovanadate (Na_3VO_4) (Sigma Aldrich, S-6508)

1x TAE buffer   50x TAE buffer diluted in ddH_2O

Western blot (WB) Blocking buffer   PBST with 5% (w/v) dried milk powder (Millipore, 70166)

WB Running buffer   10% (v/v) 10x Tris-Glycine-SDS (TGS) buffer (Fisher Scientific, BP1341-1) and 90% ddH_2O

WB Stripping buffer   Restore stripping buffer (ThermoFisher, 21063)

WB 2x Transfer buffer   80% ddH_2O with 10% (v/v) methanol, 10% (v/v) NuPAGE transfer buffer (Invitrogen, NP0006-1)

2.1.3 Antibodies

Table 2.3: Antibodies used in this thesis.

Target protein and fluorophore	*Company and product code*	*Clone*	*Dilution and use*
α-V5 tag	Abcam, ab9116	Polyclonal	1:2000 (IF) 1:5000 (WB)
α-HA tag	Invitrogen, 26183	2-2.2.14	1:500 (IF) 1:1000 (WB)
α-ADAM17	Abcam, ab39162	Polyclonal	1:2000 (WB)
α-ADAM17	R&D systems, MAB9301	111633	1:50 (FC)
α-ADAM17	Abcam, ab215268	D1(A12)	100nM (F)
α-ADAM17	Abcam, ab57484	1F6	1:500 (IF)
α-actin	Sigma-Aldrich, A2066	Polyclonal	1:2000 (WB)
α-PLCG2	Santa Cruz, sc-5283	B-10	1:1000 (WB)
α-CRKL	Bio-Techne, MAB5127	515405	1:1000 (WB)
α-SerbinB5	Sigma-Aldrich, MABC603	5C6.2	1:1000 (WB)
α-Nexilin	Sigma-Aldrich, SAB4200124	NX-38	1:1000 (WB)
α-RHBDD1	Sigma-Aldrich, HPA013972	Polyclonal	1:1000 (WB)
α-Furin	Abcam, ab3467	Polyclonal	1:1000 (WB)
α-PACS1	Bio-techne, NBP2-24496	Polyclonal	1:1000 (WB)
α-IE1	Merck, MAB810R	8B1.2	1:5000 (WB)

α-gO	Provided by Stipan Jonjić, University of Rijeka Center for Proteomics	Cl.M74.01	1:1000 (WB)
α-Nectin2	Abcam, ab135246	EPR6717	1:1000 (WB)
α-MICA	Bamomab	Bam01	1:2000 (WB)
α-Jagged1	GeneTex, GTX52879	4A24	1:25 (IF)
α-Nectin1-PE	BD, 565766	CK41	1:200 (FC)
α-Nectin1	BioLegend, 340402	R1.302	10µg/ml (F) 1:50 (FC)
α-Nectin1	SantaCruz, sc-21722	CK6	10µg/ml (F) 1:50 (FC)
α-Vasorin	Abnova, H00114990-M05	4G7	1:1000 (WB)
α-CD3-BV711	BioLegend, 344838	SK7	1:200 (FC)
α-CD3-PE	BioLegend, 300308	HIT3a	1:200 (FC)
α-CD14-BV510	BioLegend, 367124	63D3	1:200 (FC)
α-CD19-BV510	BioLegend, 302242	HIB19	1:200 (FC)
α-CD56-BV510	BioLegend, 318340	NCAM	1:200 (FC)
α-CD56-APC	BioLegend, 362504	NCAM	1:200 (FC)
α-CD4-AF700	BioLegend, 300526	RPA-T4	1:200 (FC)
α-CD4-PeCy7	Beckman Coulter, 737660	SFCI12T4D11	1:200 (FC)
α-CD25-APC	BioLegend, 302610	BC96	1:200 (FC)
α-FoxP3-PE	BioLegend, 320008	150D	1:200 (FC)
α-CD107a-FITC	BioLegend, 328606	LAMP-1	1:200 (FC)
α-CD96-PE-Cy7	BioLegend, 338416	NK92.39	1:200 (FC)
α-CD96	BioLegend, 338421	NK92.39	10 µg/ml (F)
α-CD45RA-FITC	BD Pharmingen, 555488	HI100	1:200 (FC)
α-PROCR-APC	BioLegend, 351906	RCR-401	1:200 (FC)

α-mouse IgG-AF647	Invitrogen, A-21235	Polyclonal	1:500 (IF, FC)
α-rabbit IgG-AF488	Invitrogen, A-11070	Polyclonal	1:500 (IF, FC)
α-mouse-IgG-HRP	BioRad, 1721011	Polyclonal	1:5000 (WB)
α-rabbit-IgG-HRP	BioRad, 170- 6515	Polyclonal	1:5000 (WB)

Key: WB – Western Blot, IF – Immunofluorescence, FC – Flow Cytometry, F – Functional studies.

2.2   Tissue Culture

2.2.1   Cell Lines

Immortalised human foetal foreskin fibroblast (HFFF) lines (HF-TERTs and HF-CARs) were generated by Brian McSharry. HF-TERTs were immortalised using a human telomerase reverse transcriptase (hTERT) (McSharry et al. 2001), whereas HF-CARs were generated by transducing HF-TERTs with a retrovirus expressing the Coxsackie adenovirus receptor (McSharry et al. 2008). HF-TERTs expressing V5-tagged UL148 or UL148D, as well as control cell line GAW containing a small non-coding sequence instead of viral gene, were generated by Luis Nobre by lentivirus transduction (Nobre et al. 2019). Cell lines from donor derived skin fibroblasts (SFi) for autologous T cell assays were established by Prof Eddie Wang and immortalised by Sian Llewellyn-Lacey or Dawn Roberts as previously described (McSharry et al. 2001). β2mKO-TERTs were generated by Dr Pragati Amratia using the CRISPR-Cas9 method (Amratia 2022). NK cell lines were generated and provided on request by Dr Simon Kollnberger. Other cell lines used were primary HFFFs, 293T, HT-29 and K562 cells, acquired from either MRC cell bank or ATCC.

2.2.2   Cell Maintenance

Unless stated otherwise adherent cells were grown in DMEM-10 in a 37°C incubator with 5% CO_2, apart from HT-29 cells which were cultured in McCoy's 5A media. Cells were passaged on average once or twice a week, once they had reached >90% confluency. Cell monolayers were washed in PBS, followed by a 5 min incubation at 37°C with trypsin to facilitate cell detachment. Trypsin was neutralised with DMEM-10 and cells were either used for experiments or split appropriately to continue passage. Suspension cells were cultured in RPMI-10 in a 37°C incubator with 5% CO_2 and split once or twice a week by removing part of the cell suspension and replacing it with fresh RPMI-10, unless stated otherwise. Established NK cell lines were maintained and fed with NK cell media twice a week by Dr Simon Kollnberger. All tissue culture reagents were warmed in a 37°C water bath prior to use.

2.2.3   Cell Counting

Cells were mixed thoroughly and 10 µl of cell suspension was loaded into a chamber of a Neubauer haemocytometer. The number of cells per 1 ml of cell suspension was determined by calculating the number of cells within a 4x4 grid and multiplying by 10^4. Cells were then resuspended at desired cell density and plated for experiments.

2.2.4   Cryopreservation of Cells

To freeze cell stocks, cells were centrifuged at 327x *g* (for detached adherent cells) or 209x *g* (for suspension cells) for 5 min and resuspended in freezing media. Cells were aliquoted into cryovials at 1 ml of cell suspension per cryovial and frozen at -80˚C using "Mr Freezy" pots (NALGENE, 5100-0001). The following day cryovials were put into liquid nitrogen for long-term storage. To recover cells from liquid nitrogen, cells were thawed in a 37˚C water bath and added dropwise to 15 ml of media (DMEM-10 for adherent cells and RPMI-10 for suspension cells). Cells were centrifuged as described previously, resuspended in fresh media, counted, and plated accordingly.

2.3   Generation of Vasorin- and Jagged1-expressing lines

2.3.1   Preparation of lentivirus vector

To generate Vasorin- and Jagged1-expressing cell lines, Vasorin and Jagged1 cDNA were cloned with lentivirus vector, which was later packaged into lentivirus particles used to transduce cells. The lentivirus vector used in the lab (pAL2636; a gift from Prof Michael Weekes) already had an existing insert, which needed to be removed and replaced with Vasorin and Jagged1 cDNA. To remove the existing insert, pAL2636 was digested using SalI (New England BioLabs, R0138L) and NotI (New England BioLabs, R0189L) for 3 hrs at 37°C before running on an agarose gel and visualising DNA bands (**Section 2.8.2**). Restriction digest reaction consisted of 5 µl of pAL2636 DNA, 2 µl of each restriction enzyme, 5 µl of NEB 3.1 buffer (New England BioLabs, B7203) and

36 µl of dH$_2$O. Restriction digest generated 2 bands of ~7 and ~1 kb, corresponding to the lentivirus vector and insert, respectively. The ~7 kb band was cut out and DNA was purified using a FastGene Gel/PCR Extraction Kit (Nippon Genetics, FG-91302) from gel slices. Stellar competent *E. coli* (Takara, 636763) were transfected with purified DNA, followed by DNA minipreparation (**Section 2.8.4**).

2.3.2 Generation of Vasorin and Jagged1 lentivirus plasmids

Sequence-verified Vasorin and Jagged1 cDNA were purchased from Horizon Discovery (MHS6278-202806299 & MHS6278-202806346) provided as *E. coli* cultures in LB broth with 8% glycerol. Minipreparation of Vasorin and Jagged1 cDNA from *E. coli* cultures was performed as described in **Section 2.8.4** and purified DNA was prepared to be inserted into lentivirus vector by Phusion PCR (**Section 2.8.1**) using primers with arms of homology to the lentivirus vector (**Table 2.4**). PCR products were then digested with 1 µl of DnpI (New England BioLabs, R0176S) for 30 min at 37°C to remove methylated DNA (i.e., the PCR template), stained with DNA loading dye and run on an electrophoresis gel (**Section 2.8.2**). FastGene Gel/PCR Extraction Kit was used to purify PCR products from gel slices. DNA was then cloned by Gibson assembly with previously prepared lentivirus vector plasmid using NEBuilder HiFi DNA Assembly Cloning Kit (New England BioLabs, E5520S) before transforming NEB 5-alpha Competent *E. coli* (New England BioLabs, C2987I). Transformed bacteria were cultured on LB agar plates with 100 µg/ml of ampicillin for 24-48 hrs at 37°C and four colonies from each cloning experiment were chosen for DNA minipreparation and restriction digest using SalI and NotI to confirm successful recombination, as described previously (**Section 2.3.1**). If the banding pattern of the restriction digest appeared normal, recombineered Vasorin or Jagged1 lentivirus vector DNA was sent for sequencing (**Section 2.8.5**) using sequencing primers. Since Vasorin and Jagged1 inserts were large, multiple regions of the inserts were sequenced in addition to the outside of the region of the insert (**Table 2.5**).

Table 2.4: Cloning primers used to prepare Vasorin and Jagged1 cDNA for insertion into lentivirus vector. Primers were designed using CLC Main Workbench 8.1 application and purchased from Eurofins.

Target	Primer*
Vasorin	Forward AAGTTTGTACAAAAAAGCAGGCTGCGGCCGCGCCACCATGTGCTCCAGGGTCC
	Reverse CCACTTTGTACAAGAAAGCTGGGTGTCGACTTAGATGTAGGGCTTTGCG
Jagged1	Forward AAGTTTGTACAAAAAAGCAGGCTGCGGCCGCGCCACCATGCGTTCCCCACG
	Reverse CCACTTTGTACAAGAAAGCTGGGTGTCGACCTATACGATGTACTCCATTCGGTTTAAGCTCTGGG

* Blue colour indicates arms of homology to the vector

Table 2.5: Sequencing primers used to confirm Vasorin and Jagged1 recombineering with lentivirus vector. Primers were designed using CLC Main Workbench 8.1 application and purchased from Eurofins.

Target	*Primers**
Vasorin	Forward
	1) GCTCACAACCCCTCACT
	2) AAGCTGCAGGACAACG
	3) GCTTGACTACGCCGACT
	4) CGCCACTTACTCCGTCT
	Reverse
	1) ACTTGTCATCGTCGTCCT
Jagged1	Forward
	1) GCTCACAACCCCTCACT
	2) AAGGCTTCTCACTCGGG
	3) ACCCAACTGTGAAATTGCT
	4) TCCAGTGTCTGTGTCCC
	5) AAATGGGTGGAAAGGAAAGAC
	6) TGCTCAAAGGTCTGGTGT
	7) TGTGGCTTGGATCTGTTGCT
	Reverse
	1) ACTTGTCATCGTCGTCCT

2.3.3   Lentivirus Production

293T cells were seeded in DMEM-10 at 1.1×10^6 cells/well in a 6 well plate one day before the transfection. The next day transfection mix was prepared using 1.337 µg of each packaging plasmid (pMDL, pRSV-REV, pTAT, pVSVG; a gift from Prof Michael Weekes), as well as 1.337 µg of previously prepared Vasorin or Jagged1 lentivirus plasmids (**Section 2.3.2**). Transfection reagent GeneJuice (15 µl, Merck Millipore, 70967) was mixed with 510 µl of RPMI (Sigma, R0883) and incubated for 5 min at room temperature (RT) before adding dropwise to the plasmid mix. Transfection complexes were allowed to form for 30 min at RT before 150 µl of transfection mix was added per well of previously seeded 293T, containing 6 ml of fresh DMEM-10. Cells were incubated at 37°C with 5% CO_2 for 72 hrs. After 72 hrs, supernatants were harvested and centrifuged at 1308x g for 15 min to remove cells and debris. Supernatants were then filtered using 0.45 µm low adsorption filters and stored at -80°C in 2 ml aliquots.

2.3.4   Transduction and selection of cell lines

HF-TERTs or β2mKO-TERTs were seeded at 1×10^6 in a 25 cm^2 flask in DMEM-10. The following day 2 ml of filtered lentivirus aliquot was thawed in a 37°C water bath and added to the cells together with 4 ml of DMEM10. After 48 hrs antibiotic selection began and 1 µg/ml puromycin (Santa Cruz, sc-108071B) was added to cells twice a week until the control cells that lacked antibiotic resistance marker completely died. Puromycin was applied to lentivirus transduced cells for an additional week to ensure complete selection, after which cells were expanded and cultured in DMEM-10. Vasorin and Jagged1 expression was validated by Western Blot (WB) and flow cytometry, respectively (**Sections 2.6.1 & 2.7.6**).

2.3.5   Cell Sorting

To generate β2mKO-Vasn-Jag1-TERT line, β2mKO-Vasn-TERTs were first generated by Vasorin lentivirus transduction as described previously, followed by a Jagged1 lentivirus transduction. Since both Vasorin and Jagged1

constructs had puromycin resistance markers, Jagged1+ cells were required to be cell sorted 48 hrs following Jagged1 lentivirus transduction of β2mKO-Vasn-TERTs. Cells were stained using α-Jagged1 antibody as described in **Section 2.6.1**. Jagged1+ cells were sorted by Kelly Miners using a BD FACSAria. Following cell sorting, cells were cultured in DMEM-10 at 37°C with 5% CO_2 incubator.

2.4   Virology

2.4.1   Generation of HCMV stocks

To grow out HCMV stocks, HF-TERTs were either transfected with a HCMV BAC or infected using a low multiplicity of infection (MOI) with a previously generated viral stock.

2.4.1.1   Transfection with HCMV BACs

HF-TERTs (1×10^6) were detached using Trypsin as described previously and transfected with 2 µg HCMV BAC DNA using the Amaxa Basic Nucleofector Kit for Primary Mammalian Fibroblasts (Lonza, VPI-1002) according to manufacturer's instructions. Transfected cells were seeded into a 25 cm^2 flask in DMEM-10 and cultured until the flasks demonstrated ~90% cytopathic effect (CPE), with media changed twice a week. At ~90% CPE supernatant containing HCMV virions was harvested and stored at -80°C. Supernatants were harvested every two days until the monolayer had died.

2.4.1.2   Growing HCMV stocks

Five confluent HF-TERTs 150 cm^2 flasks were infected with either existing titrated viral stock at a low MOI of 0.03, or with the harvest from HCMV BAC transfected cells described in **Section 2.4.1.1**. Infected HF-TERTs were cultured in DMEM-10 which was changed twice a week until the cells reached ~90% CPE. Supernatants were then harvested every two days and stored at -80°C until the cell monolayer had died. To concentrate the virus, frozen supernatants were thawed in a 37°C water bath and centrifuged at 581x *g* for 5 min to pellet any cells and debris. Supernatants were then pooled into virus

pots and centrifuged at 29416x *g* for 2 hrs at 22°C. A dense formed pellet was resuspended in 5 ml of DMEM-10 and pushed through a 19G needle six times to get rid of any clumps. Final viral stocks were frozen at -80°C in 300 µl aliquots and thawed in a 37°C water bath when needed. HCMV stocks used in this project are listed in **Table 2.6**.

Table 2.6: HCMV variants used in this project.

pAL number	*HCMV backbone*	*Modification*	*Creator*
1111	Merlin	Mutations in RL13 and UL128 locus (present in all Merlin derived viruses used in this project)	(Stanton et al. 2010)
1845	Merlin	ΔUL148D	Eva Ruckova
2035	Merlin	ΔUL148	Ceri Fielding
2393	Merlin	ΔUL148/ΔUL148D	Mihil Patel
2445	Merlin	V5 tag at C-terminus of UL148	Mihil Patel
2929	Merlin	V5 tag at C-terminus of UL148 and HA tag at C-terminus of UL148D	Anzelika Trinca

2.4.1.3   Titration of HCMV by plaque assay

Primary HFFFs were seeded onto a 6-well plate at 2.5×10^5 cells/well in DMEM-10. The next day cells were infected with three dilutions of previously concentrated and aliquoted HCMV stock: 10^{-4}, 10^{-5} and 10^{-6}, with all dilutions prepared in DMEM-10. Inoculum (100 µl/well) was added in duplicate and rocked for 2 hrs at 37°C, after which the inoculum was replaced with a 50:50 mixture of 2% Avicel and DMEM X2 media. Cells were left in a 37°C, 5% CO_2 incubator and not disturbed for 14 days allowing plaques to form. To count the plaques, wells were washed twice with PBS and plaques were manually counted in duplicate under a light microscope. Titre (plaque forming units (PFU)) was calculated as number of plaques (in 100 µl) x 10 x dilution factor.

2.4.1.4　HCMV Infections

For HCMV infection, HF-TERTs were seeded in DMEM at desired cell density the night before the infection to increase the effectiveness of the viral entry into fibroblasts. The following day HCMV was added to the cells at MOI of 5 or 10, following a 2 hr incubation at 37°C with 5% CO_2 on a rocker before replacing the inoculum with fresh DMEM. The following day, at 24 hpi, DMEM was substituted to DMEM-10.

2.4.2　Adenovirus Infections

Replication-deficient recombinant adenovirus (RAds) infections in HF-CARs followed the same principle as HCMV infections, however DMEM-10 was used throughout the process. MOI of 10 was used when HF-CARs were infected with individual UL148-RAd and UL148D-RAd, however when UL148-RAd and UL148D-RAd were used in combination, MOI of 5 was used for each RAd achieving a total MOI of 10. RAds used in this thesis were recombineered by Dr Sepehr Seirafian, Dr James Davies and Prof Richard Stanton.

2.5　Immunofluorescence

2.5.1　Seeding cells for Microscopy

Adherent cell lines were seeded into a glass-bottom 96-well plate (Ibidi, 89626) at 4×10^3 cells/well the day before staining. For HCMV infections, 1×10^4 cells/well were seeded and infected the following day as described in **Section 2.4.1.4**. For RAd infections (**Section 2.4.2**), as well as Mock-infected cells, cells were seeded at 3×10^3 cells/well. Staining was performed at indicated timepoints *post* infection.

2.5.2　Immunofluorescence assay

Cells were washed once in PBS, fixed using fixing solution for 15 min at RT and permeabilised with 0.5% NP-40 solution for 15 min at RT. Infected cells were incubated with IgG from an HCMV-seronegative donor (1:250 of lab stock) for 30 min at RT to block Fc receptors to avoid nonspecific staining.

Staining was performed in PBS at 37°C for 30 min, with PBS washes in between primary and secondary antibody staining. Hoescht stain (Sigma Aldrich, D9564) was added into the secondary antibody master mix at 10 ng/ml to stain the nuclei. Cells were finally washed twice in PBS before the addition of DABCO as a mounting medium. The plates were stored in the dark at 4°C before being imaged on a Zeiss microscope (Axio Observer Z1) with the Apotome function engaged to provide a clearer image of one focal plane without scattered light. A magnification of x63 was used.

2.6   Flow Cytometry

2.6.1   Surface staining for Flow Cytometry

Adherent cell lines were washed with PBS and detached using TrypLE for 5 min at 37°C. TrypLE was neutralised with DMEM-10 and detached cells were washed twice with PBS by centrifugation at 327x g for 5 min. Suspension cells, such as PBMCs, T- and NK-cells, were washed twice with PBS by centrifugation at 209x g for 5 min. Cells were resuspended in 50 µl of surface antibody master mix diluted in PBS and incubated for 30 min at 4°C in the dark. If viability stain was included, LIVE/DEAD™ Fixable Aqua (Invitrogen, L34965) was added to the master mix at 1:1000. Cells were then washed twice in PBS as previously described and in the case of unconjugated antibodies, secondary antibody master mix was applied and cells were incubated for 30 min at 4°C in the dark. Stained cells were washed twice in PBS and fixed using fixing solution for 15 min at 4˚C. If cells were analysed immediately, they remained in the fixing solution, however if the flow cytometry analysis was postponed until the next day cells were washed once with PBS, resuspended in 200 µl of FACS buffer and left at 4°C in the dark.

2.6.2   Intracellular staining for Flow Cytometry

For Forkhead box protein P3 (FoxP3) intracellular staining FOXP3 Fix/Perm Buffer Set was used (BioLegend, 421403) according to manufacturer's instructions. Briefly, cells were surfaced stained as described in **Section 2.6.1**, however the fixing step was performed using 1X BioLegend's FOXP3

Fix/Perm solution for 20 min at RT in the dark, followed by two washes in FACS buffer (5 min, 209x g). Cells were next washes once in 1X BioLegend's FOXP3 Perm buffer and incubated in the same buffer for 15 min at RT in the dark, followed by the addition of α-FoxP3-PE antibody and further 30 min incubation under the same conditions. Cells were finally washed twice in FACS buffer and resuspended in 200 μl of FACS buffer ready for flow cytometric analysis.

2.7 Immunoblotting of cell proteins

2.7.1 Preparation of lysates

Cells were seeded in 25 cm^2 flasks at 1x10^6 cells/flask, infected with HCMV- or Mock-infected and harvested at indicated timepoints. Cell monolayer was washed twice with ice cold PBS and 250 μl of NuPAGE lysis buffer was added to the flask. Cells were scraped into the lysis buffer and heated in a heat block for 10 min at 90°C. To study soluble proteins, cells were seeded in DMEM and after indicated time in culture, media was collected and centrifuged at 327x g for 5 min. Supernatant was collected and centrifuged using Vivaspin 20 sample concentrators (Sartorius, VS2091) following manufacturer's instructions. To reduce the sample, 25% (v/v) 4x NuPAGE LDS buffer and 10% (v/v) DTT were added, following by a 10 min incubation at 90°C in a heat block. Lysates were either used immediately or stored at -20°C until resolution by SDS-PAGE.

2.7.2 Immunoprecipitation

For immunoprecipitation (IP), cells were seeded in 25 cm^2 flasks at 1x10^6 cells/flask, infected with HCMV- or Mock-infected and harvested at indicated timepoints. Cell monolayers were washed twice with ice cold PBS and 500 μl of Pierce IP lysis buffer was added to the flask. Cells were scraped into a 1.5 ml collection tube and rotated on a 360° rotor for 20 min at 4°C. Supernatants were collected by centrifugation at 16,000x g for 10 min at 4°C. Each lysate (30 μl) was mixed with 25% (v/v) 4x NuPAGE LDS buffer and 10% (v/v) DTT and heated in a heat block for 10 min at 90°C to make input samples. The rest of the clarified lysates were mixed with 20 μl of either V5 or HA agarose slurry

(Abcam, ab214758 & ab1229) and incubated for 2 hrs at 4°C on a 360° rotor. The beads were washed with 500 µl of Pierce IP lysis buffer three times by centrifugation at 470x *g* for 1 min and replacement of the supernatant with the lysis buffer. After the final wash, proteins were eluted by adding 70 µl of NuPAGE lysis buffer to the beads, followed by a 10 min incubation at 90°C in a heat block. Beads were centrifuged at 16,000x *g* for 1 min and supernatant were collected and either used immediately or frozen down at -20°C for later use.

2.7.3   Enrichment of glycoproteins by Concanavalin A

Concanavalin A (ConA) enrichment of glycoproteins was specifically used to study ADAM17 levels in cells in a WB setting. HF-TERTs (1x106) were HCMV- or Mock-infected in a 25 cm2 flask and harvested at indicated timepoints *post* infection. Cells monolayers were washed twice with ice-cold PBS and lysed in 1 ml of ConA lysis buffer for 10 min on a rocker at 4°C. Cells were scraped into a 1.5 ml tube and centrifuged at 16,000x g for 10 min. Supernatants were collected and incubated with 50 µl of ConA beads (Sigma Aldrich, C9017) for 3 hrs at 4°C on a 360° rotor to capture glycoproteins. Beads were washed three times with ConA lysis buffer by centrifuging the lysates at 470x g for 3 min, removing the supernatant and resuspending the beads in 1 ml of ConA lysis buffer. To elute the glycoproteins bound to the beads, 70 µl of ConA elution buffer was added to beads, followed by a 15 min incubation at 65˚C on a heat block. Eluted samples were centrifuged at 16,000x g for 3 min and the supernatants were collected and either used immediately or frozen at -20˚C until resolution by SDS-PAGE.

2.7.4   EndoH and PNGaseF digest

For ADAM17 Endoglycosidase H (EndoH) and Peptide:N-glycosidase F (PNGaseF) digestion experiment, ConA enrichment was performed as described previously, however the elution step was performed using EndoH/PNGaseF ConA elution buffer instead of ConA elution buffer. Eluted samples were then split into 3 parts (20 µl each) and treated with either 2 µl

EndoH (New England BioLabs, P07025), 2 µl PNGaseF (New England BioLabs, P07045) or 2 µl of dH$_2$O. Digestion reactions were completed with reagents from Endoglycosidase Reaction Buffer Pack (New England Labs, B0701S). EndoH reaction was completed with 4 µl of 10x Glycobuffer 3 and 14 µl of dH$_2$O, whereas PNGaseF reaction was completed with 4 µl of 10x Glycobuffer 2, 4 µl of 10% NP-40 and 10 µl of dH$_2$O. Untreated reaction was topped up with 20 µl of dH$_2$O. Samples were digested for 16 hrs at 37°C using a PCR machine before incubating digested samples at 75°C heating block for 10 min to inactivate the enzymes. Sample were either used immediately or frozen at -20°C until resolution by SDS-PAGE.

2.7.5 Separation of polypeptides by electrophoresis

A BioRad Criterion SDS-PAGE system was used to perform gel electrophoresis on cell lysates. A 10% or gradient 4-15% pre-cast BioRad gel (BioRad, 5678034 & 5678084) was placed into Criterion electrophoresis cell with 500 ml of WB running buffer. Pre-stained protein ladder (10 µl, Geneflow, S6-0024) was used to determine protein size. For whole cell lysates (WCL) 30 µl of sample was loaded per well, for IP samples 15 µl was used. The gel was run at 150V for 1 hr.

2.7.6 Western Blotting

Semi-dry transfer method was used to transfer proteins onto a membrane. PVDF membrane (Merck, GE10600023) was soaked in 100% methanol for 5 min, followed by a 15 min soak in WB 2x transfer buffer together with two sheets of blotting paper. Soaked membrane, blotting paper and electrophoresis SDS-PAGE gel were assembled together and run at 20V for 1 hr. Following transfer, membrane was blocked in WB blocking buffer for 1 hr at RT or 16 hr at 4°C. The membrane was then stained with primary antibody diluted in WB blocking buffer for 1 hr at RT or 16 hr at 4°C. Excess antibody was removed by 3x 5 min PBST washes at RT. Secondary antibody was also diluted in WB blocking buffer and used to stain the membrane for 1 hr at RT, followed by 3x 5 min PBST washes. All blocking, staining was washing steps

were carried out on a rocker. To develop the membrane SuperSignal West Pico PLUS Chemiluminescent Substrate (Thermo Scientific, 34578) was added according to manufacturer's instructions for 5 min and visualised with a GeneSys GelDoc (Syngene). If reprobing of the blot was required, the membrane was washed with PBST (3x 5 min washes) and WB stripping buffer was applied according to manufacturer's instructions. The membrane was then washed (5x 5 min washes) and blocked again before antibody staining.

2.8 Molecular Biology

2.8.1 Polymerase Chain Reaction

Generation of Vasorin- and Jagged1-expressing cell lines, as well as UL148D-HA *En passant* relied on PCR reactions for amplification, recombineering and sequencing purposes.

Phusion High-Fidelity (HiFi) DNA Polymerase kit (New England BioLabs, M0530) was used to amplify Vasorin and Jagged1 cDNA for insertion into lentivirus plasmid vector. The PCR reaction consisted of 0.5 µl Phusion DNA polymerase, 10 µl Phusion HF buffer, 1 µM each of the forward and reverse recombineering primers specific to either Vasorin of Jagged1 (**Table 2.4**), 1 µl of either Vasorin or Jagged1 cDNA template, 1 µl dNTP mix (10mM; New England BioLabs, N0447L), 1.5 µl DMSO and 35 µl dH2O. The reactions were amplified using the programme found in **Table 2.7**.

For *En passant* recombineering PCR reactions were set up using Expand HiFi PCR System (Sigma, 11732650001) and consisted of 37.4 µl dH$_2$O, 1.5 µl DMSO, 1 µl dNTP mix, 5 µl Buffer #3 (HiFi Buffer (10x) without MgCl$_2$), 3.1 µl Buffer #4 (MgCl^2 25 mM Stock Solution), 0.25 µl of each of the forward and reverse primers (**Table 2.9**), 1 µl *En Passant* template pAL2638 and 0.5 µl of Buffer #1 (HiFi enzyme mix). The reactions were amplified using the programme found in **Table 2.8**.

Taq DNA Polymerase kit (Invitrogen, 18038-042) was used to check HCMV BACs after each round of *En passant*. The PCR reactions consisted of 0.25 µl Taq polymerase, 5 µl 10X PCR buffer, 1.5 µl MgCl$_2$, 1.5 µl DMSO, 1 µM each

of the forward and reverse primers (**Table 2.10**), 1 μl of template (BAC DNA), 1 μl dNTPs, and 37.75 μl dH$_2$O. The reactions were amplified using the HiFi programme found in **Table 2.8**.

Table 2.7: Phusion PCR programme used to amplify Vasorin and Jagged1 cDNA.

Phusion Programme Stages	Temperature	Time	Cycles
Pre-Heating	99°C	-	-
Initial Denaturation	98°C	30 s	1
Denaturation	98°C	10 s	35
Annealing	55°C	30 s	
Extension	72°C	3 min	
Final Extension	72°C	12 min	1
Hold	4°C	∞	-

Table 2.8: High Fidelity PCR programme used to amplify *En passant* cassette with UL148D-HA primers. The same programme was used for Taq polymerase PCR reactions.

HiFi Programme Stages	Temperature	Time	Cycles
Pre-Heating	99°C	-	-
Initial Denaturation	95°C	2 min	1
Denaturation	95°C	30 s	35
Annealing	55°C	30 s	
Extension	72°C	2 min	
Final Extension	72°C	7 min	1
Hold	4°C	∞	-

2.8.2 Gel Electrophoresis

DNA was separated on a 0.7% agarose-TAE gel at 100V for 45-60 min. To stain DNA Midori Green was added to liquid agarose gel before it solidified. The mixture was poured into a cassette with a comb and allowed to cool. Once solidified, the gel was placed into a tank filled with TAE buffer. HighRanger 1 kb DNA Ladder (Norgen, 11900) was added to the first well for size reference. Samples were mixed with DNA loading dye before loading onto the gel.

2.8.3 *En Passant* mutagenesis

To generate double tagged UL148-V5 and UL148D-HA HCMV, *En Passant* mutagenesis was performed as described previously (Tischer et al. 2010).

2.8.3.1 Transformation of GS1783 bacteria with a BAC

E. coli strain GS1783 lacking a BAC (pAL2315) were grown overnight in LB broth in a 32°C Stuart SI500 shaking incubator at 200 rpm. Overnight culture (500 µl) was inoculated in 25 ml LB broth the following day and grown in a shaking incubator (200 rpm) at 32°C until bacteria reached an optical density (OD600) of 0.6 (~3.5 hrs). Bacteria were then cooled on ice for 15 min and washed twice with 25 ml of cold water by centrifugation at 3347x *g* for 5 min at 4°C. Pelleted bacteria were resuspended in water dregs and 25 µl of bacterial culture was mixed with 1 µl of UL148-V5 tagged BAC (pAL2445) or 1 µl of dH2O as control. Bacteria were then transferred to 2 mm electroporation cuvettes (Geneflow, E6-0060) and electroporated with a BioRad MicroPulser, program EC3. Transformed bacteria were recovered for 1 hr in LB broth in a shaking incubator at 32°C (200 rpm) before spreading on LB agar plates containing 30 µg/ml chloramphenicol and incubating for 24-48 hrs at 32°C until the colonies form.

2.8.3.2 Inserting the *En Passant* Cassette

Up to four GS1783 colonies containing pAL2445 were picked and inoculated as described previously until bacteria reached OD600 of 0.6. The lambda red proteins were then induced by incubating the bacteria in a 42°C water bath for

15 min. Bacteria were then cooled down on ice for 15 min, washed, pelleted and transformed as before (**Section 2.8.3.1**). DNA for transformation was prepared by amplifying the *En Passant* cassette (pAL2638) (**Section 2.8.1**) using primers containing arms of homology to UL148D along with an inserted HA tag (**Table 2.9**). PCR product was digested with DpnI as described previously, run on a 0.7% agarose gel and ~1 kb band was cut out and purified from gel slices as before, and used to transform bacteria prepared earlier. Transformed bacteria were spread on a LB agar plate containing 30 µg/ml chloramphenicol and 30 µg/ml kanamycin and incubated for 24-48 hrs at 32°C until colonies formed.

Table 2.9: En passant primers used to HA-tag UL148D. Primers were designed using CLC Main Workbench 8.1 application and purchased from Eurofins.

Primer	*Sequence*
*Forward**	TTTACGCAGCAGCAGGCACGCAACGGGAGCGGCAGCGG CAGCGCTTACCCCTACGACGTGCCCGACTACGCCTAGAC AATAGGGATAACAGGGTAATGGC
Reverse	CCGGCTACGGCGCTTGGAGCTGTAGCCGCCTGGGACTTG TCTAGGCGTAGTCGGGCACGTCGTAGGGGTAAGCGCTTC AGAAGAACTCGTCAAGAAGGCG

* Green colour indicates sequence of the HA tag.

2.8.3.3 Confirming *En passant* round one results

To confirm that the en passant cassette had inserted correctly, four colonies were selected from previously prepared plates and individually incubated in a 32°C shaker overnight in 5 ml LB broth with 30 µg/ml chloramphenicol. DNA minipreparation was performed, followed by Taq polymerase PCR analysis (**Section 2.8.1**) using sequencing primers that bound just outside the region being modified (**Table 2.10**), before mixing with DNA loading dye and running on 0.7% agarose gel to check banding pattern. An alternative way of checking

that BAC integrity had not been grossly altered by the *en passant* process, HCMV BAC was subjected to restriction digest by combining 8 µl of DNA with 1 µl of NE Buffer #2.1 (New England BioLabs, B7202S) and 1 µl of HindIII (New England BioLabs, R0104L), and incubating for 1 hr at 37°C. Banding pattern was then checked by running digested DNA on a 0.7% agarose gel after the addition of DNA loading dye.

Table 2.10: Sequencing primers for UL148D-HA En passant. Primers were designed using CLC Main Workbench 8.1 application and purchased from Eurofins.

Primer	*Sequence*
Forward	CACCACCACGACCTATCT
Reverse	TCCACACGTTGTACGCC

2.8.3.4   Resolution of *En passant* cassette

Overnight cultures (10 µl) that demonstrated a correct banding pattern by either PCR or HindIII digest were inoculated in 1 ml LB broth containing 30 µg/ml chloramphenicol and incubated for 2 hrs at 32° in a shaking Stuart SI500 incubator at 200 rpm. Following incubation, 1 ml of 2% L-Arabinose solution (prepared in LB broth containing 30 µg/ml chloramphenicol) was then added to bacteria and incubated for another hour before placing the tube with bacteria into a 42°C water bath for 30 min. The culture was then returned to the 32°C shaking incubator (200 rpm) for a further 2 hrs, after which the OD600 of the culture was measured, and the bacteria were diluted accordingly and spread on a LB agar plate containing 30 µg/ml chloramphenicol and 1% L-Arabinose. Plates were incubated for 24-48 hrs at 32°C until colonies formed. Colonies that had grown on the chloramphenicol and L-arabinose plates were checked for kanamycin sensitivity – bacteria that had *En passant* cassette successfully removed were sensitive to kanamycin. This was done by picking a colony and spreading it on LB agar plate containing 30 µg/ml chloramphenicol alone, and another containing both 30 µg/ml of chloramphenicol and 30 µg/ml of

kanamycin. This was performed for at least 10 individual colonies, and kanamycin sensitive colonies were inoculated in 5 ml of LB broth with 30 µg/ml chloramphenicol and incubated overnight at 32°C shaking incubator (200 rpm), followed by DNA minipreparation and sequencing. If sequencing validated the modification, HCMV BAC maxipreparation (**Section 2.8.6**) was performed to generate enough DNA for transfections (**Section 2.4.1.1**).

2.8.4   Minipreparation of DNA

A Universal tube containing 5 ml of LB broth with appropriate antibiotic was used to inoculate bacteria overnight in a shaking (200 rpm) Stuart SI500 incubator at 32°C. Bacteria were inoculated by either a loop scrape from a glycerol stock or a colony picked from a LB agar plate. A 500 µl aliquot of the overnight culture was stored at 4°C to be made into a glycerol stock later on, whilst the rest of the culture was centrifuged at 3347x g for 5 min at 4°C, following DNA extraction using QIAprep Spin Mini Prep kit (Qiagen, 27106). Minipreparations of DNA were stored at 4°C short term or -20°C long term.

2.8.5   Sequencing

Sequencing was performed by Eurofins using the Eurofins Mix2Seq overnight kit and sequencing primers specific to HCMV BAC or Vasorin/Jagged1 plasmids. Sequencing was checked using CLC Main Workbench 8.1, where returned sequences were assembled to the predicted sequence.

2.8.6   Maxipreparation of BAC DNA

Maxipreparation of DNA was performed similarly to minipreparation (**Section 2.8.4**), however it was on a larger scale. Similar to minipreparation, an Universal tube containing 5 ml of LB broth with 30 µg/ml chloramphenicol was used to inoculate bacteria with desired BAC in a shaking (200 rpm) Stuart SI500 incubator at 32°C, however instead of overnight inoculation, bacteria were incubated throughout the day for ~7 hrs. At the end of the day bacteria were added to a 2 L conical flask containing 250 ml of LB broth supplemented with 30 µg/ml chloramphenicol. The culture was incubated overnight at 32°C in a shaking incubator at 200 rpm. Following overnight growth, the culture was

harvested and centrifuged in a 250 ml pot for 15 min at 6,000x *g* at 4°C. NucleoBond Xtra Maxi kit (Machery Nagel, 12748412) was then used for the maxipreparation according to manufacturer's instructions. The BAC DNA was then quantified and checked for quality using the NanoDrop and stored at -20°C ready to be used for transfections (**Section 2.4.1.1**).

2.9 Proteomics

2.9.1 Preparing Heavy-SILAC media

Dialysed FBS was centrifuged at 2325x *g* for 10 min to get rid of residual protein by pelleting and filtered using a 0.45 µm filter – if not removed it can subsequently interfere with protein identification by MS. Filtered dialysed FBS (50 ml) was added into a 500 ml bottle of SILAC DMEM Flex Media to make 10% media. Other media components were mixed together first and filtered used a 0.22 µl sterile filter before being added to the media bottle. This included adding 500 µl of 280 mg/ml L-Proline stock, 500 µl of 50 mg/ml L-Lysine:2HCl and 500 µl of 50 mg/ml L-Arginine:HCl to 5 ml of L-glutamine and 5 ml of D-glucose. Media was stored at 4°C and used as normal tissue culture media.

2.9.2 Generating samples for secretome analysis

For secretome analysis HF-TERTs were grown in Heavy-SILAC-DMEM-10 for 2 weeks prior to HCMV infection. HCMV infection of fibroblasts for secretome analysis was carried out as described in **Section 2.4.1.4** with Merlin, ΔUL148, ΔUL148D, ΔUL148/ΔUL148D (dKO) HCMV and Mock, using Heavy-SILAC-DMEM-0. At 24 and 72 hpi, culture media from infected cells were harvested and centrifuged at 327x *g* for 5 min to get rid of cells and debris. Harvests were required to be serum-free since proteins from FBS can interfere with secretome analysis. To achieve this, cells were incubated in Heavy-SILAC-DMEM-0 immediately after infection and when 24 hpi culture media was harvested, it was replaced with Heavy-SILAC-DMEM-10. At 48 hpi media was replaced again with Heavy-SILAC-DMEM-0 media which was then harvested

at 72 hpi. Secreted proteins from harvested and centrifuged media were concentrated using Amicon Ultra-15 Centrifugal Filter Unit (Merck, UFC900324) for 2 hrs at 4000x *g*, 4°C, resulting in a final concentrated protein sample of 250 µl. Concentrated samples were then snap-frozen in dry ice and methanol and shipped on ice to Prof Michael Weekes at the University of Cambridge for proteomics analysis.

2.9.3   Single Shot and Fractionation of samples

Proteomics work was performed by Martin Potts at the University of Cambridge. Briefly, shipped samples were digested into peptides and labelled with 10-plex tandem mass tag (TMT) reagents. All samples were mixed together and analysed by MS allowing for accurate comparative quantitation of protein levels between mixed samples. Samples were initially run as an unfractionated single shot before fractionation of the samples was performed to increase the detection range (Weekes et al. 2014).

2.10 Functional Assays

2.10.1 Protein Degradation Inhibition assays

To inhibit ER-associated protein degradation (ERAD) two ERAD inhibitors were used Eeyarestatin I (EerI) (Sigma-Aldrich, E1286) and Kifunensine (Kif) (Sigma-Aldrich, K1140). HF-TERTs were infected with HCMV as described in **Section 2.4.1.4**, however prior to infection, cell monolayer was pre-treated with either 5 µM EerI or 2.5 µM Kif for 2 hrs in DMEM-0. HCMV infections were carried out as normal however EerI or Kif were included in the media during infections, followed by an 18 hr incubation in DMEM-10 with 5 µM EerI or 2.5 µM Kif before sample processing. Additional experimental condition was set up using Kif in which Kif was added 72 hpi to cells, followed by a 24 hr incubation and sample processing at 96 hpi.

Inhibition of proteasomal and lysosomal degradation pathways were performed using proteasome inhibitor MG132 at 10 µM (Calbiochem, 474787) and lysosome inhibitor leupeptin at 200 µM (Calbiochem, 108975). HF-TERTs

were infected as normal, with inhibitors added 24 hpi in DMEM-10 for an additional 18 hrs before sample processing.

2.10.2   Treg Expansion assay

2.10.2.1   Preparation of target cells

A number of different HF-TERT and β2mKO-TERTs cell lines were used as targets, such as standard lines and Vasorin- and/or Jagged1-expressing lines. Target cells were infected with HCMV as described previously and harvested 72 hpi by detachment using TrypLE. Cells were washed twice with DMEM-10 by centrifugation at 327x g for 5 min and γ-irradiated at 6000 rad to halt cell division. Cells were washed again, counted and resuspended in RPMI-10 with 1% AB serum at appropriate cell density. When isolated naïve CD4$^+$ T cells were used as effectors, targets were resuspended at 2×10^4 cells per 100 µl, whereas when PBMC were used as effectors, targets were resuspended at 10^5 cells per 300 µl.

2.10.2.2   Preparation of responder cells

PBMC or isolated naïve CD4$^+$ T cells were used as responder cells. Peripheral blood was either donated by healthy volunteers or obtained from apheresis cones (leukoreduction system chambers) from the Welsh Blood Service. Apheresis cones containing ~5 ml of blood were washed with 45 ml of PBS into a tube containing 500 µl of Heparin Sodium (stock 1000 U/ml, Wockhardt). Blood donated by volunteers was collected into a tube containing 250 µl of Heparin Sodium. To obtain PBMCs, 25 ml of blood was carefully layered over 15 ml of Histopaque (Sigma Aldrich, 10771) and centrifuged at 470x g for 20 min with the brake off. Cloudy PBMC layer was removed and washed in RT PBS three times with the following settings for each spin: 1) 470x g, 10 min, brake on; 2) 327x g, 7 min; 3) 246x g, 3 min. PBMC were resuspended in RPMI-10, counted, centrifuged at 209x g for 5 min and resuspended at appropriate cell density. When PBMC were used as responders, 10^6 cells were resuspended in 300 µl of 2x Treg media ready for assay set up.

Naïve CD4$^+$ T cells were isolated by magnetic activated cell sorting (MACS) using the Naïve CD4$^+$ T Cell Isolation Kit II from Miltenyi Biotec (130-094-131) following manufacturer's instructions. The purity of isolated populations were checked by surface flow cytometry staining for CD4 and CD45RA markers. Purified populations were counted, centrifuged at 209x g for 5 min and resuspended in 2x Treg media at 10^5 cells per 100 µl.

2.10.2.3   Co-culture and Flow Cytometry staining

Co-cultures using PBMC were set up in triplicate or quadruplicate in 48-well flat bottom tissue culture plates by mixing 300 µl of targets and 300 µl of earlier prepared responders per well. Co-cultures using purified naïve CD4$^+$ cells were set up in 96-well U bottom tissue culture plates, which were covered with OKT3 CD3 antibody the day before the assay. OKT3 was diluted in PBS at the desired concentration and coated at 200 µl/well overnight at 4°C. OKT3 concentrations used were 1 µg/ml (BioLegend, 317326), 440 pg/ml, 44 pg/ml and 4.4 pg/ml (lab's own hybridoma stock). On the day of the assay, PBS/OKT3 mix was pipetted out if the wells and replaced with 100 µl of targets and 100 µl of earlier prepared responders per well in triplicate or quadruplicate. Outer wells of the plates were filled with PBS, plates were placed in plastic containers and incubated in 37°C incubator for 7 days. On day 3 or 4 (depending on the colour of the media), half of the media was carefully removed from each well without disturbing the cells at the bottom and replaced with equal amount of 2x Treg media. After co-culture cells were harvested, washed and surface stained for LIVE/DEAD Aqua Viability Dye, CD14, CD19, CD56, CD3, CD4 and CD25, as well as intracellularly stained for FoxP3 (**Section 2.6.2**) before being analysed by flow cytometry (**Figure 2.1**). To calculate cell counts per each well Precision Counting Beads (BioLegend, 424902) were used according to manufacturer instructions.
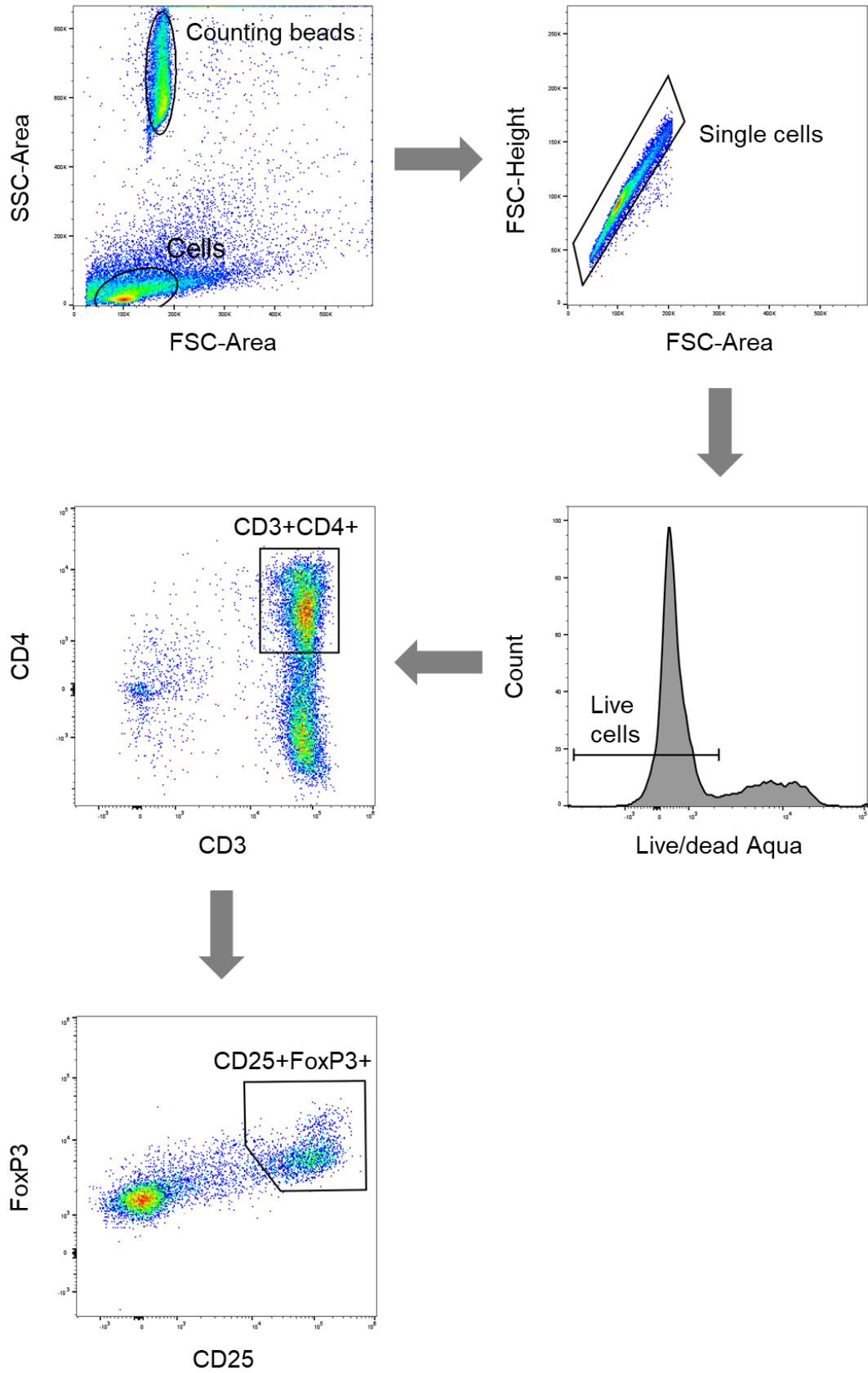
Figure 2.1: Flow cytometry gating strategy for Treg identification.

2.10.2.4   Preparation of target cells

HF-TERTs were infected with indicated HCMV strains with MOI = 10 as described previously (**Section 2.4.1.4**) and harvested 72 hpi using TrypLE to detach cells. Cells were washed twice with DMEM-10 by centrifugation at 327x *g* for 5 min, counted, centrifuged again, and resuspended in RPMI-10 at appropriate seeding density. When NK cell lines were used as effectors, targets were resuspended at 5×10^3 cells per 100 µl, whereas when PBMC were used as effectors, targets were resuspended at 5×10^4 cells per 100 µl. For ADAM17 blocking experiments, anti-ADAM17 D1(A12) antibody or human IgG control were added to target cells (100 nM) at 48 hpi and incubated for 24 hrs, followed by detachment and washing steps, unless stated otherwise. For Nectin1 blocking experiments, target cells were incubated with anti-Nectin1 antibodies (10 µg/ml) for 1 hr after target cells were detached using TrypLE.

2.10.2.5   Preparation of effector cells

PBMC or NK cell lines were used as effector cells for CD107a degranulation assay. PBMC were either thawed from frozen or isolated fresh from a blood donor (**Section 2.10.2.2**) one day before the assay and incubated with 10^3 U/ml of IFNα (Biotechne, 11100-1) in RPMI-10 overnight. NK cell lines were generated and stimulated by Dr Simon Kollenberger. Briefly, CD14−CD3−CD56+ NK cells were purified directly *ex vivo* via fluorescence-activated cell sorting (FACS) and stimulated with γ-irradiated allogeneic PBMCs, LCL-721.221 cells (1:1 ratio) and PHA-P (10 µg/ml) in NK cell medium for 3 days at 37 °C. Lines were maintained at $1–2 \times 10^6$ cells/ml by replenishing NK cell medium every 3–4 days. The purity of all cell lines was >96% and rested cell lines were harvested for functional assays after 2 weeks in culture. On the day of the assay effector cells were processed similarly to the target cells, however centrifugation steps were performed at 209x *g* for 5 min. NK cell lines were resuspended at 5×10^4 cells per 100 µl, whereas PBMC were resuspended at 5×10^5 cells per 100 µl.

2.10.2.6   Co-culture and Flow Cytometry staining

Co-cultures were set up in 96-well U-bottom tissue culture plates, filling the outer well with PBS. Previously prepared target cells (100 µl) were seeded with 100 µl of effector cells into wells in triplicate or quadruplicate depending on cell number. Each well also received Monensin (BD GolgiStop, 0.26% monensin, 554724) at a final dilution of 1:400 and anti-CD107a-FITC antibody at a final dilution of 1:200. For CD96 blocking experiments, anti-CD96 antibody was also included at 10 µg/ml per well. The plate was incubated in a plastic container at 37°C incubator for 5 hrs. Suspension cells were then harvested and washed twice in cold PBS before getting surface stained with 1:1000 LIVE/DEAD Aqua Viability Dye, CD3 and CD56 antibodies, as described previously (**Section 2.6.1**).

3 Investigating the global impact of UL148 and UL148D-driven ADAM17 impairment using proteomics

3.1 Introduction

Dr Mihil Patel previously described the effect of ADAM17 impairment by HCMV UL148 and UL148D on TNFα signalling due to increased levels of ADAM17 substrates TNFR1 and TNFR2 (Patel 2018). However, with ADAM17 cleaving over 100 currently known substrates from the cell surface, it was likely that the consequences of ADAM17 impairment in HCMV infection went beyond TNFα signalling. It was hypothesised that numerous ADAM17 substrates were affected as a result of ADAM17 impairment by UL148 and UL148D, resulting in an increase of their surface-expressed forms and a reduction in the levels of soluble proteins. To study the consequences of ADAM17 impairment, multiplexed quantitative proteomics was used to scrutinise the changes in plasma membrane (PM) and secreted proteins following infection with HCMV lacking UL148 and UL148D. This approach has previously been used to investigate the effect of HCMV infection (strain Merlin) on the composition of PM and whole cell protein levels in fibroblasts, defining quantitation of the entire proteome under multiple different treatments and conditions (Weekes et al. 2014).

3.2 Sample preparation

To study the role of ADAM17 impairment in HCMV infection two proteomics datasets were generated: PM and secretome. Samples for PM profiling (PMP) were generated by Dr Mihil Patel, however the analysis and validation of the data was performed by me. I also generated and analysed the secretome dataset.

To generate samples for secretome analysis, HF-TERTs were cultured in Heavy-SILAC-DMEM-10 DMEM for two weeks prior to HCMV infections.

Following HCMV infections with Merlin, single or double UL148 and UL148D knockouts, supernatants were collected at 24 and 72 hpi, filtered, concentrated and sent to Martin Potts at University of Cambridge for MS analysis. Prior to MS, proteins were digested into peptides and labelled with 10-plex TMT reagents, before being mixed together, fractionated and analysed (**Figure 3.1 A**). Samples for PM analysis were prepared by Dr Mihil Patel with isolation of PM proteins at 72 hpi following infections with Merlin, single or double UL148 and UL148D knockouts. dKO-infected HF-TERTs were also treated with anti-ADAM17 D1(A12) antibody for 24 hrs prior to protein harvest to block ADAM17 and facilitate direct study of ADAM17-dependent changes to the proteome. Samples for PMP were processed by Dr Katie Nightingale at the University of Cambridge (**Figure 3.1 B**).
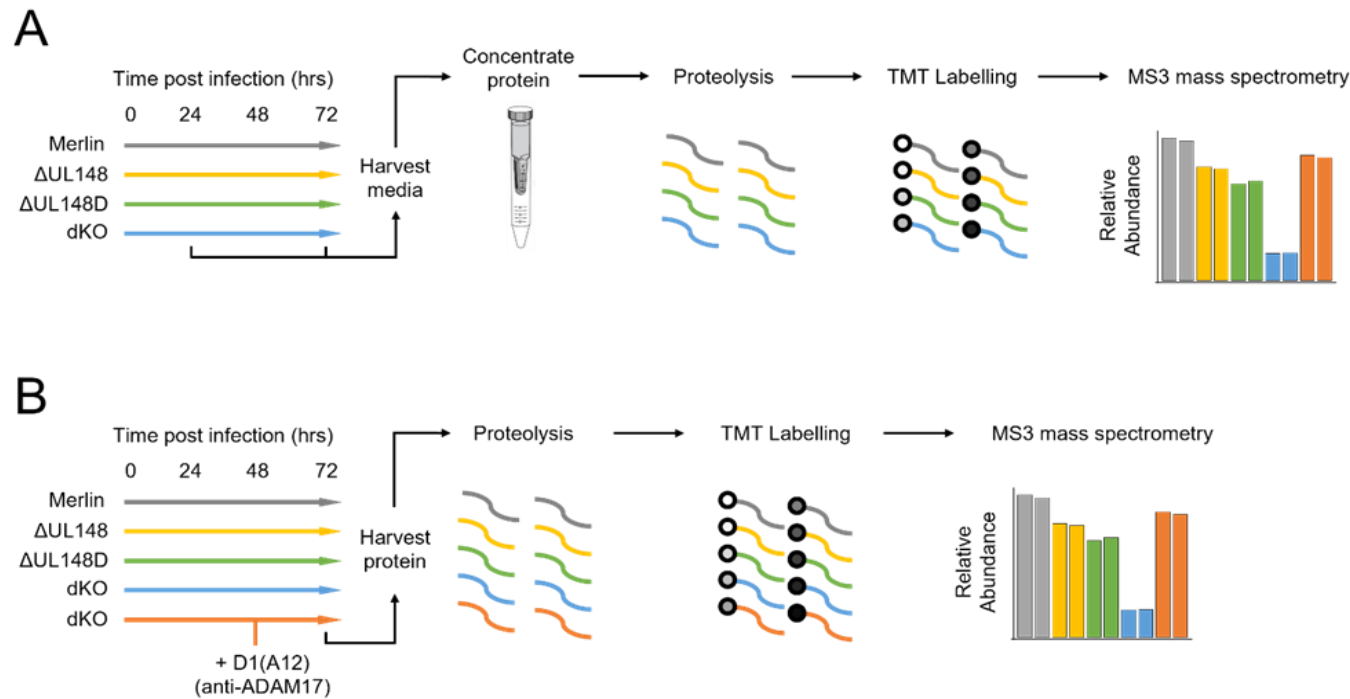
Figure 3.1: Workflow of proteomics experiments. (A) Sample preparation and experimental workflow for secretome dataset generation 24 and 72 hpi following infection with indicated HCMV strains. **(B)** Sample preparation (performed by Dr Mihil Patel) and experimental workflow for PMP dataset generation 72 hpi following infection with indicated HCMV strains. Mock-infected cells were included in preparation of both datasets. Anti-ADAM17 D1(A12) treatment (24 hrs) was used on dKO-infected HF-TERTs in the PMP dataset. Secretome MS was performed by Martin Potts, whereas PMP MS was performed by Dr Katie Nightingale at the University of Cambridge.

3.3 Investigating the impact of HCMV infection on the secretome

Secretome proteomics quantified a total of 2594 proteins, 1026 of which were annotated as secreted. Proteins were classed as secreted based on the presence of classical or non-classical secretion signals in the protein sequence or gene annotations for the terms 'Secreted', 'Extracellular' or 'Exosome' from Uniprot. Protein abundance cluster analysis of samples from Mock-infected cells clustered together at both timepoints, but separately from HCMV-infected samples (**Figure 3.2 A**). Although the secretome of HCMV-infected cells clustered separately from Mock samples at 24 hpi, the secretome at 72 hpi was considerably different compared to 24 hpi, indicating major changes to the cellular secretome of HCMV-infected cells at later stages of infection (**Figure 3.2 A**). Interestingly, ΔUL148 HCMV clustered together with Merlin, whereas ΔUL148D was more closely related to the dKO HCMV mutant (**Figure 3.2 A**). Comparisons of fold-change over Mock further highlighted the differences between secretomes at 24 and 72 hpi, with 72 hr HCMV infection resulting in more striking changes to the cellular secretome (**Figure 3.2 B**).
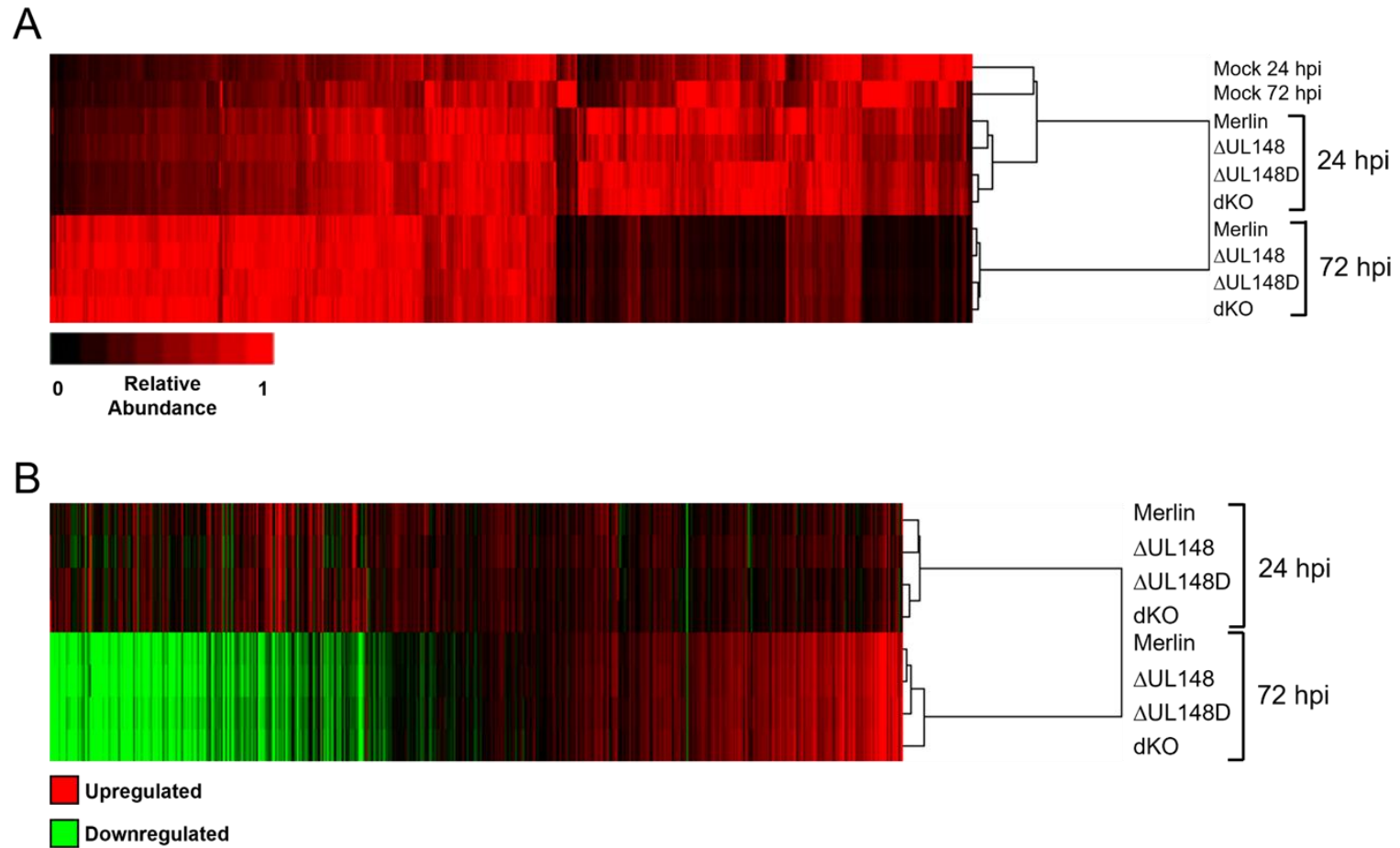
Figure 3.2: Hierarchal clustering of the secretome proteomics. (A) Relative protein abundance across all treatments at 24 and 72 hpi. **(B)** Fold change over Mock at 24 and 72 hpi

3.3.1 Identifying significantly upregulated secreted proteins following infection with HCMV lacking UL148 and UL148D

Secretomes of deletion HCMV mutants were compared against Merlin to identify any UL148- and UL148D-dependent changes to the levels of secreted proteins (**Figure 3.3**). Significance scores of $p<0.00001$ and $p<0.001$ were used to identify the most significant hits. Infection with ΔUL148 HCMV for 24 hrs resulted in one significantly upregulated protein CCL7, in contrast to ΔUL148D and dKO secretomes, which resulted in significantly upregulated secretion of multiple proteins. By 72 hpi, the ΔUL148 secretome identified additional significant hits, suggesting that UL148-dependent secretome changes develop as infection progressed (**Figure 3.3**). Although secretion of a few known ADAM17 targets, such as TNFR1 and TNFR2, was increased in the secretomes of single deletion HCMV mutants, a total of 17 proteins were identified as being highly significantly increased when both UL148 and UL148D were deleted, with five proteins identified as known ADAM17 targets and 12 as potential novel ADAM17 targets (**Table 3.1**). However, when significance was lowered to $p<0.05$, 100 and 78 proteins were identified as significantly increased in dKO-infected samples compared to Merlin at 24 and 72 phi, respectively. Since an anti-ADAM17 blocking antibody was not included in the secretome analysis, the increase in the levels of potentially novel ADAM17 targets cannot be directly linked to ADAM17 shedding, but rather to the function of viral UL148 and UL148D. Out of 17 total proteins identified as being significantly upregulated as a result of UL148 and UL148D deletion, only four had previously been reported to have a function in HCMV infection, suggesting that UL148 and UL148D may be involved in the regulation of previously unreported proteins important for HCMV (**Table 3.1**).
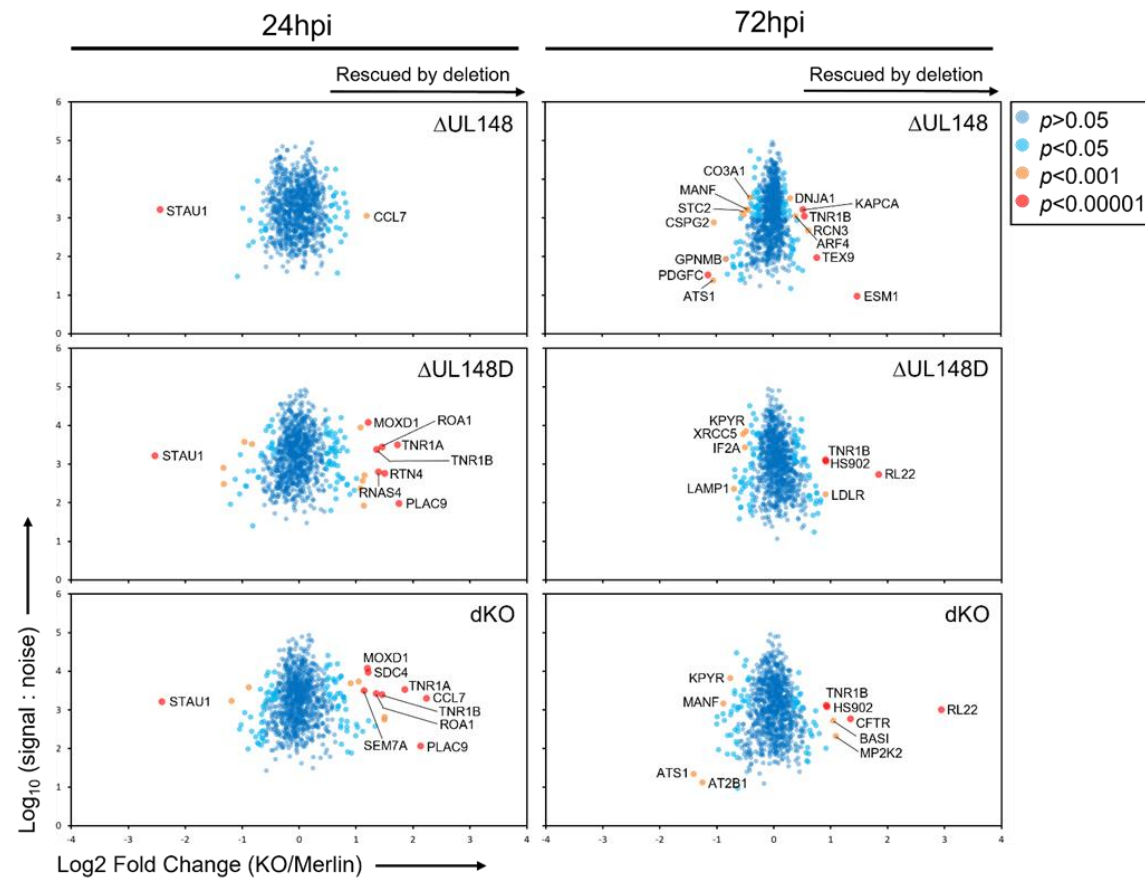
Figure 3.3: Scatterplot of secreted proteins modulated by UL148 and/or UL148D at 24 and 72 hpi. Fold change was calculated for each protein by comparing the signal:noise (S:N) ratio from each sample infected with a deletion virus against Merlin. Benjamini-Hochberg-corrected significance B was used to estimate *p*-values.

Table 3.1: Significantly upregulated proteins in the dKO secretome at 24 and 72 hpi.

Protein	24 hpi		72 hpi		Reported ADAM17 target?	Previous HCMV literature[†]
	Significance B (p-value)*	Ratio (dKO/Merlin)	Significance B (p-value)*	Ratio (dKO/Merlin)		
MOXD1	2.22E-07	2.3	ns	1	No	None
Syndecan-4	1.64E-07	2.3	ns	1.1	Yes	None
Semaphorin-7A	8.12E-07	2.2	ns	1.2	Yes	None
TNFR1	1.60E-15	3.6	ns	1.4	Yes	Upregulated by UL138 which aids HCMV reactivation (Montag et al. 2011)
TNFR2	3.36E-10	2.7	9.27E-08	1.9	Yes	Upregulated by UL148 and UL148D (Patel 2018)
CCL7	8.18E-22	4.7	ns	0.7	No	US28 binds chemokine CCL7 reducing its accumulation (Bodaghi et al. 1998)

HNRNPA1	5.52E-09	2.6	ns	0.8	No	None
PLAC9	9.84E-10	4.4	ns	0	No	None
Ribonuclease 4	1.47E-05	2.8	ns	0.7	No	None
Reticulon-4	1.60E-05	2.8	0.010728681	0.6	No	None
Neogenin	9.84E-05	1.9	ns	1.2	Yes	None
SIRPα	6.89E-06	2.1	ns	1.2	No	None
HSP 90α A2	ns	0.8	5.60E-08	1.9	No	None
CFTR	ns	1.4	1.99E-06	2.9	No	None
Basigin (CD147)	ns	1.2	0.000220577	2.1	No	Acts as entry mediator for pentamer-expressing HCMV into epithelial and endothelial cells (Vanarsdall et al. 2018)
MAP2K2	ns	0.7	0.000123103	2.1	No	None
RL22	ns	1.0	1.81E-25	7.7	No	None

* Presented are highly significant proteins from the dKO secretome dataset (**Figure 3.3**) with corresponding *p*-values and dKO/Merlin fold change values.

† Literature search for whether proteins were cleaved by ADAM17, and if any role in HCMV infection has been reported.

3.3.2 Individual examples of altered proteins from secretome analysis

Closer examination of highly significant secretome hits demonstrated expected patterns in terms of relative protein abundance. Known ADAM17 targets, such as TNFR1/2, Syndecan-4, Semaphorin-7A and Neogenin all increased in abundance at 24 hpi in the dKO secretome dataset compared to Merlin (**Figure 3.4 A**). All mentioned proteins, except for Syndecan-4, also demonstrated increased levels in the dKO secretome at 72 hpi, however the increase was less significant in most cases. Other identified proteins from the secretome analysis with no previously reported ADAM17 function demonstrated similar trends of increased levels in the dKO secretome, which was more apparent at 24 hpi. Examples included, but were not limited to, CCL7, Reticulon-4 and Basigin (**Figure 3.4 A**). A number of viral proteins were also detected in the secretome, however they were either filtered out during the selection of predicted secreted proteins or failed to pass the significance threshold of $p<0.05$, such as RL12 and UL144, respectively (**Figure 3.4 B**). Interestingly, most proteins showed similar increased relative abundance in ΔUL148D and dKO secretomes, which was true for both known and previously unreported ADAM17 targets.
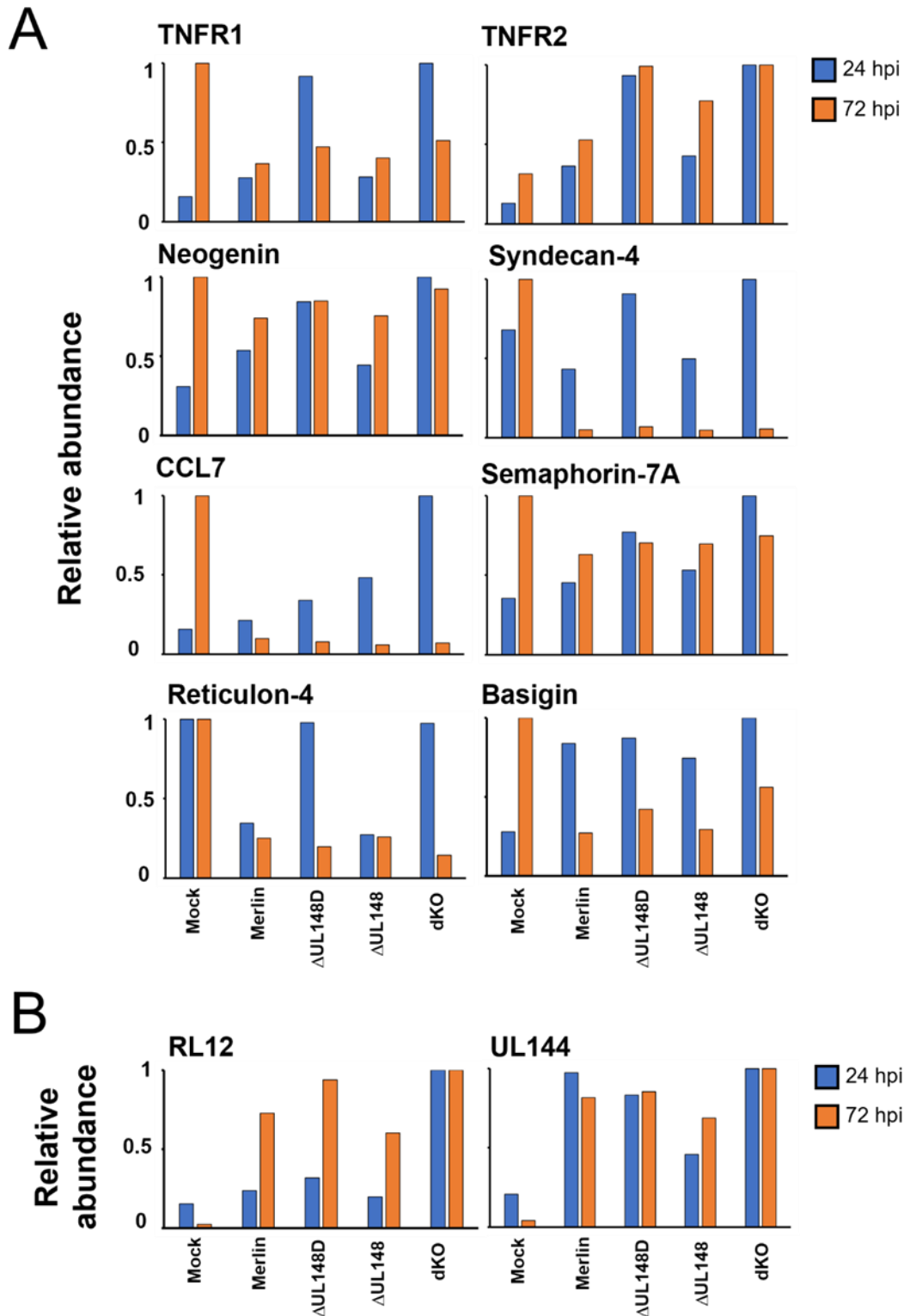
Figure 3.4: Examples of highly significant dKO secretome hits. (A) Identified secreted proteins from the host. **(B)** Viral protein hits identified but filtered out or failed to reach significance threshold.

3.4 PMP analysis studying the impact of ADAM17 impairment in HCMV infection

In addition to secretome proteomics, PMP analysis picked up a total of 2332 proteins, with 1028 identified as PM proteins. Hierarchical clustering of fold change over Mock revealed that duplicate samples clustered together suggesting consistent sample preparation and analysis (**Figure 3.5 A**). dKO HCMV infection resulted in the most different PM profile compared to other infections and clustered separately from the rest. The addition of anti-ADAM17 blocking antibody D1(A12) to dKO-infected HF-TERTs for 24 hrs prior to sample harvest altered cellular PM composition as demonstrated by these samples clustering with ΔUL148 samples and not dKO (**Figure 3.5 A**). A close up of a region where protein abundance reduced significantly following D1(A12) treatment in dKO-infected cells, revealed a number of proteins regulated in an ADAM17-dependent fashion (**Figure 3.5 B**). Further significance testing identified 114 proteins rescued by the addition of D1(A12) to dKO-infected cells reaching significance of $p<0.05$, with a number of highly significant protein hits reaching $p<0.00001$ and $p<0.00000000001$ (**Figure 3.5 C**).
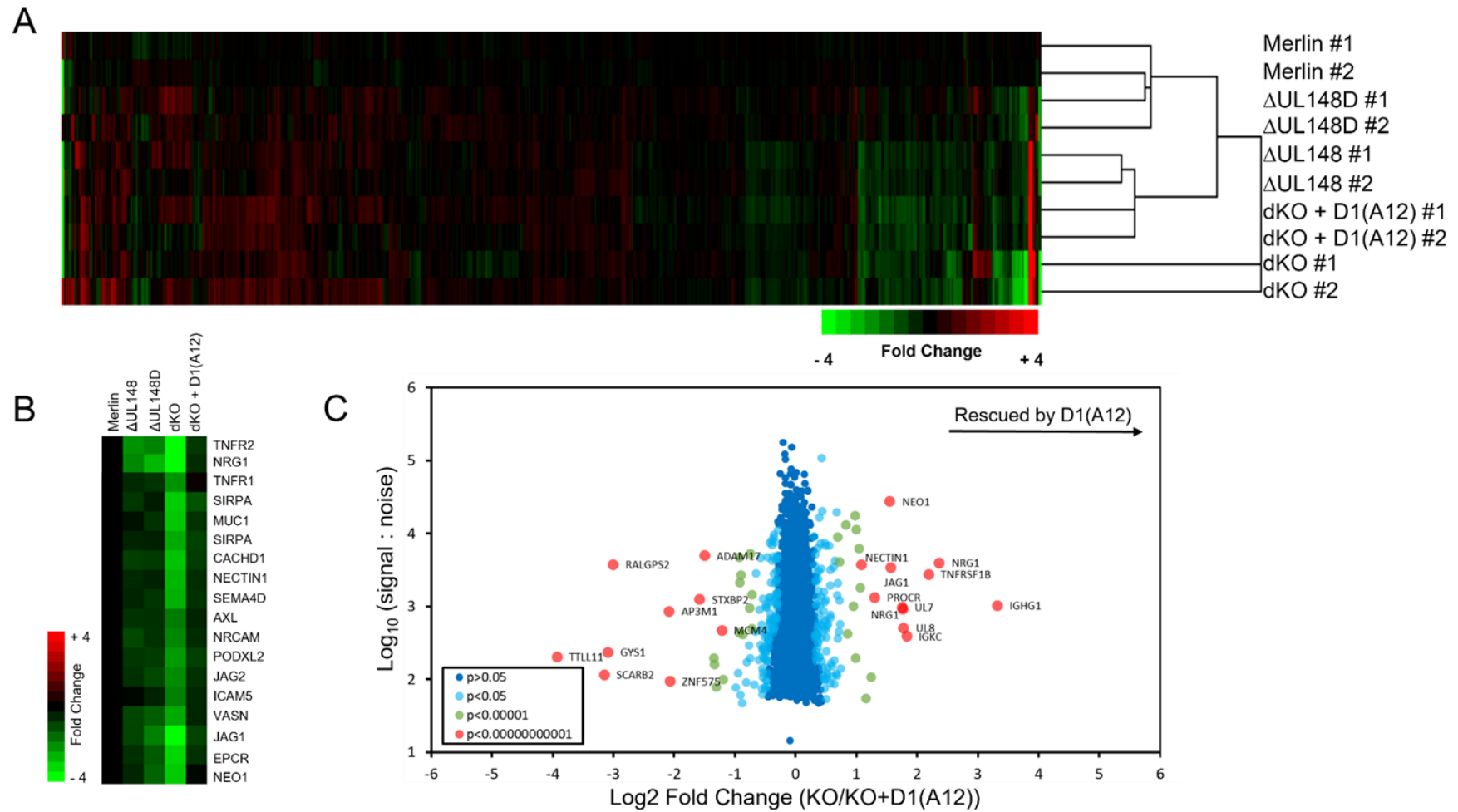
Figure 3.5: Hierarchal clustering of PMP dataset. Fold change of protein abundance of infections with indicated HCMV strains over Mock on **(A)** all proteins quantified in the experiment and **(B)** a subset of proteins. **(C)** Scatterplot of cell-surface proteins modulated by D1(A12) in dKO-infected HF-TERTs. Average values of duplicate samples were plotted.

3.4.1 Analysis of the most significant hits identified in PMP

Using significance scores of *p*<0.00001 and *p*<0.00000000001, 23 and 11 proteins respectively were recovered on the surface of dKO-infected cells in an ADAM17-dependent fashion (**Table 3.2**). Of the 23 proteins reaching significance *p*<0.00001 10 were known ADAM17 targets, such as TNFR1/2, Vasorin, and Jagged1. The remaining 13 proteins were novel ADAM17 substrates, including Nectin1, SIRPα and ICAM5. Three viral proteins UL144, UL7 and UL8 also recovered significantly in an ADAM17-dependent fashion following the addition of D1(A12) to dKO-infected cells (**Table 3.2**). Duplicate samples clustered together indicating consistent sample preparation and analysis (**Figure 3.6**). CD58 expression following D1(A12) treatment was used as a negative control, since UL148 has previously been shown to downregulate surface CD58 (Wang et al. 2018) (**Figure 3.6**), which is not reported as an ADAM17 target in the literature. All ADAM17-dependent proteins demonstrated similar relative protein abundance trends, with dKO HCMV infection resulting in considerably reduced surface protein levels, compared to a partial reduction following infection with single deletion mutants. The addition of D1(A12) recovered surface levels of named proteins similar to the levels of Merlin-infected cells, highlighting the role of ADAM17 in regulating the expression of many surface proteins in HCMV infection (**Figure 3.6**).

Table 3.2: Significantly upregulated proteins in dKO PMP following a 24 hr D1(A12) treatment.

Protein	Significance (p-value)*	Ratio (dKO+ D1(A12))/ dKO)	Known/ Novel ADAM17 Target	Previous HCMV literature†
CACHD1	7.99E-10	2.08	Novel	None
EPCR	4.73E-14	2.46	Known	None – validated in this thesis
IGHG1	6.13E-81	9.97	Novel	None
IGKC	5.25E-27	3.54	Novel	None
ICAM5	8.24E-06	1.62	Novel	None
SIRPα	3.28E-08	1.93	Novel	None
SIRPα (isoform 2)	1.14E-07	1.77	Novel	None
Pro-Neuregulin-1 (Isoform 6)	1.68E-51	5.14	Novel	None
Jagged1	1.97E-23	2.94	Known	Downregulated by AD169 (Li et al. 2015b); upregulated by Merlin - validated in this thesis
UL144	5.07E-07	1.80	Novel	HVEM ortholog that inhibits CD4^{+} T-cells (Cheung et al. 2005)
UL8	9.88E-26	3.41	Novel	Impairs myeloid proinflammatory

				cytokine production (Pérez-Carmona et al. 2018)
UL7	4.62E-24	3.37	Novel	Soluble Flt3R ligand (Crawford et al. 2018)
Mucin-1	5.39E-07	2.23	Known	None
Nectin1	5.01E-12	2.11	Novel	None – validated in this thesis
Neogenin	4.26E-23	2.92	Known	None
Neuregulin 1	2.16E-25	3.38	Known	None
PTPRG	4.15E-10	1.96	Novel	None
Semaphorin-4D	1.72E-10	1.99	Known	None
Semaphorin-7A	4.25E-06	1.64	Known	None
Syndecan-3	3.83E-09	1.98	Novel	None
TNFR1	7.86E-08	2.36	Known	Upregulated by UL138 (Montag et al. 2011)
TNFR2	1.82E-36	4.56	Known	Upregulated by UL148 and UL148D (Patel 2018)
Vasorin	2.76E-11	2.05	Known	None – validated in this thesis

* Presented are highly significant proteins from dKO+D1(A12) PMP dataset (**Figure 3.5 C**) with corresponding *p*-values ($p<0.00000000001$ and $p<0.00001$) and dKO/dKO+D1(A12) fold change values.

† A literature search identified if mentioned proteins are known or novel ADAM17 substrates and any published role in HCMV infection.
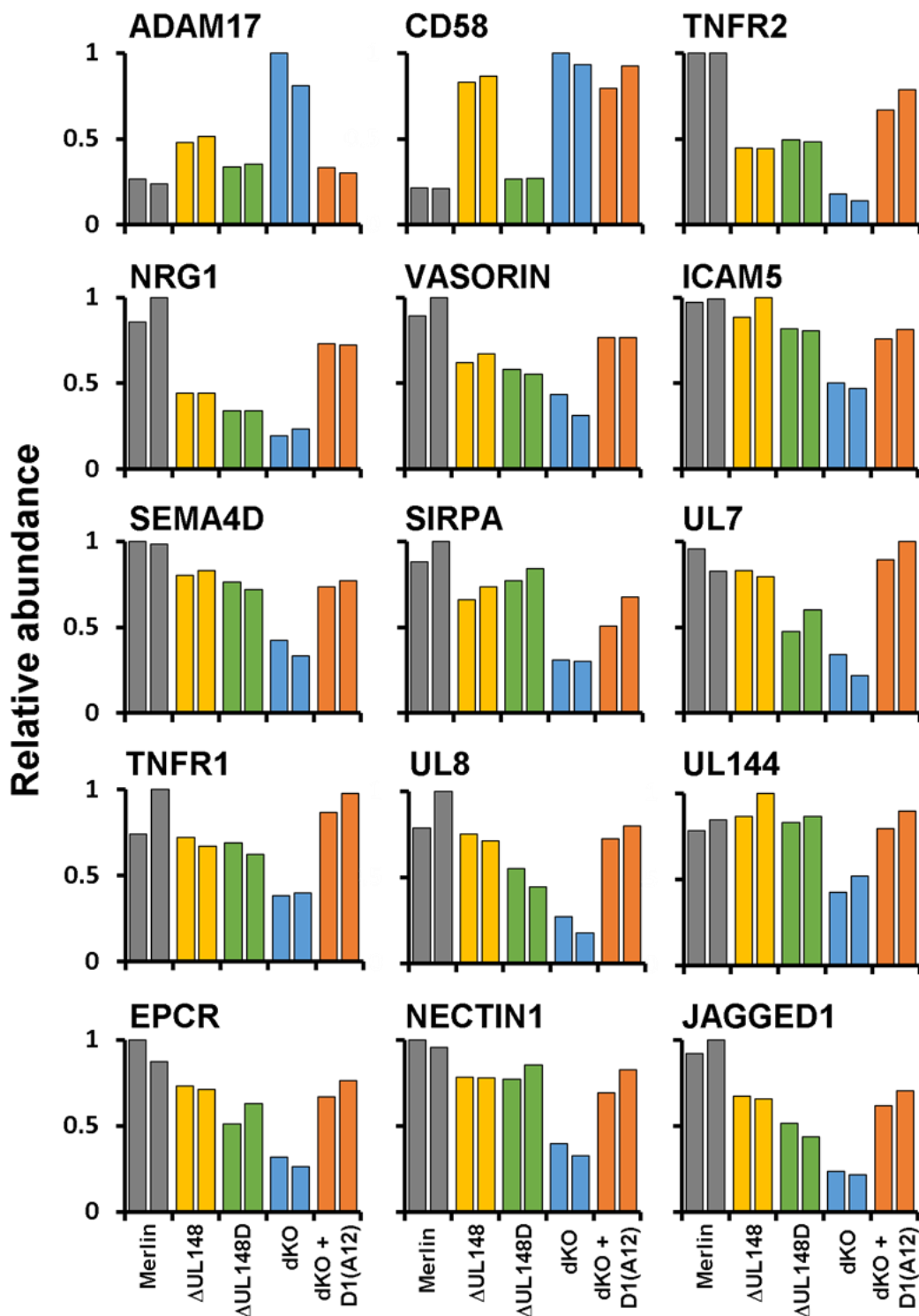
Figure 3.6: Examples of some of the highly significant hits identified in PMP, following D1(A12) treatment. Selected examples of quantified proteins in PMP analysis. CD58 was used as an internal control since it is known to be targeted by UL148 in an ADAM17-independent manner.

3.5   Combined   analysis   of   secretome proteomics and PMP

3.5.1   Shortlisting   proteomics   hits   from   two proteomics datasets

The application of anti-ADAM17 blocking antibody D1(A12) in PMP facilitated the direct study of ADAM17-dependent changes to the profile of surface proteins in HCMV infection. Out of 21 highly significant PMP hits (isoforms of SIRPα and Neuregulin were removed), 8 had previously been reported to be involved in regulation and function of neuronal cells and 15 had previously reported immune functions (**Table 3.3**). Eleven proteins were also present in the secretome dataset, with 7 proteins reaching significance of $p<0.05$ (**Table 3.3**). One viral protein UL144 was also shared between both datasets, although it failed to reach significance in the secretome proteomics. TNFR1/2 were identified in both proteomics datasets as significant hits, acting as internal positive controls for both proteomics experiments.

Table 3.3: Function/description of proteins identified in dKO PMP following a 24 h D1(A12) treatment and their secretome ratio/significance, if any.

PMP Proteins	Secretome ratio (dKO vs Merlin) †		Secretome significance (p-value) (dKO vs Merlin)*		Description/function
	24hpi	72hpi	24hpi	72hpi	
CACHD1	2.5	1.1	0.00011014	ns	Modulates voltage-gated calcium channels in neurons (Stephens and Cottrell 2019)
EPCR	-	-	-	-	Activates protein C involved in blood coagulation and responses to inflammatory stimuli; binds to activated neutrophils (Kurosawa et al. 2000); activates γδ LES T cells (Willcox et al. 2012)
IGHG1	-	-	-	-	Immunoglobulin heavy constant γ 1
IGKC	-	-	-	-	Immunoglobulin κ chain
ICAM5	1.1	1.0	ns	ns	Adhesion protein and ligand to LFA-1 that regulates neuron-microglial cell interactions (Yang 2012)
SIRPα	2.1	1.2	6.89E-06	ns	Interacts with CD47 inhibiting effector function of immune cells, such as phagocytosis (Takahashi 2018)

Jagged1	1.3	1.2	ns	ns	Ligand for Notch signalling important in development and differentiation (Li et al. 2014), involved in Treg development (Lin et al. 2019)
Neuregulin 1	-	-	-	-	Involved in nerve cell differentiation, neurite outgrowth and synapse formation (Barrenschee et al. 2015)
UL144	1.0	1.2	ns	ns	Structural mimic of HVEM, which binds BTLA, in addition to other ligands, inhibiting T cell activation (Cheung et al. 2005)
UL8	-	-	-	-	Impairs myeloid proinflammatory cytokine production (Pérez-Carmona et al. 2018)
UL7	-	-	-	-	Soluble Flt3R ligand (Crawford et al. 2018)
Mucin-1	-	-	-	-	Functions as a barrier to protect cell membranes, regulates cell adhesion, in addition to immune-regulatory functions (Chen et al. 2021)
Nectin1	-	-	-	-	Ligand for NK cell receptor CD96 regulating NK cell activation (Fuchs et al. 2004; Holmes et al. 2019)
Neogenin	1.9	1.2	9.84E-05	ns	Homologue of DCG highly expressed in neurons involved in cell migration and axon guidance (Wilson and Key 2007)
PTPRG	1.3	1.2	ns	ns	Involved in hematopoietic differentiation and sensory neuron development (Bouyain and Watkins 2010)

Semaphorin-4D	-	-	-	-	A ligand for Plexin β1 involved in immunoregulation (Lontos et al. 2018)
Semaphorin-7A	2.2	1.2	8.12E-07	ns	Interacts with Plexin C1 and β1-integrin, regulating cell migration and adhesion, neurite growth and T cell function (Czopik et al. 2006)
Syndecan-3	-	-	-	-	Plays a role in the development of neuronal and brain tissue with some evidence of inflammatory function (Arokiasamy et al. 2019)
TNFR1	3.6	1.4	1.60E-15	ns	Mediates TNF-induced inflammation and cell death (Wajant and Siegmund 2019)
TNFR2	2.7	1.9	3.36E-10	9.27E-08	Stimulates NF-κB signalling and promotes cell survival and proliferation (Wajant and Siegmund 2019)
Vasorin	1.6	1.2	0.005487463	ns	ADAM17-cleaved soluble Vasorin inhibits TGFβ signalling; and protects cells against TNFα-induced apoptosis (Ikeda et al. 2004; Choksi et al. 2011; Malapeira et al. 2011)

* Presented are descriptions/functions for highly significant ($p<0.00000000001$ and $p<0.00001$) proteins from dKO+D1(A12) PMP dataset (**Table 3.2**).

† If present in the secretome proteomics, fold change (dKO vs Merlin) values, as well as significance scores are presented for both timepoints.

3.5.2 Comparing shortlisted proteomics hits with Quantitative Temporal Viromics

Comparison of both proteomics datasets identified 11 ADAM17-dependent proteins (10 host and 1 viral) to be highly significantly affected by ADAM17 impairment by HCMV UL148 and UL148D. Shortlisted hits were then compared to a published QTV dataset to gather further evidence for the role of ADAM17 in regulating protein levels in HCMV infection. QTV proteomics were generated by infecting HF-TERTs with HCMV strain Merlin and studying protein changes over the course of 96 hrs (Weekes et al. 2014). Since HCMV stain Merlin was used in QTV, I was able to compare expression profiles of the selected 11 proteins identified in PMP/secretome proteomics to the QTV dataset (**Figure 3.7**). Most proteins demonstrated an increase in expression following infection with Merlin in QTV, such as UL144, Neogenin and TNFR2. QTV demonstrated a decrease in expression from 72 hpi onwards in the majority of the proteins, which may be explained by increased cell death associated with later HCMV infection timepoints. Interestingly, some proteins showed a consistent reduction in expression in QTV analysis, contrary to PMP and secretome proteomics. The most striking example was Vasorin, with QTV suggesting a gradual decrease of expression overtime (**Figure 3.7**), highlighting the importance of validating proteomics data prior to any functional work.
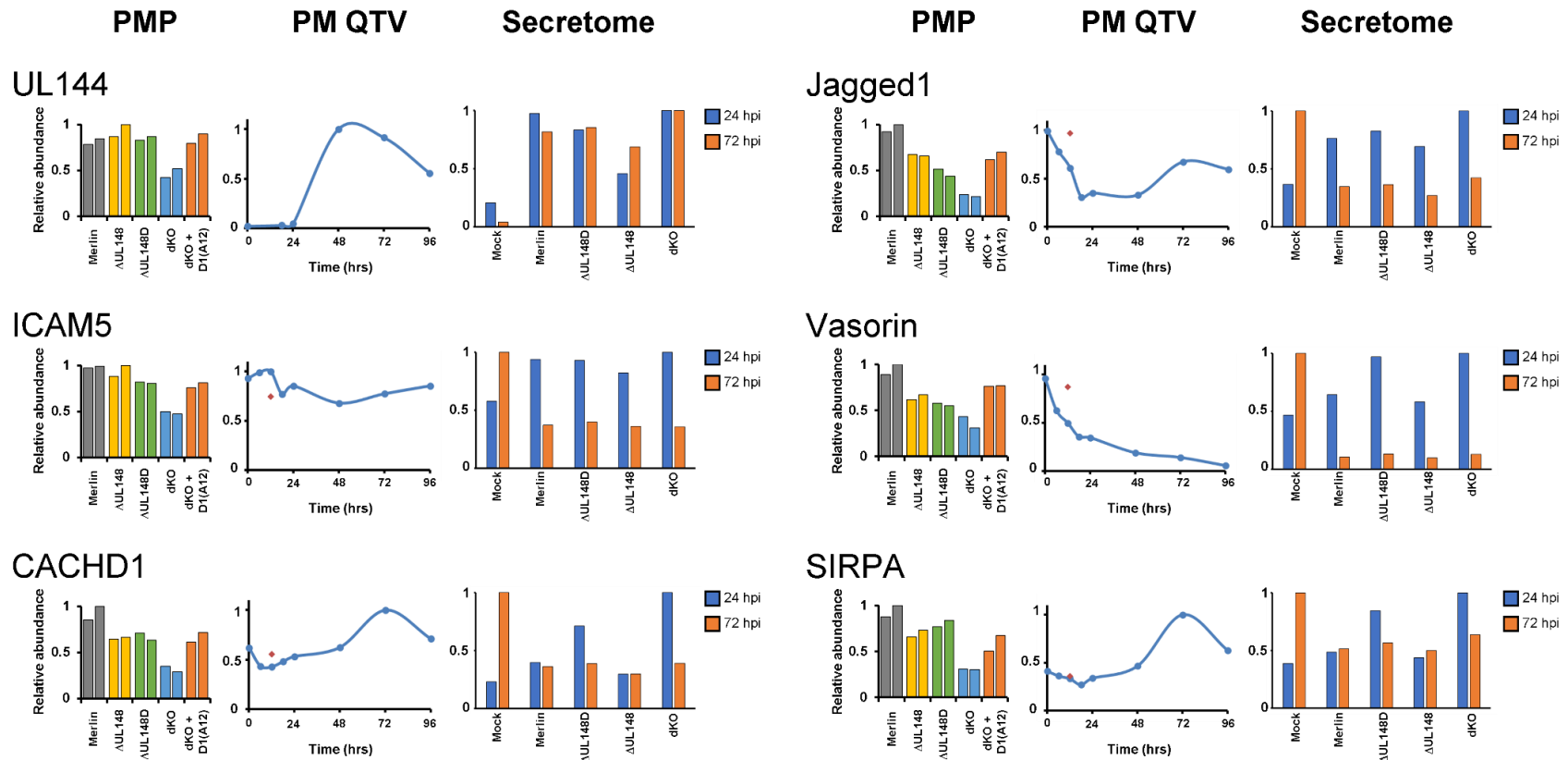
Figure 3.7: Relative protein abundance of selected proteins from 3 proteomics datasets – PMP and secretome from this thesis and previously published QTV (Weekes et al. 2014). Selected proteins were chosen on the basis of reaching significance of $p<0.00000000001$ and $p<0.00001$ in the PMP dataset and being detected in the secretome dataset (**Table 3.3**). To generate QTV graphs, Weekes et al., 2014 supplementary plotter was used.
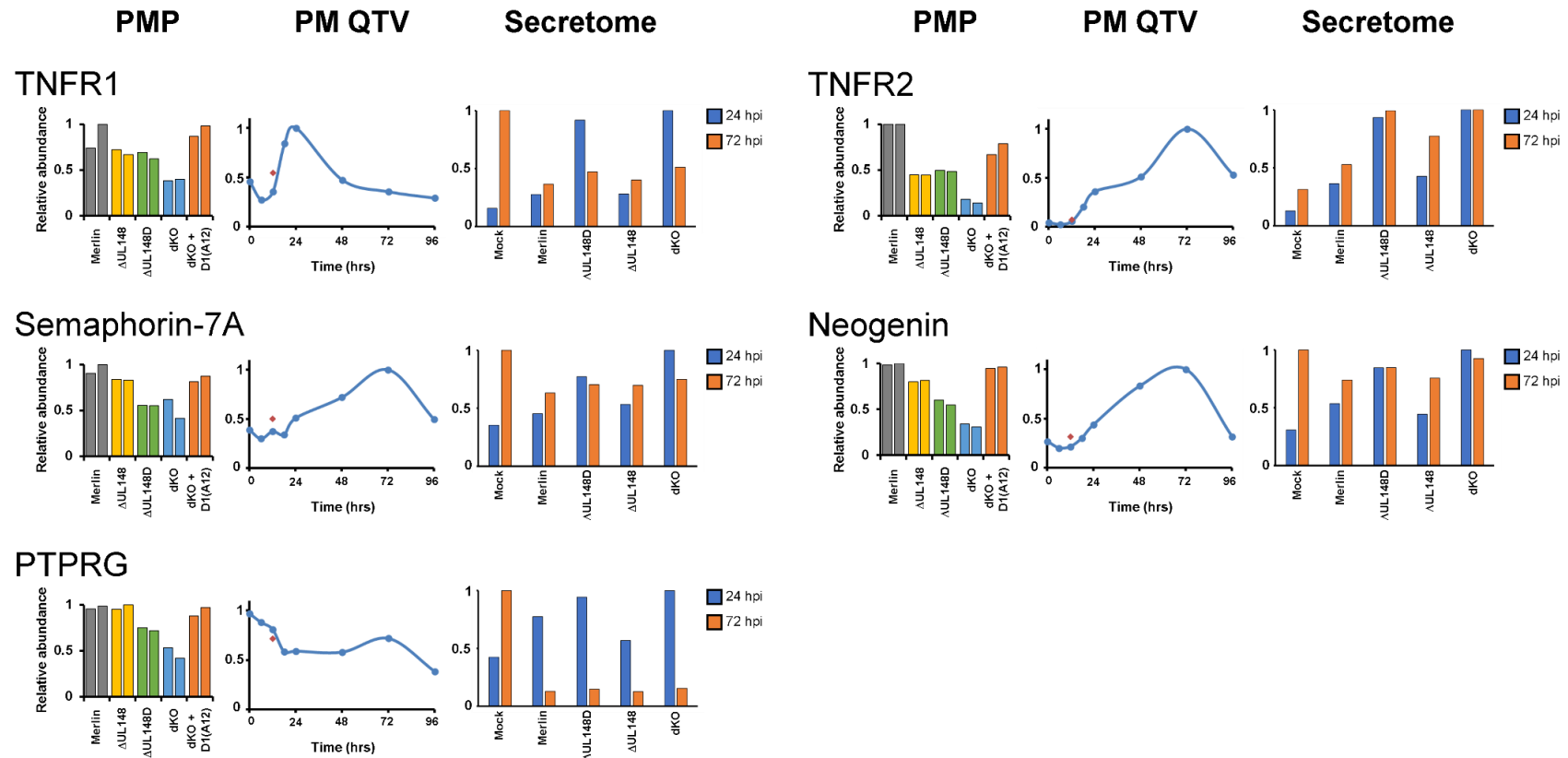
Figure 3.7 (cont.): Relative protein abundance of selected proteins from 3 proteomics datasets – PMP and secretome from this thesis and previously published QTV (Weekes et al. 2014). Selected proteins were chosen on the basis of reaching significance of $p<0.00000000001$ and $p<0.00001$ in the PMP dataset and being detected in the secretome dataset (**Table 3.3**). To generate QTV graphs, Weekes et al., 2014 supplementary plotter was used.

3.5.3   Validation of selected PMP hits

Secretome proteomics and PMP identified a number of significantly upregulated ADAM17-dependent proteins in Merlin-infected cells, some of which were also upregulated in the QTV analysis following Merlin infection (**Section 3.5.2**). Upregulation of so many surface proteins and reduction of their soluble forms as a result of UL148- and UL148D-driven ADAM17 impairment, is likely to impact multiple signalling pathways and processes. Prior to any functional work, selected hits from combined PMP and secretome proteomics were validated for expression using flow cytometry and Western blot techniques (**Figure 3.8**). Four proteins were selected for validation based on their PM and secretome profiles, as well as function – Jagged1, Vasorin, Nectin1 and EPCR (**Table 3.3**). Jagged1, Vasorin and Nectin1 had previously been reported to have immune modulatory functions. Jagged1 is known to be involved in Treg cell development, whereas soluble Vasorin has been shown to inhibit TGFβ signalling – one of the pathways involved in Treg function (**Table 3.3**). Nectin1 was selected due to its previously reported role in NK cell function, whereas EPCR was shortlisted for validation due to an intriguing aspect of EPCR associated with the activation of γδ LES T cells in response to HCMV-infected cells (**Table 3.3**).

HF-TERTs were infected for 72 hrs prior to sample processing with either Mock, HCMV strain Merlin or dKO HCMV lacking UL148 and UL148D. Surface Jagged1 staining was dim and although there was a small shift in intensity between Mock- and HCMV-infected cells, no convincing difference between Merlin- and dKO-infected cells was observed. Staining for Vasorin by Western blot showed no signal at all for surface or soluble Vasorin in whole cell lysate and supernatant, respectively (**Figure 3.8 A**). This led to the conclusion that Jagged1 and Vasorin were expressed at such low levels in HF-TERTs, they were below the sensitivity threshold for flow cytometry and Western blot detection. Proteomics is a highly sensitive method, able to detect a single peptide, hence it is not uncommon to experience issues of lack of detectable expression when validating proteomics hits with other more standard techniques. To overcome this, Jagged1 and Vasorin were overexpressed in

113

HF-TERTs using lentiviruses (hereinafter referred to Jag1-TERT for the Jagged1-expressing line and Vasn-TERT for the Vasorin-expressing line) achieving easily detectable levels in Mock-infected cells by flow cytometry for Jagged1 or Western blot for Vasorin (**Figure 3.8 B**). The use of Jag1- and Vasn-TERTs demonstrated increased protein levels in Merlin-infected, compared to dKO-infected, cells validating the proteomics results. Since Vasorin was validated using Western blot, cell supernatant (media) was also investigated for levels of the soluble form of Vasorin. A stronger signal was observed from dKO-infected cells, consistent with increased shedding of Vasorin in those cells consistent with the presence and action of ADAM17 (**Figure 3.8 B**).

In contrast to Jagged1 and Vasorin, two additional hits Nectin1 and EPCR validated without the need for overexpression. Merlin-infected cells demonstrated an expected pattern of increased surface Nectin1 compared to Mock, which reduced when UL148 and UL148D were deleted (**Figure 3.8 C**). EPCR levels in Merlin-infected cells stabilised to Mock levels and reduced dramatically when UL148 and UL148D were deleted, similarly to Nectin1 (**Figure 3.8 C**). Overall, four selected proteomics hits were validated successfully confirming upregulation of both known and novel ADAM17 targets on Merlin-infected cells.
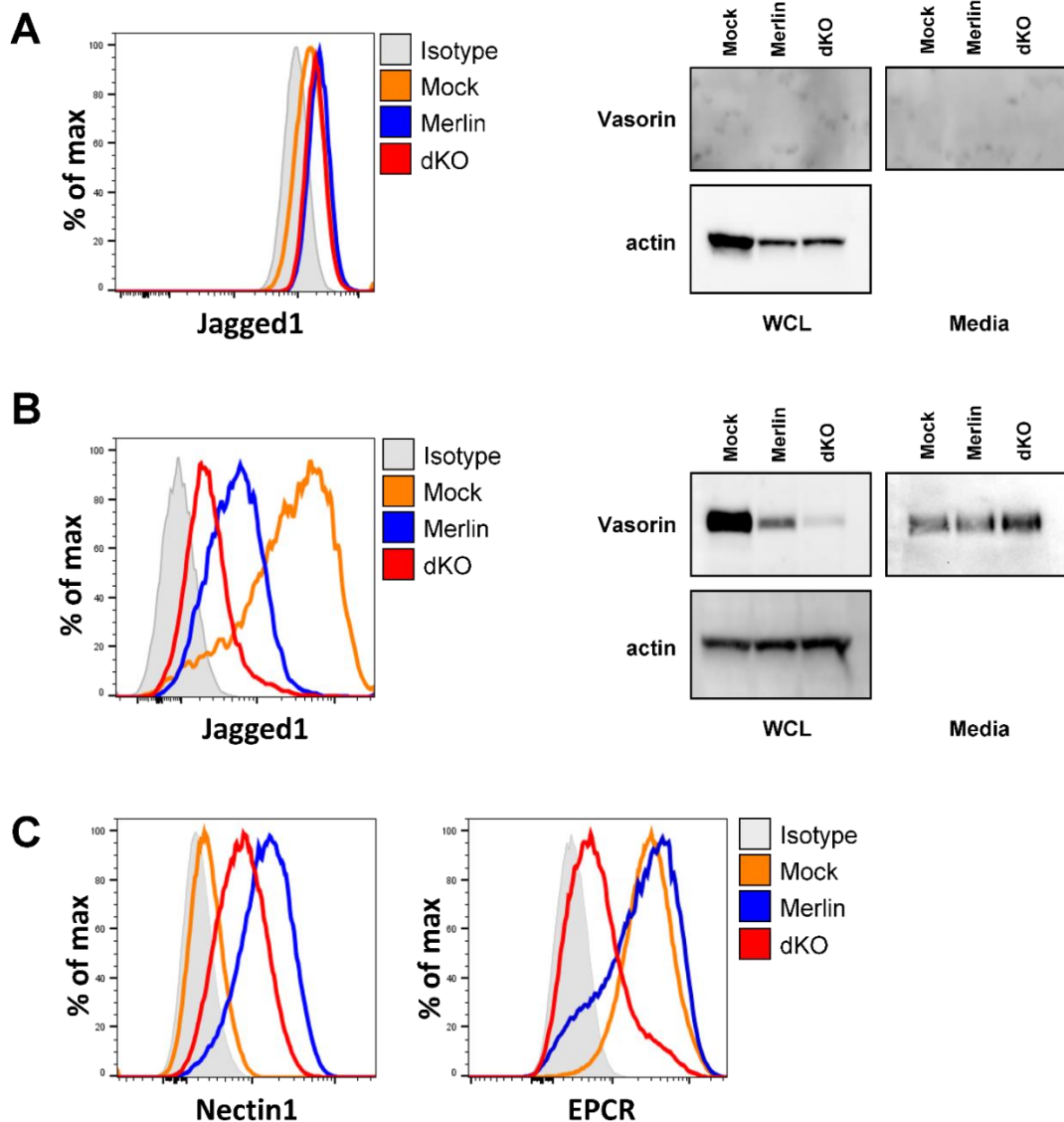
Figure 3.8: Validation of selected PMP hits. (A) Flow cytometry and Western blot analysis of Jagged1 and Vasorin, respectively, on HF-TERTs infected with indicated HCMV strains (MOI = 5, 72 hpi). **(B)** Flow cytometry and Western blot analysis of Jagged1 and Vasorin, respectively, on lentivirus transduced Jag1-TERTs and Vasn-TERTs infected with indicated HCMV strains (MOI = 5, 72 hpi). For soluble Vasorin staining, culture media from infected cells was collected at 72 hpi and concentrated using Vivaspin sample concentrators prior to lysis. **(C)** Flow cytometry staining of Nectin1 on HF-TERTs infected with indicated HCMV strains (MOI = 5, 72 hpi). Validation was performed at least twice for each protein and representative histograms/blots are presented.

3.6   Summary of findings

The PMP and secretome proteomics presented in this chapter provide important insights into the role of UL148, UL148D and ADAM17 in shaping the proteome. Following HCMV infection both proteomics datasets clearly demonstrated the effects of HCMV infection on fibroblasts, with global changes to the cellular secretome and surface protein profile. Secretome proteomics revealed that the levels of 100 and 78 secreted proteins significantly went up in dKO-infected cells compared to Merlin at 24 and 72 hpi, respectively, at a significance threshold of $p<0.05$ (**Figure 3.3**). Similarly, PMP identified 114 surface proteins as rescued by the addition of D1(A12) at $p<0.05$ (**Figure 3.5**).

When highly significant hits were examined and compared across both datasets, 11 proteins were shared with 7 reaching significance of $p<0.05$ in PMP and secretome proteomics (**Table 3.3**). Although that number may not seem high, it should be noted that significant scores of $p<0.00000000001$, $p<0.00001$ and $p<0.001$ were used to select the most significant hits, excluding a lot of proteins from more detailed analysis. This made analysis more manageable and aided shortlisting of the most promising candidates for further functional testing. In addition, the lower sensitivity of the secretome proteomics method, as well as omission of anti-ADAM17 D1(A12) treatment, may explain the differences between PMP and secretome hits.

Comparison of the results presented in this chapter to the published QTV dataset provided an additional layer of depth, putting the results of this thesis into a broader context. Increased expression of many proteins in the QTV dataset may now be explained by the impairment of ADAM17 by UL148 and UL148D (**Figure 3.7**). Although comparing a number of different proteomics datasets demonstrated the power of proteomics providing insight into important biological questions, it also highlighted the importance of validating proteomics hits prior to any functional studies. For example, Jagged1 and Vasorin validated successfully in the context of HCMV infection (**Figure 3.8 B**) despite failing to demonstrate convincing increases in the QTV dataset (**Figure 3.7**), possibly linked to the low expression of these proteins on

fibroblasts (**Figure 3.8**). Similarly, Nectin1 and EPCR were not detected in the secretome dataset but validated well in the context of HCMV infection (**Figure 3.8 C**).

Overall, with the use of global proteomics methods, this chapter demonstrated the extent of changes driven by HCMV infection on the cellular proteome, highlighting the specific impact caused by the impaired expression of a single sheddase, ADAM17, by UL148 and UL148D.

4 Investigating the mechanism of ADAM17 downregulation by UL148 and UL148

4.1 Introduction

Work presented in Chapter 3 highlighted the importance of UL148 and UL148D in regulating the cellular secretome and altering the composition of PM through the impairment of ADAM17. Previously published QTV proteomics demonstrated a rapid surface and whole cell ADAM17 reduction in host cells, with surface ADAM17 being almost completely abolished by 18 hpi (Weekes et al. 2014). Dr Mihil Patel also observed levels of surface ADAM17 go down to the level of isotype negative control staining at 24 hpi by flow cytometry (Patel 2018). Such rapid surface ADAM17 downregulation by HCMV suggests a robust and effective viral strategy. Dr Mihil Patel has already shown that viral UL148 and UL148D synergistically downregulate ADAM17 from the cell surface, however the exact mechanism of how these viral proteins downregulate ADAM17 remains unknown (Patel 2018). Some of Dr Patel's findings indicate that UL148 and UL148D disrupt ADAM17 processing, however, since ADAM17 is a tightly regulated protein due to its critical function in many cellular processes, its processing is also very complex. This chapter aimed to decipher the mechanism behind UL148- and UL148D-driven ADAM17 downregulation by studying UL148 and UL148D interactions with other proteins as well as HCMV-induced changes to ADAM17 processing.

4.2 Investigating interactions between UL148/UL148D and host proteins

4.2.1 Characterising UL148 and UL148D by immunofluorescence

To study the mechanism of ADAM17 downregulation by UL148 and UL148D, these viral proteins were first visualised by immunofluorescence to provide more insight into their biology. To achieve this a double tagged UL148-V5 and UL148D-HA HCMV was made using *En Passant* mutagenesis, as described in **Section 2.8.3**.

Immunofluorescence was performed to study localisation of UL148 and UL148D in HF-TERTs 48 hpi with the double tagged HCMV. No colocalisation was observed between UL148 and UL148D, however both viral proteins showed ER-like staining, with UL148 showing a more defined and UL148D a more diffuse pattern of staining (**Figure 4.1**). UL148 is known to be ER-resident (Siddiquey et al. 2018), while localisation of UL148D was unknown until now. Double tagged HCMV microscopy data suggested that UL148 and UL148D localise in different compartments of the ER, however due to HCMV-induced rounding up of cells it is difficult to safely interpret the result. To clarify this, immunofluorescence was performed on lentivirus transfected HF-TERT cells that stably express V5-tagged UL148 or UL148D (a gift from Prof Michael Weekes) thereby bypassing the need to infect cells with HCMV. Cells were stained for the V5-tag corresponding to either UL148 or UL148D. Staining of lentivirus cell lines also showed that UL148 and UL148D displayed distinct patterns of intracellular expression, the former more diffuse, and consistent with localisation in different ER compartments (**Figure 4.2**). UL148 and UL148D possible localisation to the ER is an important finding with regard to identifying ADAM17 downregulation mechanisms, since ADAM17 is known to undergo a wide range of processing events in the ER before maturing and becoming expressed on the cell surface.
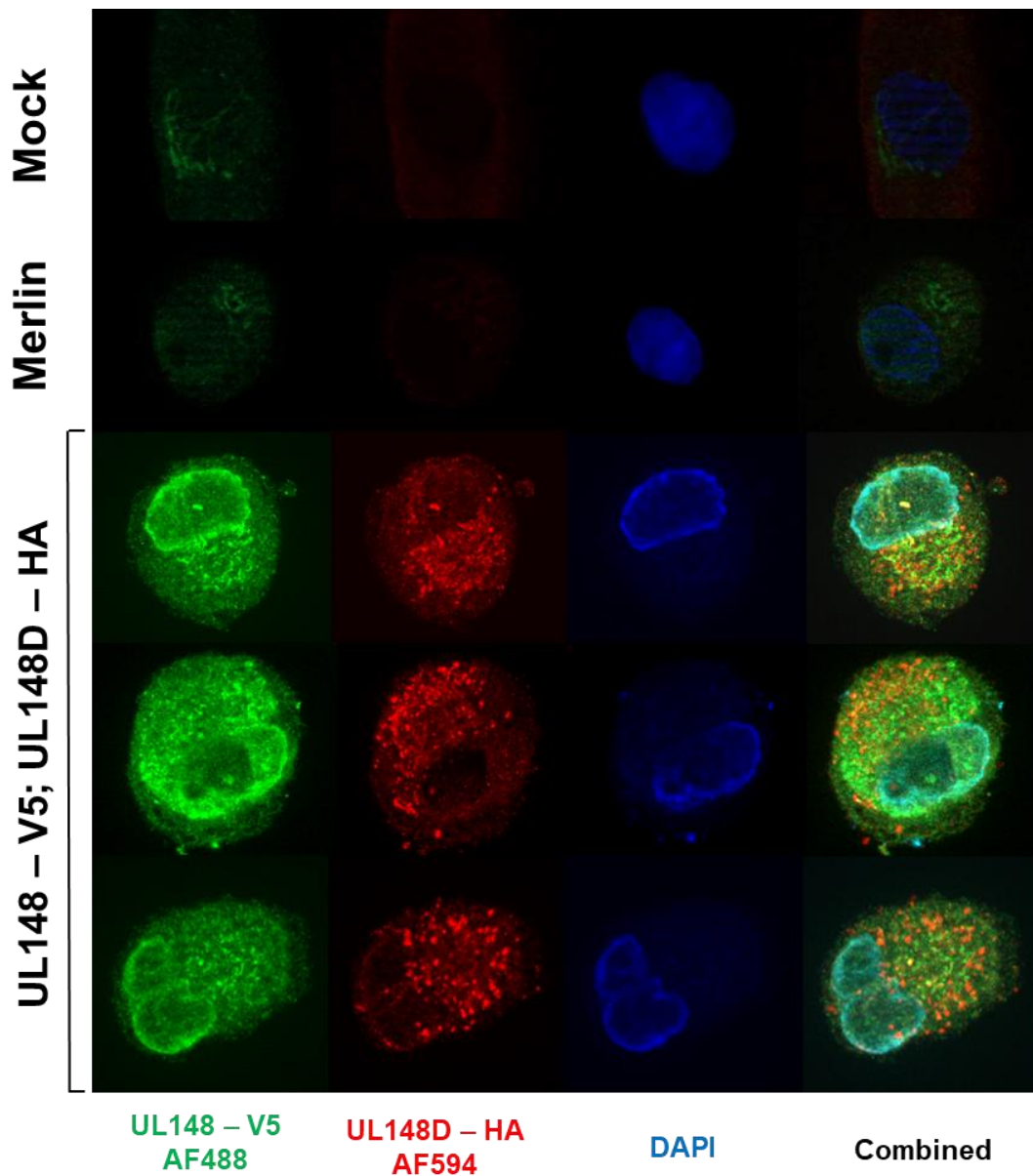
Figure 4.1: UL148 and UL148D immunofluorescence on HCMV-infected HF-TERT cells 48 hpi. Cells were infected with Mock, Merlin or double tagged UL148-V5 and UL148D-HA HCMV (MOI = 5) and 48 hpi were fixed, permeabilised and stained for DNA (405 nm), UL148-V5 (488 nm) and UL148D-HA (594 nm). Zeiss microscope (Axio Observer Z1) was used with the Apotome function to collect the images. A magnification of x63 was used. Images were processed using ImageJ software.
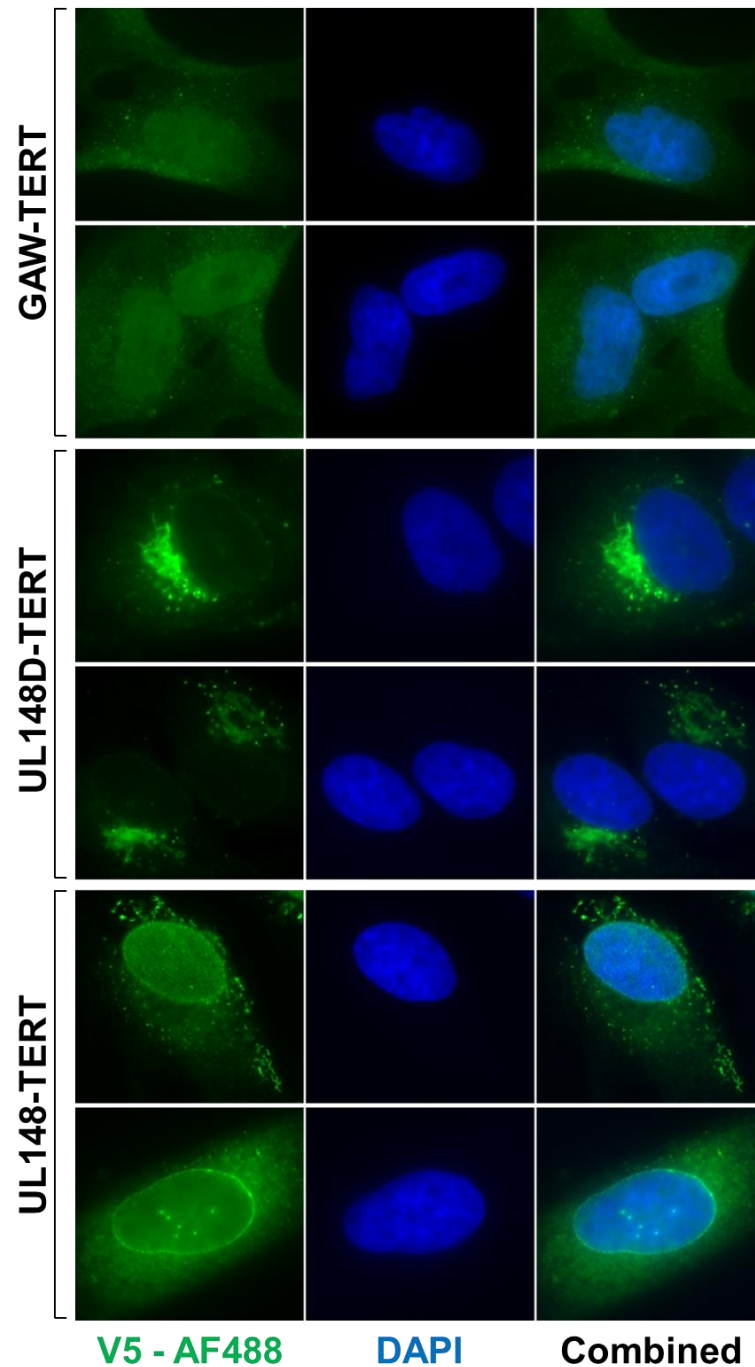
Figure 4.2: UL148 and UL148D immunofluorescence on lentivirus transfected HF-TERT cells that stably express V5-tagged UL148 or UL148D. Cells were fixed, permeabilised and stained for DNA (405 nm) and V5 corresponding to either UL148 or UL148D (488 nm). GAW-TERT cell line was used as an appropriate control for lentivirus transfected cell lines. Zeiss microscope (Axio Observer Z1) was used with the Apotome function to collect the images. A magnification of x63 was used. Images were processed using ImageJ software.

4.2.2 Characterising the expression of UL148 and UL148D by immunoblotting

To further explore localisation and trafficking of UL148 and UL148D, EndoH and PNGaseF assays were performed to assess the level of glycosylation of these proteins. EndoH sensitivity is an attribute of immature proteins still present in the ER, whereas EndoH resistance suggests protein maturity. PNGaseF cleaves nearly all N-linked glycans (Freeze and Kranz 2010).

UL148 was sensitive to EndoH digestion suggesting ER-residence, whereas UL148D was resistant to both EndoH digestion and PNGaseF digestion, suggesting that UL148D is not glycosylated (**Figure 4.3**).

In addition, total UL148 and UL148D protein expression was assessed over the course of HCMV infection using WCL to further characterise these viral proteins. Immunoblotting analysis demonstrated low levels of UL148 24 hpi, followed by a dramatic increase in protein levels 48 hpi. In contrast, UL148D retained comparable levels of expression over the course of the experiment (**Figure 4.3**).
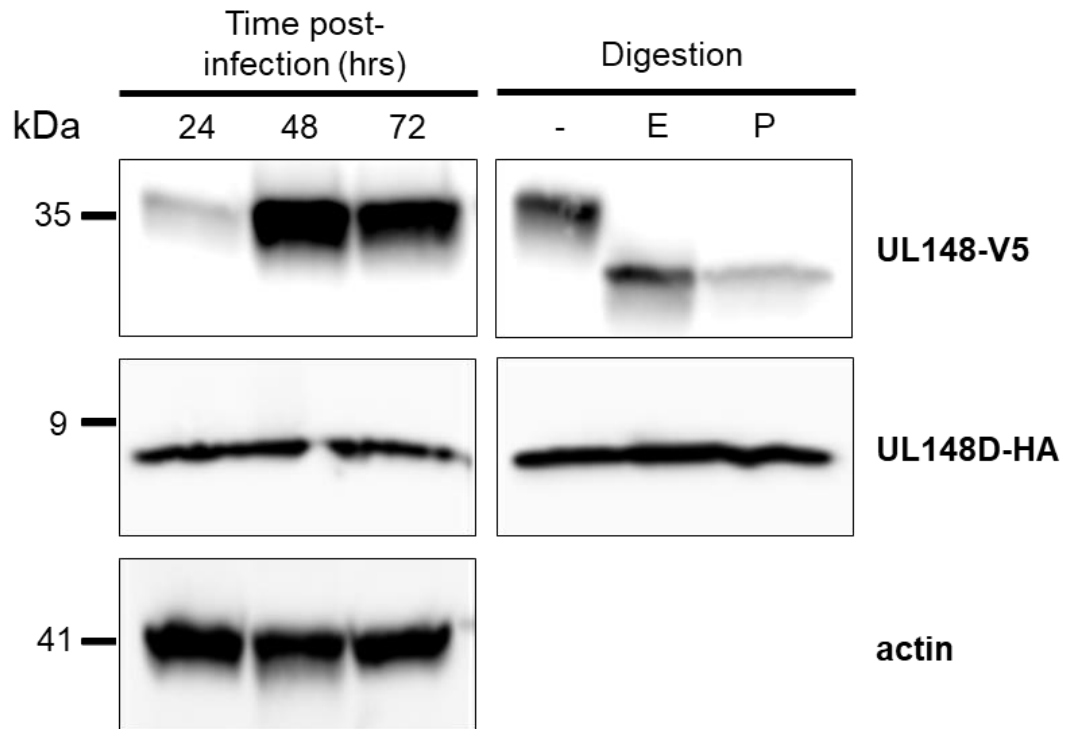
Figure 4.3: Levels of UL148-V5 and UL148D-HA 24, 48 and 72 hpi with HCMV and assessment of their glycosylation state. HF-TERT cells were infected with either Merlin or double tagged UL148-V5 and UL148D-HA HCMV (MOI = 5) and lysed at 24, 48 and 72 hpi. EndoH and PNGaseF digests were performed on 72 hpi lysates to determine the glycosylation state of proteins. Immunoblotting was performed against V5 and HA tags, representing UL148 and UL148D, respectively, as well as actin control.

4.2.3 Exploring the UL148 and UL148D interactome data set

To identify the mechanism of ADAM17 downregulation, I first wanted to investigate the proteins with which UL148 and UL148D interact. Dr Mihil Patel had already shown that UL148 and UL148D do not bind ADAM17 directly by performing IP on lentivirus transfected HF-TERTs that stably express V5-tagged UL148 or UL148D and staining for ADAM17 (Patel 2018). This suggested a more complex, indirect viral strategy of ADAM17 inhibition, potentially involving other proteins.

To identify potential proteins involved in UL148- and UL148D-driven ADAM17 impairment a HCMV IP-interactome MS dataset was used. Nobre et al. (2019) performed IP screens on each individual HCMV protein, producing an interactome of viral and host proteins. This IP screen recapitulated Dr Patel's data showing no direct binding between either viral protein and host ADAM17, consistent with the idea of an indirect and more complex mechanism behind ADAM17 inhibition. To explore this further, protein hits from the proteomics IP-interactome dataset were selected for validation in lentivirus transfected UL148-V5 and UL148D-V5 expressing HF-TERTs (**Table 4.1**). Selected hits were chosen either on the basis of their function described in the literature, and/or their Normalized Weight D (NWD) score. In interactome analysis, NWD score is an improvement on the Z score – a traditional statistical measurement of standard deviations from the mean of a group of samples. The Z score is calculated independently of the abundance of interactors, and as a result it cannot discriminate between low and high abundance interactors. To compensate for this, the NWD score takes into account interactor abundance, as well as the frequency and reproducibility of the interaction of each IP. As a result, interactors with high NWD scores fit the description of a potentially promising candidate worth following-up with further validation.

I selected Rhomboid domain containing 1 (RHBDD1) and Phospholipase C gamma 2 (PLCG2) on the basis of NWD score and functional relevance as potential UL148 interactors. Crk-like protein (CRKL) and Nexilin were chosen

as potential UL148D interactors due to their function, together with SerpinB5 which demonstrated a high NWD score of over 11 (**Table 4.1**).

Table 4.1: Hits from the Nobre et al. (2019) interactome-IP dataset chosen for validation in HF-TERTs and their function in literature.

Bait	*Protein*	*Function*	*NWD Score*
UL148	PLCG2	Regulates integrin-mediated adhesion and migration of iPSC-derived macrophages; associated with the inflammatory response in Alzheimer's disease (Obst et al. 2021; Tsai et al. 2022)	3.160
UL148	RHBDD1	Related to the ADAM17 chaperone proteins iRhom1 and iRhom2 and involved in ER-associated protein degradation (Fleig et al. 2012)	10.906
UL148D	CRKL	Crk proteins mediate signal transduction in tyrosine kinase signalling, hence playing a central role in many biological cellular processes ranging from proliferation to immune regulation (Birge et al. 2009)	0.859
UL148D	Nexilin	Actin-binding protein that plays a role in cell adhesion and migration (Liu et al. 2019)	2.049
UL148D	SerpinB5	A non-inhibitory serine protease, the exact function of which is unknown. Interacts with diverse proteins that are involved in the cellular stress response pathway, including several transcription factors (Tamazato Longhi et al. 2016)	11.739

4.2.4 Validating UL148 and UL148D IP-interactome hits

Lentivirus transfected HF-TERTs expressing V5-tagged UL148 or UL148D were used to validate selected IP-interactome hits. Surface ADAM17 staining was performed to ensure the introduced proteins were still functional (**Figure 4.4 A**). These results were consistent with previous data generated by Dr Patel, where he infected HF-CAR cells with UL148 and UL148D expressing RAds and observed ADAM17 downregulation in the presence of these HCMV genes (**Figure 4.4 B**).

To begin checking the validity of the selected interactome hits, cells were first studied for expression of the proteins by immunoblotting. SerpinB5, CRKL and PLCG2 proteins were not detected in HF-TERTs, but were present in other cell lines, such as K-562, 293T and HT-29 (**Figure 4.5 A**). In contrast, Nexilin and RHBDD1 were found in HF-TERTs (**Figure 4.5 B, WCL**). RHBDD1 was of particular interest, because it is related to the ADAM17 chaperone proteins iRhom1 and iRhom2 and is involved in ERAD and could therefore be co-opted to degrade ADAM17 (Fleig et al. 2012).

In order to test their capacity to bind UL148 or UL148D, I used the same experimental conditions that were used to generate the published interactome dataset (Nobre et al. 2019), where HCMV infection in addition to lentiviral expression was used in case other viral components were necessary for interactions to take place. The GAW cell line was used as a negative control cell line for lentivirus transfected cells. V5 Co-IP were performed on the lysates following immunoblotting for RHBDD1 and Nexilin, however no binding between UL148 and RHBDD1 or UL148D and Nexilin was observed (**Figure 4.5 B**). Both RHBDD1 and Nexilin were present in the input samples, but not in the V5 Co-IP samples.

In summary, I followed up five proposed interactors for UL148 and UL148D in pursuit of the underlying mechanism involved in ADAM17 downregulation during HCMV infection. Three were not detected at high enough

concentrations in the fibroblast line for further study, while the other two did not validate the IP-interactome data.
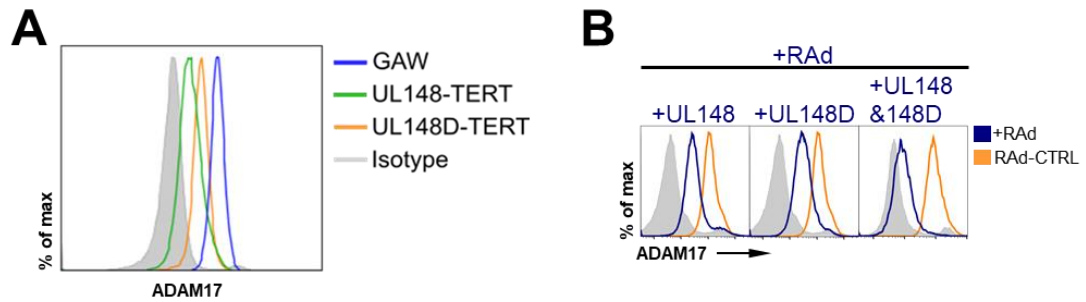
Figure 4.4: Surface ADAM17 levels are downregulated in the presence of UL148 and UL148D. (A) Surface ADAM17 levels in UL148-expressing and UL148D-expressing HF-TERTs compared to a control cell line GAW. Cell lines were stained with primary ADAM17 antibody and secondary anti-mouse AF647, as well as the isotype control IgG. X-axis values were normalised to mode. **(B)** Dr Patel's flow cytometric histograms showing surface ADAM17 following single and combined expression of UL148 and UL148D using RAd in HF-CARs (Patel 2018).
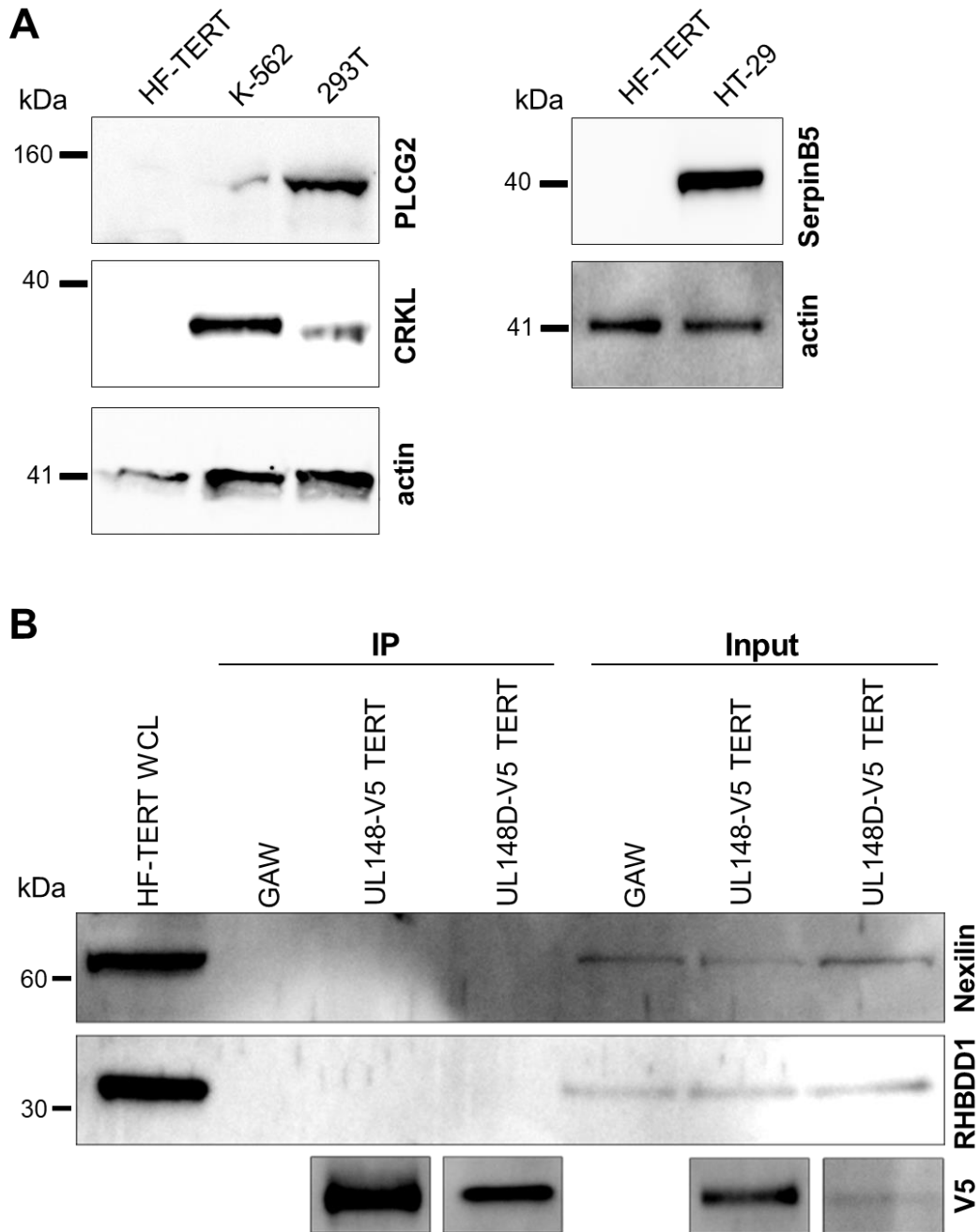
Figure 4.5: Validation of selected IP-interactome hits. (A) Immunoblotting of PLCG2 and CRKL on HF-TERT, K-562 and 293T cell lysates and Serpin B5 on HF-TERT and HT-29 cell lysates. **(B)** Immunoblotting of RHBDD1 and Nexilin in UL148 and UL148D Co-V5 IP. UL148 and UL148D expressing HF-TERTs were infected with WT HCMV (MOI = 5) and at 72 hpi cells were lysed, immunoprecipitated with V5 beads and analysed via immunoblotting. GAW cell line was used as a negative control. Inputs represent cell lysates that were not treated with V5 beads, WCL of HF-TERT cells was used as a positive control for staining.

4.2.5 Candidate approach in identifying ADAM17 downregulation mechanism

Due to its central role in many essential cellular processes, the activity of ADAM17 is tightly regulated by a range of proteins that control ADAM17 processing and trafficking (**Section 1.4.1.2**). Since UL148/UL148D IP-interactome MS dataset failed to identify proteins involved in HCMV-driven ADAM17 abolishment, a candidate approach was employed where known ADAM17 regulators were validated in the context of HCMV infection. Dr Patel has previously tested four proteins known to be involved in ADAM17 regulation in an attempt to identify the mechanism of UL148/UL148D-driven ADAM17 downregulation. He demonstrated that three ADAM17 traffickers – PACS2, iRhom1 and iRhom2, as well as iRhom1/2 adaptor protein FRMD8 were not involved in UL148- and UL148D-driven ADAM17 abolishment. To follow up, I investigated the role of two additional proteins known to play a role in ADAM17 processing and regulation – PACS1 and Furin. Furin is a protease regulated by PACS1 which cleaves pro-ADAM17 into its mature and active form (Wan et al. 1998; Gooz 2010). Furin immunoblotting demonstrated no changes in protein levels following Merlin and dKO infection compared to Mock control. In contrast, PACS1 levels dropped dramatically in HCMV infected cells compared to the Mock control, however the level of protein expression did not recover in dKO infection (**Figure 4.6 A**). To investigate further, lysates were made from HF-CARs infected with indicated HCMV strain and RAds expressing UL148 and UL148D, following immunoblotting for PACS1 (**Figure 4.6 B**). PACS1 immunoblotting in the context of HCMV infection confirmed that Merlin infection resulted in reduced PACS1 levels compared to the Mock control. This was shown to be independent of UL148 and/or UL148D as no change in PACS1 levels was observed in ΔUL148/ΔUL148D single and double HCMV infections. Furthermore, infections with UL148 and UL148D expressing RAds demonstrated the same level of PACS1 expression compared to a control RAd infection, confirming that PACS1 downregulation observed in HCMV infection is independent of UL148 and UL148D (**Figure 4.6 B**).
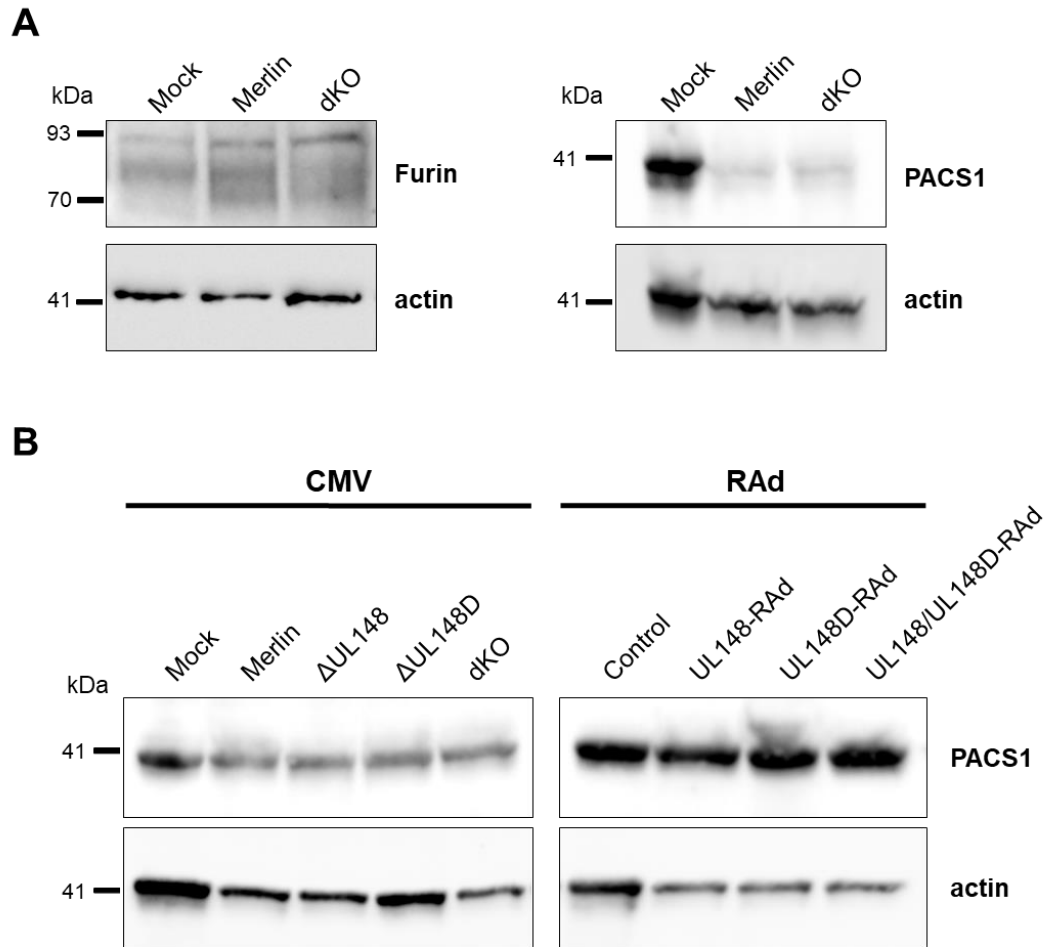
Figure 4.6: Exploring the role of potential candidates in HCMV-driven ADAM17 downregulation. (A) Immunoblotting of WCL Furin and PACS1 in the context of HCMV infection. For Furin immunoblotting lysates were made from HCMV infected HF-TERTs 72 hpi (MOI = 5). For PACS1 immunoblotting lysates were made from HCMV infected HF-CARs 72 hpi (MOI = 5). **(B)** PACS1 immunoblotting in the context of HCMV and RAd infections 72hpi. HF-CARs were infected with indicated HCMV strains (MOI = 5) and RAds (MOI = 10).

4.3 Effect of UL148 and UL148D on ADAM17 processing

4.3.1 ConA-enrichment of cell lysates for ADAM17 Western blotting

One of the ways ADAM17 processing is regulated is through glycosylation – addition or removal of certain glycans to or from the protein. As a result of glycosylation, immunoblotting results in multiple forms of ADAM17 that differ in their molecular weight (mwt) due to the presence or absence of glycans: ~120 kDa, ~95 kDa and ~70 kDa (Schlöndorff et al. 2000; Oikonomidi et al. 2018). In particular, fibroblasts have an abundance of a deglycosylated form of ADAM17 (~70 kDa) which gives the strongest ADAM17 signal in immunoblotting. The strength of this signal masks the signals from glycosylated forms of the protein (**Figure 4.7 B**). In order to resolve this, the signal from the deglycosylated form of ADAM17 can be removed by a ConA enrichment step (Oikonomidi et al. 2018). The ConA enrichment procedure was optimised to achieve clean glycosylated ADAM17 immunoblotting results, enabling study of the changes in glycosylated forms of ADAM17 (**Figure 4.7 A**).
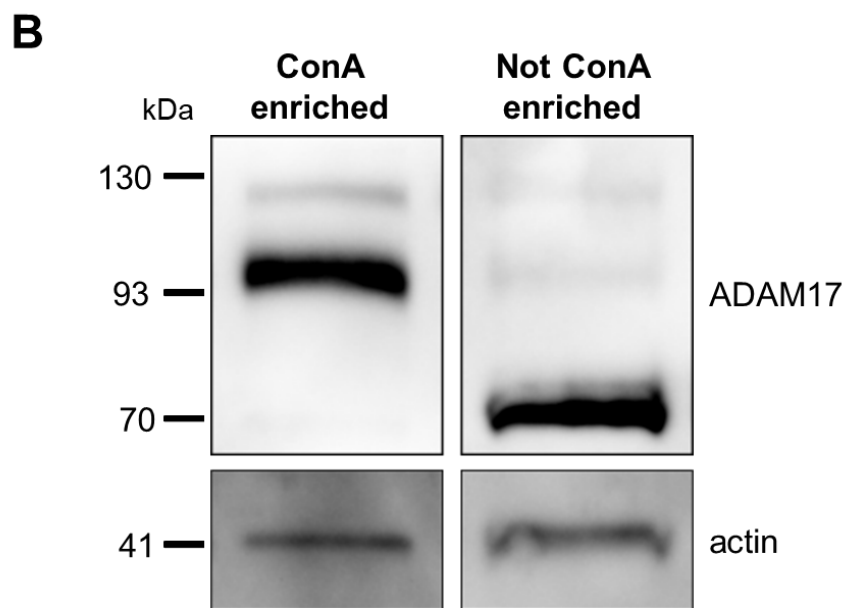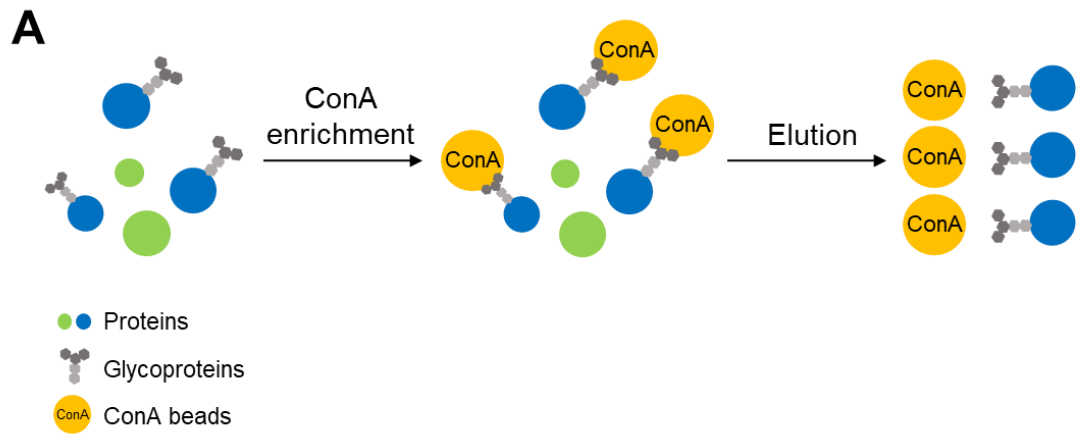
Figure 4.7: ConA enrichment of cellular lysates. (A) A schematic diagram of ConA-enrichment procedure to remove deglycosylated proteins from the lysate. **(B)** Comparison of ADAM17 immunoblotting on HF-TERTs with and without ConA enrichment step.

4.3.2 Analysis of whole cell ADAM17 by Western blotting

HF-TERTs were infected with Mock, Merlin, single and double UL148 and UL148D knockout HCMVs and processed 72 hpi by lysing the cells and performing glycoprotein enrichment using ConA beads, followed by ADAM17 immunoblotting. ADAM17 Western blots demonstrated an increased abundance of a high mwt ~120 kDa, and absence of a low mwt ~95 kDa form of ADAM17 in Merlin-infected HF-TERTs, proposed as immature and mature versions of the protein, respectively (Schlöndorff et al. 2000; Oikonomidi et al. 2018). This pattern was reversed in cells infected with the dKO HCMV variant, suggesting that UL148 and UL148D disrupts ADAM17 maturation/trafficking (**Figure 4.8 A**). This pattern was consistent with many experimental replicates, demonstrating strong evidence for UL148 and UL148D disrupting ADAM17 maturation (**Figure 4.8 B**).

To test whether these high and low mwt ADAM17 forms were indeed immature/mature, I performed EndoH and PNGaseF sensitivity assays. The high mwt form of ADAM17 (~120 kDa) was EndoH sensitive indicating its immature state, as demonstrated by the reduction in its mwt to ~97 kDa. The low mwt (~95 kDa) form was EndoH resistant, but PNGaseF sensitive, resulting in a reduction in mwt to ~70 kDa, corresponding to the deglycosylated mature form of ADAM17 (**Figure 4.8 C**).

Merlin-infected HF-TERT cells demonstrated the presence of only the ~120 kDa immature form of ADAM17, confirmed by EndoH sensitivity. Infections with single knockout HCMVs partially recovered the mature ~95 kDa form of ADAM17. However, dKO HCMV infection resulted in the rescue of mature ADAM17, comparable to the levels of mature ADAM17 found in Mock infection. This demonstrated that UL148 and UL148D interfere with ADAM17 maturation, which results in accumulation of the immature, and reduction of the mature, form of the protein.
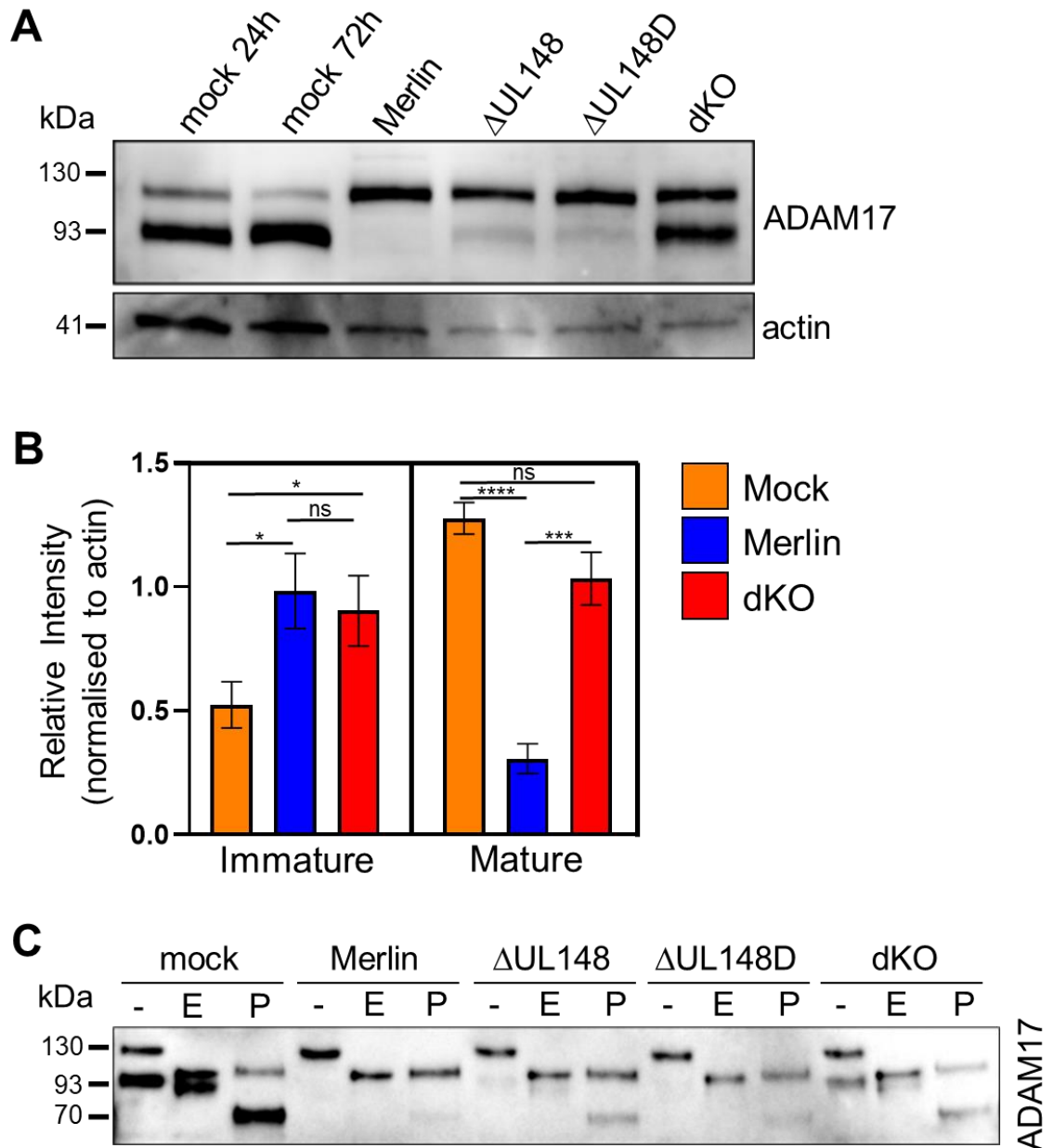
Figure 4.8. Whole cell ADAM17 biology. (A) ADAM17 levels in Mock and HCMV-infected (MOI = 5) HF-TERTs 72 hpi in ConA enriched samples. ConA enrichment successfully removed deglycosylated ADAM17 version, resulting in easier interpretation of the changes in glycosylated low mwt (~95 kDa) and high mwt (~120 kDa) ADAM17. **(B)** Relative intensity of ADAM17 staining (mature and immature forms) generated from six independent experiments, measured in ImageJ software and normalised to actin control levels. **(C)** EndoH and PNGaseF digests of HF-TERT lysates from cells infected with Mock or indicated HCMV mutant (MOI = 5) 72 hpi.

4.3.3 ADAM17 immunofluorescence during HCMV infection

Immature ADAM17 is known to be ER-resident, hence the accumulation of the immature form of the protein by HCMV is likely to be observed through immunofluorescence of ADAM17. Immunofluorescence of viral UL148 and UL148D described in **Section 4.2.1**, suggested that both proteins were probably ER-resident localising to different ER compartments. EndoH and PNGaseF digests of UL148 and UL148D (**Section 4.2.2**) further validated UL148 residence to the ER, however due to the deglycosylated status of UL148D, its localisation to the ER was not confirmed. Nevertheless, the ER is known to be a location where maturation and processing of ADAM17 occurs. To explore this further, I performed ADAM17 immunofluorescence to test for colocalization with the viral proteins, using lentivirus transfected HF-TERTs expressing V5-tagged UL148 or UL148D, with and without HCMV infection. I also used standard HF-TERTs to study changes in ADAM17 localisation following HCMV infection in an attempt to further inform on the immunoblotting results in an immunofluorescence setting.

ADAM17 immunofluorescence proved to be challenging and inconclusive, however it provided some insights into the mechanism of UL148 and UL148D-driven ADAM17 downregulation. Immunofluorescence was performed on Mock- (**Figure 4.9**) or Merlin-infected (**Figure 4.10**) V5-tagged UL148 or UL148D HF-TERTs. Cells were stained for the V5 tag corresponding to either UL148 or UL148D and ADAM17. No colocalization was observed between either UL148 or UL148D and ADAM17 in the presence or absence of HCMV infection, however this was not unexpected since ADAM17 did not come down in the IP-interactome dataset (Nobre et al. 2019), and Dr Patel failed to observe ADAM17 binding to UL148/UL148D in V5 Co-IP experiments. Nevertheless, changes in ADAM17 localisation were observed between treatments, in particular that Mock-infected cells demonstrated a dispersed ADAM17 expression across the cytoplasm, whereas HCMV-infected cells showed ADAM17 mostly localised in what possibly looks like the AC (**Figures 4.10**). To better understand the involvement of UL148 and UL148D in this

process, an experiment with ordinary HF-TERTs infected with Mock, Merlin, single and double UL148 and UL148D knockout viruses was performed, staining for ADAM17. A similar phenotype was observed in Merlin and single knockout viruses, i.e. possible ADAM17 localisation to the AC. The dKO treatment resulted in a more dispersed ADAM17 pattern, however it was difficult to interpret and compare results due to the rounding up of HCMV-infected cells (**Figure 4.11**).

In summary, ADAM17 immunofluorescence further pointed to events in the ER as being important for ADAM17 downregulation by HCMV UL148 and UL148D. Hence, I chose to investigate if HCMV UL148 and UL148D targeted ER-associated processes to downregulate ADAM17.
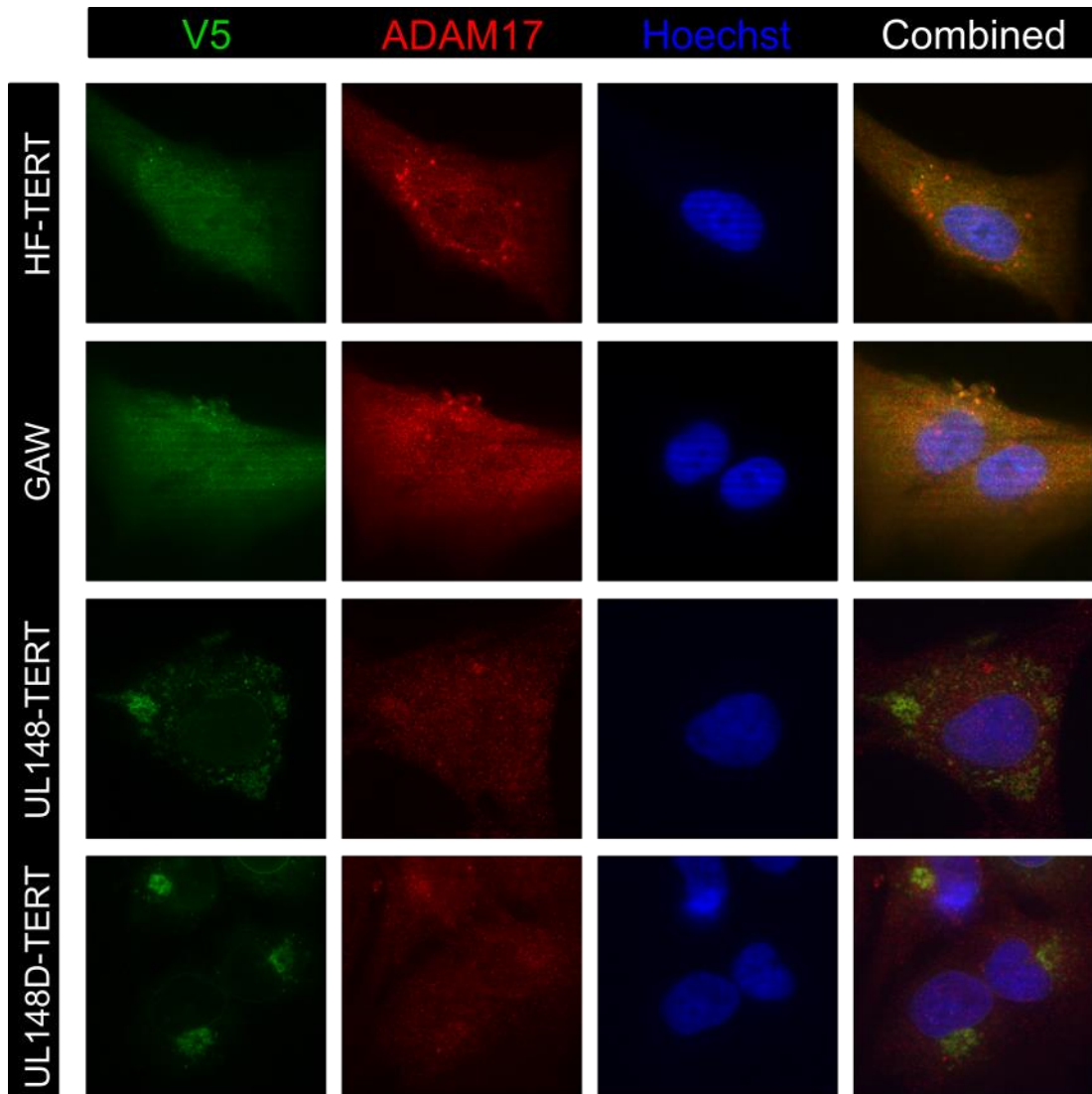
Figure 4.9. HF-TERT, GAW, UL148-V5 HF-TERT and UL148D-V5 HF-TERT immunofluorescence. Cells were fixed, permeabilised and stained for V5 (488 nm), ADAM17 (594 nm) and DNA (405 nm). Zeiss microscope (Axio Observer Z1) was used with the Apotome function to collect the images. A magnification of x63 was used. Images were processed using ImageJ software.
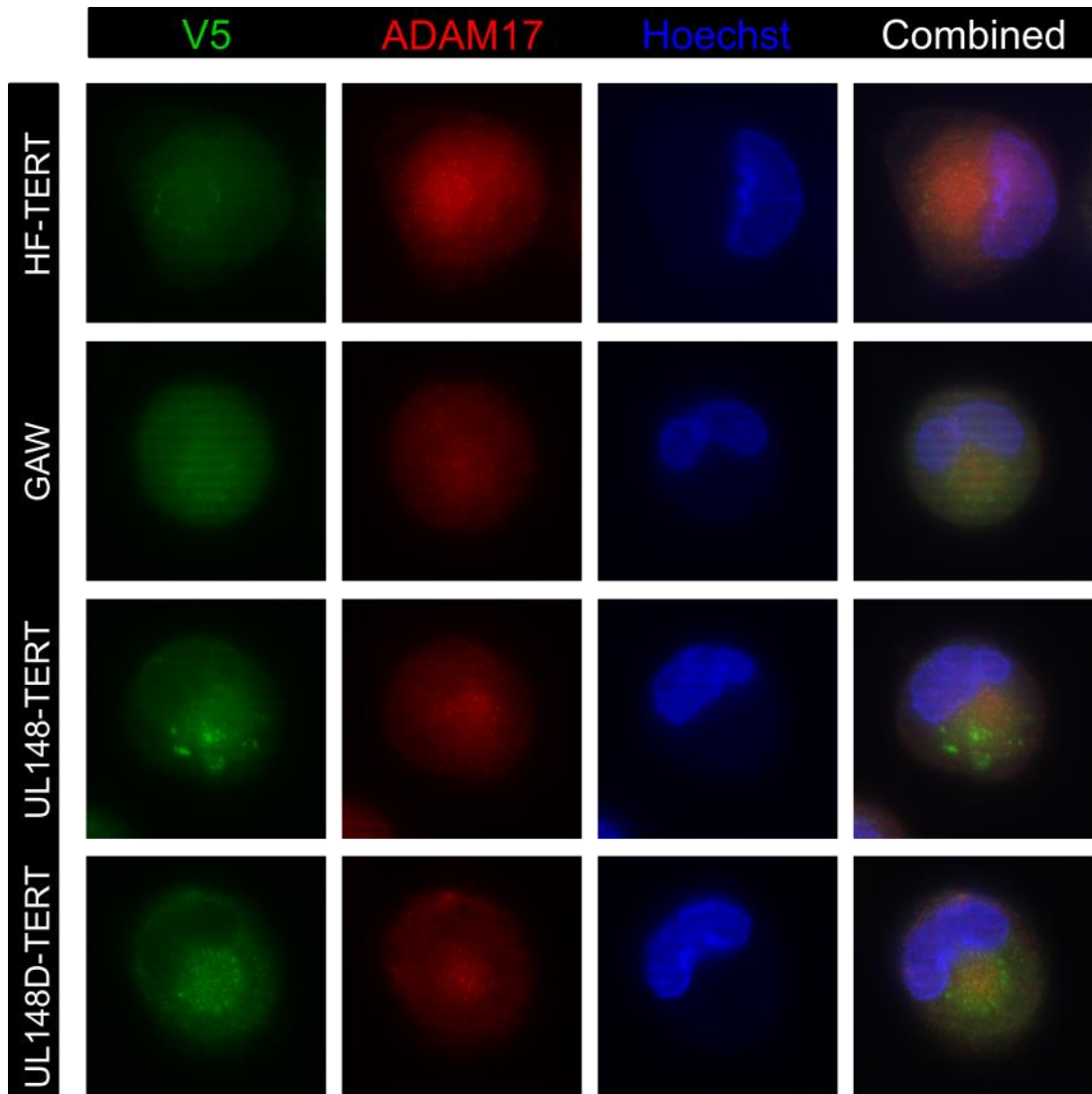
Figure 4.10. HF-TERT, GAW, UL148-V5 HF-TERT and UL148D-V5 HF-TERT immunofluorescence in the context of HCMV infection. Merlin-infected (MOI = 5) HF-TERT, GAW, UL148-V5/UL148D-V5 HF-TERT cells were fixed, permeabilised and stained for V5 (488 nm), ADAM17 (594 nm) and DNA (405 nm) 72 hpi. Zeiss microscope (Axio Observer Z1) was used with the Apotome function to collect the images. A magnification of x63 was used. Images were processed using ImageJ software.
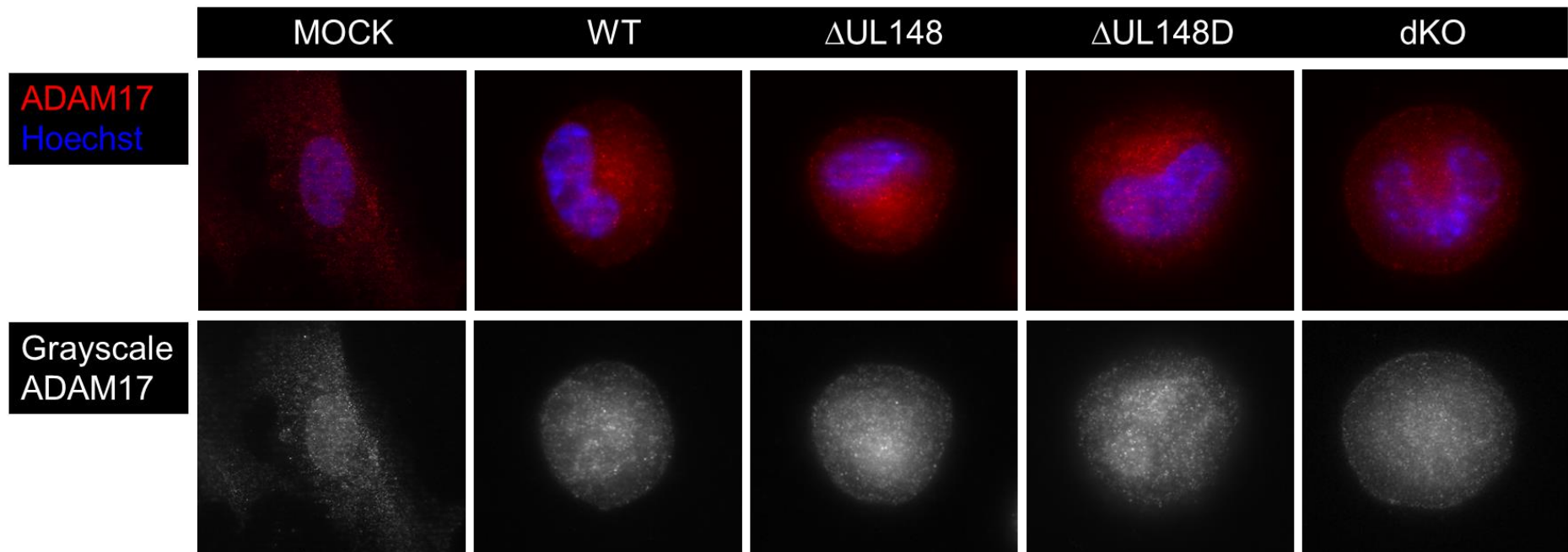
Figure 4.11. ADAM17 immunofluorescence following infection with HCMV deletion mutants. HF-TERTs were infected with Mock, Merlin, ΔUL148, ΔUL148D and dKO viruses (MOI = 5). After 72 hpi cells were fixed, permeabilised and stained for DNA (405 nm) and ADAM17 (594 nm). ADAM17 signal is also presented in grayscale for easier interpretation. Zeiss microscope (Axio Observer Z1) was used with the Apotome function to collect the images. A magnification of x63 was used. Images were processed using ImageJ software.

4.4 ER-mediated mechanism of UL148- and UL148D-driven ADAM17 downregulation

The ER is a multifunctional organelle and a major site of protein synthesis, folding, modification and transport. To ensure that only correctly folded and modified proteins leave the ER to fulfil their function, ERAD detects aggregated and misfolded proteins and targets them for proteasomal degradation. UL148 has been shown to upregulate ER-stress inducing proteins, resulting in activation of the ERAD machinery (Siddiquey et al. 2018). In addition, UL148 is also known to interact with the ERAD machinery by binding to Suppressor/Enhancer of Lin-12-like (SEL1L) protein involved in regulating ERAD (Nguyen et al. 2018). IP-interactome data described in **Section 4.2.3** identified RHBDD1 as a potential UL148 interactor, which is known to regulate ERAD processes, similarly to SEL1L. Although RHBDD1 immunoblotting failed to validate the UL148 IP-interactome result (**Section 4.2.4**), it may be explained by the high sensitivity of MS. If the interaction between RHBDD1 and UL148 is weak, immunoblotting might not detect it, however MS being a highly sensitive method capable of detecting a single peptide, may identify the interaction. Hence, I hypothesised that UL148 and UL148D utilise ERAD machinery to target ADAM17 for degradation, resulting in its downregulation from the cell surface and accumulation of the immature form of ADAM17.

4.4.1 Investigating the involvement of the ERAD pathway in ADAM17 downregulation using Eeyarestatin I

To test the involvement of ERAD in ADAM17 downregulation, I performed an ERAD inhibition assay using a common, chemical ERAD inhibitor Eeyarestatin I (EerI), which targets p97-associated deubiquitinating enzymes and prevents the translocation of polyubiquitinated misfolded proteins into the cytosol for degradation in the proteasomes (Fiebiger et al. 2004). HF-TERTs were treated with 5 µM EerI and infected with Mock, Merlin, ΔUL148, ΔUL148D and dKO

HCMV, following by sample processing 18 hpi. Inhibition of ERAD with EerI resulted in the recovery of the mature form of ADAM17 (~95 kDa) in Merlin, ΔUL148 and ΔUL148D HCMV-infected cells, suggesting that UL148 and UL148D inhibit ADAM17 by utilising cellular ERAD machinery (**Figure 4.12 A**). To attribute the recovery of mature ADAM17 in Merlin-infected cells to ERAD inhibition, I investigated whether the presence of EerI affected HCMV infection by staining for an early HCMV gene IE1. IE1 was detected across all HCMV-infected groups regardless of EerI treatment, however EerI-treated cells had 3x less IE1 in their lysates compared to control treatment. This was later attributed to loading 3x less protein to the SDS-PAGE of EerI-treated lysates compared to control lysates, as demonstrated by control lysates having 3x more actin compared to EerI-treated samples (**Figure 4.12 B**). Hence, EerI treatment did not interfere with HCMV infection and the observed ADAM17 recovery in Merlin-infected cells was likely to be real.

To further validate this result, levels of UL148 and UL148D in the presence of EerI were tested by performing an ERAD inhibition assay on HF-TERTs infected with double tagged UL148-V5 and UL148D-HA HCMV and immunoblotting for V5 and HA tags. However, both UL148 and UL148D showed reduced levels in the presence of EerI in comparison to the control treatment (**Figure 4.12 C**). There is no obvious explanation to why levels of UL148 and UL148D decrease so dramatically in the presence of EerI, however inhibition of such important cellular mechanism as ERAD is likely to have consequences on other processes beyond ERAD inhibition. EerI treatment has been shown to cause cytotoxicity, increase ER stress and induce apoptosis, all of which may explain the reduced levels of UL148 and UL148D (Wang et al. 2011). To provide more insight into the effect of EerI treatment on ADAM17 in HCMV infection, I looked at surface ADAM17 by flow cytometry.
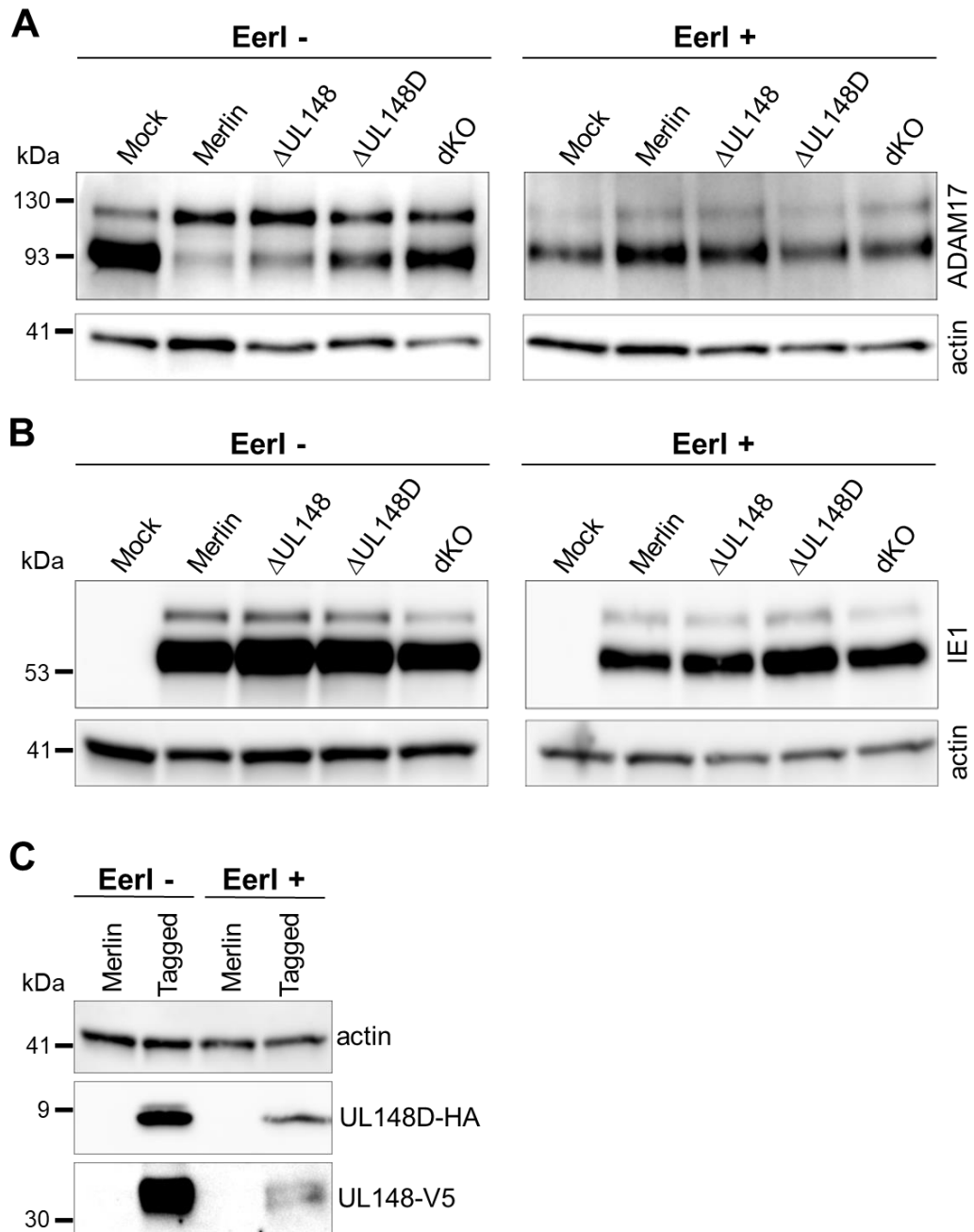
Figure 4.12. Assessing the effects of ERAD inhibition using EerI on a whole cell level. HF-TERTs were pre-treated with EerI or DMSO control, and infected with Mock, Merlin, ΔUL148, ΔUL148D and dKO HCMV (MOI = 5) for 18 hrs. **(A)** Immunoblotting of ConA enriched whole cell ADAM17 in the presence and absence of EerI treatment. **(B)** Immunoblotting of IE1 in the presence and absence of EerI treatment. **(C)** Immunoblotting of UL148-V5 and UL148D-HA in the presence and absence of EerI treatment. HF-TERTs were pre-treated with EerI or DMSO control and infected with Merlin or UL148-V5/UL148D-HA tagged HCMV (MOI = 5) and lysates were harvested 18 hpi.

4.4.2 Assessing the effect of Eeyarestatin I on surface ADAM17

Similar to the immunoblotting procedure, HF-TERTs were treated with 5 μM EerI and infected with Mock, Merlin and dKO HCMV, followed by cell staining for surface ADAM17 18 hpi. As expected, surface ADAM17 was downregulated on Merlin-infected cells and recovered in the dKO-infected cells. EerI-treated group showed similar levels of surface ADAM17 expression across all treatments, in agreements with the immunoblotting results (**Figure 4.13 A**).

Nevertheless, performing flow cytometry using EerI has proven to be problematic, hence the results generated must be interpreted with caution. The addition of EerI resulted in a significant shift in isotype staining compared to the control group (**Figure 4.13 B**). Furthermore, EerI treatment resulted in a strong autofluorescence signal in the BV510 channel in unstained cells (**Figure 4.13 B**), which spilled over into other channels across blue, violet and yellow lasers. Hence, I was unable to use any of the viability dyes routinely used in our laboratory, since they were all excited by the blue, violet or yellow lasers. The red laser was already occupied by ADAM17 staining, since there was no spill over observed from the EerI treatment in the APC channel. Hence, it is important to note that the results for surface ADAM17 staining in EerI-treated cells were generated and analysed without a viability dye and live cells were gated based purely on their location on the side and forward scatter.

In summary, EerI treatment resulted in the rescue of the mature form of ADAM17, as well as the recovery of surface ADAM17, however ERAD inhibition by EerI had significant consequences to the cells. EerI resulted in reduced levels of UL148 and UL148D, as well as issues in performing flow cytometry.
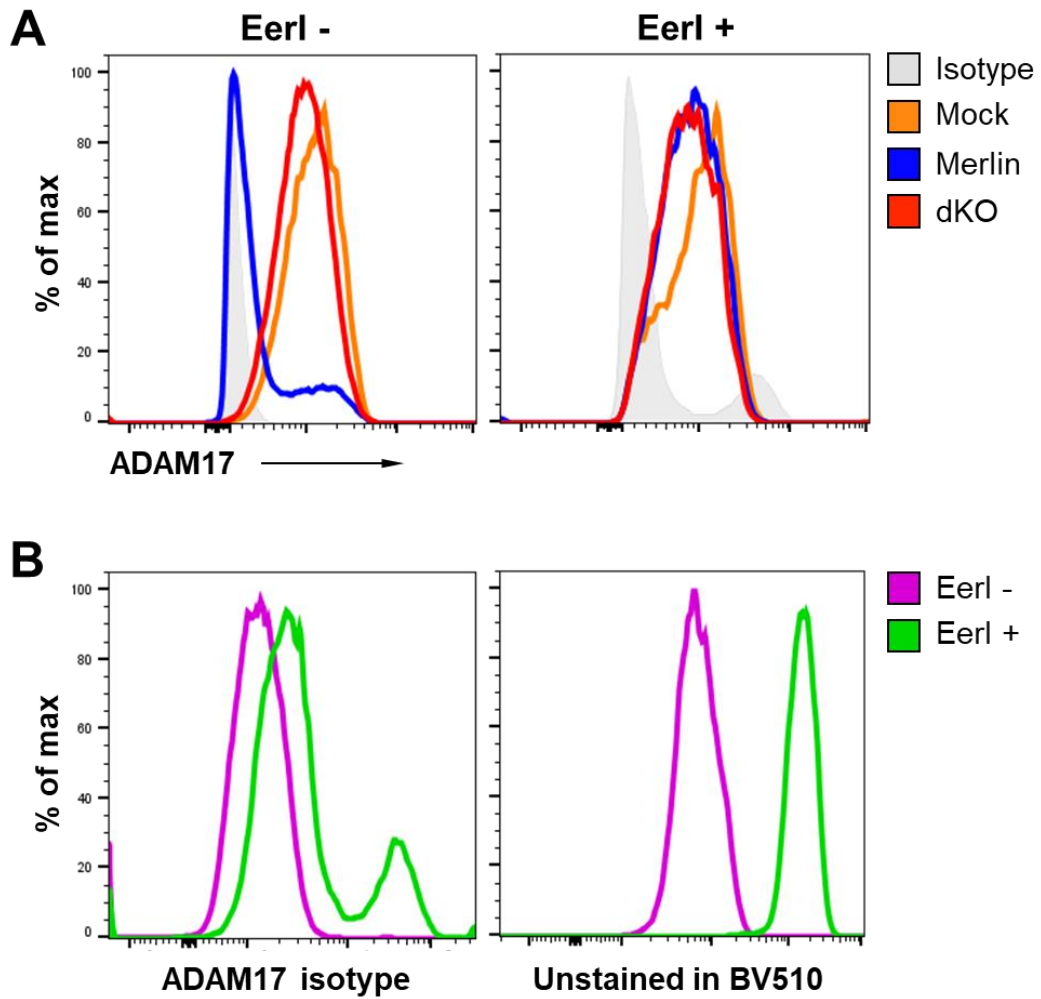
Figure 4.13. Assessing the effects of EerI treatment on surface ADAM17 levels. HF-TERTs were pre-treated with EerI or DMSO control, and infected with Mock, Merlin, or dKO HCMV (MOI = 5) for 18 hrs before staining. Cells were stained for ADAM17, fixed and ran on an Attune NxT Flow Cytometer (Thermo Fisher Scientific). **(A)** Histograms of surface ADAM17 expression in the presence and absence of EerI treatment. **(B)** Histograms representing issues associated with EerI treatment: increased binding of the isotype control and autofluorescence signal in BV510 channel in unstained samples.

4.4.3　Investigating the involvement of the ERAD pathway in ADAM17 downregulation using Kifunensine

Due to the issues associated with the use of EerI, the effect of ERAD inhibition on ADAM17 levels was tested using an alternative chemical inhibitor of the ERAD pathway. Kifunensine (Kif) employs a different mechanism of ERAD inhibition compared to EerI – it interferes with the early recognition of misfolded proteins by inhibiting ER mannosidase I, and causes minimal ER stress and limited cytotoxicity (Fagioli and Sitia 2001; Wang et al. 2011). HF-TERTs were treated with 2.5 µM Kif and infected with Mock, Merlin, single and double UL148 and UL148D knockouts, following by sample processing 18 hpi. No changes were observed between Kif-treated and control samples, with Merlin-infected cells demonstrating an abundance of the immature form of ADAM17 (~120 kDa) even in the presence of Kif. Furthermore, levels of UL148 and UL148D were not affected by Kif treatment and were comparable to the control (**Figure 4.14**). Since Kif-mediated ERAD inhibition resulted in no changes to the levels of ADAM17, UL148 and UL148D, a positive control was needed to ensure that Kif was inhibiting ERAD.

Viral gO was chosen as a positive control to test Kif-induced ERAD inhibition. gO is a heavily glycosylated protein, making it more susceptible for degradation via ERAD, but to impair its degradation, HCMV UL148 stabilises and promotes folding and assembly of gO (Nguyen et al. 2018). Hence, I assessed the levels of gO following Merlin and ΔUL148 HCMV infection in the presence and absence of Kif treatment. HF-TERTs were infected with Mock, Merlin or ΔUL148, following the addition of 2.5 µM Kif at 72 hpi and sample processing at 96 hpi as described in Nguyen et al. (2018). As expected, control samples demonstrated the importance of UL148 in stabilising gO since Merlin infection showed increased amounts of gO in comparison to ΔUL148 infection. The addition of Kif resulted in a further increase of gO levels in both Merlin and ΔUL148 HCMV infections, consistent with Kif treatment inhibiting ERAD (**Figure 4.15 A**). Finally, ADAM17 levels following Mock, Merlin, ΔUL148, ΔUL148D and dKO infections were assessed in the same experimental

setting. Kif-mediated ERAD inhibition failed to show a recovery of the mature form of ADAM17 in Merlin infection (**Figure 4.15 B**), which contradicts results from the EerI-mediated ERAD inhibition.
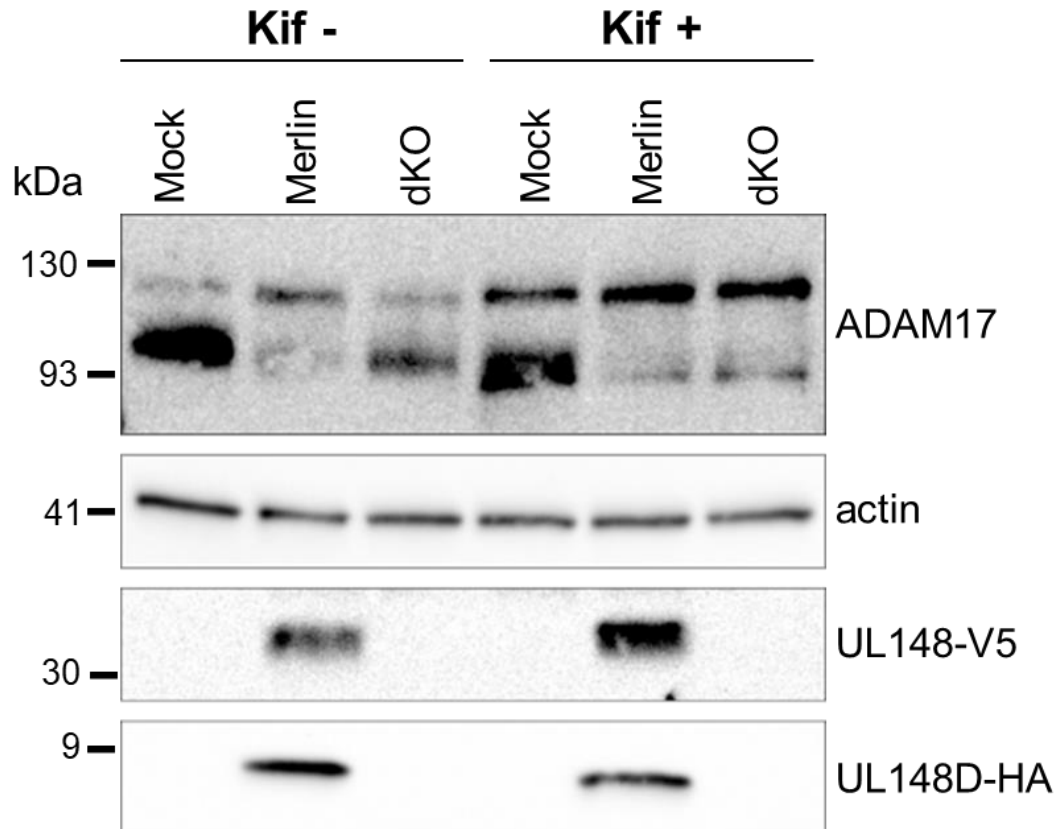
Figure 4.14. Assessing the effects of ERAD inhibition using Kif on a whole cell level. HF-TERTs were pre-treated with Kif or water control, and infected with Mock, Merlin, ΔUL148, ΔUL148D and dKO HCMV (MOI = 5) for 18 hrs. Immunoblotting of ADAM17 in the presence and absence of Kif treatment was performed after ConA enrichment. Actin, UL148-V5 and UL148D-HA immunoblotting was performed on whole cell lysates.
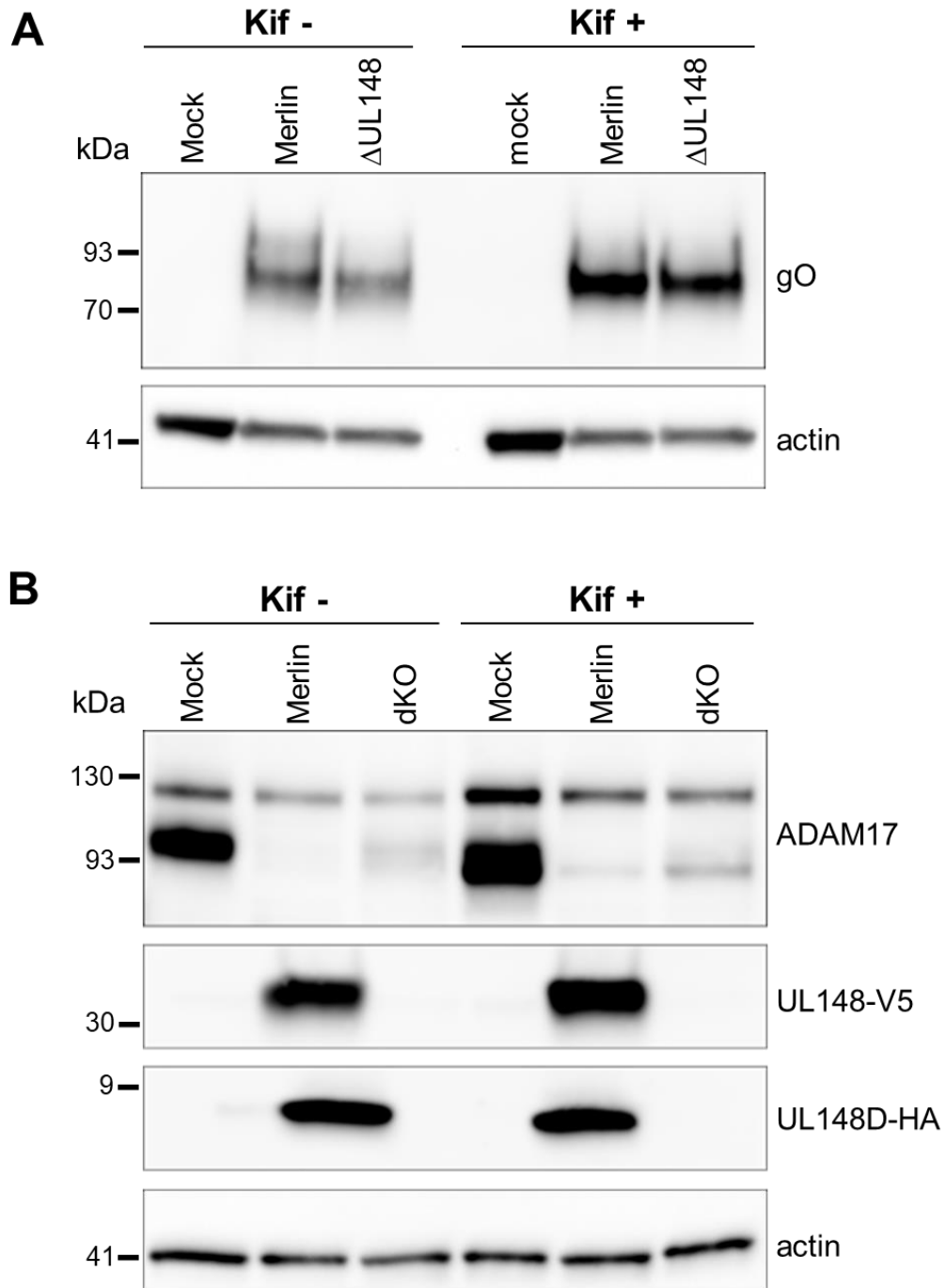
Figure 4.15. ERAD inhibition using Kif following Nguyen et al. (2018) methodology. HF-TERTs were infected with Mock, Merlin or ΔUL148, following the addition of 2.5 µM Kif or water at 72 hpi and sample processing at 96 hpi. **(A)** Immunoblotting of gO in the presence and absence of Kif as a positive control for Kif-mediated ERAD inhibition. **(B)** Immunoblotting of ConA enriched ADAM17 in the presence and absence of Kif treatment, as well as the levels of UL148-V5 and UL148D-HA (Merlin was double tagged with UL148-V5, UL148D-HA).

4.4.4 Assessing the effect of Kifunensine on surface ADAM17

Levels of surface ADAM17 in the presence of Kif were also assessed by flow cytometry. HF-TERTs were treated with 2.5 μM Kif and infected with Mock, Merlin and dKO HCMV, following by cell staining for surface ADAM17 18 hpi. In contrast to EerI treatment, Kif treatment had no effect on autofluorescence or isotype binding, hence a viability dye was included in the analysis.

As expected, the control group showed reduced levels of surface ADAM17 in Merlin-infected cells and an increase in the dKO-infected cells. However, the addition of Kif resulted in no changes to the levels of surface ADAM17, which is in keeping with ADAM17 immunoblotting results for Kif-treated HCMV-infected cells (**Figure 4.16**).
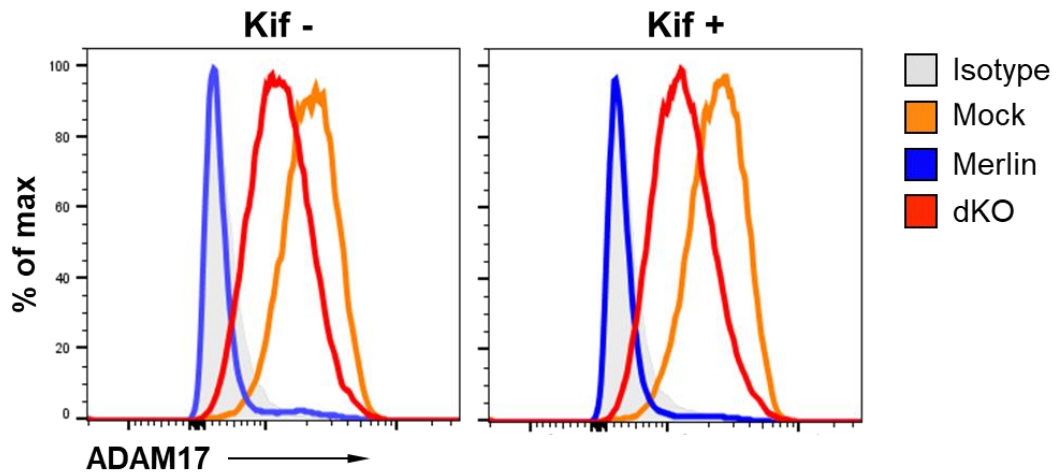
Figure 4.16. Assessing the effects of Kif treatment on surface ADAM17 levels. Histograms represent surface ADAM17 expression in the presence and absence of Kif treatment. HF-TERT cells were pre-treated with Kif or water control, and infected with Mock, Merlin, or dKO HCMV (MOI = 5) for 18 h before staining. Cells were stained for ADAM17, fixed and ran on Attune NxT Flow Cytometer (Thermo Fisher Scientific).

4.4.5 Using RAds to explore EerI- and Kif-mediated ERAD inhibition during ectopic expression of UL148 and UL148D

To explore the differences in results generated by EerI and Kif treatments, I decided to simplify ERAD inhibition assay and remove HCMV infection from the experimental setting. UL148-V5 and UL148D-V5 expressing RAds were used on HF-CARs excluding any other viral components apart from the two viral proteins of interest. HF-CARs were treated with 5 µM EerI or 2.5 µM Kif, infected with Mock, Control RAd and a combination of UL148 and UL148D RAds, following sample processing 18 hpi.

ADAM17 immunoblotting of RAd-infected cells replicated the results observed in HCMV-infected cells. Cells infected with UL148 and UL148D RAds demonstrated a recovery of mature ADAM17 (~95 kDa) in the presence of EerI, but not Kif (**Figure 4.17**). Similar to HCMV infection, levels of UL148 and UL148D were unaffected by Kif, however EerI treatment led to a significant decrease in UL148 and UL148D levels, as demonstrated by UL148-V5 and UL148D-V5 immunoblotting (**Figure 4.17**).

In summary, ADAM17 immunoblotting in ectopic expression systems of UL148 and UL148D using Kif and EerI to inhibit ERAD demonstrated the same results as ADAM17 immunoblotting on HCMV-infected cells.
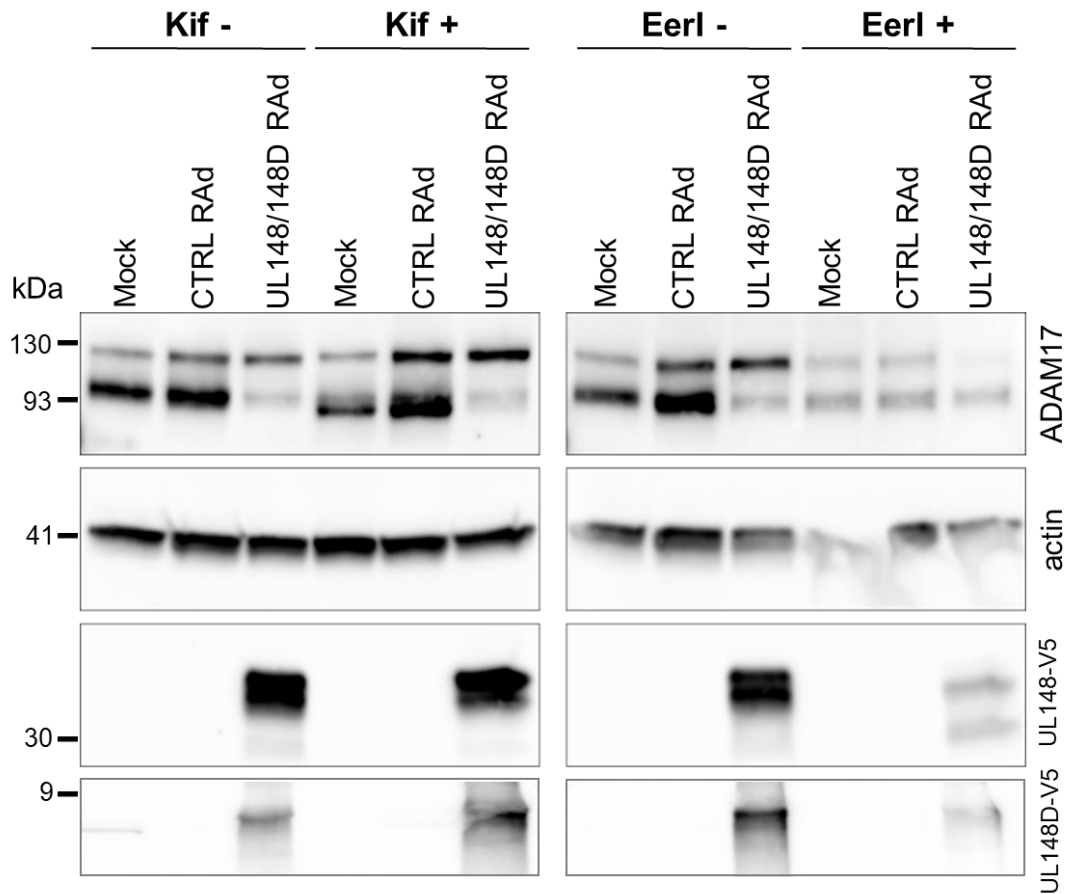
Figure 4.17. Assessing the effect of Kif- and Eerl-mediated ERAD inhibition in UL148/UL148D RAd-infected HF-CARs. HF-CARs were treated with 5 µM Eerl (DMSO for control) or 2.5 µM Kif (water for control), infected with Mock, control RAd and a combination of UL148 and UL148D RAds (MOI = 10), following sample processing 18 hpi. ADAM17 immunoblotting was performed on ConA enriched lysates. Actin, UL148-V5 and UL148D-HA immunoblotting was performed on whole cell lysates.

4.4.6 Exploring the role of degradation on whole cell ADAM17 levels using proteasome and lysosome inhibitors

Since the use of RAds in individual expression systems failed to clarify the contradicting differences observed between EerI- and Kif-treated samples, the role of degradation in the mechanism of ADAM17 downregulation was studied by inhibiting proteasomal and lysosomal degradation. If ERAD was indeed involved in ADAM17 downregulation by UL148 and UL148D, as suggested by EerI treatment, ADAM17 would pass through the ERAD machinery and be degraded by cytosolic 26S proteasomes. Hence, inhibition of proteasome complexes may clarify the role of ERAD in HCMV-induced ADAM17 downregulation. To test the role of other pathways in the degradation of ADAM17, inhibition of lysosomal degradation was performed in parallel. ER-to-lysosome-associated degradation (ERLAD) is an alternative route of degradation for proteins that fail to enter the ERAD pathway (Fregno and Molinari 2019). Although I had no evidence to think that ERLAD may be involved in ADAM17 downregulation, HCMV has been shown to target certain host proteins for lysosomal degradation in the past (Fielding et al. 2014).

HF-TERTs were infected with Mock, Merlin and dKO HCMV, following the addition of chemical inhibitors of the major protein degradation pathways 24 hpi. Cells were incubated with the inhibitors for a further 18 hrs before lysis and ConA enrichment. MG132 was chosen as a proteasome inhibitor at 10 µM, whereas leupeptin was chosen to inhibit lysosomal degradation at 200 µM since it inhibits enzymatic activity within lysosomes. ADAM17 immunoblotting demonstrated no rescue of the mature form of ADAM17 (~95 kDa) in Merlin-infected cells in the presence of either inhibitor (**Figure 4.18**). Nectin2 was chosen as a positive control for MG132-mediated inhibition of proteasomal degradation (Prod'homme et al. 2010), whereas MICA was chosen as a positive control for the inhibition of lysosomal degradation (Fielding et al. 2014). While treatment of HCMV-infected cells with MG132 or leupeptin increased levels of Nectin2 and MICA, respectively, ADAM17 levels remained

unchanged, suggesting that these degradation pathways were not involved in UL148- and UL148D-driven ADAM17 downregulation. (**Figure 4.18**).
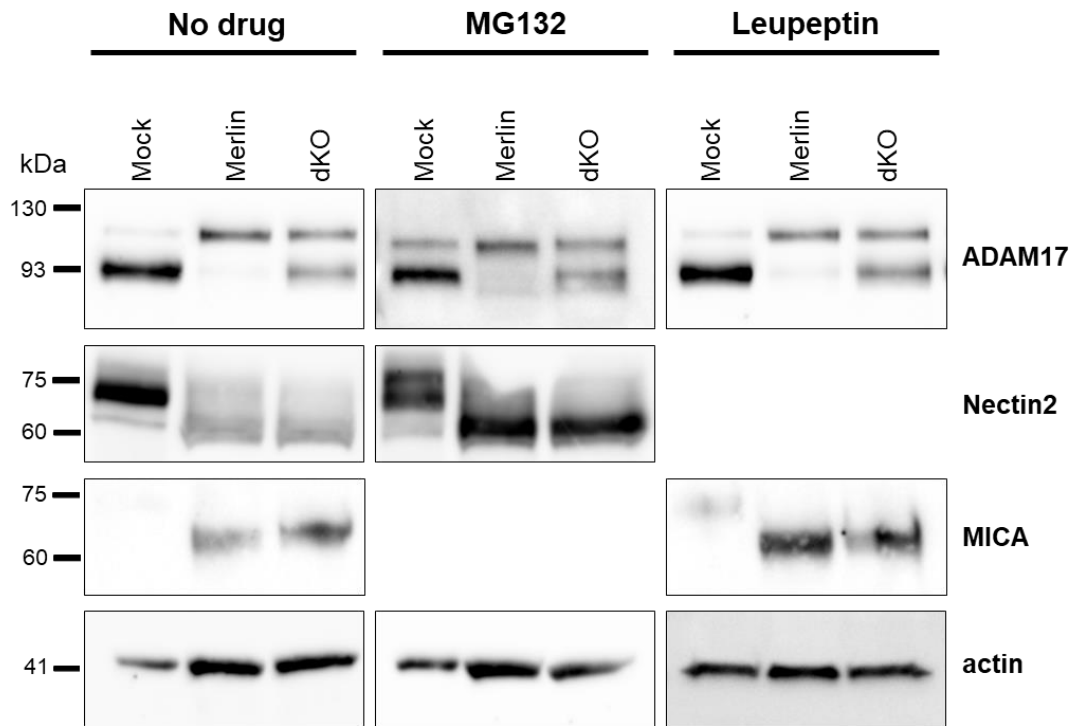
Figure 4.18. Assessing the involvement of proteasomal and lysosomal degradation in ADAM17 downregulation. HF-TERTs were infected with Mock, Merlin and dKO HCMV, following the addition of MG132 or leupeptin 24 hpi. Cells were incubated with the inhibitors for further 18 hrs before lysis and ConA enrichment. ADAM17 immunoblotting was performed on ConA enriched lysates, however actin and MHCI immunoblotting was performed on whole cell lysates.

4.5   Summary of findings

This chapter aimed to identify the mechanism of UL148- and UL148D-driven ADAM17 impairment by studying potential UL148 and UL148D interactors, as well as implementing a more targeted approach by identifying potential candidate proteins involved in ADAM17 processing.

UL148 and UL148D interactors identified through the IP-interactome dataset provided some promising mechanistic hits, such as RHBDD1, yet they failed to validate in a WB setting. In total I followed up five proposed interactors for UL148 and UL148D in pursuit of a mechanism for ADAM17 downregulation associated with the presence of UL148 and UL148D during HCMV infection. Three were not detected at high enough concentrations in our fibroblast line, while the other two did not validate the IP-interactome data. This highlights one of the problems with MS – its high sensitivity can pick up very low expressing proteins that can turn out to be false. However, unless the IP-interactome MS is repeated, it will be difficult to identify the reason behind the failed validation of these potential interactors.

Although no direct interactors of UL148 and UL148D were identified, ADAM17 immunoblotting in combination with the ConA glycoprotein enrichment methods demonstrated an accumulation of the immature form of ADAM17 in Merlin infection, as shown by its sensitivity to EndoH. dKO infection resulted in the rescue of mature ADAM17, suggesting that UL148 and UL148D interfere with ADAM17 maturation/trafficking. Six known ADAM17 regulators/traffickers were shown not be involved in UL148/UL148D-driven ADAM17 abolishment, further supporting the idea of a more complex and potentially novel method of ADAM17 regulation. Interestingly, levels of Furin-regulating protein PACS1 reduced in Merlin infection and failed to recover when UL148 and UL148D were deleted, suggesting another HCMV gene's involvement in ADAM17 regulation, consistent with the very rapid reduction in surface ADAM17 as quick as 6 hpi reported in QTV (Weekes et al, 2014).

ADAM17 immunofluorescence suggested the accumulation of ADAM17 in the ER in Merlin infection. Therefore, the involvement of ERAD in ADAM17

downregulation was assessed using two chemical ERAD inhibitors. ERAD inhibition using EerI resulted in the recovery of the mature form of ADAM17 and restored surface ADAM17 levels in Merlin-infected cells. However, EerI treatment resulted in many changes in the cell, such as downregulation of UL148 and UL148D, autofluorescence and increased isotype binding. Treatment with an alternative ERAD inhibitor Kif resulted in no changes to whole cell or surface ADAM17 levels, and there were no issues associated with the use of this inhibitor. The differences observed with the use of two different ERAD inhibitors may be explained by the different mechanism of action that these inhibitors use to target ERAD. Since both ERAD inhibitors gave conflicting results, proteasome (MG132) and lysosome (leupeptin) inhibitors were used instead to test whether ADAM17 was being targeted for degradation through these downstream and alternate pathways. Treatments with these inhibitors resulted in no changes in the whole cell levels of ADAM17, suggesting that these pathways of degradation are not involved in ADAM17 downregulation by UL148 and UL148D and implying that the primary mechanism of action is likely through impaired maturation.

5 Functional significance of ADAM17 downregulation by UL148 and UL148D

5.1 Introduction

Chapter 4 provided some valuable insights into the mechanism of UL148- and UL148D-driven ADAM17 impairment, however it failed to pinpoint the exact mechanism HCMV employs to target ADAM17. Considering that ADAM17 plays a crucial role in a broad range of biological functions, its dysregulation is likely to have a significant impact on multiple biological processes in the host. PMP and secretome proteomics results presented in Chapter 3 were consistent with this hypothesis, identifying numerous examples of ADAM17-dependent changes to the levels of surface and soluble proteins following HCMV infection. This chapter aimed to investigate the functional significance of ADAM17 downregulation by HCMV UL148 and UL148D, using protein hits identified through the PMP and secretome proteomic analysis.

Collectively, PMP and secretome proteomics identified 7 shared highly significant proteins, with Jagged1 and Vasorin detected in both datasets (**Table 3.3**) and successfully validated after lentivirus transduction to overexpress the proteins (**Section 3.5.3**). Jagged1 and Vasorin have been described previously as ADAM17-dependent substrates (Gooz 2010; Moss and Minond 2017). Overexpression of Notch ligand Jagged1 on antigen presenting EBV-transformed B cells promotes the development of immunosuppressive Treg cells (Yvon et al. 2003). In addition to Jagged1-mediated Notch signalling, TGFβ-mediated signalling maintains expression of FoxP3, the signature transcription factor involved in the differentiation and function of Treg cells (Marie et al. 2005; Lu et al. 2017). However, TGFβ signalling has been shown to be inhibited by the ADAM17-shed soluble form of Vasorin through its binding of soluble TGFβ, thereby preventing binding and downstream signalling through TGFβ receptors (Malapeira et al. 2011). Treg cells, in turn, have the capacity to impair protective host immunity and enhance viral immune evasion (Veiga-Parga et al. 2013). I hypothesised that

UL148/UL148D-mediated impairment of ADAM17 may aid HCMV's evasion of the host immune system through promoting the generation of immunosuppressive Treg cells through two distinct mechanisms; stabilization of surface Jagged1 providing Notch-mediated signalling, and stabilization of surface Vasorin with the reduction of soluble Vasorin increasing the availability of TGFβ to provide TGFβ signalling (**Figure 5.1. A**).

Nectin1 was another intriguing functional hit identified in the PMP dataset, due to its reported role in NK cell function in both humans and mice (Chan et al. 2012). Although Nectin1 was not detected in the secretome proteomics, it was identified as a highly significant hit in the PMP and validated successfully by flow cytometry in the context of HCMV infection (**Section 3.5.3**). Nectin1 is a member of the nectin and nectin-like family of cell adhesion proteins that are ligands for paired activating and inhibitory NK cell receptors that determine whether an NK cell activates (Chan et al. 2014). Both activating and inhibitory function has been attributed to CD96, the receptor for Nectin1. However, an inhibitory role as a 'stand-alone' receptor, is more compelling, because CD96 has an ITIM motif associated with inhibitory signalling (Chan et al. 2012), while mice deficient for CD96, are more sensitive to lipopolysaccharide (LPS)-induced endotoxicosis compared to WT mice due to increased IFNγ production by NK cells (Chan et al. 2014). I hypothesised that UL148/UL148D-mediated impairment of ADAM17 would act as an inhibitor of NK cells via inhibitory signals provided through CD96 and the increased levels of surface Nectin1 on an HCMV-infected target cell (**Figure 5.1. B**).
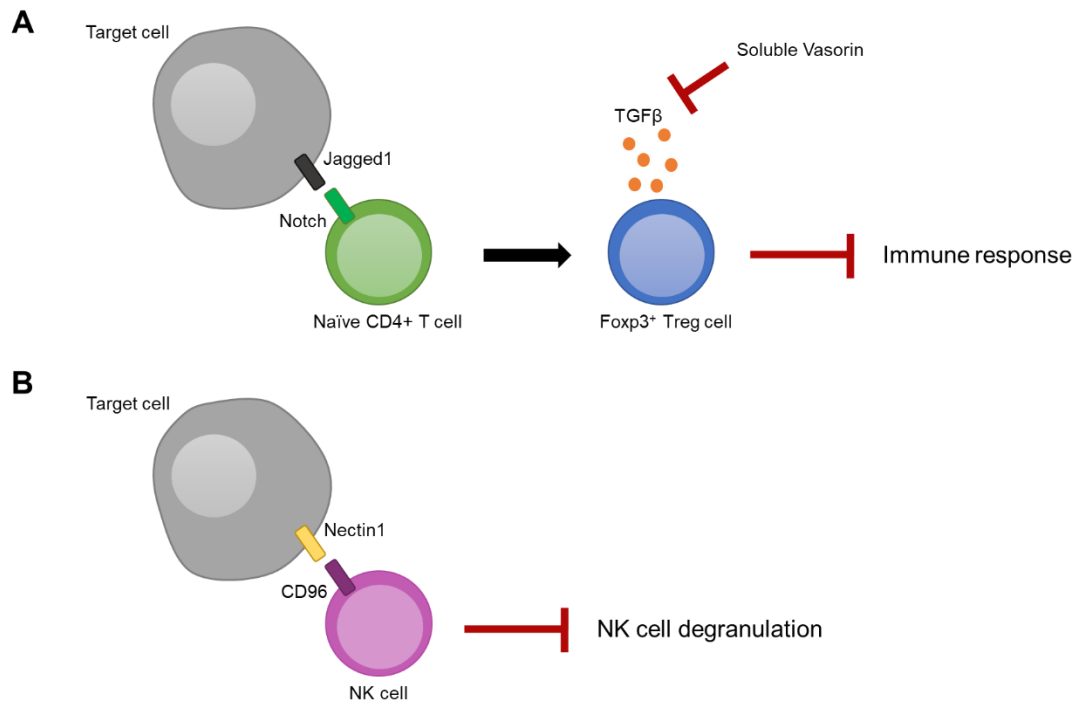
Figure 5.1: Schematic diagrams of Jagged1-, Vasorin- and Nectin1-mediated pathways. Schematic diagram of **(A)** the role of Jagged1 and Vasorin in Treg development and **(B)** the role of Nectin1 and CD96 interaction in NK cell function.

5.2 Investigating the function of ADAM17 impairment on Treg development

5.2.1 Optimising Treg expansion assay conditions

Following Jagged1 and Vasorin validation in the context of HCMV infection, I began investigating the role of ADAM17 impairment in Jagged1- and Vasorin-driven Treg development. To study the changes in Treg proliferation following co-culture with HCMV-infected targets, I designed and optimised a protocol for a Treg expansion assay. According to the literature Treg expansion can be achieved by incubating CD4$^+$ T cells with IL-2 and TGFβ for a minimum of 5 days (Ellis et al. 2012). Hence, to determine the optimal experimental conditions, an initial experiment was performed in which whole *ex vivo* PBMC were co-cultured with autologous non-infected skin fibroblasts in the absence or presence of those cytokines for 4, 7 and 10 days (**Figure 5.2**). The assay showed that in the absence of cytokines, Tregs failed to expand even over the course of 10 days. Days 7 and 10 demonstrated similar %Tregs, with IL-2 treatment resulting in 20.6% and 20.5% Tregs, respectively, and combined IL-2 and TGFβ treatment in 22.6% and 22.8%, respectively (**Figure 5.2**). Hence, it was concluded that day 7 and the combination of IL-2 and TGFβ would be used in subsequent experiments.

The optimised system is described in detail in the Materials and Methods Chapter. However, briefly responder cells (*ex vivo* PBMC or later, isolated CD4$^+$ T cells) were co-cultured with HCMV-infected cells for 7 days in the presence of IL-2 and TGFβ before they were harvested, stained and analysed by flow cytometry for Treg cells, defined as FoxP3+CD25+CD3+CD4+ (**Figure 5.3 A**). Prior to the co-culture, HCMV-infected cells were irradiated at 6000 rad to halt the proliferation of Mock-infected cells and maintain responder:stimulator ratios (**Figure 5.3 B**).
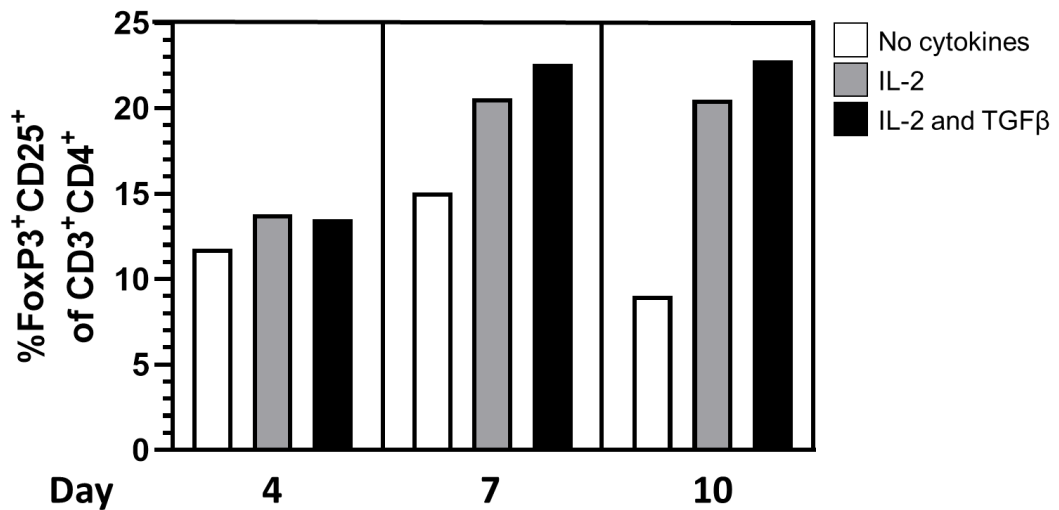
Figure 5.2: Determining optimal conditions for Treg expansion. Whole PBMC were co-cultured with non-infected autologous skin fibroblasts for 4, 7 and 10 days in the absence of cytokines, IL-2 alone or both IL-2 and TGFβ. A ratio of 10:1 responders:stimulators was used and targets were irradiated (6000 rad) prior to co-culture. At indicated time points, cells were harvested and surface stained with Fixable Aqua 405nm viability stain, CD19-BV510, CD14-BV510, CD56-BV510 (dead cells, as well as CD19+, CD14+ and CD56+ were gated out), CD3-BV711, CD4-AF700 and CD25-APC. Cells were then intracellularly stained with FoxP3-PE and analysed by flow cytometry for %FoxP3+CD25+ of CD3+CD4+ T cells. The data presented is generated from one experimental repeat on a single donor.
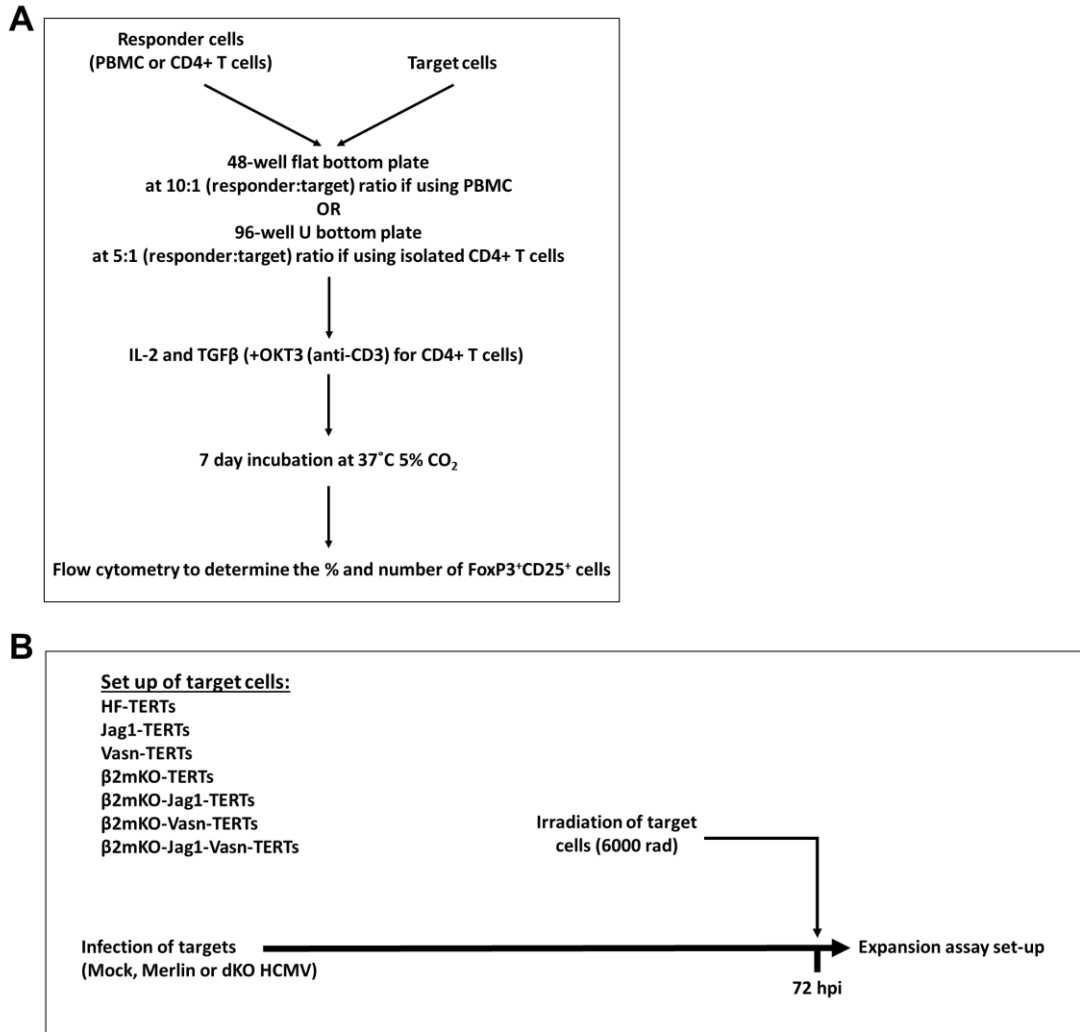
Figure 5.3: Schematic diagrams of experimental set up to study Treg cell expansions. (A) Treg expansion assay set up. **(B)** Schematic diagram of target infection and irradiation prior to assay set up.

5.2.2 Measuring Treg expansion in the context of HCMV infection

The optimised system was then used to measure Tregs expansion in the context of HCMV infection. Whole *ex vivo* PBMC from one donor were co-cultured with HCMV-infected targets for 7 days in the presence of IL-2 and TGFβ. Flow cytometry was used to determine the proportion of Treg cells in cultures, while cell counting beads (Precision Count Beads, BioLegend) were included in the assay to assess absolute cell numbers. HF-TERTs, as well as Jagged1- and Vasorin-expressing Jag1-TERTs and Vasn-TERTs were used as stimulators, testing the hypothesis that Merlin-infected targets would induce Treg expansion due to upregulated surface Jagged1 and reduced soluble Vasorin as a result of ADAM17 impairment. No significant differences in %Tregs or absolute Treg numbers were observed between Merlin- and dKO-infected targets. Interestingly, however, there was a significant increase in the proportion of Tregs generated by stimulation with Mock- versus HCMV-infected (Merlin or dKO) cells (**Figure 5.4**).
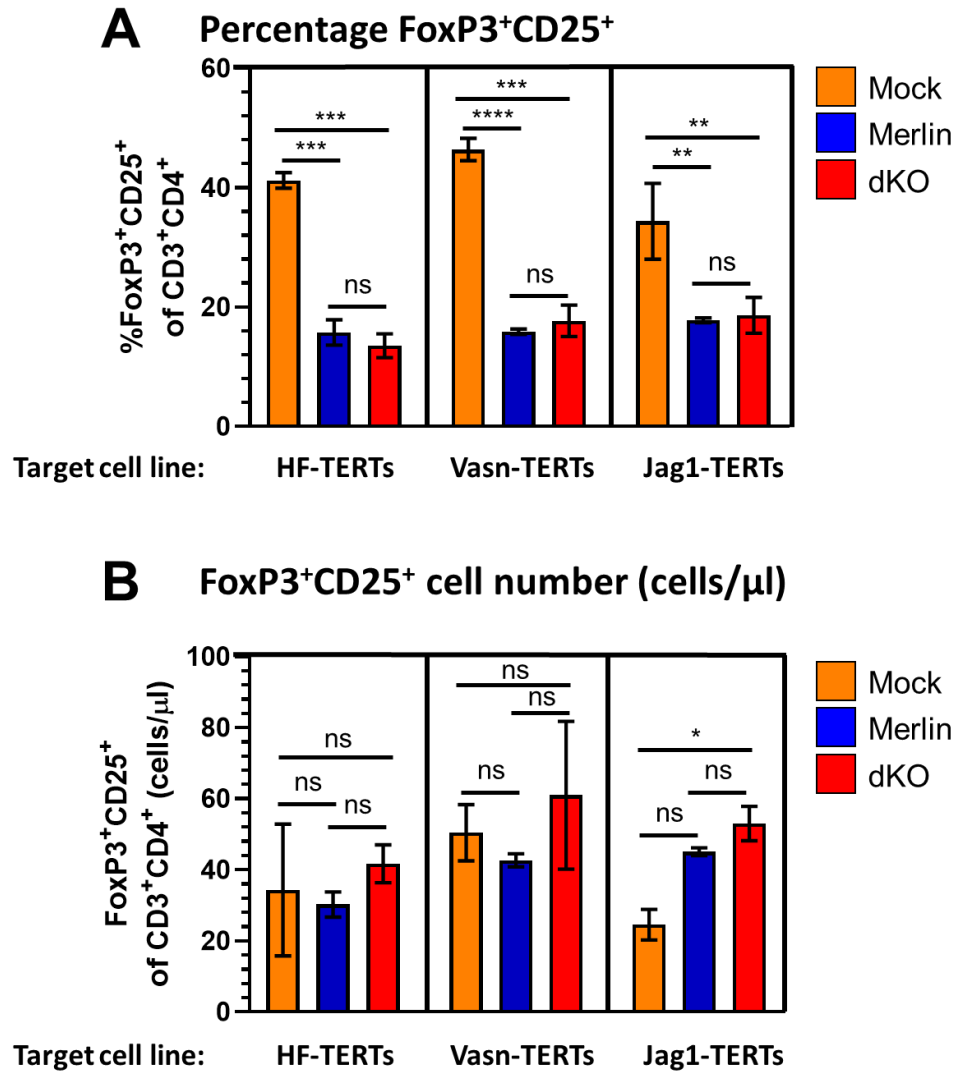
Figure 5.4: Treg expansion assay on whole PBMC using HCMV-infected Jagged1- and Vasorin-expressing targets show no significant difference in proportion or absolute Treg cell number. Whole *ex vivo* PBMC were co-cultured with irradiated (6000 rad) HCMV-infected targets (HF-TERTs, Vasn-TERTs and Jag1-TERTs) in the presence of IL-2 and TGFβ. A ratio of 10:1 of responders:stimulators was used. At 7 days of co-culture cells were harvested, stained and analysed by flow cytometry for %FoxP3+CD25+CD3+CD4+ T cells. To calculate absolute cell number Precision Counting Beads (BioLegend) were used according to manufacturer instructions. Means +/- SEM of triplicate samples are shown. The data presented is generated from one experimental repeat on a single donor. ANOVA with Tukey multiple comparison post-hoc tests showed significance at ****$p<0.0001$, ***$p<0.001$, **$p<0.01$, *$p<0.05$, ns – not significant.

5.2.3 Measuring Treg expansion in response to HCMV-infected β2mKO targets

One possible explanation for the increase in %Tregs induced by Mock-infected cells was stimulation of the CD4+ T-cells by allogeneic MHC-I. In order to eliminate this, β2 microglobulin (β2m) knockout HF-TERTs were used instead (produced and kindly provided by Dr Pragati Amratia). β2m is a critical component for HLA-I expression, hence β2mKO cells do not express surface HLA-I. Jagged1 and Vasorin were overexpressed in β2mKO-TERTs the same way they were overexpressed in regular HF-TERTs (**Section 2.3**), however in addition to single Jagged1- and Vasorin-expressing cell lines, a cell line with both overexpressed Jagged1 and Vasorin was made (β2mKO-Jag1-Vasn-TERTs). To generate this line, β2mKO-Vasn-TERTs were first selected using puromycin resistance for Vasorin expression (**Figure 5.5 A**), followed by Jagged1 lentivirus transduction and cell sorting for Jagged1+ cells (**Figure 5.5 B**).

In the absence of cell surface HLA-I, the relative increase of Tregs induced by stimulation with Mock-infected cells was reduced, consistent with allogeneic activation contributing to the effects observed in **Figure 5.4**. Stimulation with Vasorin-expressing β2mKO-TERTs infected with HCMV Merlin significantly increased Treg absolute cell numbers and proportions compared to cells infected with dKO (**Figure 5.6**). In contrast Jagged1-expressing β2mKO-TERTs showed no difference between Merlin- and dKO-infected targets, whereas targets expressing both Jagged1 and Vasorin drove an unexpected increase in Treg proliferation when infected with dKO HCMV (**Figure 5.6**). Overall, these data support a role for stabilized Vasorin in Merlin-mediated Treg development, however the phenotype was not maintained with the introduction of Jagged1.
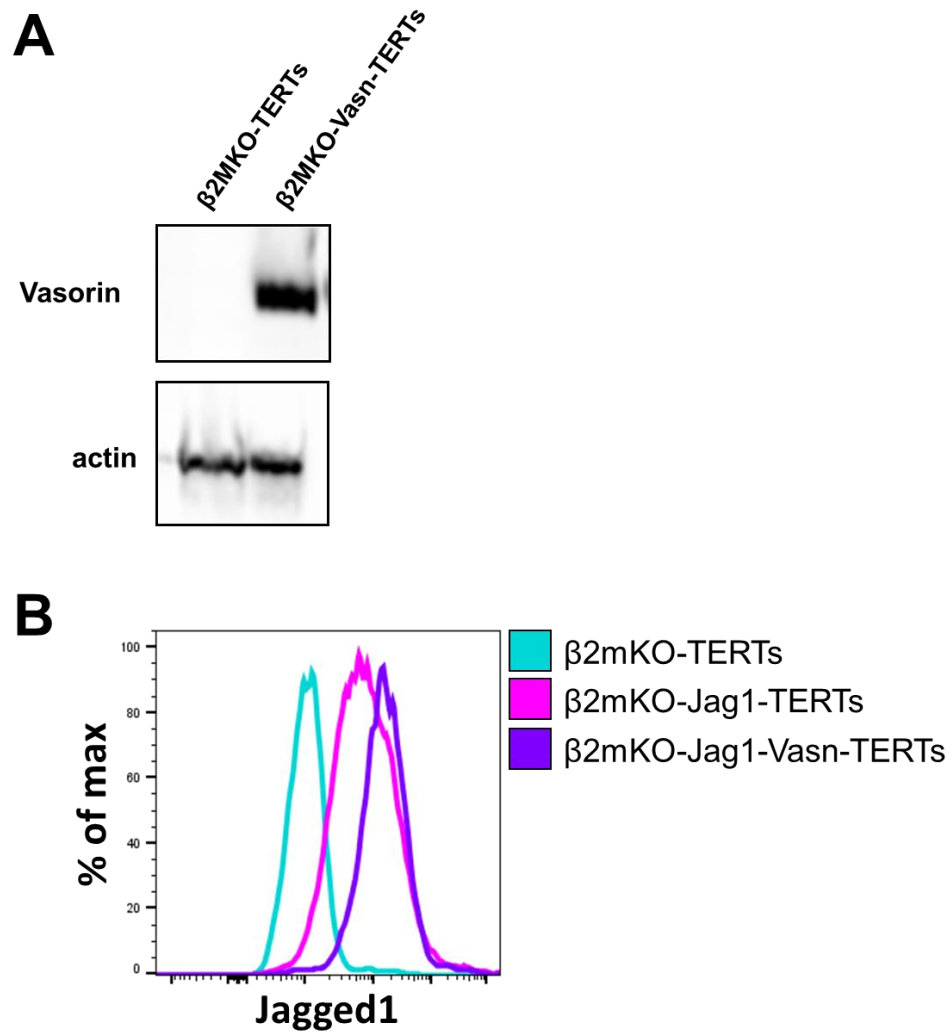
Figure 5.5: Validation of Vasorin and Jagged1 expression in lentivirus transduced β2mKO-TERTs. (A) WB analysis of Vasorin levels in β2mKO-TERTs and Vasorin lentivirus transduced β2mKO-Vasn-TERTs selected via puromycin selection. Actin was used as a loading control. **(B)** Flow cytometry analysis of surface Jagged1 levels on β2mKO-TERTs and Jagged1 lentivirus transduced β2mKO-Jag1-TERTs and β2mKO-Jag1-Vasn-TERTs. β2mKO-Jag1-TERTs were selected via puromycin selection, whereas β2mKO-Jag1-Vasn-TERTs were cell sorted on Jagged1+ cells.
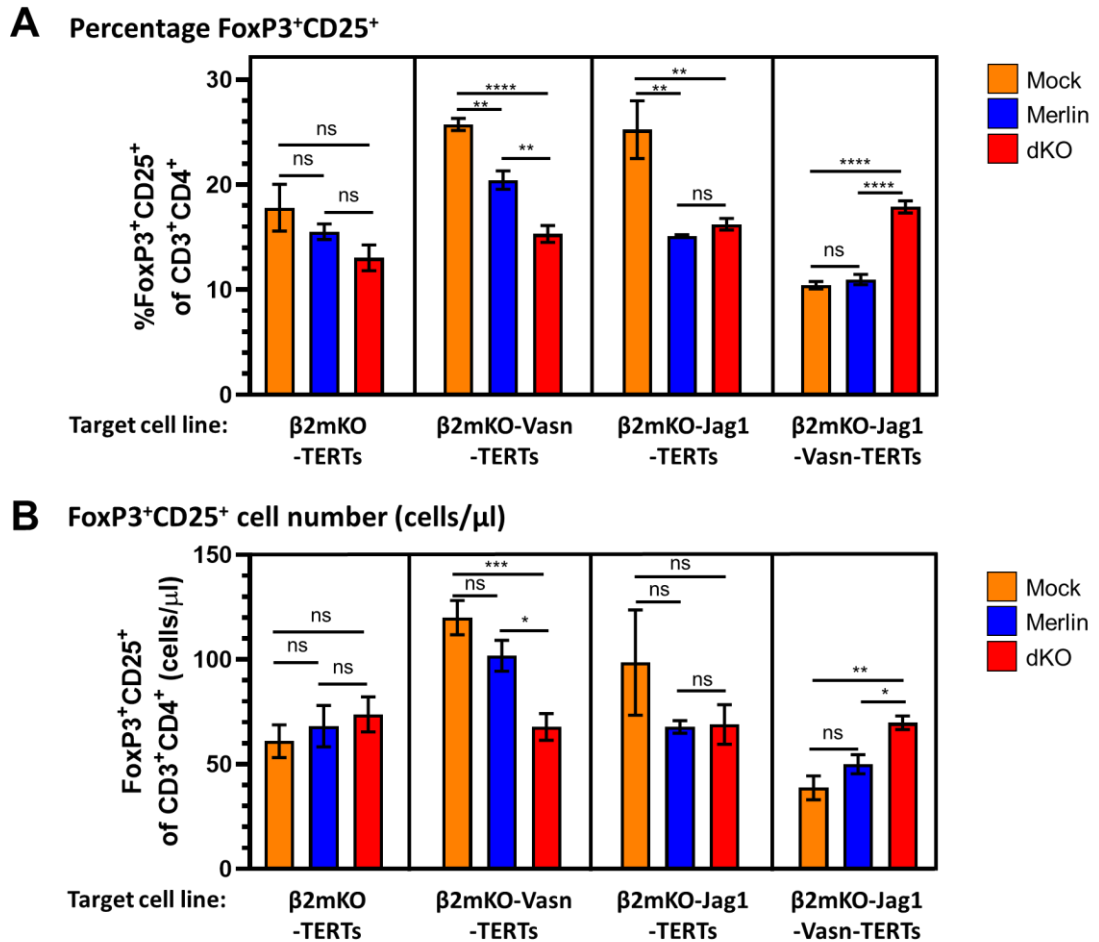
Figure 5.6: Treg expansion assay on whole PBMC using HCMV-infected β2mKO targets suggest that Vasorin plays a role in Treg expansions in response to Merlin-infected targets. Whole PBMC were co-cultured with irradiated (6000 rad) HCMV-infected β2mKO targets (β2mKO-TERTs, β2mKO-Vasn-TERTs, β2mKO-Jag1-TERTs and β2mKO-Jag1-Vasn-TERTs) in the presence of IL-2 and TGFβ. A ratio of 10:1 of responders:stimulators was used. At 7 days of co-culture cells were harvested, stained and analysed by flow cytometry for %FoxP3+CD25+ of CD3+CD4+ T cells. To calculate absolute cell number Precision Counting Beads (BioLegend) were used according to manufacturer instructions. Means +/- SEM of triplicate samples are shown. The data presented is generated from one experimental repeat on a single donor. ANOVA with Tukey multiple comparison post-hoc tests showed significance at ****$p<0.0001$, ***$p<0.001$, **$p<0.01$, *$p<0.05$, ns – not significant.

5.2.4 The effect of TCR signalling on HCMV-driven Treg expansion

The varied responses observed in my initial data highlighted the complex interactions within the Treg expansion assay and implied that simplification of the system could aid the generation of larger differential effects and dissection of the phenotype. The use of purified naïve CD4+ T cells would ensure responses were not dependent on other cell types in PBMC. However, the same lack of other immune cells plus the use of β2mKO targets with no surface MHC-I meant that no allogeneic signalling through mismatched MHC-I would be provided to CD4+ T cells. Use of agonistic anti-CD3 monoclonal antibodies (mAbs) would provide such a signal that could also be varied to mimic optimal and sub-optimal signalling through the TCR. Anti-CD3 antibody (clone OKT3) was chosen and co-culture plates were pre-treated with different concentrations of OKT3 for 16 hrs at 4°C prior to the assay setup. There were two separate batches of OKT3 used – a commercially available OKT3 from BioLegend at 1 µg/ml, as well as three different dilutions of our own lab stock of OKT3 hybridoma (1:500, 1:5000 and 1:50,000). The concentration of OKT3 hybridoma stock was unknown prior to the experiment, however I performed an ELISA using an IgG2a Mouse ELISA kit, confirming that the stock concentration of OKT3 hybridoma was 220 ng/ml. Hence, corresponding OKT3 concentrations for the three dilutions used were 440 pg/ml, 44 pg/ml and 4.4 pg/ml for 1:500, 1:5000 and 1:50,000, respectively.

The assay showed that at higher OKT3 concentrations (1 µg/ml and 440 pg/ml) no significant differences were observed in absolute Treg cell numbers generated by stimulation with Merlin- and dKO-infected β2mKO and Vasorin-expressing targets (**Figure 5.7**). This was in contrast to the previous experiment using whole PBMC (**Figure 5.6**). Interestingly Jagged1-expressing β2mKO targets, as well as targets expressing both Jagged1 and Vasorin, demonstrated significant increases in absolute Treg numbers against dKO-infected targets (**Figure 5.7**). Previous data using whole PBMC showed a similar phenotype but only when both Jagged1 and Vasorin were overexpressed (**Figure 5.6**).

OKT3 concentrations of 44 pg/ml and 4.4 pg/ml resulted in a striking difference in expansion of Tregs in response to Merlin-infected, compared to dKO-infected, cells across all types of target cells, with WT β2mKO targets and Vasorin-expressing β2mKO targets demonstrating higher absolute Treg numbers compared to target cells expressing Jagged1 (**Figure 5.7**). This suggests that differences in Treg generation only occur when CD4+ T cells receive sub-optimal TCR signals. Comparing the two OKT3 lower concentrations, 4.4 pg/ml resulted in higher variability across datapoints, as indicated by larger error bars, hence an OKT3 concentration of 44 pg/ml to stimulate T cells was chosen for future experiments.
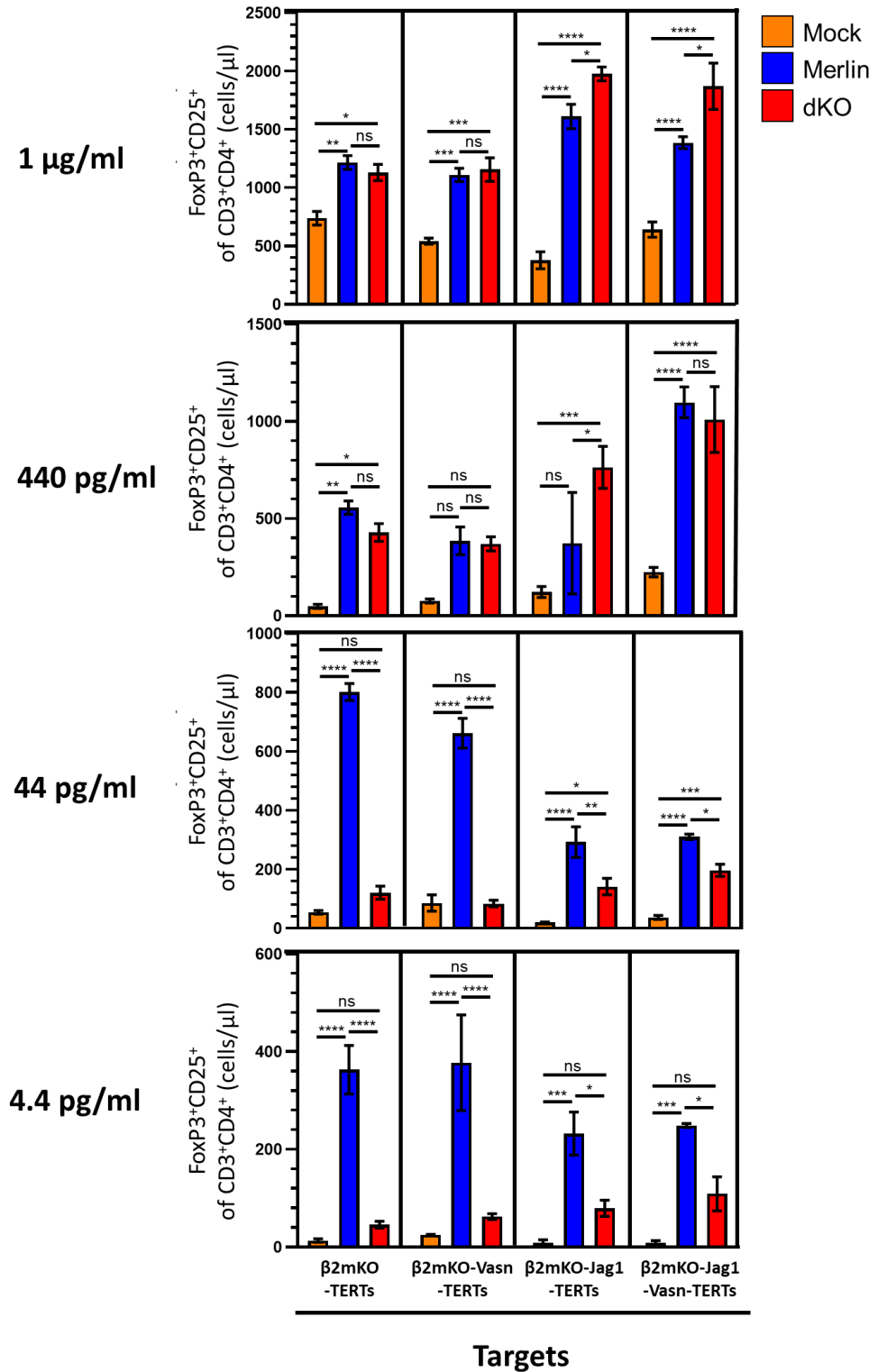
Figure 5.7: Optimisation of anti-CD3 OKT3 concentrations for stimulation of purified naïve CD4+ T cells revealed significant Treg expansions in response to Merlin-infected cells when sub-optimal OKT3 concentrations were used. 96-well U bottom co-culture plates were coated

prior to co-culture with different OKT3 concentrations at 4°C overnight. Purified naïve CD4$^+$ T cells were co-cultured with irradiated (6000 rad) HCMV-infected β2mKO targets (β2mKO-TERTs, β2mKO-Vasn-TERTs, β2mKO-Jag1-TERTs and β2mKO-Jag1-Vasn-TERTs) in the presence of IL-2 and TGFβ. A ratio of 5:1 of responders:stimulators was used. At 7 days of co-culture cells were harvested, stained and analysed by flow cytometry for %FoxP3+CD25+ of CD3+CD4+ T cells. To calculate absolute cell number Precision Counting Beads (BioLegend) were used according to manufacturer instructions. Means +/- SEM of triplicate samples are shown. The data presented is generated from one experimental repeat on a single donor. ANOVA with Tukey multiple comparison post-hoc tests showed significance at ****p<0.0001, ***p<0.001, **p<0.01, *p<0.05, ns - not significant.

5.2.5 Phenotypic analysis of cell subsets induced by HCMV in Treg expansion assays

Assessment of absolute Treg numbers following different OKT3 treatments suggested huge Treg expansions in response to Merlin-infected targets, however %Treg data only showed significant increases in proportions when using WT β2mKO Merlin-infected targets (**Figure 5.8 A**). Absolute cell number is a measure of the combined effect of proliferation, expansion and cell death within a culture, while percentage data records changes in cellular dynamics. Percentage of CD3+CD4+ T cells was assessed since Tregs were derived from a CD3+CD4+ gate (**Figure 5.8 B**). Interestingly, independent of expression of Jagged1 or Vasorin, the phenotype within lymphocyte gates altered according to the type of stimulation with Mock-infection resulting in the lowest %CD3+CD4+ and Merlin-infection in the highest (**Figure 5.8 B**). This indicated the presence of other populations besides CD3+CD4+ T cells, proportions of which altered after stimulation. Further analysis revealed that at lower OKT3 concentrations (4.4 pg/ml and 44 pg/ml) two other populations besides CD3+CD4+ were expanding – CD3+CD4- and CD3-CD4- (**Figure 5.9 A**). These populations were only present when cells were stimulated with sub-optimal concentrations of OKT3, and not 1 µg/ml and 440 pg/ml OKT3 (**Figure 5.9 B**). Although the nature of these additional populations is unknown and would be beyond the scope of this PhD to investigate, it is intriguing to observe the differences in immune cell responses to Merlin- and dKO-infected targets.
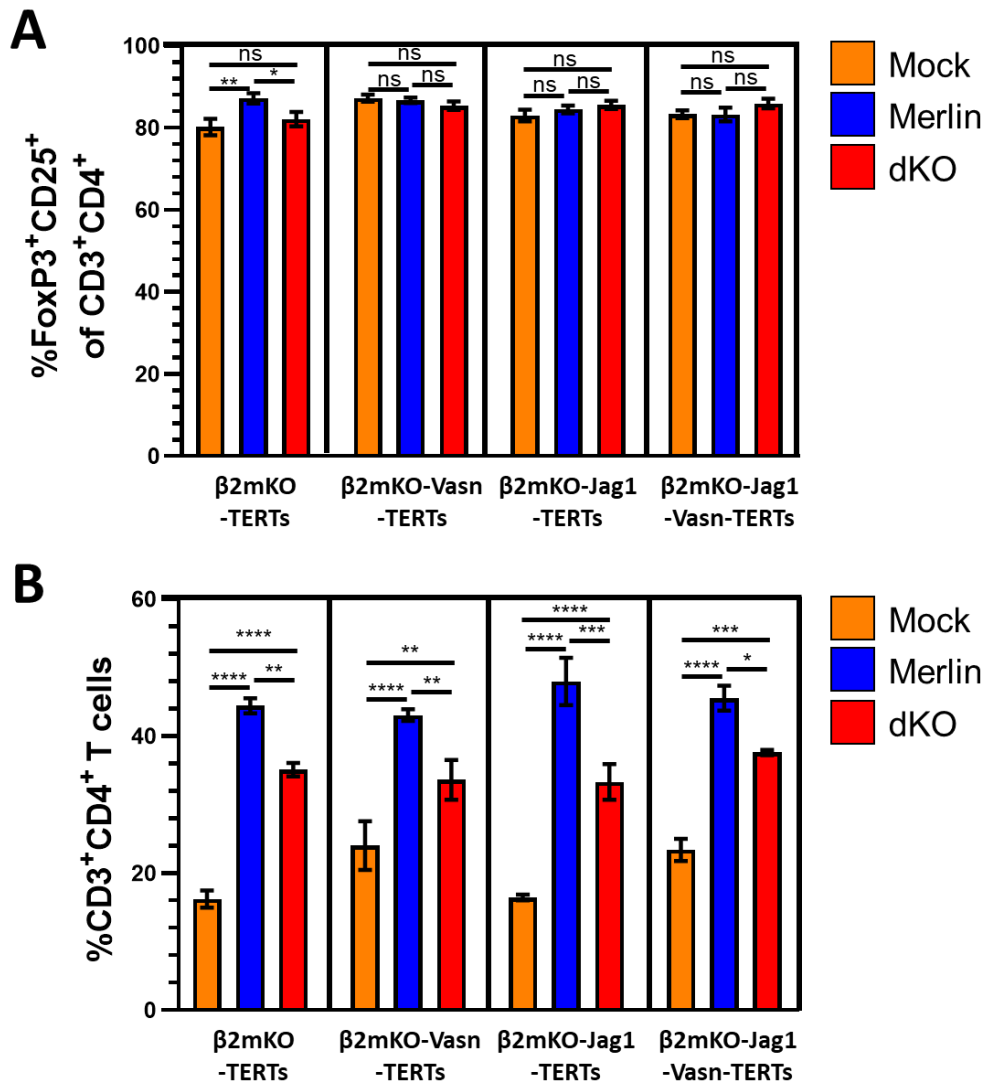
Figure 5.8: Stimulation of purified naïve CD4+ T cells with 44 pg/ml OKT3 reveals phenotypic changes within the lymphocyte gate. Purified naïve CD4+ T cells were stimulated with 44 pg/ml OKT3 and co-cultured with irradiated (6000 rad) HCMV-infected β2mKO targets in the presence of IL-2 and TGFβ. Percentages of **(A)** Tregs and **(B)** CD3+CD4+ T cell population are shown. A ratio of 5:1 of responders:stimulators was used. At 7 days of co-culture cells were harvested, stained and analysed by flow cytometry for %FoxP3+CD25+ of CD3+CD4+ T cells. To calculate absolute cell number Precision Counting Beads (BioLegend) were used according to manufacturer instructions. Means +/- SEM of triplicate samples are shown. ANOVA with Tukey multiple comparison post-hoc tests showed significance at ****$p<0.0001$, ***$p<0.001$, **$p<0.01$, *$p<0.05$, ns – not significant.
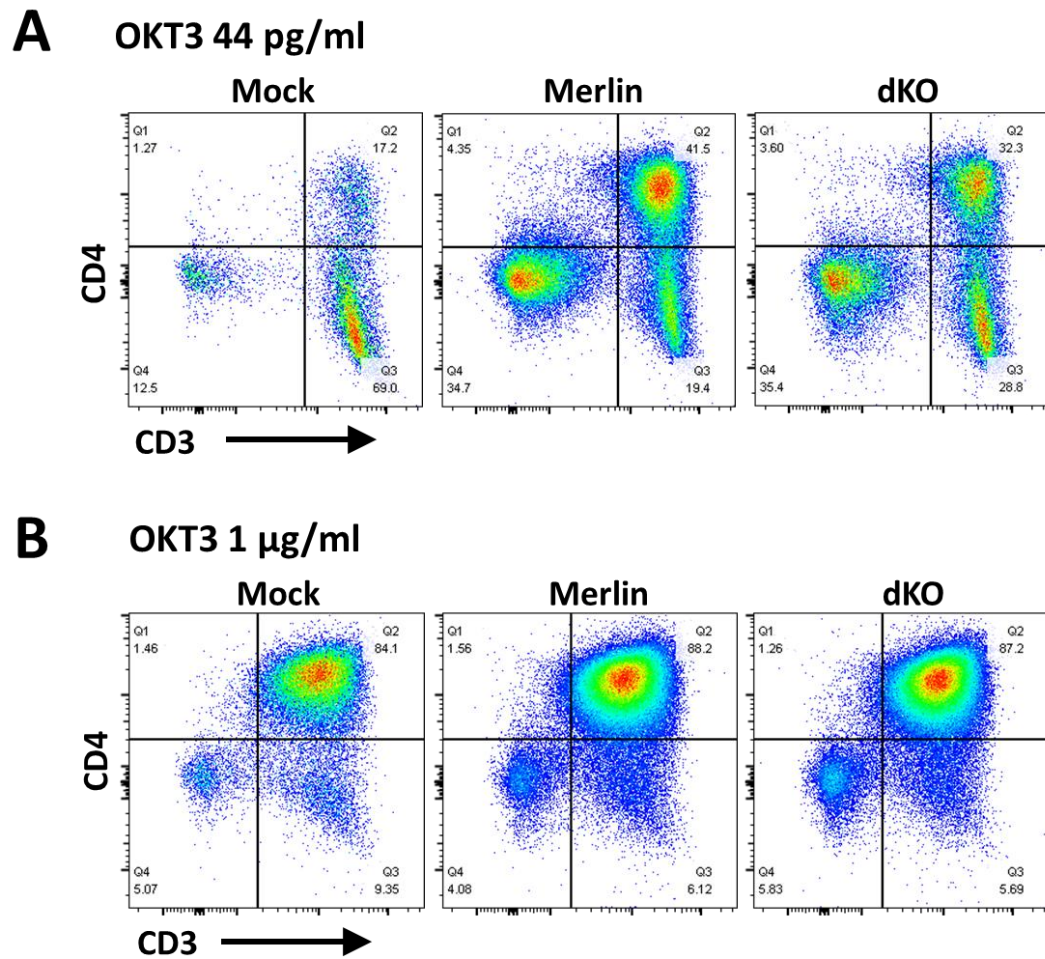
Figure 5.9: CD3 vs CD4 flow cytometry dot plots of responder cells stimulated with (A) 44 pg/ml OKT3 and (B) 1 µg/ml OKT3. Treg expansion assay result in which purified naïve CD4+ T cells were stimulated with either 1 µg/ml or 44 pg/ml OKT3 and co-cultured with irradiated (6000 rad) HCMV-infected β2mKO targets (β2mKO-TERTs) in the presence of IL-2 and TGFβ. A ratio of 5:1 of responders:stimulators was used. At 7 days of co-culture cells were harvested, stained and analysed by flow cytometry.

5.2.6 Treg expansion of multiple donors in response to Merlin-infected targets

While the data in **Section 5.2.4**. was highly significant within the described experiment, I wanted to test the biological significance of my findings. Therefore, I performed Treg expansion assays using sub-optimal TCR stimulation (44 pg/ml OKT3) on an additional five donors. Summary graphs were created in which the data was plotted as a fold change over Mock (**Figure 5.10**). Overall, no significant differences were observed in %Tregs (**Figure 5.10 A**) or absolute Treg numbers (**Figure 5.10 B**) between donors. Nevertheless, some variability in donor responses was observed. Two out of six donors demonstrated a considerable decrease in both %Treg and absolute Treg numbers in response to dKO-infected targets compared to Merlin, whereas two donors demonstrated a decrease in absolute Treg numbers with only a slight decrease or no change in %Treg. In contrast, the remaining two donors demonstrated increase in %Treg and absolute Treg numbers, with one donor showing only a marginal increase in %Treg and absolute Treg numbers (**Figure 5.10**).

%FoxP3+CD25+ of CD3+CD4+

A

p = 0.3066

FoxP3+CD25+ of CD3+CD4+ (cells/µl)

B

p = 0.2188
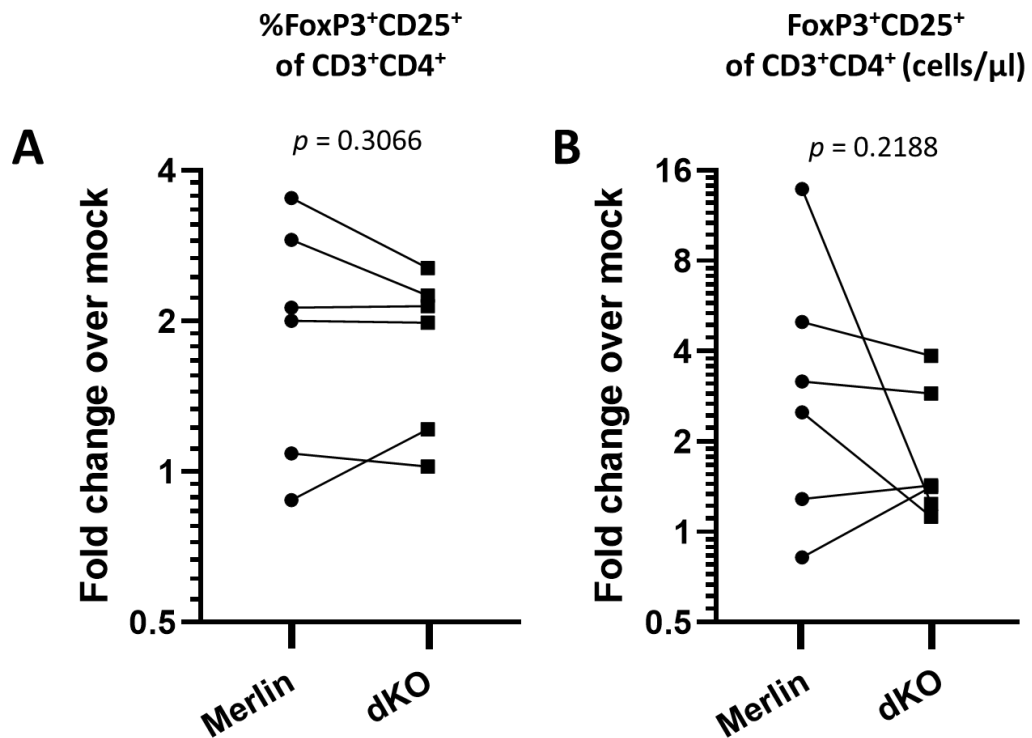
Figure 5.10: Treg expansion in response to Merlin-infected targets on multiple donors reveals no significant change in %Treg and absolute Treg cell numbers. Summary plots of **(A)** %Tregs and **(B)** absolute Treg number performed on isolated naïve CD4+ T cells from 6 different donors. Purified naïve CD4+ T cells were stimulated with 44 pg/ml OKT3 and co-cultured with irradiated (6000 rad) HCMV-infected β2mKO targets (β2mKO-TERTs only) in the presence of IL-2 and TGFβ. A ratio of 5:1 of responders:stimulators was used. At 7 days of co-culture cells were harvested and stained and analysed by flow cytometry for %FoxP3+CD25+ of CD3+CD4+ T cells. To calculate absolute cell number Precision Counting Beads were used according to manufacturer instructions. Results are presented as fold change over Mock. For **(A)** a paired *t*-test showed the *p*-value indicated, for **(B)** non-parametric Wilcoxon test (data not normally distributed) showed the *p*-value indicated. The data presented is generated from four experimental repeats on six different donors.

5.2.7 Maintenance of Jagged1 expression on β2mKO lines

Due to the observed variability in Treg expansion experiments, I decided to test if Jagged1 and Vasorin levels in lentivirus transduced β2mKO cell lines were altered by prolonged time in cell culture (>4 months). Surface Jagged1 levels on older β2mKO-Jag1-Vasn-TERTs were low with non-infected cells showing similar Jagged1 levels to the isotype (**Figure 5.11**). This was in contrast to the expression of Jagged1 on freshly transduced cells (**Figure 5.5**). Such low expression of Jagged1 on older β2mKO-Jag1-Vasn-TERTs suggests loss of Jagged1 expression possibly due to a lack of selection pressure. As a result of low baseline Jagged1 levels, it was difficult to observe significant changes in Jagged1 expression following HCMV infection with Merlin or dKO (**Figure 5.11**). This could at least partially explain similar %Treg and absolute Treg cell numbers in response to Merlin- and dKO-infected targets in later experiments. Vasorin expression was not specifically tested.
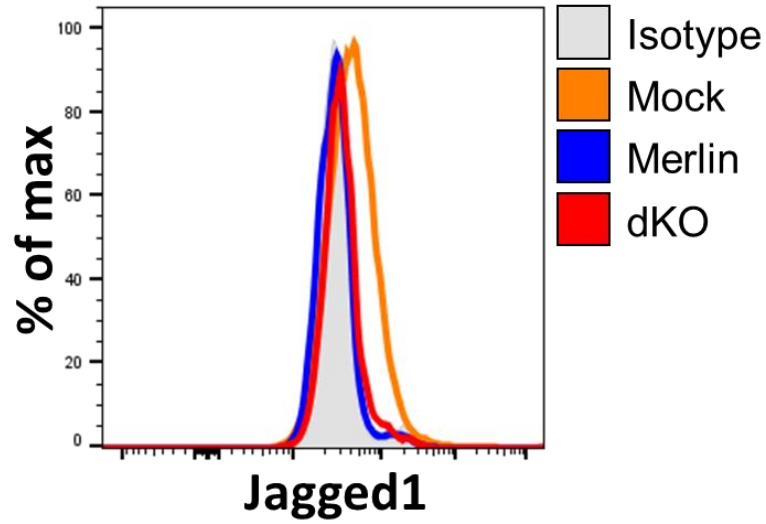
Figure 5.11: Surface Jagged1 expression in lentivirus transduced β2mKO-TERTs after >4 months of being in culture. Flow cytometry analysis of Jagged1 levels on β2mKO-Jag1-Vasn-TERTs infected with indicated HCMV strains (MOI = 5, 72 hpi). Cells were in culture for >4 months prior to infections and staining.

5.3   Investigating the function of ADAM17 impairment on NK cell activation

Section 5.2 focused on investigating the consequences of HCMV-mediated ADAM17 impairment on Treg development, however, with over 100 proteins stabilised during HCMV infection (**Chapter 3**), the functional consequences of ADAM17 downregulation are likely to go beyond Treg development. Hence, I investigated the role of ADAM17 impairment on NK cell function. The rationale behind studying the effect of ADAM17 impairment on NK cell activation was the identification and validation of Nectin1 as a significant hit in the PMP dataset (**Section 5.1**) combined with the laboratory's expertise in dissecting HCMV-encoded NK cell modulators (Wilkinson et al. 2008; Patel et al. 2018). To investigate the functional significance of UL148- and UL148D-mediated ADAM17 impairment on NK cell function, CD107a degranulation assays were performed as described in Section 2.10.3. Briefly, HCMV-infected target cells (HF-TERTs) were co-cultured for 5 hrs with effector cells (*ex vivo* PBMC or NK cell lines) in the presence of FITC-conjugated anti-CD107a antibody and GolgiStop (BD), followed by flow cytometry staining and analysis to detect %CD3-CD56+CD107a+ NK cells (**Figure 5.12 A**). For ADAM17 blocking studies, anti-ADAM17 antibody D1(A12) was used to treat target cells 24 hrs prior to assay set up to block ADAM17 in dKO-infected cells and allow enough time for the levels of ADAM17-dependent substrates to increase on the cell surface (**Figure 5.12 B**).
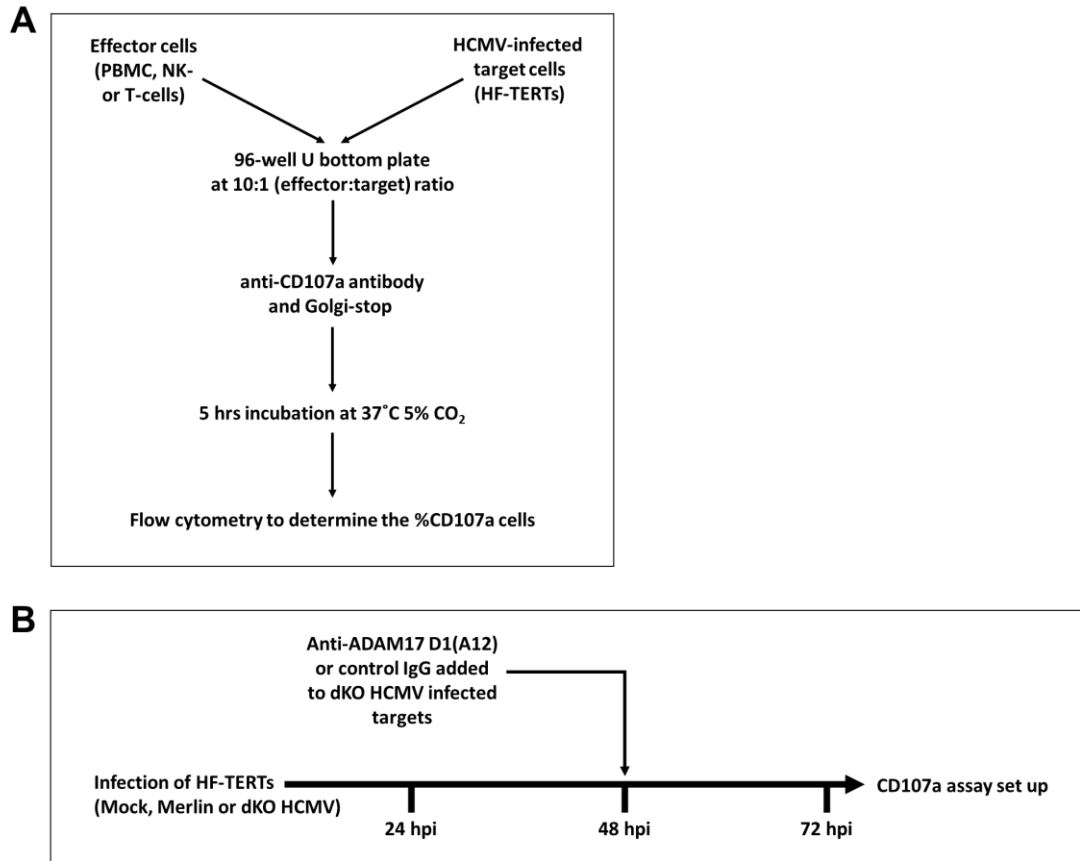
Figure 5.12: Schematic diagram of CD107a degranulation assay set up to study NK cell function. (A) Schematic of the CD107a degranulation assay set up. **(B)** Schematic of anti-ADAM17 D1(A12) antibody addition to HCMV dKO-infected cells.

5.3.1 Investigating the effect of ADAM17 impairment on NK cell activation using *ex vivo* PBMC

To begin exploring the effect ADAM17 impairment has on NK cell function, CD107a degranulation assays were first performed using *ex vivo* PBMC from frozen stocks (**Figure 5.13 A**). However, the overall levels of NK cell activation across all conditions and all donors were very low, with D003 NK cells demonstrating less than 1% activation in some instances. Typically, a higher level of degranulation is expected in response to HF-TERTs when using *ex vivo* PBMC. In our laboratory we routinely perform CD107a degranulation assays with PBMC and achieve NK cell degranulation of ~20-30% to Mock-infected HF-TERTs. Hence, a repeat of the assay was performed using fresh PBMC isolated one day prior to the assay to test if freezing down PBMC had a negative effect on their activation.

Using fresh PBMC from four different donors resulted in low NK cell degranulation, similar to the result observed when previously frozen PBMC were used (**Figure 5.13 B**). Since results generated using fresh *ex vivo* PBMC did not provide a large enough differential for my studies, the CD107a assay was further optimised in an attempt to achieve 20-30% degranulation to Mock-infected HF-TERTs before continuing.
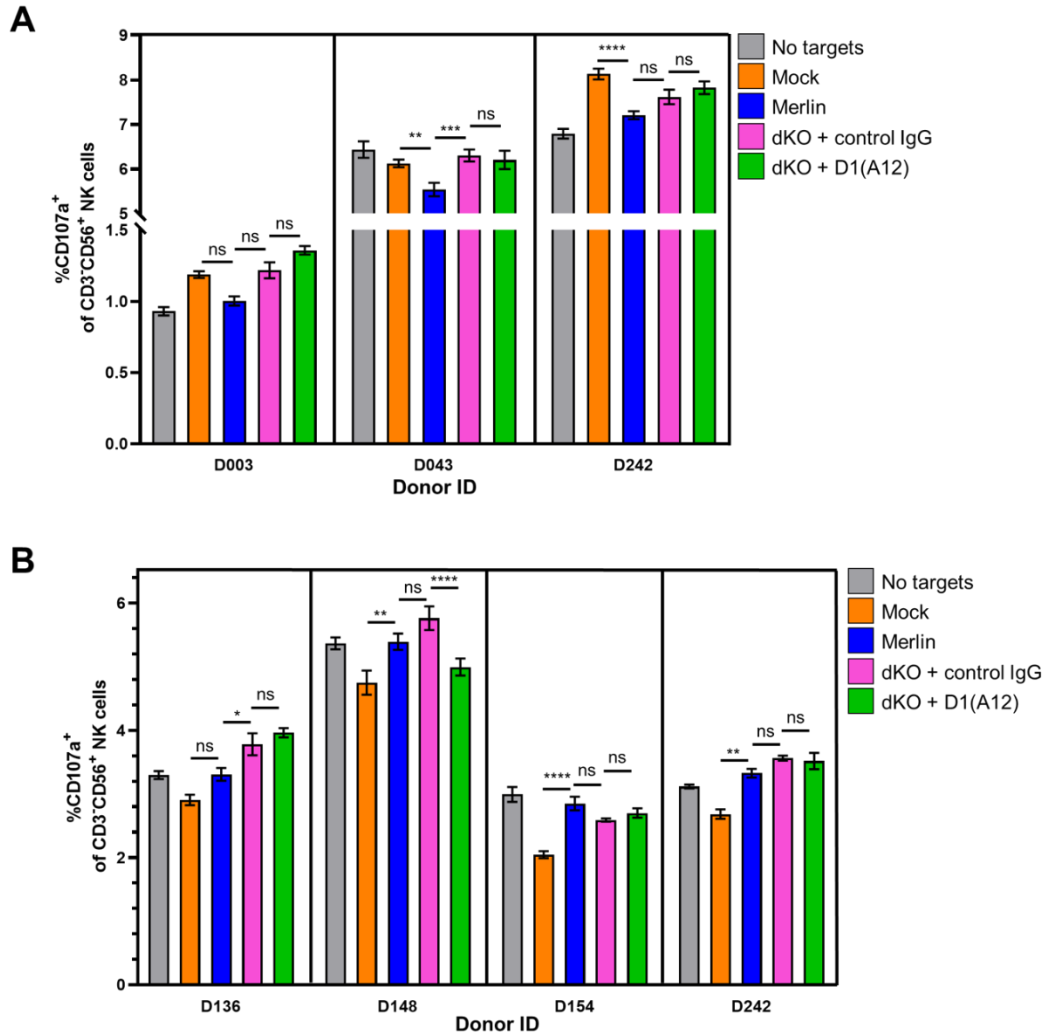
Figure 5.13: Initial CD107a degranulation assays demonstrated poor NK cell activation with both fresh and frozen ex vivo PBMC. CD107a degranulation assay on **(A)** frozen and **(B)** fresh *ex vivo* PBMC from three and four donors, respectively. HF-TERT cells were infected with indicated HCMV strain or Mock-infected (MOI = 10, 72 hrs). Targets infected with dKO HCMV were treated with D1(A12) anti-ADAM17 blocking antibody or control human IgG 24 hrs prior to harvest. At 72 hpi infected HF-TERT cells were co-cultured with *ex vivo* PBMC, which have previously been incubated with IFNα overnight. Effector:target ratio of 10:1 was used for the co-culture, following a 5 hr incubation in the presence of anti-CD107a antibody and GolgiStop (BD). Effectors were analysed by flow cytometry for %CD107a of CD3-CD56+ NK cells. Means +/- SEM of quadruplicate samples are shown. ANOVA with Tukey multiple comparison post-hoc tests showed significance at ****$p<0.0001$, ***$p<0.001$, **$p<0.01$, *$p<0.05$, ns – not significant.

## 5.3.2 Optimisation of CD107a degranulation assay on *ex vivo* PBMC

Two variables were tested – the IFNα stock used to stimulate PBMC overnight and the HF-TERTs used as targets. It was noted that both IFNα stock and cultured HF-TERTs were not new, with the IFNα stock aliquoted and frozen down in 2017, while the HF-TERTs had been cultured for at least 3 months prior to assays. A side by side comparison was made by setting up a CD107a degranulation assay using *ex vivo* PBMC from one donor as effectors against old and fresh HF-TERTs as targets. Effectors were also stimulated with either old or fresh stock of IFNα.

A combination of both old IFNα and old HF-TERTs resulted in the lowest NK cell degranulation of 8.85% CD107a$^+$ NK cells, similar to the values observed previously (**Figure 5.14**). The use of either fresh HF-TERTs or fresh IFNα increased NK cell degranulation, however the use of both fresh reagent and targets together resulted in NK cell degranulation of 23% (**Figure 5.14**).
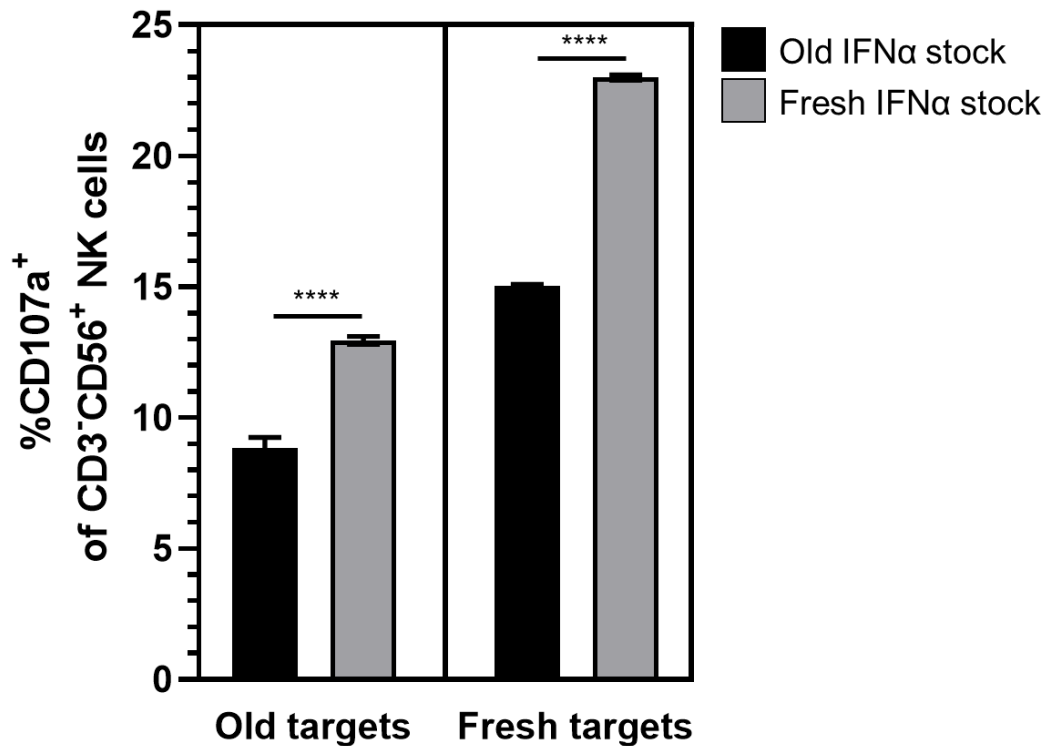
Figure 5.14: Optimisation of CD107a degranulation assay testing old and fresh stocks of IFNα and HF-TERTs as targets. Two different stocks of IFNα were used to stimulate *ex vivo* PBMC from one donor, followed by a co-culture with either 3-month old or 2-week old HF-TERTs, old and fresh, respectively. Effector:target ratio of 10:1 was used for the co-culture, following a 5 hr incubation in the presence of anti-CD107a antibody and GolgiStop (BD). Effectors were stained with Fixable Aqua 405nm viability stain, CD3-PE and CD56-APC, and analysed by flow cytometry for %CD107a of CD3-CD56+ NK cells. Means +/- SEM of quadruplicate samples are shown. ANOVA with Tukey multiple comparison post-hoc tests showed significance at ****$p < 0.0001$.

5.3.3 Investigating the effect of ADAM17 impairment on NK cell activation using *ex vivo* PBMC under optimised assay conditions

The optimised CD107a degranulation assay was performed on two donors with the addition of anti-ADAM17 D1(A12) antibody to dKO-infected targets to study the involvement of ADAM17 in NK cell function. NK cells of both donors responded to Merlin- and dKO-infected targets as expected, with Merlin-infected targets significantly inhibiting NK cell activation compared to Mock, and dKO-infected targets recovering NK function (**Figure 5.15**). However, the addition of D1(A12) to dKO-infected targets to block ADAM17 did not reduce NK cell degranulation, suggesting that the inhibitory effect of UL148 and UL148D on NK cells was independent of their role in ADAM17 impairment (**Figure 5.15**). It is important to note that only two donors were tested under optimised CD107a assay conditions, with both donors demonstrating a small reduction in NK cell activation following D1(A12) treatment that did not reach a statistical significance of $p < 0.05$ (**Figure 5.15**).
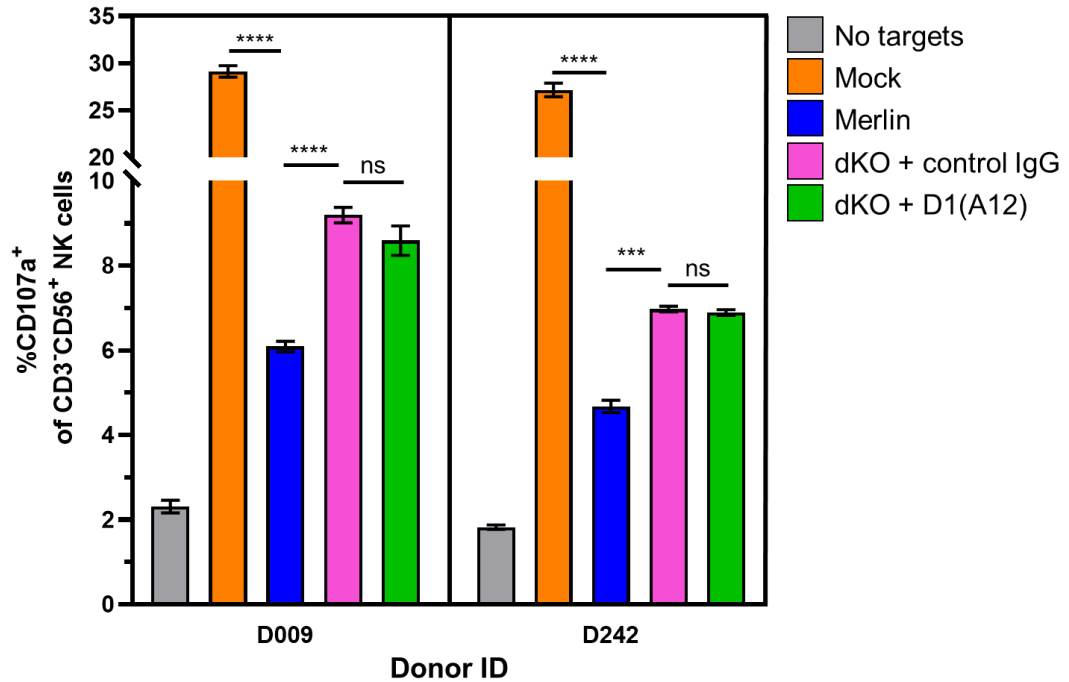
Figure 5.15: CD107a degranulation assay on ex vivo PBMC under optimised assay conditions showed no ADAM17 involvement in NK cell function. Fresh (3 week old) HF-TERT cells were infected with indicated HCMV strain or Mock-infected (MOI = 10, 72 hrs). Targets infected with dKO HCMV were treated with D1(A12) anti-ADAM17 blocking antibody or control human IgG 24 hrs prior to harvest. At 72 hpi infected HF-TERT cells were co-cultured with *ex vivo* PBMC from different donors, which have previously been incubated with fresh IFNα overnight to stimulate NK cells. Effector:target ratio of 10:1 was used for the co-culture, following a 5 hr incubation in the presence of anti-CD107a antibody and GolgiStop (BD). Effectors were stained with Fixable Aqua 405nm viability stain, CD3-PE and CD56-APC, and analysed by flow cytometry for %CD107a of CD3-CD56+ NK cells. Means +/- SEM of quadruplicate samples are shown. The data presented is generated from one experimental repeat on two different donors. ANOVA with Tukey multiple comparison post-hoc tests showed significance at ****$p<0.0001$, ***$p<0.001$, ns – not significant.

5.3.4 Investigating the effect of ADAM17 impairment on NK cell activation using NK cell lines

At the same time as I was performing *ex vivo* PBMC assays, Dr Simon Kollnberger in the laboratory was generating NK cell lines for a separate project, allowing me to test a different set of effectors. Three NK cell lines were tested against HCMV-infected HF-TERTs with dKO-infected targets treated with anti-ADAM17 D1(A12) (**Figure 5.16**). In contrast to the data generated using *ex vivo* PBMC, D1(A12) treatment resulted in significant decreases in NK cell activation across all three donor NK cell lines compared to control IgG-treated targets, suggesting ADAM17 involvement in NK cell function in these cell lines (**Figure 5.16 A**). Although it was an encouraging result, NK lines D043 and D169 did not respond as expected to Merlin-infected targets, with D043 demonstrating an increase in %CD107a$^+$ cells and D169 no change in the levels of %CD107a compared to Mock (**Figure 5.16 A**). In addition, control IgG-treated dKO-infected targets resulted in increases in NK cell activation across all three donors, with the D043 line demonstrating an 8-fold increase in %CD107a$^+$ NK cells compared to Mock-infected targets (**Figure 5.16 A**). Such increases in %CD107a$^+$ NK cells, suggested control IgG treatment of dKO-infected targets was activating NK cells.

A repeat of the assay was performed and untreated dKO-infected targets were included into the experimental set up to assess if control IgG treatment of targets had any effect on NK cells activation (**Figure 5.16 B**). The same NK lines were used as in **Figure 5.16 A**, 7 days after the initial experiment. No significant differences were observed in %CD107a$^+$ NK cells against dKO-infected targets with and without control IgG, consistent with the increase in NK cell activation in response to dKO-infected targets being caused by the lack of UL148 and UL148D, and not control IgG (**Figure 5.16 B**). Furthermore, all three NK cell lines responded to Merlin-infected cells as expected, demonstrating a significant reduction in NK cell activation compared to Mock, as measured by proportion of CD107a+ cells (**Figure 5.16 B**). This was later repeated with different NK cell lines demonstrating similar results.

A total of 7 NK cell lines were tested and summary graphs were generated showing consistent increases in NK cell activation to dKO-infected targets compared to Merlin (**Figure 5.16 C**). Addition of anti-ADAM17 D1(A12) to dKO-infected targets significantly reduced NK cell activation in all tested NK cell lines, demonstrating biological reproducibility for the role of ADAM17 impairment in NK cell activation.
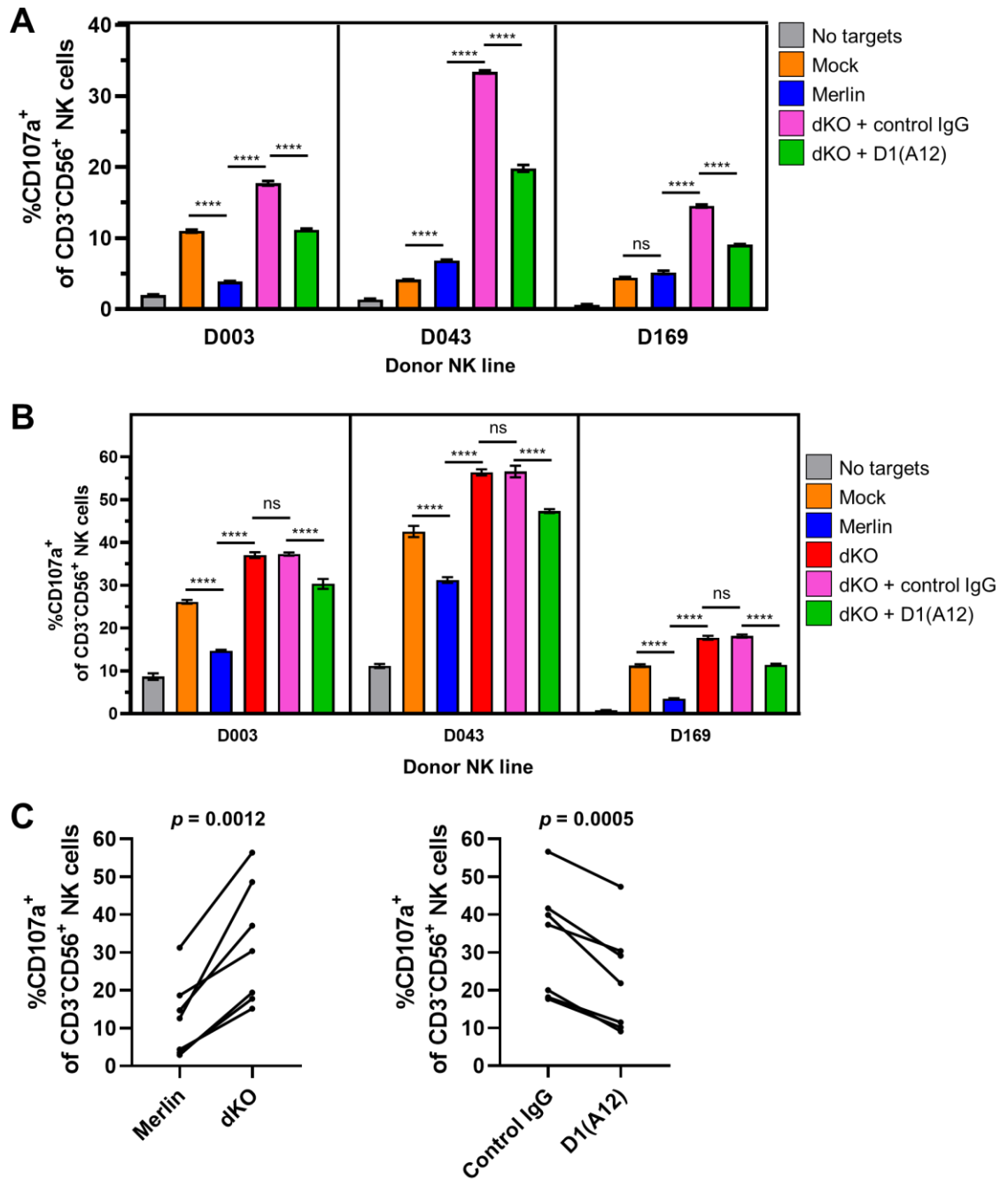
Figure 5.16: CD107a degranulation assay on NK cell lines using anti-ADAM17 D1(A12) antibody demonstrated ADAM17-dependent role in NK cell inhibition in Merlin-infected cells. (A) HF-TERT cells were infected with indicated HCMV strain or Mock-infected (MOI = 10, 72 hrs). Targets infected with dKO HCMV were treated with D1(A12) anti-ADAM17 blocking antibody or control human IgG 24 hrs prior to harvest. At 72 hpi infected HF-TERT cells were co-cultured indicated NK cell lines. Effector:target ratio of 10:1 was used for the co-culture, following a 5 hrs incubation in the presence of anti-CD107a

antibody and GolgiStop (BD). Effectors were stained with Fixable Aqua 405nm viability stain, CD3-PE and CD56-APC, and analysed by flow cytometry for %CD107a of CD3-CD56+ NK cells. Means +/- SEM of quadruplicate samples are shown. ANOVA with Tukey multiple comparison post-hoc tests showed significance at ****$p<0.0001$, ns – not significant. **(B)** A repeat experiment of (A) with the addition of untreated dKO-infected targets. **(C)** CD107a degranulation of 7 NK lines challenged with HF-TERT target cells infected with dKO-infected HCMV and treated with either control human IgG or D1(A12) anti-ADAM17 antibody. Points are means of quadruplicate samples. A paired t-test showed the p-value indicated. NK cell lines for summary plots were generated from four donors, with three NK cell lines stimulated on two separate occasions, generating 6 different NK cell lines.

5.3.5 Assessing the role of ADAM17 downregulation in the inhibition of NK cell activation

Although anti-ADAM17 D1(A12) treatment on dKO-infected targets confirmed that HCMV-mediated ADAM17 impairment inhibited NK cell activation, the exact mechanism was unclear. There were two possible explanations. It was possible that ADAM17 itself was acting as an activating ligand to the NK cells. PMP data (**Chapter 3**) suggested that 24 hrs of anti-ADAM17 D1(A12) treatment not only blocked ADAM17 function, but also reduced surface ADAM17 levels presumably through protein endocytosis (**Figure 3.6**). Hence, if ADAM17 was itself a novel activating NK cell ligand, its downregulation following anti-ADAM17 D1(A12) treatment may explain NK cell inhibition. An alternative explanation was that the impairment of ADAM17 shedding function was the reason behind altered NK cell responses, i.e., one or more ADAM17-dependent inhibitory NK cell ligands (such as Nectin1) accumulated on the cell surface as a consequence of ADAM17 blocking by D1(A12) and provided NK inhibitory signals.

To test the role of ADAM17 in HCMV-mediated NK cell inhibition an experiment was performed in which D1(A12) treatment was applied for short and long periods - 1 hr and 24 hrs, respectively (**Figure 5.17**). It was hypothesised that 1 hr anti-ADAM17 D1(A12) treatment would be sufficient to block and downregulate surface ADAM17, without impacting the levels of its substrates. Whereas a 24 hrs D1(A12) application would allow for the accumulation of ADAM17-dependent substrates on the cell surface, as suggested by the PMP analysis (**Chapter 3**). Before functional CD107a assay could be performed to assess the role of ADAM17 in NK cell inhibition, ADAM17 and Nectin1 expression were studied by flow cytometry following these different D1(A12) treatments to see which correlated better with blocking.

ADAM17 flow cytometry staining on 24 hrs D1(A12)-treated dKO-infected HF-TERTs demonstrated abolishment of surface ADAM17 close to the levels of

Merlin-infected HF-TERTs, validating PMP proteomics results and confirming significant downregulation of ADAM17 following 24 hrs D1(A12) treatment (**Figure 5.18 A**). In contrast, 1 hr D1(A12) treatment resulted in a partial ADAM17 downregulation, however ADAM17 levels were still lower than that of control IgG-treated cells (**Figure 5.18 B**). An additional treatment was tested, in which target cells were treated with D1(A12) for 1 hr, following 5 hrs D1(A12)-free incubation to monitor the changes in ADAM17 and Nectin1 expression levels thereby mirroring events in a CD107a degranulation assay (**Figure 5.17**). Five hrs incubation following 1 hr D1(A12) treatment resulted in a recovery of surface ADAM17, yet not enough time had passed to recover it to the levels of control IgG-treated cells (**Figure 5.18 B**).

ADAM17 expression correlated with the expression of its substrate Nectin1. D1(A12) treatment for 24 hrs on dKO-infected HF-TERTs resulted in surface Nectin1 increasing to levels observed on Merlin-infected cells (**Figure 5.19**). However, 1 hr of D1(A12) treatment on dKO-infected HF-TERTs failed to upregulate surface Nectin1 levels, confirming that 1 hr D1(A12) treatment is sufficient to downregulate ADAM17, without altering the levels of its substrates (**Figure 5.19**). Finally, 5 hrs incubation in the absence of D1(A12) resulted in a partial increase in surface Nectin1 levels compared to Nectin1 levels immediately after 1 hr D1(A12) treatment (**Figure 5.19**). This indicated that Nectin1 started to slowly accumulate on the cell surface after 5 hrs D1(A12)-free incubation.
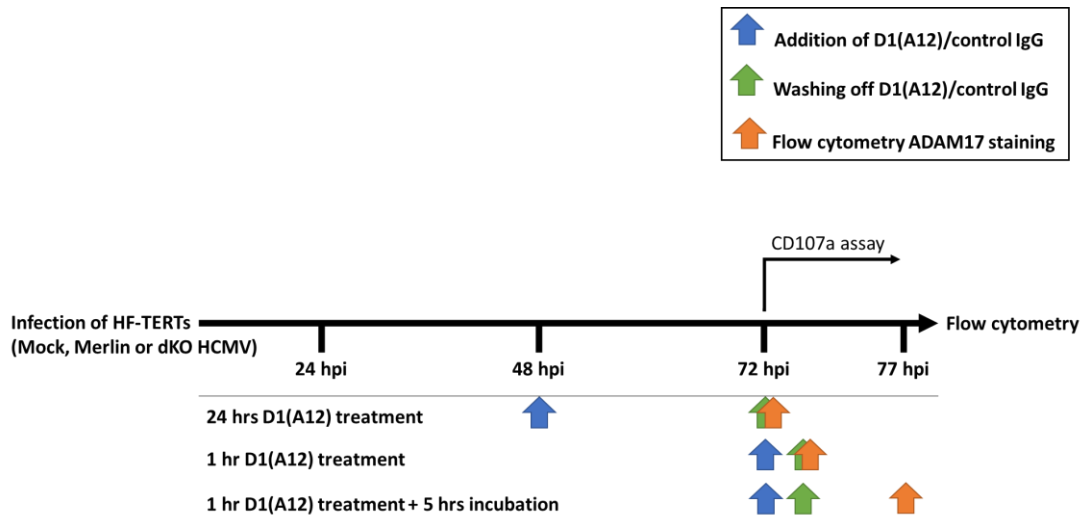
Figure 5.17: A schematic of the assay designed to assess the role of ADAM17 impairment in NK cell function. Briefly, dKO-infected HF-TERTs were treated with anti-ADAM17 D1(A12) for different durations prior to ADAM17 flow cytometry staining. '24 hrs' treatment consisted of continuous 24 hrs D1(A12) application prior to washing and staining. '1 hr' treatment consisted of 1 hr D1(A12) application followed by immediate wash and flow cytometry staining. '1 hr + 5 hrs incubation' treatment consisted of 1 hr D1(A12) application, followed by a wash to wash off any residual D1(A12) antibody and a 5 hrs incubation in the absence of D1(A12) prior to flow cytometry staining.
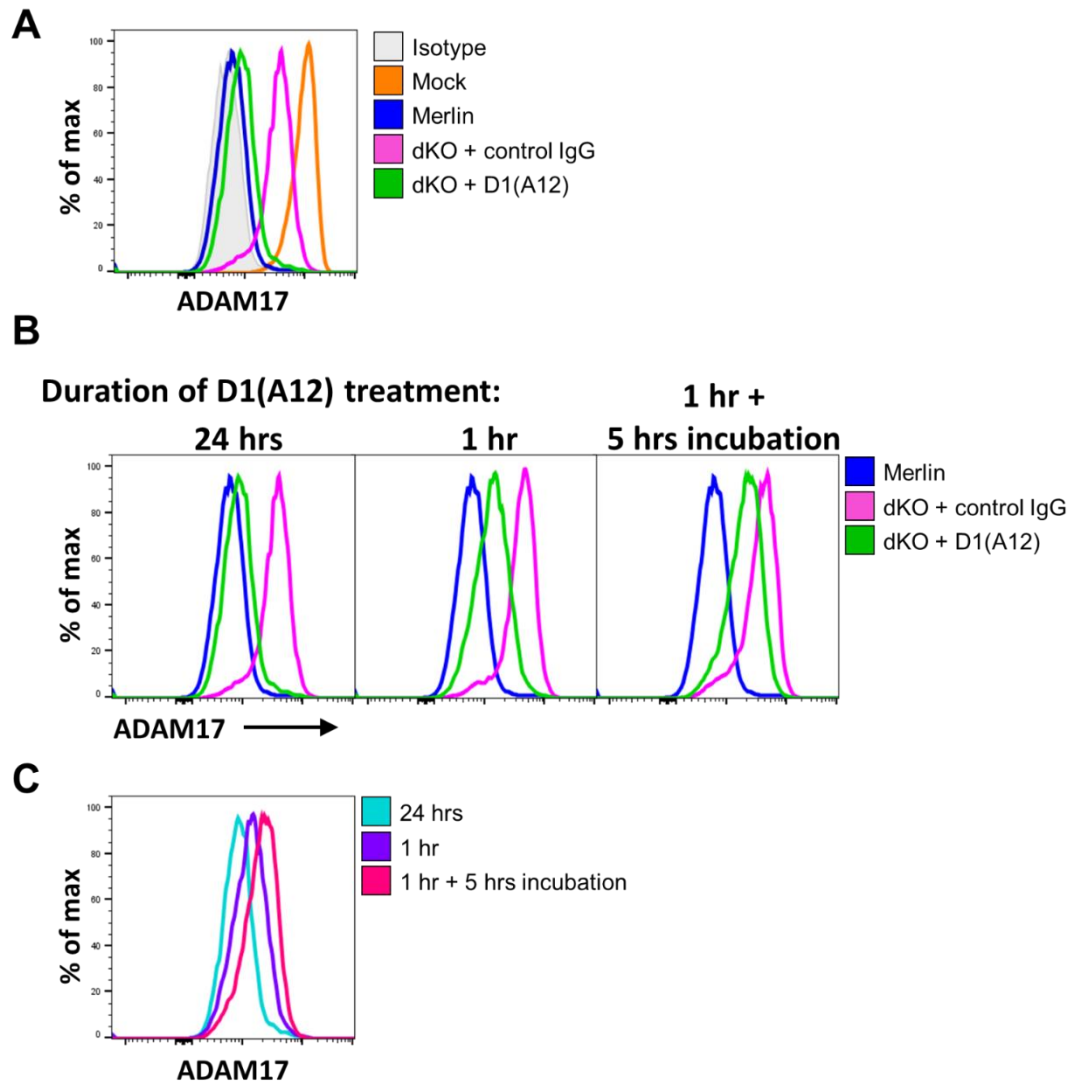
Figure 5.18: Flow cytometry surface ADAM17 staining following multiple D1(A12) treatment regimes. (A) ADAM17 flow cytometry staining on HF-TERTs infected with indicated HCMV strains (MOI = 10, 72 hpi). Anti-ADAM17 D1(A12) or control IgG treatments were added to dKO-infected cells 24 hrs prior to cell harvest and staining. **(B)** ADAM17 flow cytometry staining on HF-TERTs infected with indicated HCMV strains (MOI = 10, 72 hpi), following different regimes of anti-ADAM17 D1(A12) treatment. **(C)** An overlay of surface ADAM17 staining from (B) following different anti-ADAM17 D1(A12) treatment schedules.

Duration of D1(A12) treatment:
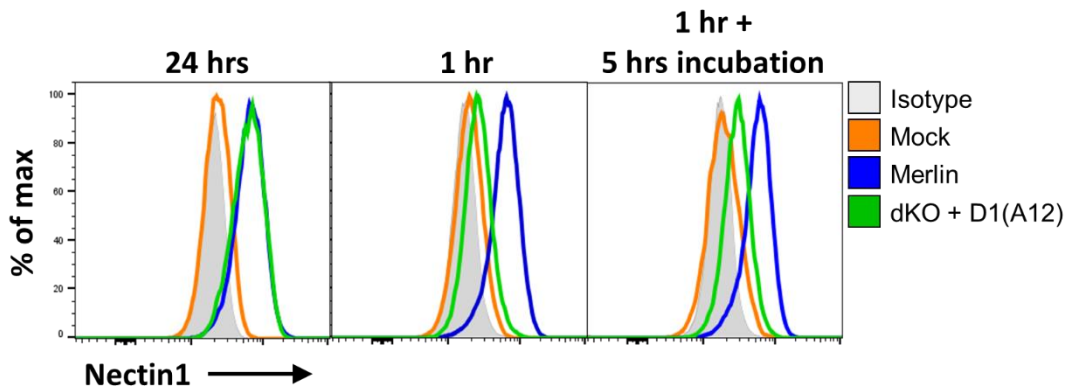
Figure 5.19: Flow cytometry surface Nectin1 staining on HF-TERTs infected with indicated HCMV strains (MOI = 10, 72 hpi) and treated with D1(A12). dKO-infected HF-TERTs were treated with anti-ADAM17 D1(A12) for 1 and 24 hrs prior to cell harvest and staining. Additionally, a subset of cells was incubated for 5 hrs after 1 hr D1(A12) treatment in D1(A12)-free media prior to staining to mimic CD107a degranulation assay incubation.

5.3.6 Investigating the effect of D1(A12) blocking of ADAM17 on NK cell inhibition by Merlin

Differential expression of surface ADAM17 and Nectin1 levels after 24 hrs and 1 hr D1(A12) treatment on dKO-infected HF-TERTs facilitated a comparison of CD107a degranulation assay by NK cells at these timepoints to assess the role of ADAM17 in NK cell inhibition. CD107a degranulation assays were performed on two NK cell lines where dKO-infected targets were treated with anti-ADAM17 D1(A12) 1 hr or 24 hrs prior to co-culture. Both NK cell lines demonstrated decreases compared to Mock and recovery in NK cell activation in response to Merlin- and dKO-infected targets, respectively (**Figure 5.20**). The D003 NK cell line showed a non-significant (p = 0.5683) downward trend in NK cell activation against Merlin-infected targets, while the differences of the D169 NK line were highly significant. Anti-ADAM17 D1(A12) treatment for 24 hrs showed a significant reduction in NK cell activation in both NK lines, whereas 1 hr treatment failed to inhibit NK cells (**Figure 5.20**). Thus, inhibition of NK cell activation did not correlate with ADAM17 expression, indicating that ADAM17 was unlikely to be a novel NK cell activating ligand and that the observed ADAM17-dependent NK cell inhibition was due to an upregulation of an ADAM17 substrate on the cell surface as a result of ADAM17 impairment by HCMV.
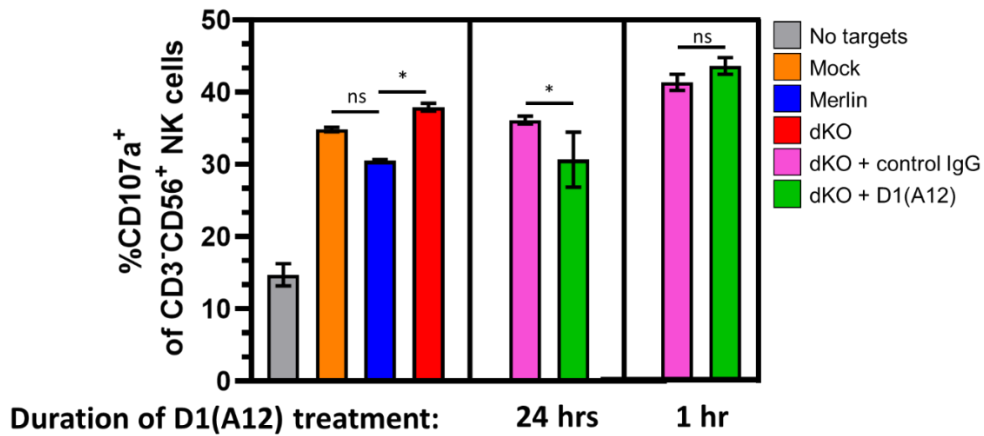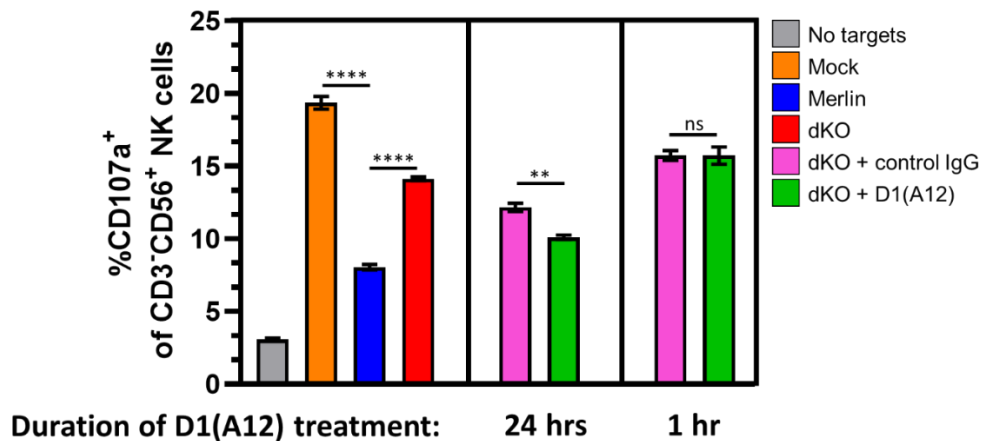
Figure 5.20: CD107a degranulation assay on D003 and D169 NK cell lines following different D1(A12) treatments on dKO-infected targets reveals the importance of ADAM17-dependent substrate in NK cell function. HF-TERT cells were infected with indicated HCMV strain or Mock-infected (MOI = 10, 72 hrs). dKO-infected targets were treated with D1(A12) anti-ADAM17 blocking antibody or control human IgG 24 hrs or 1 hr prior to harvest. At 72 hpi infected HF-TERT cells were co-cultured indicated NK cell lines. Effector:target ratio of 10:1 was used for the co-culture, following a 5 hrs incubation in the presence of anti-CD107a antibody and GolgiStop (BD). Effectors were stained and analysed by flow cytometry for %CD107a of CD3-CD56+ NK cells. Means +/- SEM of quadruplicate samples are shown. ANOVA with Tukey multiple comparison post-hoc tests showed significance at ****$p<0.0001$, ***$p<0.001$, **$p<0.01$, *$p<0.05$, ns – not significant.

5.3.7 Nectin1 expression on keratinocytes and its effect on NK cell function

Data presented in **Figure 5.20** implied that it was the accumulation of at least one ADAM17 substrate on the cell surface that was responsible for ADAM17-dependent NK cell inhibition by HCMV. One potential candidate was Nectin1. There have been contradictory reports in the literature implicating Nectin1 as both an activator (Holmes et al. 2019) and inhibitor (Chan et al. 2012) of NK cells. To test this in our own systems, Nectin1 KO and WT keratinocyte cell lines (a kind gift from Dr Gill Elliott) were used as targets in a CD107a degranulation assay with NK cell lines as effectors. Staining of the keratinocyte cell lines confirmed the presence or absence of Nectin1 (**Figure 5.21 A**). Both NK cell lines responded similarly, with significantly increased activation in response to Nectin1 KO, compared to WT, keratinocyte targets (**Figure 5.21 B**), consistent with an inhibitory function for NK cells with these NK cell lines.
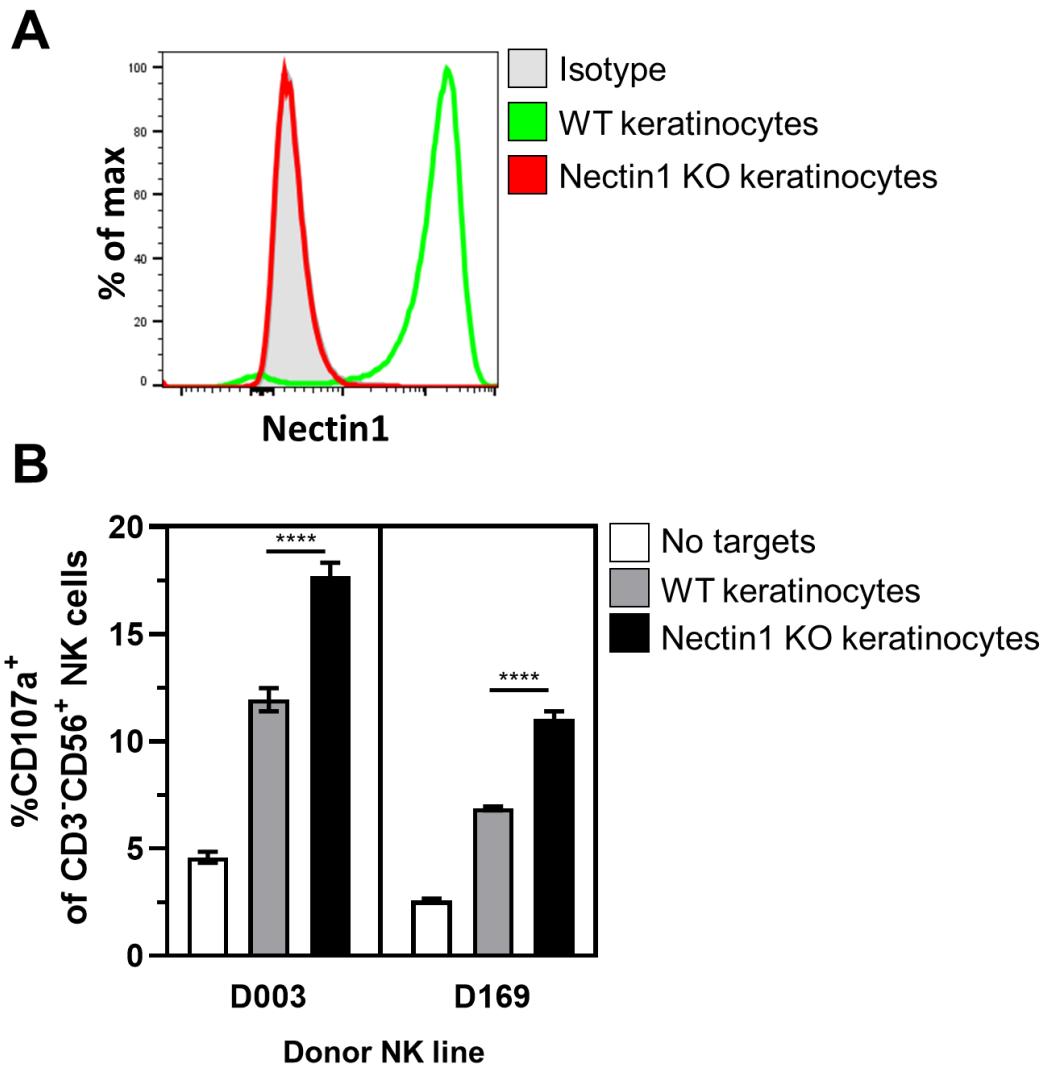
Figure 5.21: NK CD107a levels in response to keratinocytes suggest inhibitory Nectin1 role in NK cell function. (A) Flow cytometry staining of surface Nectin1 on keratinocyte cell lines. **(B)** CD107a degranulation assay on D003 and D169 NK cell lines in response to keratinocyte cell lines. Nectin1 KO keratinocytes were kindly provided by Gill Elliot. Effector:target ratio of 10:1 was used for the co-culture, following 5 hrs incubation in the presence of anti-CD107a antibody and GolgiStop (BD). Effectors were stained with Fixable Aqua 405nm viability stain, CD3-PE and CD56-APC, and analysed by flow cytometry for %CD107a of CD3-CD56+ NK cells. Means +/- SEM of quadruplicate samples are shown. ANOVA with Tukey multiple comparison post-hoc tests showed significance at ****$p < 0.0001$.

5.3.8 CD96 expression on NK cells and correlations with NK inhibition

Since Nectin1 is a ligand for the CD96 receptor on NK cells, I assessed the levels of CD96 on the effector cells in my assays, namely NK cells from PBMC and NK cell lines. NK cells from PBMC had low levels of surface CD96, that was not particularly induced by IFNα stimulation (<2% in all three donors) (**Figure 5.22 A**). In contrast, NK cell lines showed high levels of CD96 expression, with almost all cells being CD96+ (**Figure 5.22 B**). It was important to note that NK cell lines stimulated on different occasions demonstrated varied levels of CD96 expression, and on some occasions NK cell lines showed less CD96, however the lowest %CD96+ cells recorded was 60%. This was consistent with Nectin1 being inhibitory to NK cell function, where such large differences in CD96 levels between NK cells from PBMC and NK cell lines could explain the differential effects of D1(A12) treatment on NK activation against dKO-infected targets when using PBMC as effectors (no effect) (**Figure 5.15**) compared to the large and consistent inhibition observed using NK cell lines (**Figure 5.16**).
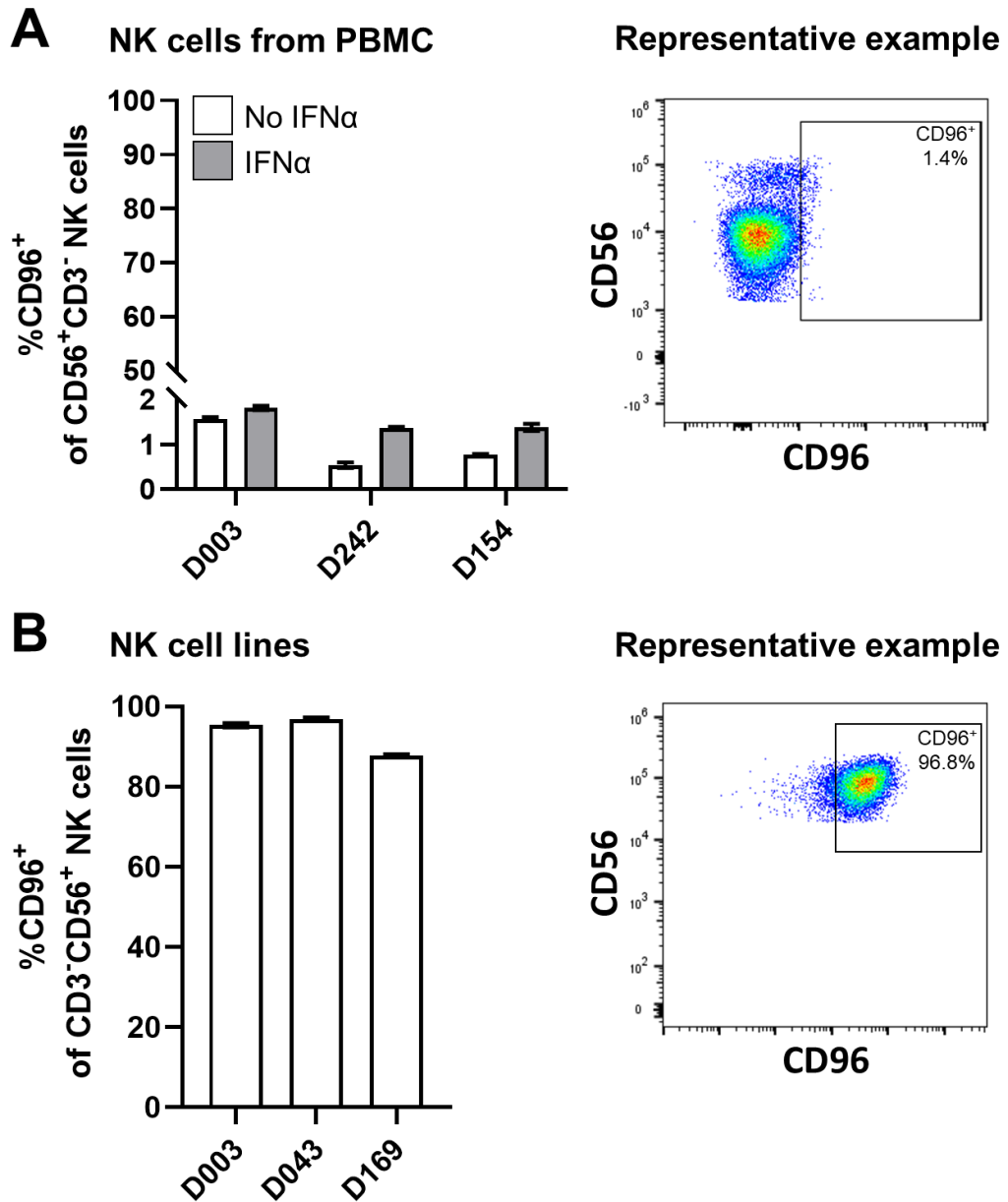
Figure 5.22: CD96 expression on NK cells correlates with NK inhibition.
%CD96+ cells of **(A)** NK cells from PBMC from three donors and **(B)** three NK cell lines. *Ex vivo* PBMC were stimulated with IFNα overnight prior to staining. Cells were stained with Fixable Aqua 405nm viability stain, CD3-PE, CD56-APC, CD96-PeCy7 and analysed by flow cytometry for %CD96+ of CD3-CD56+ NK cells. Means +/- SEM of duplicate samples are shown.

5.3.9 Binding of anti-Nectin1 antibodies

While the increase in NK activation following exposure to Nectin1 KO keratinocytes and good levels of CD96 expression on NK cell lines were consistent with an NK inhibitory function for Nectin1, this did not demonstrate its role in the context of HCMV infection. HCMV cannot infect keratinocytes, so I returned to our standard HCMV permissive line, HF-TERTs. There was limited literature on antagonistic anti-Nectin1 antibodies, therefore I selected two to test in functional assays (R1.302 from BioLegend and CK6 from SantaCruz). HF-TERTs were first stained with the mAbs to ensure they could bind surface Nectin1. Uninfected HF-TERTs had low levels of Nectin1 on their surface, therefore cells were infected with HCMV strain Merlin to upregulate the protein prior to flow cytometric analysis. Both anti-Nectin1 antibodies demonstrated good Nectin1 staining, with R1.302 producing the higher fluorescence signal (MFI 48170 and 11728 for R1.302 and CK6 mAbs, respectively) (**Figure 5.23**).
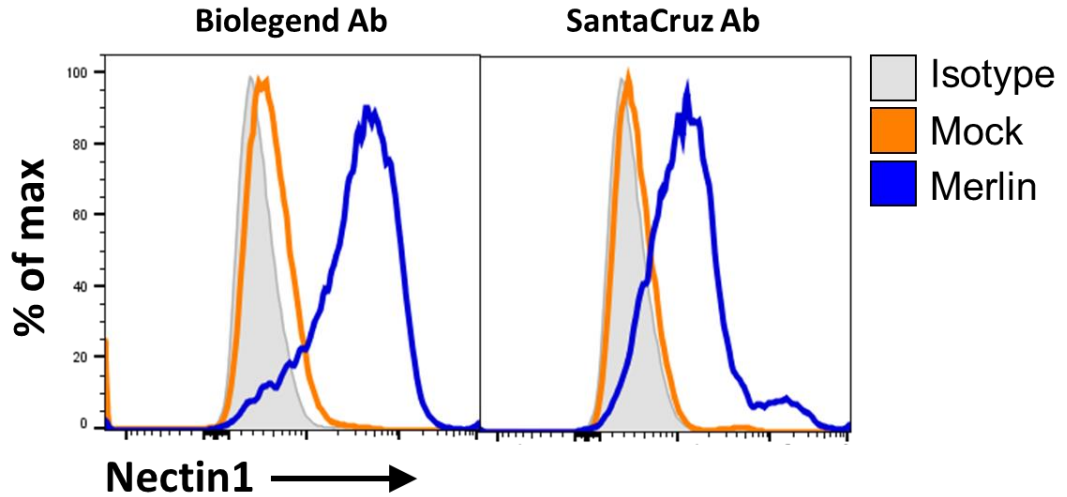
Figure 5.23: Flow cytometry staining of surface Nectin1 on HF-TERTs using two different anti-Nectin1 antibodies (R1.302 from BioLegend and CK6 from SantaCruz). HF-TERT cells were infected with HCMV strain Merlin or Mock-infected (MOI = 10, 72 hrs) prior to staining. MFI 48170 and 11728 for R1.302 and CK6 mAbs, respectively.

5.3.10 Effect of anti-Nectin1 antibodies on NK activation following ADAM17 blockage on HCMV-infected cells

CK6 anti-Nectin1 antibody was first tested in a CD107a degranulation assay to assess its capacity to alter NK activation in the context of an HCMV infection. The working hypothesis was that if Nectin1 was acting as an inhibitory ligand, blocking it would result in increased NK cell activation in response to Merlin-infected targets. CD107a degranulation assays were performed using three NK cell lines, in which Merlin-infected targets were pre-treated with the anti-Nectin1 CK6 mAb 1 hr prior to co-culture. No significant differences in NK cell activation were observed in the NK responses to Merlin-infected targets treated with anti-Nectin1 antibody or control IgG using any of the cell lines (**Figure 5.24**).

R1.302 anti-Nectin1 antibody was then used in a CD107a degranulation assay in a second set of experiments, set up in a similar fashion to the assay performed with CK6. In addition to Merlin-infected cells, anti-Nectin1 mAb was also applied to dKO-infected cells following anti-ADAM17 D1(A12) treatment, which also had Nectin1 on their surface. Treatment of Merlin-infected targets with R1.302 anti-Nectin1 antibody showed no significant difference in NK cell activation compared to control IgG-treated cells, similar to the results obtained using CK6 mAb (**Figure 5.25**). The D003 NK cell line showed a small but significant reduction in NK cell activation in response to dKO-infected targets treated with anti-Nectin1 antibody. Additionally, both D003 and D043 NK cell lines demonstrated significantly reduced NK cell activation against dKO-infected D1(A12)- and anti-Nectin1-treated targets (**Figure 5.25**).

Both sets of data were not consistent with my hypothesis that Nectin1 acts as an inhibitory ligand for CD96 on NK cells against HCMV-infected targets, with the D003 data suggesting the opposite. However, neither antibody had been shown previously to antagonise the interaction between CD96 and Nectin1 and therefore, conclusions from this dataset should be approached with caution.
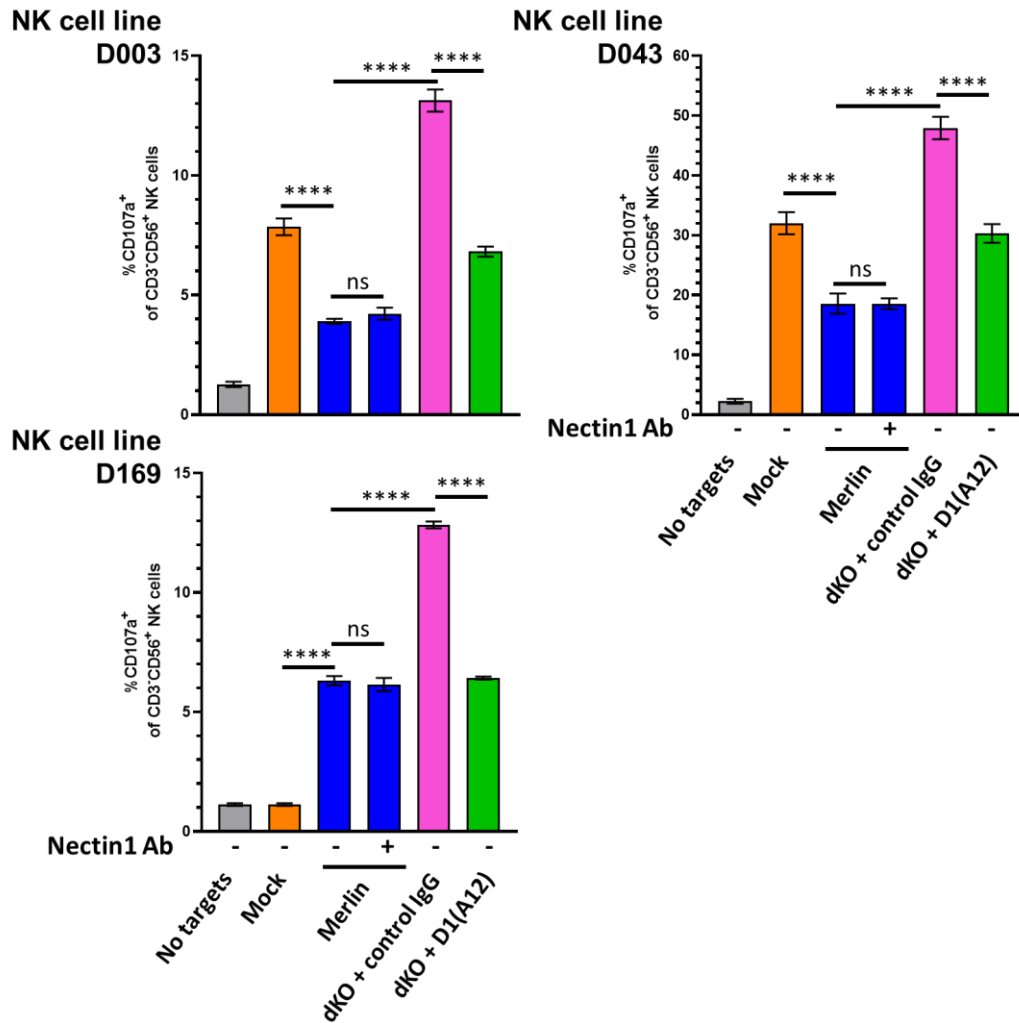
Figure 5.24: CD107a degranulation assay using D003, D043 and D169 NK cell lines following anti-Nectin1 antibody treatment (CK6, SantaCruz) on Merlin-infected targets. HF-TERT cells were infected with the indicated HCMV strain or Mock-infected (MOI = 10, 72 hrs). Targets infected with dKO HCMV were treated with D1(A12) anti-ADAM17 blocking antibody or control human IgG 24 hrs prior to co-culture. Targets infected with Merlin were treated with SantaCruz anti-Nectin1 antibody or control IgG 1 hr prior to co-culture. At 72 hpi infected HF-TERT cells were co-cultured with the indicated NK cell lines. An effector:target ratio of 10:1 was used for the co-culture. Following a 5 hrs incubation in the presence of anti-CD107a antibody and GolgiStop (BD), effectors were stained and analysed by flow cytometry for %CD107a of CD3-CD56+ NK cells. Means +/- SEM of quadruplicate samples are shown for three NK lines. ANOVA with Tukey multiple comparison post-hoc tests showed significance at ****$p<0.0001$, ns – not significant.
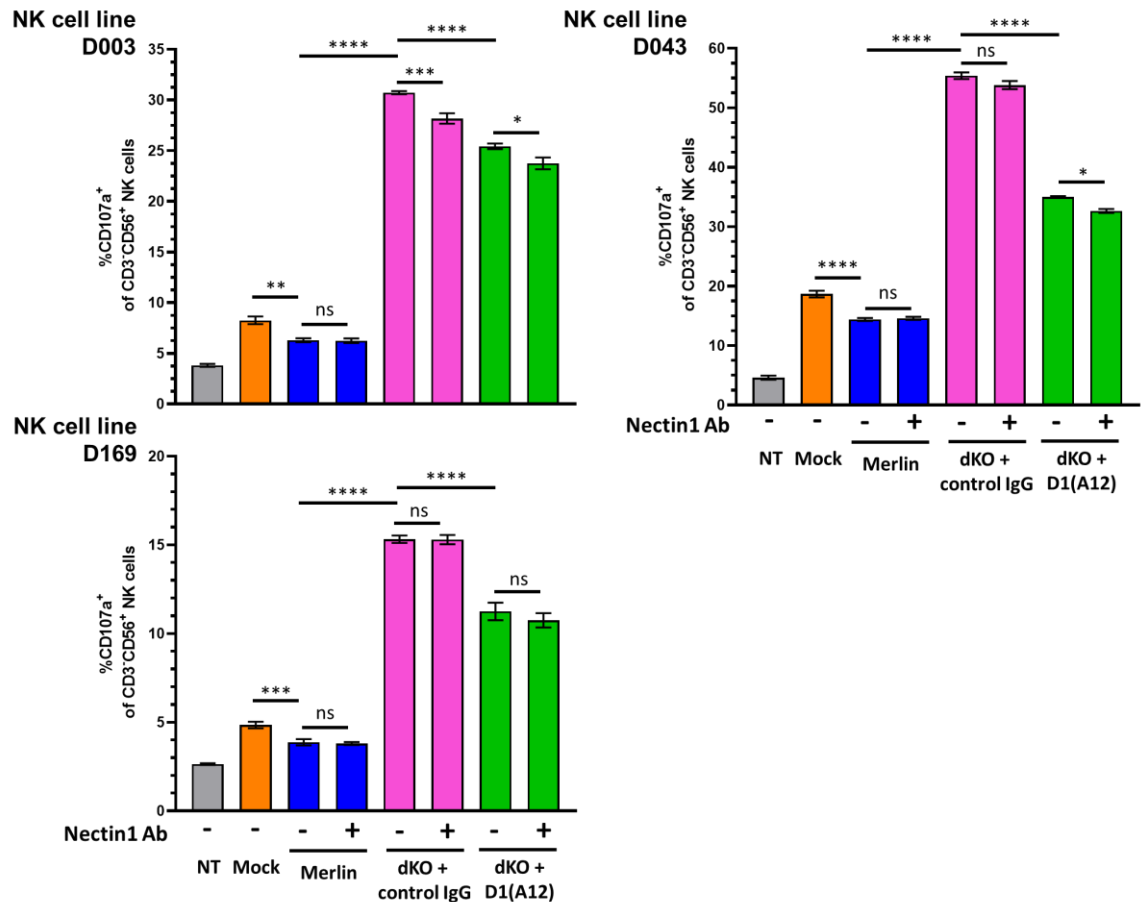
Figure 5.25: CD107a degranulation assay using D003, D043 and D169 NK cell lines following anti-Nectin1 antibody (R1.302, BioLegend) treatment on HCMV-infected targets. HF-TERT cells were infected with indicated HCMV strain or Mock-infected (MOI = 10, 72 hrs). Targets infected with dKO HCMV were treated with D1(A12) anti-ADAM17 blocking antibody or control human IgG 24 hrs prior to co-culture. Targets infected with Merlin were treated with BioLegend anti-Nectin1 antibody or control IgG 1 hr prior to co-culture. At 72 hpi infected HF-TERT cells were co-cultured with the indicated NK cell lines. An effector:target ratio of 10:1 was used for the co-culture. Following a 5 hrs incubation in the presence of anti-CD107a antibody and GolgiStop (BD), effectors were stained and analysed by flow cytometry for %CD107a of CD3$^-$CD56$^+$ NK cells. Means +/- SEM of quadruplicate samples are shown for three NK lines. ANOVA with Tukey multiple comparison post-hoc tests showed significance at ****$p<0.0001$, ***$p<0.001$, **$p<0.01$, *$p<0.05$, ns – not significant. NT – no targets.

5.3.11 Assessing the effect of anti-CD96 mAbs on NK cell function

To explore this further, I investigated mAbs against CD96. Two NK cell lines were treated with anti-CD96 antibody prior to use in a CD107a degranulation assay. The D003 NK cell line failed to show any differences in NK cell activation against HCMV-infected targets in the presence or absence of anti-CD96 antibody, or significant differences between any targets although the previously reported trends were observed (**Figure 5.26 A**). In contrast, the D169 NK line responded to HCMV-infected targets as expected, demonstrating significant differences in response to Merlin-, dKO- and dKO-infected D1(A12)-treated targets (**Figure 5.26 B**). However, anti-CD96 antibody treatment had no effect on NK cell activation across all targets (**Figure 5.26 B**). Again, this was not consistent with the hypothesis that the CD96/Nectin1 axis is inhibitory during HCMV infection, but the pitfalls of using mAb to block the function will be discussed.
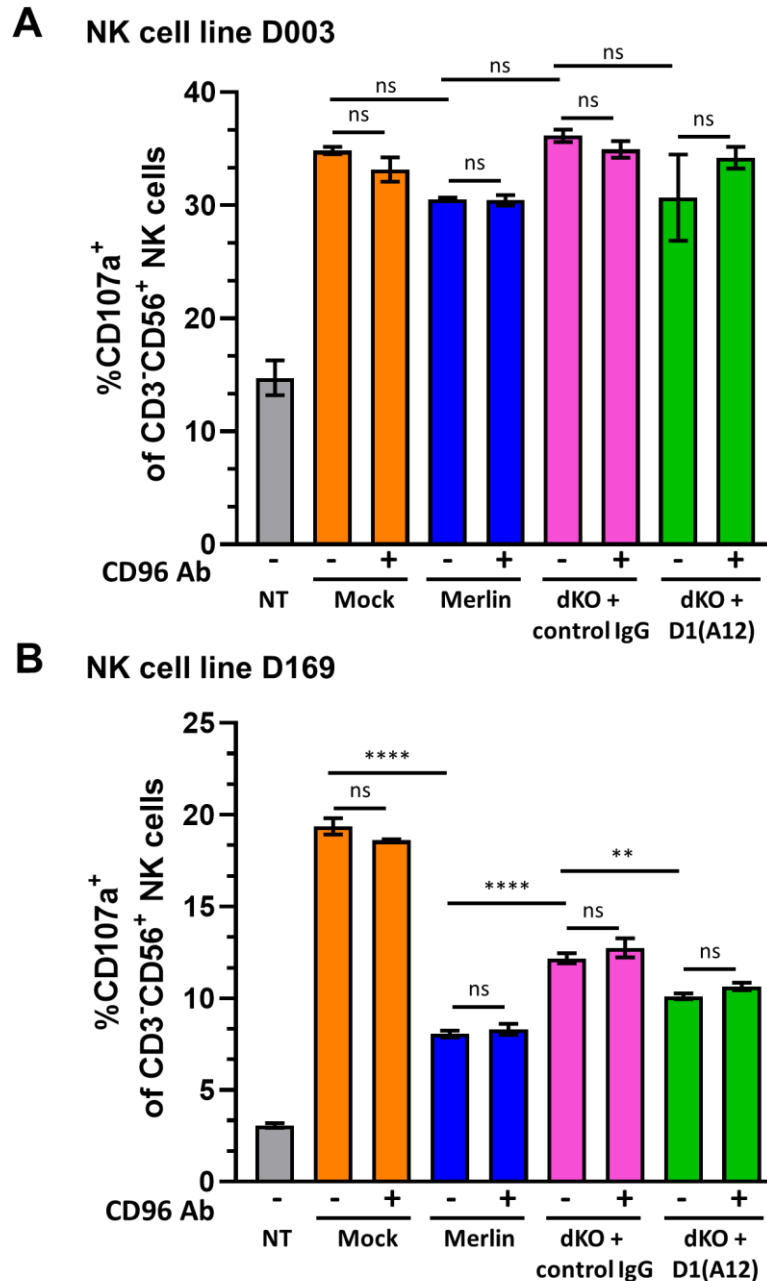
Figure 5.26: CD107a degranulation assay using anti-CD96 antibody treatment on NK cell lines. (A) D003 and **(B)** D169 NK cell lines following anti-CD96 antibody treatment on HCMV-infected targets. HF-TERT cells were infected with indicated HCMV strain or Mock-infected (MOI = 10, 72 hrs). Targets infected with dKO HCMV were treated with D1(A12) anti-ADAM17 blocking antibody or control human IgG 24 hrs prior to co-culture. At 72 hpi infected HF-TERT cells were co-cultured indicated NK cell lines. NK cell lines were pre-treated with anti-CD96 antibody for 15 minutes prior to the co-culture, and the antibody was left in the media for the duration of the assay. An

effector:target ratio of 10:1 was used for the co-culture. Following a 5 hrs incubation in the presence of anti-CD107a antibody and GolgiStop cells were stained and analysed by flow cytometry for %CD107a of CD3-CD56+ NK cells. Means +/- SEM of quadruplicate samples are shown. ANOVA with Tukey multiple comparison post-hoc tests showed significance at ****p<0.0001, **p<0.01, ns – not significant. NT – no targets.

5.4   Summary of findings

This chapter aimed to investigate the functional consequences of UL148/UL148D-mediated ADAM17 impairment. Of the many proteins detected in PMP and secretome proteomics to be significantly altered as a result of ADAM17 impairment, three were selected for functional validation because of their potential for immune modulation. Jagged1 and Vasorin were selected due to their established role in TGFβ signalling and Treg development, whereas Nectin1 was chosen due to its proposed function in NK cell regulation.

Treg expansion assays were designed and optimised in order to investigate the potential of HCMV infection to drive Treg development. The use of whole *ex vivo* PBMC as responders, as well as WT HF-TERTs as stimulators, failed to induce significant Treg expansions against Merlin-infected cells. Assays using purified naïve CD4+ T cells as responders provided some evidence of Treg proliferation in response to Merlin-infected targets, however effects appeared to be donor specific. In addition, assays on purified naïve CD4+ T cells demonstrated expansions of additional CD3+CD4- and CD3-CD4- populations at lower OKT3 concentrations, possibly linked to contamination by other immune cell types during the separation process.

NK cell CD107a degranulation assays also required a level of optimisation, however they conclusively demonstrated a connection between UL148/UL148D-mediated ADAM17 impairment and inhibition of NK cell function. NK inhibition was only achieved when treating dKO-infected cells with anti-ADAM17 D1(A12) mAb for 24 hrs, and not 1 hr, prior to NK assays. This correlated with the time needed to stabilise surface expression of ADAM17 substrates and not with expression of ADAM17 itself, suggesting a role for at least one ADAM17-dependent substrate in this process. Although Nectin1 was shown to be inhibitory to NK cells in the context of keratinocytes, and CD96 expression on NK cell effectors correlated with the inhibitory phenotype, antibodies to Nectin1 or CD96 failed to alter NK cell responses to either Merlin-infected cells or dKO-infected cells treated with D1(A12) ADAM17 blocking antibody. The data suggests that upregulated surface Nectin1 is not

dominantly involved in NK cell inhibition by HCMV, however it is also possible that the antibodies used were targeted against areas not involved in the interaction between CD96 and Nectin1. The underlying ADAM17 substrate(s) responsible for NK cell inhibition remain unproven, but there are many other candidates.

6 General Discussion

HCMV has been described as a paradigm of immune evasion due to the variety and complexity of immune evasion strategies it employs to manipulate host immune responses and establish a life-long infection. Nevertheless, many aspects of HCMV biology remain poorly understood. Recent advances in proteomic techniques facilitated the study of global temporal changes in viral and host proteomes during HCMV infection using PM and WCL profiling. This approach led to the discovery of proteins important in host defence and viral pathogenesis, as well as identification of a number of viral cell-surface glycoproteins that could potentially be used as therapeutic targets in the future (Weekes et al. 2014). Regardless, our understanding of the viral genes and mechanisms involved in shaping the cellular proteome following HCMV infection remain limited. This thesis demonstrated the importance of two viral genes UL148 and UL148D in significantly altering the composition of many surface and secreted proteins simultaneously in the host by impairing the function of a single 'sheddase' ADAM17. The mechanism of ADAM17 downregulation was investigated, as well as the functional impact of ADAM17 impairment in the context of Treg and NK cell function, demonstrating the significance of ADAM17 manipulation by HCMV.

6.1 HCMV induces global changes to the cellular proteome by impairing a single 'sheddase' ADAM17

6.1.1 Using proteomics to identify global changes to the cellular and viral proteomes

This thesis combined two proteomics approaches investigating HCMV-induced protein changes on PM and secreted proteins on fibroblasts infected with different HCMV mutants. Global protein secretion in HCMV-infected cells has previously been studied by others (Dumortier et al. 2008; Botto et al.

2011), however those studies looked at just one time point after HCMV infection and used HCMV strains that are known to have compromised genetic integrity, such as AD169 and VR1814 (Wilkinson et al. 2015). Strain AD169 had previously been shown to have no effect on ADAM17 levels which can be attributed to the deletion of the U_L/b' region in that strain, and therefore a lack of UL148 and UL148D to downregulate ADAM17 (Esteso et al. 2014). Similarly, a previous report suggesting that HCMV downregulated surface Jagged1 may be explained by the use of HCMV strain Towne, which like strain AD169, lacks UL148 and UL148D (Li et al. 2015b).

Considering the importance of ADAM17 shedding function in regulating the cellular proteome, results generated from secretome proteomic studies using HCMV strains lacking UL148 and UL148D should be interpreted carefully. Although a genetically intact HCMV strain Merlin, and Merlin derived KO mutants, were used to generate the secretome data in this thesis, it was surprising to observe that the secretome of dKO HCMV-infected cells was not hugely different to Merlin and the single deletion HCMV mutants (**Figure 3.2**). It was thought that the presence of functioning ADAM17 would lead to increased shedding of ADAM17 substrates, resulting in a significantly different secretome, however hierarchal clustering analysis did not strongly support that. Out of 17 highly significant hits increased in the dKO HCMV secretome, only five were previously reported as known ADAM17 targets (**Table 3.1**).

In contrast, PMP hierarchal clustering of fold change over Mock revealed a distinct section of upregulated proteins in dKO HCMV infection, some of which were identified as known ADAM17 targets (**Figure 3.5 B**). PMP detected a higher proportion of known ADAM17 targets (10 out of 23 most significant hits), suggesting that secretome proteomics may not be sensitive enough to reliably detect ADAM17-mediated changes to the composition of secreted proteins. Indeed, secretome studies have reported difficulties in detection of low abundance proteins (Chen et al. 2019; Deshmukh et al. 2019). For example, proteomic analysis of serum and plasma has shown that the presence of highly abundant albumin, representing up to 80% of total protein composition, results in limited detection of lower abundance proteins (Georgiou et al. 2001).

Furthermore, secretome proteomics require the culture of cells in serum-free media from 12 to 24 hrs prior to supernatant harvest to avoid the interference from serum contaminants during the MS step. This might further alter the cell secretome profile, reducing the correlation to the true physiological secretome (Brown et al. 2012). Another explanation for reduced sensitivity in the secretome proteomics is how the raw MS data is filtered to remove any non-soluble proteins from the analysis. In this thesis, secreted proteins were defined by the presence of classical or non-classical secretion signals in the protein sequence or gene annotations for the terms 'Secreted', 'Extracellular' or 'Exosome' from Uniprot. Since this method of filtering relies on external databases which are not always up to date, secreted hits can accidently be excluded from analysis, which is particularly true for pathogens due to the use of alternative secretion signals. This may explain why highly significant protein hits, such as RL12, identified in the secretome proteomics were excluded from final analysis, despite demonstrating significant fold changes in the dKO secretome compared to Merlin (over 4x fold increase in RL12 levels in dKO secretome compared to Merlin at 24 hpi) (**Figure 3.4 B**).

Although, secretome proteomics may have demonstrated limited detection sensitivity, nevertheless it provided valuable insight into the role of UL148 and UL148D in regulating the secretome. Hierarchal clustering of fold change over Mock at 24 hpi showed that the dKO secretome was more similar to the ΔUL148D secretome, whereas the ΔUL148 secretome clustered with Merlin, suggesting that UL148D may play a more dominant role in early stages of ADAM17 impairment than UL148 (**Figure 3.2**). This observation is further supported by the results of UL148/UL148D immunoblotting, demonstrating high levels of UL148D at 24 hpi, in contrast to UL148 which peaked at 48 hpi (**Figure 4.3**). Furthermore, secretion of a few known ADAM17 targets, such as TNFR1 and TNFR2, was also increased in the secretomes of single deletion HCMV mutants, possibly due to a partial recovery of ADAM17 on those cells, further supporting the idea that synergistic action of UL148 and UL148D is required to effectively impair ADAM17 (**Figure 3.3**) (Patel 2018).

Since anti-ADAM17 D1(A12) blocking antibody was not included in the secretome proteomics experiment, observed changes in protein secretion

could only be attributed to UL148 and UL148D function, rather than the impairment of ADAM17. However, by comparing hits identified in the secretome to those identified in PMP, which included D1(A12) anti-ADAM17 blocking antibody in the experimental design, I was able to shortlist 11 proteins that were significantly affected by UL148- and UL148D-driven ADAM17 abolishment in both datasets (**Table 3.3, Figure 3.7**). The presence of shared hits between these datasets support the contention that alterations in the dKO secretome are likely to be caused by ADAM17 impairment mediated by UL148 and UL148D. All shortlisted proteins were also compared to an already published proteomics QTV dataset, with most of them demonstrating an increase in PM levels by 72 hpi in the QTV. Thus, these changes may be explained by the lack of ADAM17 shedding in dKO-infected cells (**Figure 3.7**) (Weekes et al. 2014). However, not all proteins in the QTV showed convincing increases in expression, particularly Vasorin, which later was successfully validated in the context of HCMV infection (**Figure 3.8**). It is possible that due to low baseline Vasorin levels in HF-TERTs (**Figure 3.8 A**), there were very few peptides detected during QTV MS, leading to inconsistent results across multiple proteomics datasets. This highlights the importance of utilising multiple proteomics datasets, if available, and validating selected proteomics results before starting any functional or mechanistic work.

6.1.2 ADAM17 specific impact on the HCMV proteome

One key advantage of the PMP was the use of D1(A12) anti-ADAM17 blocking antibody in the experimental design allowing for a direct comparison of cell surface protein changes and ADAM17 function. It identified a number of novel ADAM17 targets, which is particularly important for studying overall ADAM17 biology, since ADAM17 dysregulation has been implicated in many disorders, including inflammation, cancer and neurological pathologies (Gooz 2010). Some of the newly identified ADAM17 substrates have previously been shown to be cleaved by other members of the ADAMs family of metalloproteinases, as well as other matrix metalloproteinases (MMPs). ICAM5 is known to be cleaved into its soluble form by MMP-2 (Tian et al. 2007), whereas Syndecan-

3 has cleavage sites for MMP-2, -9 and -14, although its shedding is yet to be confirmed experimentally (Arokiasamy et al. 2019; Bertrand and Bollmann 2019). Both SIRPα and Nectin1 are cleaved by ADAM10 – an ADAM protease sharing some functional similarities with ADAM17 (Kim et al. 2010; Londino et al. 2015). A number of surface substrates are shed by both ADAM10 and ADAM17 while others are shed by either protease (Pruessmeyer and Ludwig 2009). In this thesis I have validated Nectin1 as a novel ADAM17 target (**Figure 3.8 C**), and although SIRPα was not validated, it came up in the dKO secretome proteomics as well as PMP, suggesting that it is likely to be cleaved by both ADAM10 and ADAM17 (**Table 3.3, Figure 3.7**). Other proteins previously reported to be cleaved by metalloproteases that were discovered in the secretome analysis were CCL7 and Basigin (**Table 3.1**). MMP-13 cleaves CCL7, whereas Basigin is a known ADAM12 target (Liu et al. 2018; Albrechtsen et al. 2019). Together with many other proteins identified in both proteomics experiments as significantly altered due to UL148- and UL148D-mediated ADAM17 impairment, these findings would suggest that ADAM17 cleaves even more substrates than originally thought.

PMP demonstrated a significant reduction in surface protein levels of 114 proteins at significance threshold of $p<0.05$, with only 13 proteins identified as known ADAM17 targets and 101 as novel (**Appendix 8.1**). It is possible that D1(A12) anti-ADAM17 antibody had poor specificity to ADAM17 and inhibited other ADAMs in the PMP experiment. However, that seems unlikely since D1(A12) was originally designed for specificity and use therapeutically (Tape et al. 2011; Richards et al. 2012). It was designed to target the ancillary domains of ADAM17, which are absent in the MMPs and less conserved than the catalytic domain among other members of the ADAMs family (Tape et al. 2011).

In contrast to such an abundance of potentially novel ADAM17 targets identified, many known ADAM17 substrates were not detected in dKO HCMV proteomes. This may in part be explained by ADAM17 shedding activity being cell type and cellular context dependent, as well as by the differences in the levels of ADAM17 substrates among different cell types (Edwards et al. 2008; Ebsen et al. 2013). However, a more interesting explanation is active

downregulation of undesired ADAM17 targets by separate HCMV mechanisms. For example, members of the HCMV US12 gene family modulate the expression of known ADAM17 substrates, such as CD166, ICOS ligand, Sydecan-4, as well as MICA and MICB (Fielding et al. 2017). MICA and MICB serve as ligands for the activating NK cell receptor NKG2D, however HCMV retains MICA and MICB in the cis-Golgi via UL142 and UL16 respectively, targets MICA for lysosomal degradation via US18 and US20 (Dunn et al. 2003a; Ashiru et al. 2009; Fielding et al. 2014), and proteasomal degradation via UL147A (Seidel et al. 2021). This indicates complex viral strategies where the upregulation of certain surface proteins caused by inhibition of ADAM17 function is blocked if unfavourable for HCMV. Accumulation of selected ADAM17 substrates on the surface of HCMV-infected cells is therefore likely to be of high importance to the virus.

Excluding host proteins, it was intriguing to observe a number of viral proteins stabilized on the cell surface as a result of ADAM17 blocking by D1(A12) (**Table 3.2**). Three viral proteins showing highly significant cell surface stabilization were identified in PMP - UL144, UL7 and UL8, with UL144 detected in the secretome also (**Table 3.3**). All these viral proteins have previously reported immune functions. UL7 promotes myelopoiesis as a ligand for Fms-like tyrosine kinase 3 receptor, UL8 impairs myeloid proinflammatory cytokine production, and UL144 inhibits CD4+ T-cell proliferation through its interaction with B and T lymphocyte attenuator (BTLA) (Cheung et al. 2005; Crawford et al. 2018; Pérez-Carmona et al. 2018). Indeed, more viral proteins were detected at lower significance thresholds, such as RL12 and UL40, further highlighting the importance of ADAM17 impairment during HCMV infection through preventing the shedding of a number of viral proteins from the surface of the infected cell where they can interact with ligands (**Appendix 8.1**).

6.2 The mechanism of ADAM17 impairment by UL148 and UL148D is complex

With proteomics results evidently demonstrating the extent of ADAM17 impairment by HCMV to the cellular proteome, the next question was how UL148 and UL148D impaired ADAM17 expression. ADAM17 is tightly regulated by a number of chaperones (**Figure 1.8**). However, in his thesis Dr Mihil Patel showed no interactions between UL148 and UL148D and the established ADAM17 regulators iRhom1/2, FRMD8 and PACS2 (Patel 2018). Similarly, I failed to observe UL148- and UL148D-dependent changes to the levels of Furin and PACS1 (**Figure 4.6**). Indeed, none of the known ADAM17 regulating proteins were reported to bind UL148 and/or UL148D in a recently published HCMV interactome dataset (Nobre et al. 2019), suggesting that UL148 and UL148D impair ADAM17 maturation through a distinct as yet undiscovered mechanism distinct from currently known ADAM17 traffickers and regulators. A number of selected UL148- and UL148D-binding proteins identified in the interactome proteomics failed to validate in our experiments and, consequently, were ruled out as proteins involved in HCMV-mediated ADAM17 dysregulation (**Figure 4.5**). It is important to note that published interactome hits may not be representative of the *in vivo* scenario, since overexpressing V5-tagged HCMV protein-expressing cell lines were used to pull down HCMV proteins of interest and their interactors, instead of using gene-tagged complete viruses (Nobre et al. 2019). Furthermore, weaker, and more transient interactions could have easily been missed by IP.

Interestingly, PACS1 immunoblotting demonstrated reduced levels of PACS1 in Merlin-infected cells that failed to recover when UL148 and UL148D were deleted. It is likely that at least one more HCMV gene is involved in ADAM17 impairment acting on downregulating PACS1 levels, leading to potential inhibition of Furin-mediated pro-ADAM17 cleavage into mature ADAM17 (**Figure 4.6**). Flow cytometric ADAM17 staining on dKO-infected cells failed to completely recover ADAM17 to the levels observed in Mock-infected cells, and, in fact, demonstrated similar levels of ADAM17 expression when compared to cells infected with AD169 (Patel 2018), implying that the third

gene targeting PACS1 is located outside the U$_L$/*b'* region of the HCMV genome. Together these findings suggest that ADAM17 is being targeted via multiple mechanisms and by at least three HCMV genes.

Although UL148 and UL148D were shown to act synergistically in reducing ADAM17 levels, they may act via distinct mechanisms. UL148D is expressed earlier than UL148, with temporal protein profile Tp2 kinetics, whereas UL148 is predominantly expressed later, with temporal protein profile Tp5 kinetics (**Figure 4.3**) (Weekes et al. 2014). Both proteins have ER-retention motifs (RRR at residues 314-316 for UL148 and IRR at residues 27-29 for UL148D) (elm.eu.org), however they failed to co-localise in immunofluorescence experiments (**Figure 4.1 & 4.2**) and did not bind each other or ADAM17 in the interactome proteomics (Nobre et al. 2019), further supporting distinct gene-specific ADAM17 targeting strategies. ADAM17 impairment is the only known function associated with UL148D reported thus far (Patel 2018), while UL148 has previously been described as an ER-resident glycoprotein associated with a number of viral functions.

UL148 has previously been shown to bind a key regulator of the ERAD pathway Sel1L, facilitate ER-stress signalling by inducing unfolded protein response (UPR) and retain CD58 inside the infected cell (Li et al. 2015a; Nguyen et al. 2018; Siddiquey et al. 2018; Wang et al. 2018). Hence, the ERAD pathway was investigated as a potential ADAM17 targeting strategy employed by UL148 and UL148D. While EerI treatment recovered mature ADAM17 in Merlin-infected cells, it is likely that increased levels of the mature form of ADAM17 were a result of reduced expression of UL148 and UL148D caused by EerI treatment. Indeed, the use of EerI treatment demonstrated some cellular toxicity, as well as major nonspecific signal spill over during flow cytometric analysis (**Figure 4.13**). As a result, our viability dyes could not be used in the staining panel, and live cells were gated based purely on the side and forward scatter. Data generated using an alternative, non-toxic ERAD inhibitor Kif, as well as proteasomal and lysosomal degradation inhibitors MG132 and leupeptin, demonstrated that ADAM17 impairment could not be attributed to the established degradation related functions of UL148, since they failed to recover the mature form of ADAM17 in HCMV-infected cells

(**Figure 4.15 & 4.18**). Although during this PhD I was unable to identify the exact mechanism behind UL148- and UL148D-mediated ADAM17 downregulation, results presented here imply that, apart from its established role in ERAD processes, UL148 may be an important immune modulator in an array of biological processes.

Cellular toxicity associated with ERAD inhibition, was not the only issue encountered whilst investigating the mechanism underlying ADAM17 targeting. All ADAM17 antibodies tested in immunofluorescence experiments, showed a disperse and non-specific staining of ADAM17, which could potentially be explained by the abundance of the deglycosylated mature form of ADAM17 in fibroblasts (**Figure 4.7**). In immunoblotting, ConA enrichment was used to remove this form of ADAM17 from cell lysates, resulting in clean immunoblotting of glycosylated forms of ADAM17. Anti-ADAM17 antibodies used for immunofluorescence were not specific to the glycosylated forms of the protein, therefore it is most likely that they were staining all forms of ADAM17, including the highly abundant deglycosylated ADAM17, the function of which remains unknown. Collectively, this demonstrates the issues associated with studying ADAM17 regulation, contributing to the failure to define the exact mechanism behind UL148- and UL148D-mediated impairment of ADAM17 during this PhD.

6.3   Functional significance of ADAM17 impairment

Proteomics results presented in Chapter 3 clearly highlighted the significance of ADAM17 impairment in HCMV infection facilitating the changes to the levels of surface and soluble proteins of host and viral origin. It was important to investigate the functional consequences of such changes to assess how they would benefit the virus. Dr Mihil Patel previously demonstrated the impact of ADAM17 impairment on TNFα-mediated pathways, demonstrating ADAM17-dependent changes to TNFα-mediated cytokine production (Patel 2018). However, he also observed inhibitory UL148 and UL148D function on TNFα-mediated cytokine production that occurred even in the absence of treatment

with D1(A12). This added an extra level of complexity to an already complex system and made it difficult to decipher the role of ADAM17 in TNFα-mediated signalling. Hence, I decided to look at other functional consequences of ADAM17 impairment by studying additional immune readouts, namely Treg expansions and NK cell activation.

6.3.1 Effect of HCMV-driven ADAM17 impairment on Treg development

Tregs have been shown to be implicated in acute MCMV infection. *In vitro* Treg cells were able to suppress MCMV-specific CD8$^+$ T cells, whereas *in vivo* Treg depletion enhanced MCVM-specific T cell responses resulting in decreased viral load (Li et al. 2010; Jost et al. 2014). However, there is limited research on Treg function in HCMV infection. Depletion of CD25+ T cells from PBMCs have previously been shown to increase T cell responses to CMV antigens in HIV-infected patients (Aandahl et al. 2004), while Jesser et al. (2006) described a subpopulation of CMV-specific T cells phenotypically defined as CD4+CD27-CD28- with regulatory characteristics, such as *de novo* inhibition of autologous PBMC in response to CMV antigenic stimulation, reduced activation, and increased apoptosis of CD4+ and CD8+ T cells (Jesser et al. 2006; Tovar-Salazar et al. 2010; Tovar-Salazar and Weinberg 2020). However, in those studies the expression of classical Treg markers FoxP3 and CD25 was only detected in a proportion of CD4+CD27-CD28- T cells (Tovar-Salazar and Weinberg 2020). FoxP3 and CD25 are considered to be the minimum required markers to define human Tregs (Santegoets et al. 2015). Hence, cells identified in the mentioned studies may not be describing Treg cells, but rather a subpopulation of T cells with regulatory properties. In contrast, this thesis used the combination of classic Treg markers FoxP3 and CD25, in addition to CD4 and CD3, to identify Tregs.

Treg expansion assays demonstrated that two of six donors showed significant increases in Tregs in response to Merlin-infected targets compared to dKO-infected targets, suggesting that in some individuals UL148 and UL148D may drive increases in Treg numbers (**Figure 5.10**). Other donors demonstrated slight increases, decreases or no change in Treg numbers and proportions,

possibly explained by the reduced levels of Jagged1, and perhaps Vasorin, on the surface of lentivirus-transduced cell lines as a result of longterm cell culture (**Figure 5.11**). Overtime, the expression of lentivirus-transduced proteins in cell lines may drop, which is particularly true for the polyclonal populations. Due to the random integration of the lentivirus into the host genome, transduced cells express varied levels of introduced transgene with low-expressors potentially overgrowing high-expressors, resulting in lower levels of the overexpressed protein overtime (Li and Rossi 2007). Although the involvement of Jagged1 and Vasorin was not directly tested by blocking studies, their established involvement in Treg development and TGFβ signalling make them appealing candidates for mediating Treg expansion during HCMV infection. This would be the first evidence for HCMV gene involvement in this process.

Another interesting finding that unexpectedly came up during the Treg work was the expansion of other cell subsets induced by HCMV, which was dependent on the strength of TCR signalling (**Figure 5.9**). Purification of naïve CD4+ T cells using beads isn't totally efficient. A small aliquot of isolated cells was always tested for purity by staining for the naïve T cell marker CD45RA *post* separation, and the percentage of CD4+CD45RA+ cells was on average around 95%. Therefore, the most likely explanation for the unexpected phenotype at lower OKT3 concentrations, is expansion of other immune cell types present in the isolated CD4+ T cell culture. The reason for not observing this phenotype at higher OKT3 concentrations may be due to stronger activation and proliferation of CD3+CD4+ T cells in those wells. Furthermore, in addition to CD4 and CD45RA other CD4+ T cell markers, such as CD62L and CCR7, should be used in the future to better define the populations within purified and cultured cells, considering effector memory T cells (TEMRAs) are also known to re-express CD45RA (Tian et al. 2017; Caccamo et al. 2018). The differences in immune cell responses to Merlin- and dKO-infected targets further highlight the roles of UL148 and UL148D in immune modulation.

Finally, it is important to note that Treg expansion assays required a substantial amount of optimisation and manipulation to obtain results, such as Jagged1 and Vasorin overexpression on target cells, the use of MHC-I lacking

β2mKO cells and 'naïve' CD4+ T cell isolation/stimulation. Although a differential Treg response between Merlin- and dKO-infected targets was observed in some donors, the manipulations may be far removed from a physiological situation where multiple cell types and signalling pathways are in crosstalk with one another.

6.3.2 Effect of HCMV-driven ADAM17 impairment on NK cell function

The use of NK cell lines facilitated robust experimental results demonstrating an inhibitory role for ADAM17 in NK cell function, however there were also requirements for conditions to observe these effects. For example, the first attempt of the NK cell CD107a assay was performed using NK cell lines 7 days *post* stimulation, and resulted in an increase in NK activation against Merlin-infected targets compared to Mock in two of three lines tested (**Figure 5.16 A**). However, a repeat experiment on the same NK cell lines 14 days post stimulation showed decreased responses to Merlin-infected targets (**Figure 5.16 B**), the effect that is regularly seen when using PBMC *ex vivo*. The difference in NK cell responses 1 week and 2 weeks *post* stimulation can be explained by the use of IL-15 and irradiated allogeneic feeder PBMC to drive NK cell expansions, resulting in potential over stimulation of NK cells (Huntington et al. 2009; Granzin et al. 2017). Furthermore, NK cell work highlighted the importance of regular reagent testing, as well as potential risks of culturing cell lines in vitro for prolonged periods of time, as shown by the lack of CD107a response when using old IFNα stocks and target cells (**Figure 5.14**).

HCMV is known to heavily target NK cell responses by downregulating activating ligands and providing inhibitory ones (Patel et al. 2018). Indeed, HCMV dedicates a large proportion of its genome to NK cell inhibition – the U$_L$/*b'* region alone contains at least five genes that disrupt NK cell function (Patel et al. 2018). Upregulation of Nectin1 expression caused by ADAM17 targeting is appealing mechanistically as it would be the first example of the upregulation of a potential inhibitory ligand caused by genes within the U$_L$/*b'* region. Although studies in mice attributed inhibitory functions to Nectin1, its

overexpression in K562 cells has also been shown to increase susceptibility of K562 cells to NK cell cytotoxicity, suggesting an activating function of Nectin1 in humans (Holmes et al. 2019). Hence, exploring the functional significance of ADAM17-dependent Nectin1 upregulation in HCMV infected cells was important for two reasons: to investigate the functional significance of ADAM17 impairment in HCMV infection and to clarify the role of Nectin1 in NK cell activation.

UL148 has previously been shown to inhibit NK cell function by downregulating activating adhesion protein CD58, however CD58 is not cleaved by ADAM17 (**Figure 3.6**), hence the observed impairment of NK cell responses cannot be attributed to this established UL148 function (Wang et al. 2018). NK cell responses to Nectin1 KO keratinocytes provided strong evidence to support Nectin1 being inhibitory to NK cells (**Figure 5.21**), however that did not seem to bear out in the context of HCMV infection (**Figure 5.24 – 5.26**). In contrast to the CRISPR-ed Nectin1 KO keratinocyte line, it is possible that the antibodies used to block Nectin1 and CD96 were not antagonistic. The anti-CD96 antibody (clone NK92.398) has previously been reported to successfully block the CD96 interaction with the poliovirus receptor (PVR/CD155) (Fuchs et al. 2004), but not CD96-Nectin1 interactions. Indeed, there are no reports of Nectin1-CD96 blocking with the antibodies used in this thesis. A Nectin1 KO fibroblast line would allow for a definitive study of the role of Nectin1 in NK cell function in the context of HCMV infection.

CD96 is one of three receptors together with DNAM-1 and T cell immunoglobulin and ITIM domain (TIGIT) on NK and T cells that share nectins and nectin-like molecules as ligands. These include Nectin1, Nectin2, Nectin3 and PVR (CD155), and regulate lymphocyte cytotoxicity (Sanchez-Correa et al. 2019; Harjunpää and Guillerey 2020). TIGIT stimulation promotes NK and T cell inhibition via its ligands Nectin2, Nectin3 and PVR (CD155), whereas stimulation of DNAM-1 via PVR (CD155) or Nectin2 delivers activating signals to the effectors (Harjunpää and Guillerey 2020). In contrast to the other two receptors, CD96 contains both inhibitory and activating motifs and has been shown to induce activating signals via its interaction with PVR (CD155) and Nectin1 in humans, as well as having inhibitory capacity through the CD96-

Nectin1 interaction in mice (Chan et al. 2012; Holmes et al. 2019). It is intriguing that HCMV upregulates Nectin1 on the surface of infected cells, especially since PVR (CD155) and Nectin2 are downregulated by viral UL141 and this has a dominant inhibitory effect on NK cells (Tomasec et al. 2005; Prod'homme et al. 2010). With this dual capacity, a dominant inhibitory function for CD96 may be context dependent and require the downregulation of PVR(CD155) and Nectin2 as observed during HCMV infection. This may explain the wider contradictory functions reported for the CD96-Nectin1 axis for NK cells. It would also be consistent with the correlation between levels of CD96 and NK inhibition against HCMV-infected cells observed in this thesis, whereby only NK lines with significantly higher levels of CD96 on their surface than NK cells from PBMC, were activated by dKO-infected cells in an ADAM17-dependent fashion (**Figure 5.22**).

6.3.3 Overall functional impact of ADAM17 impairment

This thesis demonstrated the functional consequences of ADAM17 impairment by HCMV in the context of Treg and NK cell function. However, there were many other protein hits that were significantly upregulated in PMP and downregulated in secretome proteomics, which may be functionally relevant to the virus (**Table 3.3**). EPCR was one of the proteins that was validated in the context of HCMV infection and was shown to be stabilised on the surface of Merlin-infected cells in UL148- and UL148D-dependent fashion (**Figure 3.8**). EPCR is known to bind a γδ T cell antigen receptor and facilitate the expansion of the Vδ2− γδ T cell population (Willcox et al. 2012), observed in recipients of solid organ transplants, as well as healthy individuals (Déchanet et al. 1999; Pitard et al. 2008). γδ T cells are involved in stress-surveillance responses and have been associated with a better clinical outcome in malignancies or infectious diseases (Wilhelm et al. 2003; Costa et al. 2011). Although it seems counterintuitive for HCMV to stabilise a γδ T cell ligand on infected cells, γδ TCR repertoires are diverse with some γδ T cell subsets demonstrating immunosuppressive properties, such as promoting tumour progression by inhibiting anti-tumour responses (Li et al. 2020). Hence,

it is possible that ADAM17-mediated EPCR stabilisation in HCMV infection may contribute to the expansions of γδ T cell subsets and be relevant to viral survival and pathogenesis.

Mucin-1 is another protein identified as significantly upregulated in PMP, which has previously been shown to inhibit NK cell killing (Zhang et al. 1997). That study demonstrated that K562 cells expressing higher levels of Mucin-1 had increased resistance to NK cell lysis, compared to WT K562 cells or cells expressing lower Mucin-1 levels (Zhang et al. 1997). Hence, Mucin-1 may play a role in inhibitory NK cell function mediated by ADAM17 impairment by UL148 and UL148D.

In addition to HCMV-driven ADAM17 impairment affecting a number of immunoregulatory processes, a substantial number of proteins identified in the PMP analysis have been shown to be involved in other biological functions. The role for ADAM17 in foetal development is well established (**Section 1.4.2.1**). ADAM17$^{\Delta Zn/\Delta Zn}$ mice lacking exon 11 from the catalytic active site of the metalloprotease domain show lethality within two weeks of birth (Peschon et al. 1998; Horiuchi et al. 2007). ADAM17 is also implicated in the development of the central nervous system (CNS) and contributes to brain repair (Gooz 2010). A large proportion of the proteomics hits are known to regulate neuronal function, growth, development, and migration (**Table 3.3**). It is tempting to speculate that HCMV-driven ADAM17 impairment could potentially be important in the context of cCMV infection. cCMV is associated with severe neurodevelopmental deficits, mental retardation, vision and hearing loss, with almost 90% of symptomatic neonates suffering from the damage caused to the CNS or affected organs (**Section 1.2.3**) (Fowler et al. 1992; Dietrich and Schieffelin 2019). With no effective treatment options or vaccines against cCMV currently available, understanding the mechanisms behind cCMV-caused neurodevelopmental abnormalities is of critical importance, with the modulation of ADAM17 an appealing starting point.

6.4 Future directions and concluding remarks

This thesis aimed to describe the global and functional impact of ADAM17 dysregulation by HCMV, as well as identify the mechanisms behind UL148- and UL148D-driven impairment of this 'sheddase'. Using proteomics, it reports the impact of ADAM17 impairment on the levels of surface, as well as secreted, proteins, validating a number of them by classical biochemical and flow cytometric techniques, and then provides studies that demonstrate functional significance. While the underlying mechanism of ADAM17 downregulation was not defined, some insight was gained by showing that inhibition of protein degradation did not recover mature ADAM17 expression, while known ADAM17 regulators were unaffected by the effects of UL148 and UL148D. This highlights a number of areas for future study.

The broad impact on many surface and secreted proteins implies that ADAM17 impairment is part of a carefully coordinated HCMV strategy. Surface ADAM17 downregulation occurs as early as 6 hpi (Weekes et al. 2014) and is mediated by at least three viral genes, highlighting its importance to the virus. The laboratory has an adenovirus library of all 170 canonical HCMV genes that may be screened for other genes outside the U$_L$/*b'* region for ADAM17 downregulating function. The data from this thesis provides a testable mechanism for any newly identified HCMV gene(s) in the form of PACS1, which I show to be impaired by HCMV independent of UL148 and UL148D. The impact of PACS1 targeting on Furin and its colocalization with ADAM17 can then also be investigated by microscopy and other standard techniques.

Identifying the underlying mechanism used by UL148 and UL148D to impair ADAM17 maturation would help advance the field of ADAM17 biology. One could systematically validate UL148 and UL148D interactome hits (Nobre et al. 2019) and test whether knocking out expression by RNA interference or CRISPR influences ADAM17 expression. Furthermore, to improve the sensitivity of the UL148 and UL148D interactome and identify weaker, but perhaps more important protein interactions, other methods of protein-protein

interactions could be considered. Proximity labelling, such as BioID method, could be used to fuse biotin ligase to a protein of interest (UL148, UL148D and ADAM17), facilitating biotinylation of the interacting proteins upon supplementation of the culture medium with biotin. Biotinylated proteins can then be isolated and identified by MS, which would allow for identification of weaker and more transient protein interactions, which may play an essential role in ADAM17 regulation (Roux et al. 2012).

With regards functional impact, expansions of immunosuppressive Treg cells in response to Merlin-infected targets were observed in a number of donors dependent on UL148 and UL148D, providing the first mechanistic evidence of how HCMV infection may drive Treg development. However, the readout was full of variables, requiring overexpression of Jagged1 and Vasorin, use of β2mKO fibroblasts and provision of a varying range of TCR signals, making experiments very unwieldy. One possibility is to use cells that intrinsically express Jagged1, such as dendritic cells. While these would solve the problems of mismatched HLA as they could be derived from the same donor as CD4+ T cells, the system has its own difficulties in being markedly harder to infect at high levels with HCMVs based on a Merlin background.

NK cell function was also negatively affected by UL148- and UL148D-driven ADAM17 downregulation. This thesis did not identify the underlying mechanism, with attempts to antagonise the Nectin1-CD96 axis using mAbs failing. A definitive set of experiments would be to generate a Nectin1 KO fibroblast line using CRISPR and testing it following HCMV infection as a target for NK cells. There is, however, also the possibility that other ADAM17-dependent host and viral proteins contribute to NK inhibition. The potential for Mucin-1 has been discussed previously, but there are also HCMV-encoded proteins that are stabilised as a result of ADAM17 targeting that could be screened for NK evasion function, such as UL144 and UL40. Indeed, BTLA, the inhibitory ligand for UL144, has recently been reported to be expressed on NK cells in certain clinical settings (Sordo-Bahamonde et al. 2021), while UL40 is an established inhibitor of NKG2A+ NK cells (Wang et al. 2002; Prod'homme et al. 2012). There is the testable possibility that UL40 requires membrane expression inside the cell to deliver HLA-E binding peptides into the ER and

therefore needs ADAM17 targeting to function properly during HCMV infection.

Due to the complex nature of ADAM17 dysregulation, studying the functional importance, as well as the mechanism behind ADAM17 impairment, proved technically difficult. This can partially be explained by the global action of ADAM17, and consequently the use of D1(A12) to inhibit ADAM17 function on dKO-infected cells. Although the use of D1(A12) in functional assays allowed global definition of ADAM17-dependent responses, it resulted in the accumulation of all ADAM17 substrates simultaneously. This adds an additional layer of complexity to an already complex system and makes it difficult to decipher the role of ADAM17 in individual biological processes and signalling pathways. Future work should address this by focusing on validating individual examples of ADAM17-dependent proteins and the role they have in HCMV infection. For example, Jagged1 and Vasorin blocking experiments could be performed to investigate their role in Treg expansions.

However, the importance of ADAM17 impairment in HCMV infection should also be studied beyond its role in Treg and NK cell function. Indeed, Sun et al. (2020) modelled the effects of HCMV infection on human brain development, demonstrating that infection with a "clinical-like" HCMV strain TB40/E impairs the growth and cortical structure of human induced pluripotent stem cell (hiPSC)-derived brain organoids (Sun et al. 2020). Similar studies with the dKO virus and D1(A12) treatment may give some insight into the role of ADAM17 targeting by UL148 and UL148D in neuronal changes observed in cCMV-associated disease. Such information may inform on how to attenuate HCMVs for safe vaccine vector use in the future.

Finally, apart from demonstrating the significance of ADAM17 regulation in HCMV infection, this thesis contributes to our understanding of overall ADAM17 biology, identifying many novel ADAM17 targets. With the widely recognised importance of ADAM17 in disease, this is significant and provides a database as a foundation for future research. This should focus on deciphering UL148- and UL148D-mediated impairment of ADAM17 to shed light on complex ADAM17 regulation mechanisms. Furthermore, novel

ADAM17 targets can be validated and used to establish the importance of ADAM17 shedding function in previously unknown signalling pathways, thereby improving our understanding of ADAM17 biology.

7   References

Aandahl, E. M., Michaëlsson, J., Moretto, W. J., Hecht, F. M. and Nixon, D. F. 2004. Human CD4+ CD25+ regulatory T cells control T-cell responses to human immunodeficiency virus and cytomegalovirus antigens. *J Virol* 78(5), pp. 2454-2459. doi: 10.1128/jvi.78.5.2454-2459.2004

Abate, D. A., Watanabe, S. and Mocarski, E. S. 2004. Major human cytomegalovirus structural protein pp65 (ppUL83) prevents interferon response factor 3 activation in the interferon response. *J Virol* 78(20), pp. 10995-11006. doi: 10.1128/JVI.78.20.10995-11006.2004

Adair, R., Douglas, E. R., Maclean, J. B., Graham, S. Y., Aitken, J. D., Jamieson, F. E. and Dargan, D. J. 2002. The products of human cytomegalovirus genes UL23, UL24, UL43 and US22 are tegument components. *J Gen Virol* 83(Pt 6), pp. 1315-1324. doi: 10.1099/0022-1317-83-6-1315

Adrain, C., Zettl, M., Christova, Y., Taylor, N. and Freeman, M. 2012. Tumor necrosis factor signaling requires iRhom2 to promote trafficking and activation of TACE. *Science* 335(6065), pp. 225-228. doi: 10.1126/science.1214400

Ager, A. 2012. ADAMs and Ectododomain Proteolytic Shedding in Leucocyte Migration: Focus on L-Selectin and ADAM17. *Current Immunology Reviews* 8, 103-117.

Aicheler, R. J., Wang, E. C. Y., Tomasec, P., Wilkinson, G. W. G. and Stanton, R. J. 2013. Potential for Natural Killer Cell-Mediated Antibody-Dependent Cellular Cytotoxicity for Control of Human   Cytomegalovirus. *Antibodies* 2(4):617-635.

Albrechtsen, R., Wewer Albrechtsen, N. J., Gnosa, S., Schwarz, J., Dyrskjøt, L. and Kveiborg, M. 2019. Identification of ADAM12 as a Novel Basigin Sheddase. *Int J Mol Sci* 20(8), doi: 10.3390/ijms20081957

Alexopoulou, L. et al. 2006. Transmembrane TNF protects mutant mice against intracellular bacterial infections, chronic inflammation and autoimmunity. *Eur J Immunol* 36(10), pp. 2768-2780. doi: 10.1002/eji.200635921

Alwine, J. C. 2012. The human cytomegalovirus assembly compartment: a masterpiece of viral manipulation of cellular processes that facilitates assembly and egress. *PLoS Pathog* 8(9), p. e1002878. doi: 10.1371/journal.ppat.1002878

Amratia, P. 2022. *Identification and characterisation of host factors essential for Human Cytomegalovirus Infection.* PhD thesis. Cardiff University.

Anders, D. G., Kacica, M. A., Pari, G. and Punturieri, S. M. 1992. Boundaries and structure of human cytomegalovirus oriLyt, a complex origin for lytic-phase DNA replication. *J Virol* 66(6), pp. 3373-3384. doi: 10.1128/JVI.66.6.3373-3384.1992

Arokiasamy, S., Balderstone, M. J. M., De Rossi, G. and Whiteford, J. R. 2019. Syndecan-3 in Inflammation and Angiogenesis. *Front Immunol* 10, p. 3031. doi: 10.3389/fimmu.2019.03031

Arvin, A. M., Fast, P., Myers, M., Plotkin, S., Rabinovich, R. and Committee, N. V. A. 2004. Vaccine development to prevent cytomegalovirus disease: report from the National Vaccine Advisory Committee. *Clin Infect Dis* 39(2), pp. 233-239. doi: 10.1086/421999

Ashiru, O., Bennett, N. J., Boyle, L. H., Thomas, M., Trowsdale, J. and Wills, M. R. 2009. NKG2D ligand MICA is retained in the cis-Golgi apparatus by human cytomegalovirus protein UL142. *J Virol* 83(23), pp. 12345-12354. doi: 10.1128/JVI.01175-09

Atabani, S. F. et al. 2012. Cytomegalovirus replication kinetics in solid organ transplant recipients managed by preemptive therapy. *Am J Transplant* 12(9), pp. 2457-2464. doi: 10.1111/j.1600-6143.2012.04087.x

Ataya, M. et al. 2020. Pretransplant adaptive NKG2C+ NK cells protect against cytomegalovirus infection in kidney transplant recipients. *Am J Transplant* 20(3), pp. 663-676. doi: 10.1111/ajt.15658

Azevedo, L. S. et al. 2015. Cytomegalovirus infection in transplant recipients. *Clinics (Sao Paulo)* 70(7), pp. 515-523. doi: 10.6061/clinics/2015(07)09

Baasch, S., Ruzsics, Z. and Henneke, P. 2020. Cytomegaloviruses and Macrophages-Friends and Foes From Early on? *Front Immunol* 11, p. 793. doi: 10.3389/fimmu.2020.00793

Baldick, C. J. and Shenk, T. 1996. Proteins associated with purified human cytomegalovirus particles. *J Virol* 70(9), pp. 6097-6105. doi: 10.1128/JVI.70.9.6097-6105.1996

Bandsma, R. H. et al. 2015. Loss of ADAM17 is associated with severe multiorgan dysfunction. *Hum Pathol* 46(6), pp. 923-928. doi: 10.1016/j.humpath.2015.02.010

Barrenschee, M., Lange, C., Cossais, F., Egberts, J. H., Becker, T., Wedel, T. and Böttner, M. 2015. Expression and function of Neuregulin 1 and its signaling system ERBB2/3 in the enteric nervous system. *Front Cell Neurosci* 9, p. 360. doi: 10.3389/fncel.2015.00360

Battista, M. C., Bergamini, G., Boccuni, M. C., Campanini, F., Ripalti, A. and Landini, M. P. 1999. Expression and characterization of a novel structural protein of human cytomegalovirus, pUL25. *J Virol* 73(5), pp. 3800-3809. doi: 10.1128/JVI.73.5.3800-3809.1999

Baxter, M. K. and Gibson, W. 2001. Cytomegalovirus basic phosphoprotein (pUL32) binds to capsids in vitro through its amino one-third. *J Virol* 75(15), pp. 6865-6873. doi: 10.1128/JVI.75.15.6865-6873.2001

Bechtel, J. T. and Shenk, T. 2002. Human cytomegalovirus UL47 tegument protein functions after entry and before immediate-early gene expression. *J Virol* 76(3), pp. 1043-1050. doi: 10.1128/jvi.76.3.1043-1050.2002

Bertrand, J. and Bollmann, M. 2019. Soluble syndecans: biomarkers for diseases and therapeutic options. *Br J Pharmacol* 176(1), pp. 67-81. doi: 10.1111/bph.14397

Birge, R. B., Kalodimos, C., Inagaki, F. and Tanaka, S. 2009. Crk and CrkL adaptor proteins: networks for physiological and pathological signaling. *Cell Commun Signal* 7, p. 13. doi: 10.1186/1478-811X-7-13

Biron, C. A., Byron, K. S. and Sullivan, J. L. 1989. Severe herpesvirus infections in an adolescent without natural killer cells. *N Engl J Med* 320(26), pp. 1731-1735. doi: 10.1056/NEJM198906293202605

Biron, C. A. and Tarrio, M. L. 2015. Immunoregulatory cytokine networks: 60 years of learning from murine cytomegalovirus. *Med Microbiol Immunol* 204(3), pp. 345-354. doi: 10.1007/s00430-015-0412-3

Black, R. A. et al. 1997. A metalloproteinase disintegrin that releases tumour-necrosis factor-alpha from cells. *Nature* 385(6618), pp. 729-733. doi: 10.1038/385729a0

Blaydon, D. C. et al. 2011. Inflammatory skin and bowel disease linked to ADAM17 deletion. *N Engl J Med* 365(16), pp. 1502-1508. doi: 10.1056/NEJMoa1100721

Bodaghi, B. et al. 1998. Chemokine sequestration by viral chemoreceptors as a novel viral escape strategy: withdrawal of chemokines from the environment of cytomegalovirus-infected cells. *J Exp Med* 188(5), pp. 855-866. doi: 10.1084/jem.188.5.855

Boeckh, M. and Nichols, W. G. 2004. The impact of cytomegalovirus serostatus of donor and recipient before hematopoietic stem cell transplantation in the era of antiviral prophylaxis and preemptive therapy. *Blood* 103(6), pp. 2003-2008. doi: 10.1182/blood-2003-10-3616

Boehme, K. W., Guerrero, M. and Compton, T. 2006. Human cytomegalovirus envelope glycoproteins B and H are necessary for TLR2 activation in permissive cells. *J Immunol* 177(10), pp. 7094-7102. doi: 10.4049/jimmunol.177.10.7094

Boppana, S. B. and Fowler, K. B. 2007. Persistence in the population: epidemiology and transmisson. In: Arvin A, Campadelli-Fiume G, Mocarski E, et al., editors. Human Herpesviruses: Biology, Therapy, and Immunoprophylaxis. Cambridge: Cambridge University Press, Chapter 44.

Botto, S., Streblow, D. N., DeFilippis, V., White, L., Kreklywich, C. N., Smith, P. P. and Caposio, P. 2011. IL-6 in human cytomegalovirus secretome promotes angiogenesis and survival of endothelial cells through the stimulation of survivin. *Blood* 117(1), pp. 352-361. doi: 10.1182/blood-2010-06-291245

Boutet, P. et al. 2009. Cutting edge: the metalloproteinase ADAM17/TNF-alpha-converting enzyme regulates proteolytic shedding of the MHC class I-related chain B protein. *J Immunol* 182(1), pp. 49-53. doi: 10.4049/jimmunol.182.1.49

Bouyain, S. and Watkins, D. J. 2010. The protein tyrosine phosphatases PTPRZ and PTPRG bind to distinct members of the contactin family of neural recognition molecules. *Proc Natl Acad Sci U S A* 107(6), pp. 2443-2448. doi: 10.1073/pnas.0911235107

Bradley, A. J. et al. 2009. High-throughput sequence analysis of variants of human cytomegalovirus strains Towne and AD169. *J Gen Virol* 90(Pt 10), pp. 2375-2380. doi: 10.1099/vir.0.013250-0

Bresnahan, W. A. and Shenk, T. E. 2000. UL82 virion protein activates expression of immediate early viral genes in human cytomegalovirus-infected cells. *Proc Natl Acad Sci U S A* 97(26), pp. 14506-14511. doi: 10.1073/pnas.97.26.14506

Bristow, B. N., O'Keefe, K. A., Shafir, S. C. and Sorvillo, F. J. 2011. Congenital cytomegalovirus mortality in the United States, 1990-2006. *PLoS Negl Trop Dis* 5(4), p. e1140. doi: 10.1371/journal.pntd.0001140

Britt, W. J. and Auger, D. 1986. Synthesis and processing of the envelope gp55-116 complex of human cytomegalovirus. *J Virol* 58(1), pp. 185-191. doi: 10.1128/JVI.58.1.185-191.1986

Bronzini, M., Luganini, A., Dell'Oste, V., De Andrea, M., Landolfo, S. and Gribaudo, G. 2012. The US16 gene of human cytomegalovirus is required for efficient viral infection of endothelial and epithelial cells. *J Virol* 86(12), pp. 6875-6888. doi: 10.1128/JVI.06310-11

Brown, K. J. et al. 2012. Advances in the proteomic investigation of the cell secretome. *Expert Rev Proteomics* 9(3), pp. 337-345. doi: 10.1586/epr.12.21

Browne, E. P. and Shenk, T. 2003. Human cytomegalovirus UL83-coded pp65 virion protein inhibits antiviral gene expression in infected cells. *Proc Natl Acad Sci U S A* 100(20), pp. 11439-11444. doi: 10.1073/pnas.1534570100

Bruno, L. et al. 2016. Human cytomegalovirus pUL10 interacts with leukocytes and impairs TCR-mediated T-cell activation. *Immunol Cell Biol* 94(9), pp. 849-860. doi: 10.1038/icb.2016.49

Caccamo, N., Joosten, S. A., Ottenhoff, T. H. M. and Dieli, F. 2018. Atypical Human Effector/Memory CD4. *Front Immunol* 9, p. 2832. doi: 10.3389/fimmu.2018.02832

Calligaris, M., Cuffaro, D., Bonelli, S., Spanò, D. P., Rossello, A., Nuti, E. and Scilabra, S. D. 2021. Strategies to Target ADAM17 in Disease: From its Discovery to the iRhom Revolution. *Molecules* 26(4), doi: 10.3390/molecules26040944

Cannon, M. J. 2009. Congenital cytomegalovirus (CMV) epidemiology and awareness. *J Clin Virol* 46 Suppl 4, pp. S6-10. doi: 10.1016/j.jcv.2009.09.002

Cannon, M. J., Schmid, D. S. and Hyde, T. B. 2010. Review of cytomegalovirus seroprevalence and demographic characteristics associated with infection. *Rev Med Virol* 20(4), pp. 202-213. doi: 10.1002/rmv.655

Cantrell, S. R. and Bresnahan, W. A. 2006. Human cytomegalovirus (HCMV) UL82 gene product (pp71) relieves hDaxx-mediated repression of HCMV replication. *J Virol* 80(12), pp. 6188-6191. doi: 10.1128/JVI.02676-05

Cappenberg, A. et al. 2019. L-selectin shedding affects bacterial clearance in the lung: a new regulatory pathway for integrin outside-in signaling. *Blood* 134(17), pp. 1445-1457. doi: 10.1182/blood.2019000685

Cavaletto, N., Luganini, A. and Gribaudo, G. 2015. Inactivation of the Human Cytomegalovirus US20 Gene Hampers Productive Viral Replication in Endothelial Cells. *J Virol* 89(21), pp. 11092-11106. doi: 10.1128/JVI.01141-15

Cesaro, A. et al. 2009. Differential expression and regulation of ADAM17 and TIMP3 in acute inflamed intestinal epithelia. *Am J Physiol Gastrointest Liver Physiol* 296(6), pp. G1332-1343. doi: 10.1152/ajpgi.90641.2008

Cha, T. A., Tom, E., Kemble, G. W., Duke, G. M., Mocarski, E. S. and Spaete, R. R. 1996. Human cytomegalovirus clinical isolates carry at least 19 genes not found in laboratory strains. *J Virol* 70(1), pp. 78-83.

Chalupny, N. J., Rein-Weston, A., Dosch, S. and Cosman, D. 2006. Down-regulation of the NKG2D ligand MICA by the human cytomegalovirus glycoprotein UL142. *Biochem Biophys Res Commun* 346(1), pp. 175-181. doi: 10.1016/j.bbrc.2006.05.092

Chambers, J. et al. 1999. DNA microarrays of the complex human cytomegalovirus genome: profiling kinetic class with drug sensitivity of viral gene expression. *J Virol* 73(7), pp. 5757-5766. doi: 10.1128/JVI.73.7.5757-5766.1999

Chan, C. J., Andrews, D. M. and Smyth, M. J. 2012. Receptors that interact with nectin and nectin-like proteins in the immunosurveillance and immunotherapy of cancer. *Curr Opin Immunol* 24(2), pp. 246-251. doi: 10.1016/j.coi.2012.01.009

Chan, C. J., Smyth, M. J. and Martinet, L. 2014. Molecular mechanisms of natural killer cell activation in response to cellular stress. *Cell Death Differ* 21(1), pp. 5-14. doi: 10.1038/cdd.2013.26

Chaplin, D. D. 2010. Overview of the immune response. *J Allergy Clin Immunol* 125(2 Suppl 2), pp. S3-23. doi: 10.1016/j.jaci.2009.12.980

Chee, M. S. et al. 1990. Analysis of the protein-coding content of the sequence of human cytomegalovirus strain AD169. *Curr Top Microbiol Immunol* 154, pp. 125-169. doi: 10.1007/978-3-642-74980-3_6

Chen, G. et al. 2019. Comprehensive Identification and Characterization of Human Secretome Based on Integrative Proteomic and Transcriptomic Data. *Front Cell Dev Biol* 7, p. 299. doi: 10.3389/fcell.2019.00299

Chen, W., Zhang, Z., Zhang, S., Zhu, P., Ko, J. K. and Yung, K. K. 2021. MUC1: Structure, Function, and Clinic Application in Epithelial Cancers. *Int J Mol Sci* 22(12), doi: 10.3390/ijms22126567

Cheung, T. C. et al. 2005. Evolutionarily divergent herpesviruses modulate T cell activation by targeting the herpesvirus entry mediator cosignaling pathway. *Proc Natl Acad Sci U S A* 102(37), pp. 13218-13223. doi: 10.1073/pnas.0506172102

Choksi, S. et al. 2011. A HIF-1 target, ATIA, protects cells from apoptosis by modulating the mitochondrial thioredoxin, TRX2. *Mol Cell* 42(5), pp. 597-609. doi: 10.1016/j.molcel.2011.03.030

Christova, Y., Adrain, C., Bambrough, P., Ibrahim, A. and Freeman, M. 2013. Mammalian iRhoms have distinct physiological functions including an essential role in TACE regulation. *EMBO Rep* 14(10), pp. 884-890. doi: 10.1038/embor.2013.128

Ciferri, C. et al. 2015. Structural and biochemical studies of HCMV gH/gL/gO and Pentamer reveal mutually exclusive cell entry complexes. *Proc Natl Acad Sci U S A* 112(6), pp. 1767-1772. doi: 10.1073/pnas.1424818112

Cohen, J. I. 2020. Herpesvirus latency. *J Clin Invest* 130(7), pp. 3361-3369. doi: 10.1172/JCI136225

Colberg-Poley, A. M. 1996. Functional roles of immediate early proteins encoded by the human cytomegalovirus UL36-38, UL115-119, TRS1/IRS1 and US3 loci. *Intervirology* 39(5-6), pp. 350-360. doi: 10.1159/000150506

Compton, T., Kurt-Jones, E. A., Boehme, K. W., Belko, J., Latz, E., Golenbock, D. T. and Finberg, R. W. 2003. Human cytomegalovirus activates inflammatory cytokine responses via CD14 and Toll-like receptor 2. *J Virol* 77(8), pp. 4588-4596. doi: 10.1128/jvi.77.8.4588-4596.2003

Compton, T., Nepomuceno, R. R. and Nowlin, D. M. 1992. Human cytomegalovirus penetrates host cells by pH-independent fusion at the cell surface. *Virology* 191(1), pp. 387-395. doi: 10.1016/0042-6822(92)90200-9

Corrales-Aguilar, E. et al. 2014. Human cytomegalovirus Fcγ binding proteins gp34 and gp68 antagonize Fcγ receptors I, II and III. *PLoS Pathog* 10(5), p. e1004131. doi: 10.1371/journal.ppat.1004131

Cosman, D. et al. 2001. ULBPs, novel MHC class I-related molecules, bind to CMV glycoprotein UL16 and stimulate NK cytotoxicity through the NKG2D receptor. *Immunity* 14(2), pp. 123-133. doi: 10.1016/s1074-7613(01)00095-4

Costa, G. et al. 2011. Control of Plasmodium falciparum erythrocytic cycle: γδ T cells target the red blood cell-invasive merozoites. *Blood* 118(26), pp. 6952-6962. doi: 10.1182/blood-2011-08-376111

Cox, M., Kartikasari, A. E. R., Gorry, P. R., Flanagan, K. L. and Plebanski, M. 2021. Potential Impact of Human Cytomegalovirus Infection on Immunity to Ovarian Tumours and Cancer Progression. *Biomedicines* 9(4), doi: 10.3390/biomedicines9040351

Crawford, L. B. et al. 2018. Human Cytomegalovirus Encodes a Novel FLT3 Receptor Ligand Necessary for Hematopoietic Cell Differentiation and Viral Reactivation. *mBio* 9(2), doi: 10.1128/mBio.00682-18

Czopik, A. K., Bynoe, M. S., Palm, N., Raine, C. S. and Medzhitov, R. 2006. Semaphorin 7A is a negative regulator of T cell responses. *Immunity* 24(5), pp. 591-600. doi: 10.1016/j.immuni.2006.03.013

Dargan, D. J. et al. 2010. Sequential mutations associated with adaptation of human cytomegalovirus to growth in cell culture. *J Gen Virol* 91(Pt 6), pp. 1535-1546. doi: 10.1099/vir.0.018994-0

Das, S., Ortiz, D. A., Gurczynski, S. J., Khan, F. and Pellett, P. E. 2014. Identification of human cytomegalovirus genes important for biogenesis of the cytoplasmic virion assembly complex. *J Virol* 88(16), pp. 9086-9099. doi: 10.1128/JVI.01141-14

Das, S., Vasanji, A. and Pellett, P. E. 2007. Three-dimensional structure of the human cytomegalovirus cytoplasmic virion assembly complex includes a reoriented secretory apparatus. *J Virol* 81(21), pp. 11861-11869. doi: 10.1128/JVI.01077-07

Davison, A. J. 2011. Evolution of sexually transmitted and sexually transmissible human herpesviruses. *Ann N Y Acad Sci* 1230, pp. E37-49. doi: 10.1111/j.1749-6632.2011.06358.x

Davison, A. J. and Bhella, D. 2007. Comparative genome and virion structure. Human herpesviruses: biology, therapy, and immunoprophylaxis. Cambridge University Press.

Davison, A. J. et al. 2003. The human cytomegalovirus genome revisited: comparison with the chimpanzee cytomegalovirus genome. *J Gen Virol* 84(Pt 1), pp. 17-28. doi: 10.1099/vir.0.18606-0

Davison, A. J. et al. 2009. The order Herpesvirales. *Arch Virol* 154(1), pp. 171-177. doi: 10.1007/s00705-008-0278-4

Deshmukh, A. S. et al. 2019. Proteomics-Based Comparative Mapping of the Secretomes of Human Brown and White Adipocytes Reveals EPDR1 as a Novel Batokine. *Cell Metab* 30(5), pp. 963-975.e967. doi: 10.1016/j.cmet.2019.10.001

Dietrich, M. L. and Schieffelin, J. S. 2019. Congenital Cytomegalovirus Infection. *Ochsner J* 19(2), pp. 123-130. doi: 10.31486/toj.18.0095

Dolan, A. et al. 2004. Genetic content of wild-type human cytomegalovirus. *J Gen Virol* 85(Pt 5), pp. 1301-1312. doi: 10.1099/vir.0.79888-0

Dombernowsky, S. L. et al. 2015. The sorting protein PACS-2 promotes ErbB signalling by regulating recycling of the metalloproteinase ADAM17. *Nat Commun* 6, p. 7518. doi: 10.1038/ncomms8518

Dominitzki, S. et al. 2007. Cutting edge: trans-signaling via the soluble IL-6R abrogates the induction of FoxP3 in naive CD4+CD25 T cells. *J Immunol* 179(4), pp. 2041-2045. doi: 10.4049/jimmunol.179.4.2041

Drew, W. L. 1988. Cytomegalovirus infection in patients with AIDS. *J Infect Dis* 158(2), pp. 449-456. doi: 10.1093/infdis/158.2.449

Duffy, M. J., McKiernan, E., O'Donovan, N. and McGowan, P. M. 2009. The role of ADAMs in disease pathophysiology. *Clin Chim Acta* 403(1-2), pp. 31-36. doi: 10.1016/j.cca.2009.01.007

Dumortier, J. et al. 2008. Human cytomegalovirus secretome contains factors that induce angiogenesis and wound healing. *J Virol* 82(13), pp. 6524-6535. doi: 10.1128/JVI.00502-08

Dunn, C., Chalupny, N. J., Sutherland, C. L., Dosch, S., Sivakumar, P. V., Johnson, D. C. and Cosman, D. 2003a. Human cytomegalovirus glycoprotein UL16 causes intracellular sequestration of NKG2D ligands, protecting against natural killer cell cytotoxicity. *J Exp Med* 197(11), pp. 1427-1439. doi: 10.1084/jem.20022059

Dunn, W. et al. 2003b. Functional profiling of a human cytomegalovirus genome. *Proc Natl Acad Sci U S A* 100(24), pp. 14223-14228. doi: 10.1073/pnas.2334032100

Déchanet, J. et al. 1999. Implication of gammadelta T cells in the human immune response to cytomegalovirus. *J Clin Invest* 103(10), pp. 1437-1449. doi: 10.1172/JCI5409

Düsterhöft, S., Jung, S., Hung, C. W., Tholey, A., Sönnichsen, F. D., Grötzinger, J. and Lorenzen, I. 2013. Membrane-proximal domain of a disintegrin and metalloprotease-17 represents the putative molecular switch of its shedding activity operated by protein-disulfide isomerase. *J Am Chem Soc* 135(15), pp. 5776-5781. doi: 10.1021/ja400340u

Eagle, R. A., Traherne, J. A., Hair, J. R., Jafferji, I. and Trowsdale, J. 2009. ULBP6/RAET1L is an additional human NKG2D ligand. *Eur J Immunol* 39(11), pp. 3207-3216. doi: 10.1002/eji.200939502

Ebsen, H., Schröder, A., Kabelitz, D. and Janssen, O. 2013. Differential surface expression of ADAM10 and ADAM17 on human T lymphocytes and tumor cells. *PLoS One* 8(10), p. e76853. doi: 10.1371/journal.pone.0076853

Edwards, D. R., Handsley, M. M. and Pennington, C. J. 2008. The ADAM metalloproteinases. *Mol Aspects Med* 29(5), pp. 258-289. doi: 10.1016/j.mam.2008.08.001

Elder, E. and Sinclair, J. 2019. HCMV latency: what regulates the regulators? *Med Microbiol Immunol* 208(3-4), pp. 431-438. doi: 10.1007/s00430-019-00581-1

Elek, S. D. and Stern, H. 1974. Development of a vaccine against mental retardation caused by cytomegalovirus infection in utero. *Lancet* 1(7845), pp. 1-5. doi: 10.1016/s0140-6736(74)92997-3

Ellis, G. I., Reneer, M. C., Vélez-Ortega, A. C., McCool, A. and Martí, F. 2012. Generation of induced regulatory T cells from primary human naïve and memory T cells. *J Vis Exp* (62), doi: 10.3791/3738

Endres, K., Anders, A., Kojro, E., Gilbert, S., Fahrenholz, F. and Postina, R. 2003. Tumor necrosis factor-alpha converting enzyme is processed by proprotein-convertases to its mature form which is degraded upon phorbol ester stimulation. *Eur J Biochem* 270(11), pp. 2386-2393. doi: 10.1046/j.1432-1033.2003.03606.x

Esteso, G. et al. 2014. Altered microRNA expression after infection with human cytomegalovirus leads to TIMP3 downregulation and increased shedding of metalloprotease substrates, including MICA. *J Immunol* 193(3), pp. 1344-1352. doi: 10.4049/jimmunol.1303441

Fabits, M. et al. 2020. The Cytomegalovirus Tegument Protein UL35 Antagonizes Pattern Recognition Receptor-Mediated Type I IFN Transcription. *Microorganisms* 8(6), doi: 10.3390/microorganisms8060790

Fagioli, C. and Sitia, R. 2001. Glycoprotein quality control in the endoplasmic reticulum. Mannose trimming by endoplasmic reticulum mannosidase I times the proteasomal degradation of unassembled immunoglobulin subunits. *J Biol Chem* 276(16), pp. 12885-12892. doi: 10.1074/jbc.M009603200

Feire, A. L., Koss, H. and Compton, T. 2004. Cellular integrins function as entry receptors for human cytomegalovirus via a highly conserved disintegrin-like domain. *Proc Natl Acad Sci U S A* 101(43), pp. 15470-15475. doi: 10.1073/pnas.0406821101

Feire, A. L., Roy, R. M., Manley, K. and Compton, T. 2010. The glycoprotein B disintegrin-like domain binds beta 1 integrin to mediate cytomegalovirus entry. *J Virol* 84(19), pp. 10026-10037. doi: 10.1128/JVI.00710-10

Fiebiger, E., Hirsch, C., Vyas, J. M., Gordon, E., Ploegh, H. L. and Tortorella, D. 2004. Dissection of the dislocation pathway for type I membrane proteins with a new small molecule inhibitor, eeyarestatin. *Mol Biol Cell* 15(4), pp. 1635-1646. doi: 10.1091/mbc.e03-07-0506

Fielding, C. A. et al. 2014. Two novel human cytomegalovirus NK cell evasion functions target MICA for lysosomal degradation. *PLoS Pathog* 10(5), p. e1004058. doi: 10.1371/journal.ppat.1004058

Fielding, C. A. et al. 2017. Control of immune ligands by members of a cytomegalovirus gene expansion suppresses natural killer cell activation. *Elife* 6, doi: 10.7554/eLife.22206

Fleig, L., Bergbold, N., Sahasrabudhe, P., Geiger, B., Kaltak, L. and Lemberg, M. K. 2012. Ubiquitin-dependent intramembrane rhomboid protease promotes ERAD of membrane proteins. *Mol Cell* 47(4), pp. 558-569. doi: 10.1016/j.molcel.2012.06.008

Foley, B. et al. 2012. Human cytomegalovirus (CMV)-induced memory-like NKG2C(+) NK cells are transplantable and expand in vivo in response to recipient CMV antigen. *J Immunol* 189(10), pp. 5082-5088. doi: 10.4049/jimmunol.1201964

Forte, E., Zhang, Z., Thorp, E. B. and Hummel, M. 2020. Cytomegalovirus Latency and Reactivation: An Intricate Interplay With the Host Immune Response. *Front Cell Infect Microbiol* 10, p. 130. doi: 10.3389/fcimb.2020.00130

Fowler, K. et al. 2022. A systematic literature review of the global seroprevalence of cytomegalovirus: possible implications for treatment, screening, and vaccine development. *BMC Public Health* 22(1), p. 1659. doi: 10.1186/s12889-022-13971-7

Fowler, K. B. et al. 2017. A Targeted Approach for Congenital Cytomegalovirus Screening Within Newborn Hearing Screening. *Pediatrics* 139(2), doi: 10.1542/peds.2016-2128

Fowler, K. B., Stagno, S., Pass, R. F., Britt, W. J., Boll, T. J. and Alford, C. A. 1992. The outcome of congenital cytomegalovirus infection in relation to maternal antibody status. *N Engl J Med* 326(10), pp. 663-667. doi: 10.1056/NEJM199203053261003

Freeze, H. H. and Kranz, C. 2010. Endoglycosidase and glycoamidase release of N-linked glycans. *Curr Protoc Mol Biol* Chapter 17, p. Unit 17.13A. doi: 10.1002/0471142727.mb1713as89

Fregno, I. and Molinari, M. 2019. Proteasomal and lysosomal clearance of faulty secretory proteins: ER-associated degradation (ERAD) and ER-to-

lysosome-associated degradation (ERLAD) pathways. *Crit Rev Biochem Mol Biol* 54(2), pp. 153-163. doi: 10.1080/10409238.2019.1610351

Fu, Y. Z. et al. 2017. Human Cytomegalovirus Tegument Protein UL82 Inhibits STING-Mediated Signaling to Evade Antiviral Immunity. *Cell Host Microbe* 21(2), pp. 231-243. doi: 10.1016/j.chom.2017.01.001

Fuchs, A., Cella, M., Giurisato, E., Shaw, A. S. and Colonna, M. 2004. Cutting edge: CD96 (tactile) promotes NK cell-target cell adhesion by interacting with the poliovirus receptor (CD155). *J Immunol* 172(7), pp. 3994-3998. doi: 10.4049/jimmunol.172.7.3994

Furman, M. H., Dey, N., Tortorella, D. and Ploegh, H. L. 2002. The human cytomegalovirus US10 gene product delays trafficking of major histocompatibility complex class I molecules. *J Virol* 76(22), pp. 11753-11756. doi: 10.1128/jvi.76.22.11753-11756.2002

Gabaev, I. et al. 2011. The human cytomegalovirus UL11 protein interacts with the receptor tyrosine phosphatase CD45, resulting in functional paralysis of T cells. *PLoS Pathog* 7(12), p. e1002432. doi: 10.1371/journal.ppat.1002432

Gatherer, D. et al. 2011. High-resolution human cytomegalovirus transcriptome. *Proc Natl Acad Sci U S A* 108(49), pp. 19755-19760. doi: 10.1073/pnas.1115861108

Gazit, R. et al. 2004. Expression of KIR2DL1 on the entire NK cell population: a possible novel immunodeficiency syndrome. *Blood* 103(5), pp. 1965-1966. doi: 10.1182/blood-2003-11-3796

Gebremariam, H. G., Qazi, K. R., Somiah, T., Pathak, S. K., Sjölinder, H., Sverremark Ekström, E. and Jonsson, A. B. 2019. Suppresses the Production of Proinflammatory Cytokines in. *Front Immunol* 10, p. 2326. doi: 10.3389/fimmu.2019.02326

Georgiou, H. M., Rice, G. E. and Baker, M. S. 2001. Proteomic analysis of human plasma: failure of centrifugal ultrafiltration to remove albumin and other high molecular weight proteins. *Proteomics* 1(12), pp. 1503-1506. doi: 10.1002/1615-9861(200111)1:12<1503::aid-prot1503>3.0.co;2-m

Gerna, G., Kabanova, A. and Lilleri, D. 2019. Human Cytomegalovirus Cell Tropism and Host Cell Receptors. *Vaccines (Basel)* 7(3), doi: 10.3390/vaccines7030070

Gibson, W. 2008. Structure and Formation of the Cytomegalovirus Virion. In: Shenk, T.E., Stinski, M.F. (eds) Human Cytomegalovirus. Current Topics in Microbiology and Immunology, vol 325. Springer, Berlin, Heidelberg.

Gillespie, G. M. et al. 2000. Functional heterogeneity and high frequencies of cytomegalovirus-specific CD8(+) T lymphocytes in healthy seropositive donors. *J Virol* 74(17), pp. 8140-8150. doi: 10.1128/jvi.74.17.8140-8150.2000

Gooz, M. 2010. ADAM-17: the enzyme that does it all. *Crit Rev Biochem Mol Biol* 45(2), pp. 146-169. doi: 10.3109/10409231003628015

Granzin, M., Wagner, J., Köhl, U., Cerwenka, A., Huppert, V. and Ullrich, E. 2017. Shaping of Natural Killer Cell Antitumor Activity by. *Front Immunol* 8, p. 458. doi: 10.3389/fimmu.2017.00458

Grefte, A., Harmsen, M. C., van der Giessen, M., Knollema, S., van Son, W. J. and The, T. H. 1994. Presence of human cytomegalovirus (HCMV) immediate early mRNA but not ppUL83 (lower matrix protein pp65) mRNA in polymorphonuclear and mononuclear leukocytes during active HCMV infection. *J Gen Virol* 75 (Pt 8), pp. 1989-1998. doi: 10.1099/0022-1317-75-8-1989

Griffiths, P., Baraniak, I. and Reeves, M. 2015. The pathogenesis of human cytomegalovirus. *J Pathol* 235(2), pp. 288-297. doi: 10.1002/path.4437

Griffiths, P. and Reeves, M. 2021. Pathogenesis of human cytomegalovirus in the immunocompromised host. *Nat Rev Microbiol* 19(12), pp. 759-773. doi: 10.1038/s41579-021-00582-z

Grinde, B. 2013. Herpesviruses: latency and reactivation - viral strategies and host response. *J Oral Microbiol* 5, doi: 10.3402/jom.v5i0.22766

Grob, J. P. et al. 1987. Immune donors can protect marrow-transplant recipients from severe cytomegalovirus infections. *Lancet* 1(8536), pp. 774-776. doi: 10.1016/s0140-6736(87)92800-5

Grosse, S. D., Ross, D. S. and Dollard, S. C. 2008. Congenital cytomegalovirus (CMV) infection as a cause of permanent bilateral hearing loss: a quantitative assessment. *J Clin Virol* 41(2), pp. 57-62. doi: 10.1016/j.jcv.2007.09.004

Grötzinger, J., Lorenzen, I. and Düsterhöft, S. 2017. Molecular insights into the multilayered regulation of ADAM17: The role of the extracellular region. *Biochim Biophys Acta Mol Cell Res* 1864(11 Pt B), pp. 2088-2095. doi: 10.1016/j.bbamcr.2017.05.024

Han, J. et al. 2013. Human cytomegalovirus (HCMV) US2 protein interacts with human CD1d (hCD1d) and down-regulates invariant NKT (iNKT) cell activity. *Mol Cells* 36(5), pp. 455-464. doi: 10.1007/s10059-013-0221-8

Hanley, P. J. and Bollard, C. M. 2014. Controlling cytomegalovirus: helping the immune system take the lead. *Viruses* 6(6), pp. 2242-2258. doi: 10.3390/v6062242

Harjunpää, H. and Guillerey, C. 2020. TIGIT as an emerging immune checkpoint. *Clin Exp Immunol* 200(2), pp. 108-119. doi: 10.1111/cei.13407

Hartl, D. et al. 2018. A rare loss-of-function variant of ADAM17 is associated with late-onset familial Alzheimer disease. *Mol Psychiatry* 25(3), pp. 629-639. doi: 10.1038/s41380-018-0091-8

Ho, M. 2008. The history of cytomegalovirus and its diseases. *Med Microbiol Immunol* 197(2), pp. 65-73. doi: 10.1007/s00430-007-0066-x

Holmes, V. M., Maluquer de Motes, C., Richards, P. T., Roldan, J., Bhargava, A. K., Orange, J. S. and Krummenacher, C. 2019. Interaction between nectin-1 and the human natural killer cell receptor CD96. *PLoS One* 14(2), p. e0212443. doi: 10.1371/journal.pone.0212443

Hook, L. M. et al. 2014. Cytomegalovirus miRNAs target secretory pathway genes to facilitate formation of the virion assembly compartment and reduce cytokine secretion. *Cell Host Microbe* 15(3), pp. 363-373. doi: 10.1016/j.chom.2014.02.004

Horiuchi, K., Kimura, T., Miyamoto, T., Takaishi, H., Okada, Y., Toyama, Y. and Blobel, C. P. 2007. Cutting edge: TNF-alpha-converting enzyme (TACE/ADAM17) inactivation in mouse myeloid cells prevents lethality from endotoxin shock. *J Immunol* 179(5), pp. 2686-2689. doi: 10.4049/jimmunol.179.5.2686

Horiuchi, T., Mitoma, H., Harashima, S., Tsukamoto, H. and Shimoda, T. 2010. Transmembrane TNF-alpha: structure, function and interaction with anti-TNF agents. *Rheumatology (Oxford)* 49(7), pp. 1215-1228. doi: 10.1093/rheumatology/keq031

Houldcroft, C. J. et al. 2020. Assessing Anti-HCMV Cell Mediated Immune Responses in Transplant Recipients and Healthy Controls Using a Novel Functional Assay. *Front Cell Infect Microbiol* 10, p. 275. doi: 10.3389/fcimb.2020.00275

Hu, X., Wang, H. Y., Otero, C. E., Jenks, J. A. and Permar, S. R. 2022. Lessons from Acquired Natural Immunity and Clinical Trials to Inform Next-Generation Human Cytomegalovirus Vaccine Development. *Annu Rev Virol* 9(1), pp. 491-520. doi: 10.1146/annurev-virology-100220-010653

Huber, M. T. and Compton, T. 1997. Characterization of a novel third member of the human cytomegalovirus glycoprotein H-glycoprotein L complex. *J Virol* 71(7), pp. 5391-5398. doi: 10.1128/JVI.71.7.5391-5398.1997

Huber, M. T. and Compton, T. 1998. The human cytomegalovirus UL74 gene encodes the third component of the glycoprotein H-glycoprotein L-containing envelope complex. *J Virol* 72(10), pp. 8191-8197. doi: 10.1128/JVI.72.10.8191-8197.1998

Huber, M. T., Tomazin, R., Wisner, T., Boname, J. and Johnson, D. C. 2002. Human cytomegalovirus US7, US8, US9, and US10 are cytoplasmic glycoproteins, not found at cell surfaces, and US9 does not mediate cell-to-cell spread. *J Virol* 76(11), pp. 5748-5758. doi: 10.1128/jvi.76.11.5748-5758.2002

Huntington, N. D. et al. 2009. IL-15 trans-presentation promotes human NK cell development and differentiation in vivo. *J Exp Med* 206(1), pp. 25-34. doi: 10.1084/jem.20082013

Ikeda, Y. et al. 2004. Vasorin, a transforming growth factor beta-binding protein expressed in vascular smooth muscle cells, modulates the arterial response to injury in vivo. *Proc Natl Acad Sci U S A* 101(29), pp. 10732-10737. doi: 10.1073/pnas.0404117101

Ioudinkova, E. et al. 2006. Control of human cytomegalovirus gene expression by differential histone modifications during lytic and latent infection of a monocytic cell line. *Gene* 384, pp. 120-128. doi: 10.1016/j.gene.2006.07.021

Irmiere, A. and Gibson, W. 1983. Isolation and characterization of a noninfectious virion-like particle released from cells infected with human

strains of cytomegalovirus. *Virology* 130(1), pp. 118-133. doi: 10.1016/0042-6822(83)90122-8

Isaacson, M. K., Juckem, L. K. and Compton, T. 2008. Virus entry and innate immune activation. *Curr Top Microbiol Immunol* 325, pp. 85-100. doi: 10.1007/978-3-540-77349-8_5

Isomura, H. and Stinski, M. F. 2013. Coordination of late gene transcription of human cytomegalovirus with viral DNA synthesis: recombinant viruses as potential therapeutic vaccine candidates. *Expert Opin Ther Targets* 17(2), pp. 157-166. doi: 10.1517/14728222.2013.740460

Issuree, P. D. et al. 2013. iRHOM2 is a critical pathogenic mediator of inflammatory arthritis. *J Clin Invest* 123(2), pp. 928-932. doi: 10.1172/JCI66168

Ivetic, A., Hoskins Green, H. L. and Hart, S. J. 2019. L-selectin: A Major Regulator of Leukocyte Adhesion, Migration and Signaling. *Front Immunol* 10, p. 1068. doi: 10.3389/fimmu.2019.01068

Jackson, S. E., Mason, G. M. and Wills, M. R. 2011. Human cytomegalovirus immunity and immune evasion. *Virus Res* 157(2), pp. 151-160. doi: 10.1016/j.virusres.2010.10.031

Jahn, G., Scholl, B. C., Traupe, B. and Fleckenstein, B. 1987. The two major structural phosphoproteins (pp65 and pp150) of human cytomegalovirus and their antigenic properties. *J Gen Virol* 68 (Pt 5), pp. 1327-1337. doi: 10.1099/0022-1317-68-5-1327

Janes, P. W. et al. 2005. Adam meets Eph: an ADAM substrate recognition module acts as a molecular switch for ephrin cleavage in trans. *Cell* 123(2), pp. 291-304. doi: 10.1016/j.cell.2005.08.014

Jean Beltran, P. M. and Cristea, I. M. 2014. The life cycle and pathogenesis of human cytomegalovirus infection: lessons from proteomics. *Expert Rev Proteomics* 11(6), pp. 697-711. doi: 10.1586/14789450.2014.971116

Jenkins, C., Garcia, W., Godwin, M. J., Spencer, J. V., Stern, J. L., Abendroth, A. and Slobedman, B. 2008. Immunomodulatory properties of a viral homolog of human interleukin-10 expressed by human cytomegalovirus during the latent phase of infection. *J Virol* 82(7), pp. 3736-3750. doi: 10.1128/JVI.02173-07

Jesser, R. D., Li, S. and Weinberg, A. 2006. Regulatory T cells generated during cytomegalovirus in vitro stimulation of mononuclear cells from HIV-infected individuals on HAART correlate with decreased lymphocyte proliferation. *Virology* 352(2), pp. 408-417. doi: 10.1016/j.virol.2006.04.035

Jiang, X. J. et al. 2008. UL74 of human cytomegalovirus contributes to virus release by promoting secondary envelopment of virions. *J Virol* 82(6), pp. 2802-2812. doi: 10.1128/JVI.01550-07

Jocher, G. et al. 2022. ADAM10 and ADAM17 promote SARS-CoV-2 cell entry and spike protein-mediated lung cell fusion. *EMBO Rep* 23(6), p. e54305. doi: 10.15252/embr.202154305

Johnson, D. C. and Hegde, N. R. 2002. Inhibition of the MHC class II antigen presentation pathway by human cytomegalovirus. *Curr Top Microbiol Immunol* 269, pp. 101-115. doi: 10.1007/978-3-642-59421-2_7

Jones, G. W. et al. 2010. Loss of CD4+ T cell IL-6R expression during inflammation underlines a role for IL-6 trans signaling in the local maintenance of Th17 cells. *J Immunol* 184(4), pp. 2130-2139. doi: 10.4049/jimmunol.0901528

Jones, T. R., Hanson, L. K., Sun, L., Slater, J. S., Stenberg, R. M. and Campbell, A. E. 1995. Multiple independent loci within the human cytomegalovirus unique short region down-regulate expression of major histocompatibility complex class I heavy chains. *J Virol* 69(8), pp. 4830-4841. doi: 10.1128/JVI.69.8.4830-4841.1995

Jones, T. R., Wiertz, E. J., Sun, L., Fish, K. N., Nelson, J. A. and Ploegh, H. L. 1996. Human cytomegalovirus US3 impairs transport and maturation of major histocompatibility complex class I heavy chains. *Proc Natl Acad Sci U S A* 93(21), pp. 11327-11333. doi: 10.1073/pnas.93.21.11327

Jose, R. J. and Manuel, A. 2020. COVID-19 cytokine storm: the interplay between inflammation and coagulation. *Lancet Respir Med* 8(6), pp. e46-e47. doi: 10.1016/S2213-2600(20)30216-2

Jost, N. H. et al. 2014. Regulatory T cells and T-cell-derived IL-10 interfere with effective anti-cytomegalovirus immune response. *Immunol Cell Biol* 92(10), pp. 860-871. doi: 10.1038/icb.2014.62

Just, M., Buergin-Wolff, A., Emoedi, G. and Hernandez, R. 1975. Immunisation trials with live attenuated cytomegalovirus TOWNE 125. *Infection* 3(2), pp. 111-114. doi: 10.1007/BF01641052

Kalejta, R. F. 2008. Tegument proteins of human cytomegalovirus. *Microbiol Mol Biol Rev* 72(2), pp. 249-265, table of contents. doi: 10.1128/MMBR.00040-07

Kari, B. and Gehrz, R. 1992. A human cytomegalovirus glycoprotein complex designated gC-II is a major heparin-binding component of the envelope. *J Virol* 66(3), pp. 1761-1764. doi: 10.1128/JVI.66.3.1761-1764.1992

Kempen, J. H., Jabs, D. A., Wilson, L. A., Dunn, J. P., West, S. K. and Tonascia, J. 2003. Mortality risk for patients with cytomegalovirus retinitis and acquired immune deficiency syndrome. *Clin Infect Dis* 37(10), pp. 1365-1373. doi: 10.1086/379077

Kenneson, A. and Cannon, M. J. 2007. Review and meta-analysis of the epidemiology of congenital cytomegalovirus (CMV) infection. *Rev Med Virol* 17(4), pp. 253-276. doi: 10.1002/rmv.535

Kern, F. et al. 2002. Cytomegalovirus (CMV) phosphoprotein 65 makes a large contribution to shaping the T cell repertoire in CMV-exposed individuals. *J Infect Dis* 185(12), pp. 1709-1716. doi: 10.1086/340637

Kim, J., Lilliehook, C., Dudak, A., Prox, J., Saftig, P., Federoff, H. J. and Lim, S. T. 2010. Activity-dependent alpha-cleavage of nectin-1 is mediated by a disintegrin and metalloprotease 10 (ADAM10). *J Biol Chem* 285(30), pp. 22919-22926. doi: 10.1074/jbc.M110.126649

Kim, S. et al. 2011. Human cytomegalovirus microRNA miR-US4-1 inhibits CD8(+) T cell responses by targeting the aminopeptidase ERAP1. *Nat Immunol* 12(10), pp. 984-991. doi: 10.1038/ni.2097

Knight, A. et al. 2010. The role of Vδ2-negative γδ T cells during cytomegalovirus reactivation in recipients of allogeneic stem cell transplantation. *Blood* 116(12), pp. 2164-2172. doi: 10.1182/blood-2010-01-255166

Krishna, B. A., Wills, M. R. and Sinclair, J. H. 2019. Advances in the treatment of cytomegalovirus. *Br Med Bull* 131(1), pp. 5-17. doi: 10.1093/bmb/ldz031

Kropff, B., Burkhardt, C., Schott, J., Nentwich, J., Fisch, T., Britt, W. and Mach, M. 2012. Glycoprotein N of human cytomegalovirus protects the virus from neutralizing antibodies. *PLoS Pathog* 8(10), p. e1002999. doi: 10.1371/journal.ppat.1002999

Kurosawa, S., Esmon, C. T. and Stearns-Kurosawa, D. J. 2000. The soluble endothelial protein C receptor binds to activated neutrophils: involvement of proteinase-3 and CD11b/CD18. *J Immunol* 165(8), pp. 4697-4703. doi: 10.4049/jimmunol.165.8.4697

Köppen-Rung, P., Dittmer, A. and Bogner, E. 2016. Intracellular Distribution of Capsid-Associated pUL77 of Human Cytomegalovirus and Interactions with Packaging Proteins and pUL93. *J Virol* 90(13), pp. 5876-5885. doi: 10.1128/JVI.00351-16

Künzel, U., Grieve, A. G., Meng, Y., Sieber, B., Cowley, S. A. and Freeman, M. 2018. FRMD8 promotes inflammatory and growth factor signalling by stabilising the iRhom/ADAM17 sheddase complex. *Elife* 7, doi: 10.7554/eLife.35012

La Rosa, C. and Diamond, D. J. 2012. The immune response to human CMV. *Future Virol* 7(3), pp. 279-293. doi: 10.2217/fvl.12.8

Lan, K. and Luo, M. H. 2017. Herpesviruses: epidemiology, pathogenesis, and interventions. *Virol Sin* 32(5), pp. 347-348. doi: 10.1007/s12250-017-4108-2

Le-Trilling, V. T. K. et al. 2020. The Human Cytomegalovirus pUL145 Isoforms Act as Viral DDB1-Cullin-Associated Factors to Instruct Host Protein Degradation to Impede Innate Immunity. *Cell Rep* 30(7), pp. 2248-2260.e2245. doi: 10.1016/j.celrep.2020.01.070

Lee, M. Y., Nam, K. H. and Choi, K. C. 2016. iRhoms; Its Functions and Essential Roles. *Biomol Ther (Seoul)* 24(2), pp. 109-114. doi: 10.4062/biomolther.2015.149

Lehner, P. J., Karttunen, J. T., Wilkinson, G. W. and Cresswell, P. 1997. The human cytomegalovirus US6 glycoprotein inhibits transporter associated with antigen processing-dependent peptide translocation. *Proc Natl Acad Sci U S A* 94(13), pp. 6904-6909. doi: 10.1073/pnas.94.13.6904

Li, D., Masiero, M., Banham, A. H. and Harris, A. L. 2014. The notch ligand JAGGED1 as a target for anti-tumor therapy. *Front Oncol* 4, p. 254. doi: 10.3389/fonc.2014.00254

Li, G., Nguyen, C. C., Ryckman, B. J., Britt, W. J. and Kamil, J. P. 2015a. A viral regulator of glycoprotein complexes contributes to human

cytomegalovirus cell tropism. *Proc Natl Acad Sci U S A* 112(14), pp. 4471-4476. doi: 10.1073/pnas.1419875112

Li, M. and Rossi, J. J. 2007. Lentivirus transduction of hematopoietic cells. *Cold Spring Harb Protoc* May 1;2007:pdb.prot4755. doi: 10.1101/pdb.prot4755.

Li, X. J. et al. 2015b. Human Cytomegalovirus Infection Dysregulates the Localization and Stability of NICD1 and Jag1 in Neural Progenitor Cells. *J Virol* 89(13), pp. 6792-6804. doi: 10.1128/JVI.00351-15

Li, Y., Li, G., Zhang, J., Wu, X. and Chen, X. 2020. The Dual Roles of Human γδ T Cells: Anti-Tumor or Tumor-Promoting. *Front Immunol* 11, p. 619954. doi: 10.3389/fimmu.2020.619954

Li, Y. N., Liu, X. L., Huang, F., Zhou, H., Huang, Y. J. and Fang, F. 2010. CD4+CD25+ regulatory T cells suppress the immune responses of mouse embryo fibroblasts to murine cytomegalovirus infection. *Immunol Lett* 131(2), pp. 131-138. doi: 10.1016/j.imlet.2010.03.011

Ligat, G., Cazal, R., Hantz, S. and Alain, S. 2018. The human cytomegalovirus terminase complex as an antiviral target: a close-up view. *FEMS Microbiol Rev* 42(2), pp. 137-145. doi: 10.1093/femsre/fuy004

Lilley, B. N., Ploegh, H. L. and Tirabassi, R. S. 2001. Human cytomegalovirus open reading frame TRL11/IRL11 encodes an immunoglobulin G Fc-binding protein. *J Virol* 75(22), pp. 11218-11221. doi: 10.1128/JVI.75.22.11218-11221.2001

Lin, A., Xu, H. and Yan, W. 2007. Modulation of HLA expression in human cytomegalovirus immune evasion. *Cell Mol Immunol* 4(2), pp. 91-98.

Lin, C. L., Huang, H. M., Hsieh, C. L., Fan, C. K. and Lee, Y. L. 2019. Jagged1-expressing adenovirus-infected dendritic cells induce expansion of Foxp3. *Immunology* 156(2), pp. 199-212. doi: 10.1111/imm.13021

Link, M. A., Lücke, K., Schmid, J., Schumacher, V., Eden, T., Rose-John, S. and Mittrücker, H. W. 2017. The role of ADAM17 in the T-cell response against bacterial pathogens. *PLoS One* 12(9), p. e0184320. doi: 10.1371/journal.pone.0184320

Lischka, P. and Zimmermann, H. 2008. Antiviral strategies to combat cytomegalovirus infections in transplant recipients. *Curr Opin Pharmacol* 8(5), pp. 541-548. doi: 10.1016/j.coph.2008.07.002

Liu, C. et al. 2019. Nexilin Is a New Component of Junctional Membrane Complexes Required for Cardiac T-Tubule Formation. *Circulation* 140(1), pp. 55-66. doi: 10.1161/CIRCULATIONAHA.119.039751

Liu, F. and Zhou, Z. H. 2007. *Comparative virion structures of human herpesviruses. Chapter 3. I n: Arvin A, Campadelli-Fiume G, Mocarski E, Moore PS, Roizman B, Whitley R, Yamanishi K, editors. Human Herpesviruses: Biology, Therapy, and Immunoprophylaxis. Cambridge: Cambridge University Press.* Cambridge University Press.

Liu, Y., Cai, Y., Liu, L., Wu, Y. and Xiong, X. 2018. Crucial biological functions of CCL7 in cancer. *PeerJ* 6, p. e4928. doi: 10.7717/peerj.4928

Londino, J. D., Gulick, D., Isenberg, J. S. and Mallampalli, R. K. 2015. Cleavage of Signal Regulatory Protein α (SIRPα) Enhances Inflammatory Signaling. *J Biol Chem* 290(52), pp. 31113-31125. doi: 10.1074/jbc.M115.682914

Lontos, K., Adamik, J., Tsagianni, A., Galson, D. L., Chirgwin, J. M. and Suvannasankha, A. 2018. The Role of Semaphorin 4D in Bone Remodeling and Cancer Metastasis. *Front Endocrinol (Lausanne)* 9, p. 322. doi: 10.3389/fendo.2018.00322

Lorenzen, I. et al. 2016. Control of ADAM17 activity by regulation of its cellular localisation. *Sci Rep* 6, p. 35067. doi: 10.1038/srep35067

Lu, L., Barbi, J. and Pan, F. 2017. The regulation of immune tolerance by FOXP3. *Nat Rev Immunol* 17(11), pp. 703-717. doi: 10.1038/nri.2017.75

Lurain, N. S. et al. 2006. Analysis of the human cytomegalovirus genomic region from UL146 through UL147A reveals sequence hypervariability, genotypic stability, and overlapping transcripts. *Virol J* 3, p. 4. doi: 10.1186/1743-422X-3-4

Mach, M., Kropff, B., Dal Monte, P. and Britt, W. 2000. Complex formation by human cytomegalovirus glycoproteins M (gpUL100) and N (gpUL73). *J Virol* 74(24), pp. 11881-11892. doi: 10.1128/jvi.74.24.11881-11892.2000

Mach, M., Kropff, B., Kryzaniak, M. and Britt, W. 2005. Complex formation by glycoproteins M and N of human cytomegalovirus: structural and functional aspects. *J Virol* 79(4), pp. 2160-2170. doi: 10.1128/JVI.79.4.2160-2170.2005

Malapeira, J., Esselens, C., Bech-Serra, J. J., Canals, F. and Arribas, J. 2011. ADAM17 (TACE) regulates TGFβ signaling through the cleavage of vasorin. *Oncogene* 30(16), pp. 1912-1922. doi: 10.1038/onc.2010.565

Marchi, E., Lee, L. N. and Klenerman, P. 2019. Inflation vs. Exhaustion of Antiviral CD8+ T-Cell Populations in Persistent Infections: Two Sides of the Same Coin? *Front Immunol* 10, p. 197. doi: 10.3389/fimmu.2019.00197

Marie, J. C., Letterio, J. J., Gavin, M. and Rudensky, A. Y. 2005. TGF-beta1 maintains suppressor function and Foxp3 expression in CD4+CD25+ regulatory T cells. *J Exp Med* 201(7), pp. 1061-1067. doi: 10.1084/jem.20042276

Marschall, M. et al. 2020. Nuclear Egress Complexes of HCMV and Other Herpesviruses: Solving the Puzzle of Sequence Coevolution, Conserved Structures and Subfamily-Spanning Binding Properties. *Viruses* 12(6), doi: 10.3390/v12060683

Martinez-Martin, N. et al. 2018. An Unbiased Screen for Human Cytomegalovirus Identifies Neuropilin-2 as a Central Viral Receptor. *Cell* 174(5), pp. 1158-1171.e1119. doi: 10.1016/j.cell.2018.06.028

Marty, F. M. et al. 2017. Letermovir Prophylaxis for Cytomegalovirus in Hematopoietic-Cell Transplantation. *N Engl J Med* 377(25), pp. 2433-2444. doi: 10.1056/NEJMoa1706640

Martí-Carreras, J. and Maes, P. 2019. Human cytomegalovirus genomics and transcriptomics through the lens of next-generation sequencing: revision and future challenges. *Virus Genes* 55(2), pp. 138-164. doi: 10.1007/s11262-018-1627-3

Maskos, K. et al. 1998. Crystal structure of the catalytic domain of human tumor necrosis factor-alpha-converting enzyme. *Proc Natl Acad Sci U S A* 95(7), pp. 3408-3412. doi: 10.1073/pnas.95.7.3408

McGeoch, D. J., Cook, S., Dolan, A., Jamieson, F. E. and Telford, E. A. 1995. Molecular phylogeny and evolutionary timescale for the family of mammalian herpesviruses. *J Mol Biol* 247(3), pp. 443-458. doi: 10.1006/jmbi.1995.0152

McLaughlin-Taylor, E. et al. 1994. Identification of the major late human cytomegalovirus matrix protein pp65 as a target antigen for CD8+ virus-specific cytotoxic T lymphocytes. *J Med Virol* 43(1), pp. 103-110. doi: 10.1002/jmv.1890430119

McSharry, B. P. et al. 2008. Adenovirus E3/19K promotes evasion of NK cell recognition by intracellular sequestration of the NKG2D ligands major histocompatibility complex class I chain-related proteins A and B. *J Virol* 82(9), pp. 4585-4594. doi: 10.1128/JVI.02251-07

McSharry, B. P., Jones, C. J., Skinner, J. W., Kipling, D. and Wilkinson, G. W. G. 2001. Human telomerase reverse transcriptase-immortalized MRC-5 and HCA2 human fibroblasts are fully permissive for human cytomegalovirus. *J Gen Virol* 82(Pt 4), pp. 855-863. doi: 10.1099/0022-1317-82-4-855

Miller, D. M., Cebulla, C. M., Rahill, B. M. and Sedmak, D. D. 2001. Cytomegalovirus and transcriptional down-regulation of major histocompatibility complex class II expression. *Semin Immunol* 13(1), pp. 11-18. doi: 10.1006/smim.2001.0291

Minder, W. H. 1953. Die Aetiologie der Cytomegalia infantum. *Schweiz Med Wochenschr* 83, pp. 1180–1182.

Mocarski, E. 2007. Betaherpes viral genes and their functions. Chapter 15. In: Arvin A, Campadelli-Fiume G, Mocarski E, et al., editors. Human Herpesviruses: Biology, Therapy, and Immunoprophylaxis. Cambridge: Cambridge University Press.

Mocarski, E. S., Shank, T. and Pass, R. F. 2007. Cytomegaloviruses. p. 2701–2772. In D. M. Knipe, P. M. Howley, D. E. Griffin, R. A. Lamb, M. A. Martin, B. Roizman, and S. E. Straus (ed.), Fields virology, 5th ed., vol. 2. Lippincott Williams & Wilkins, Philadelphia, PA.

Mohammed, R. N., Watson, H. A., Vigar, M., Ohme, J., Thomson, A., Humphreys, I. R. and Ager, A. 2016. L-selectin Is Essential for Delivery of Activated CD8(+) T Cells to Virus-Infected Organs for Protective Immunity. *Cell Rep* 14(4), pp. 760-771. doi: 10.1016/j.celrep.2015.12.090

Mohammed, R. N. et al. 2019. ADAM17-dependent proteolysis of L-selectin promotes early clonal expansion of cytotoxic T cells. *Sci Rep* 9(1), p. 5487. doi: 10.1038/s41598-019-41811-z

Montag, C., Wagner, J. A., Gruska, I., Vetter, B., Wiebusch, L. and Hagemeier, C. 2011. The latency-associated UL138 gene product of human cytomegalovirus sensitizes cells to tumor necrosis factor alpha (TNF-alpha) signaling by upregulating TNF-alpha receptor 1 cell surface expression. *J Virol* 85(21), pp. 11409-11421. doi: 10.1128/JVI.05028-11

Monteil, V. et al. 2020. Inhibition of SARS-CoV-2 Infections in Engineered Human Tissues Using Clinical-Grade Soluble Human ACE2. *Cell* 181(4), pp. 905-913.e907. doi: 10.1016/j.cell.2020.04.004

Moretta, A., Marcenaro, E., Parolini, S., Ferlazzo, G. and Moretta, L. 2008. NK cells at the interface between innate and adaptive immunity. *Cell Death Differ* 15(2), pp. 226-233. doi: 10.1038/sj.cdd.4402170

Moss, M. L. et al. 1997. Cloning of a disintegrin metalloproteinase that processes precursor tumour-necrosis factor-alpha. *Nature* 385(6618), pp. 733-736. doi: 10.1038/385733a0

Moss, M. L. and Minond, D. 2017. Recent Advances in ADAM17 Research: A Promising Target for Cancer and Inflammation. *Mediators Inflamm* 2017, p. 9673537. doi: 10.1155/2017/9673537

Muller, C., Alain, S., Baumert, T. F., Ligat, G. and Hantz, S. 2021. Structures and Divergent Mechanisms in Capsid Maturation and Stabilization Following Genome Packaging of Human Cytomegalovirus and Herpesviruses. *Life (Basel)* 11(2), doi: 10.3390/life11020150

Mullooly, M., McGowan, P. M., Crown, J. and Duffy, M. J. 2016. The ADAMs family of proteases as targets for the treatment of cancer. *Cancer Biol Ther* 17(8), pp. 870-880. doi: 10.1080/15384047.2016.1177684

Murphy, E. and Shenk, T. E. 2008. Human Cytomegalovirus Genome. In: Shenk, T.E., Stinski, M.F. (eds) Human Cytomegalovirus. Current Topics in Microbiology and Immunology, vol 325. Springer, Berlin, Heidelberg.

Murrell, I., Tomasec, P., Wilkie, G. S., Dargan, D. J., Davison, A. J. and Stanton, R. J. 2013. Impact of sequence variation in the UL128 locus on production of human cytomegalovirus in fibroblast and epithelial cells. *J Virol* 87(19), pp. 10489-10500. doi: 10.1128/JVI.01546-13

Neff, B. J., Weibel, R. E., Buynak, E. B., McLean, A. A. and Hilleman, M. R. 1979. Clinical and laboratory studies of live cytomegalovirus vaccine Ad-169. *Proc Soc Exp Biol Med* 160(1), pp. 32-37. doi: 10.3181/00379727-160-40382

Nemčovičová, I., Benedict, C. A. and Zajonc, D. M. 2013. Structure of human cytomegalovirus UL141 binding to TRAIL-R2 reveals novel, non-canonical death receptor interactions. *PLoS Pathog* 9(3), p. e1003224. doi: 10.1371/journal.ppat.1003224

Nguyen, C. C. and Kamil, J. P. 2018. Pathogen at the Gates: Human Cytomegalovirus Entry and Cell Tropism. *Viruses* 10(12), doi: 10.3390/v10120704

Nguyen, C. C., Siddiquey, M. N. A., Zhang, H., Li, G. and Kamil, J. P. 2018. Human Cytomegalovirus Tropism Modulator UL148 Interacts with SEL1L, a Cellular Factor That Governs Endoplasmic Reticulum-Associated Degradation of the Viral Envelope Glycoprotein gO. *J Virol* 92(18), doi: 10.1128/JVI.00688-18

Nichols, H. 2018. *An analysis of human cytomegalovirus gene family function.* PhD Thesis. Cardiff University.

Nicolaou, A. et al. 2017. Adam17 Deficiency Promotes Atherosclerosis by Enhanced TNFR2 Signaling in Mice. *Arterioscler Thromb Vasc Biol* 37(2), pp. 247-257. doi: 10.1161/ATVBAHA.116.308682

Nightingale, K. et al. 2018. High-Definition Analysis of Host Protein Stability during Human Cytomegalovirus Infection Reveals Antiviral Factors and Viral Evasion Mechanisms. *Cell Host Microbe* 24(3), pp. 447-460.e411. doi: 10.1016/j.chom.2018.07.011

Nightingale, K. et al. 2022. Human cytomegalovirus protein RL1 degrades the antiviral factor SLFN11 via recruitment of the CRL4 E3 ubiquitin ligase complex. *Proc Natl Acad Sci U S A* 119(6), doi: 10.1073/pnas.2108173119

Nobre, L. V. et al. 2019. Human cytomegalovirus interactome analysis identifies degradation hubs, domain associations and viral protein functions. *Elife* 8, doi: 10.7554/eLife.49894

Obst, J. et al. 2021. PLCγ2 regulates TREM2 signalling and integrin-mediated adhesion and migration of human iPSC-derived macrophages. *Sci Rep* 11(1), p. 19842. doi: 10.1038/s41598-021-96144-7

Ogawa-Goto, K. et al. 2003. Microtubule network facilitates nuclear targeting of human cytomegalovirus capsid. *J Virol* 77(15), pp. 8541-8547. doi: 10.1128/jvi.77.15.8541-8547.2003

Oikonomidi, I. et al. 2018. iTAP, a novel iRhom interactor, controls TNF secretion by policing the stability of iRhom/TACE. *Elife* 7, doi: 10.7554/eLife.35032

Ong, D. S. Y. et al. 2017. Epidemiology of Multiple Herpes Viremia in Previously Immunocompetent Patients With Septic Shock. *Clin Infect Dis* 64(9), pp. 1204-1210. doi: 10.1093/cid/cix120

Pari, G. S. 2008. Nuts and bolts of human cytomegalovirus lytic DNA replication. *Curr Top Microbiol Immunol* 325, pp. 153-166. doi: 10.1007/978-3-540-77349-8_9

Park, A. et al. 2019. HCMV-encoded US7 and US8 act as antagonists of innate immunity by distinctively targeting TLR-signaling pathways. *Nat Commun* 10(1), p. 4670. doi: 10.1038/s41467-019-12641-4

Pass, R. F. and Anderson, B. 2014. Mother-to-Child Transmission of Cytomegalovirus and Prevention of Congenital Infection. *J Pediatric Infect Dis Soc* 3 Suppl 1(Suppl 1), pp. S2-6. doi: 10.1093/jpids/piu069

Patel, M. 2018. *Regulation of Cellular Immunity by Human Cytomegalovirus.* PhD thesis. Cardiff University.

Patel, M., Vlahava, V. M., Forbes, S. K., Fielding, C. A., Stanton, R. J. and Wang, E. C. Y. 2018. HCMV-Encoded NK Modulators: Lessons From. *Front Immunol* 9, p. 2214. doi: 10.3389/fimmu.2018.02214

Patente, T. A., Pinho, M. P., Oliveira, A. A., Evangelista, G. C. M., Bergami-Santos, P. C. and Barbuto, J. A. M. 2018. Human Dendritic Cells: Their Heterogeneity and Clinical Application Potential in Cancer Immunotherapy. *Front Immunol* 9, p. 3176. doi: 10.3389/fimmu.2018.03176

Paya, C. et al. 2004. Efficacy and safety of valganciclovir vs. oral ganciclovir for prevention of cytomegalovirus disease in solid organ transplant recipients. *Am J Transplant* 4(4), pp. 611-620. doi: 10.1111/j.1600-6143.2004.00382.x

Pegram, H. J., Andrews, D. M., Smyth, M. J., Darcy, P. K. and Kershaw, M. H. 2011. Activating and inhibitory receptors of natural killer cells. *Immunol Cell Biol* 89(2), pp. 216-224. doi: 10.1038/icb.2010.78

Peiretti, F., Canault, M., Deprez-Beauclair, P., Berthet, V., Bonardo, B., Juhan-Vague, I. and Nalbone, G. 2003. Intracellular maturation and transport of tumor necrosis factor alpha converting enzyme. *Exp Cell Res* 285(2), pp. 278-285. doi: 10.1016/s0014-4827(03)00052-1

Pellet, P. E. and Roizman, B. 2013. Herpesviridae. In: FIELDS, B. N., KNIPE, D. M. & HOWLEY, P. M. (eds.) Fields Virology. 6th ed. Philadelphia: Lippincott Williams & Wilkins.

Penfold, M. E., Dairaghi, D. J., Duke, G. M., Saederup, N., Mocarski, E. S., Kemble, G. W. and Schall, T. J. 1999. Cytomegalovirus encodes a potent alpha chemokine. *Proc Natl Acad Sci U S A* 96(17), pp. 9839-9844. doi: 10.1073/pnas.96.17.9839

Perera, M. R., Wills, M. R. and Sinclair, J. H. 2021. HCMV Antivirals and Strategies to Target the Latent Reservoir. *Viruses* 13(5), doi: 10.3390/v13050817

Pereyra, F. and Rubin, R. H. 2004. Prevention and treatment of cytomegalovirus infection in solid organ transplant recipients. *Curr Opin Infect Dis* 17(4), pp. 357-361. doi: 10.1097/01.qco.0000136933.67920.dd

Peschon, J. J. et al. 1998. An essential role for ectodomain shedding in mammalian development. *Science* 282(5392), pp. 1281-1284. doi: 10.1126/science.282.5392.1281

Pitard, V. et al. 2008. Long-term expansion of effector/memory Vdelta2-gammadelta T cells is a specific blood signature of CMV infection. *Blood* 112(4), pp. 1317-1324. doi: 10.1182/blood-2008-01-136713

Plachter, B., Sinzger, C. and Jahn, G. 1996. Cell types involved in replication and distribution of human cytomegalovirus. *Adv Virus Res* 46, pp. 195-261. doi: 10.1016/s0065-3527(08)60073-1

Plotkin, S. A., Furukawa, T., Zygraich, N. and Huygelen, C. 1975. Candidate cytomegalovirus strain for human vaccination. *Infect Immun* 12(3), pp. 521-527. doi: 10.1128/iai.12.3.521-527.1975

Poole, E., Juss, J. K., Krishna, B., Herre, J., Chilvers, E. R. and Sinclair, J. 2015. Alveolar Macrophages Isolated Directly From Human Cytomegalovirus (HCMV)-Seropositive Individuals Are Sites of HCMV Reactivation In Vivo. *J Infect Dis* 211(12), pp. 1936-1942. doi: 10.1093/infdis/jiu837

Prod'homme, V. et al. 2007. The human cytomegalovirus MHC class I homolog UL18 inhibits LIR-1+ but activates LIR-1- NK cells. *J Immunol* 178(7), pp. 4473-4481. doi: 10.4049/jimmunol.178.7.4473

Prod'homme, V. et al. 2010. Human cytomegalovirus UL141 promotes efficient downregulation of the natural killer cell activating ligand CD112. *J Gen Virol* 91(Pt 8), pp. 2034-2039. doi: 10.1099/vir.0.021931-0

Prod'homme, V. et al. 2012. Human cytomegalovirus UL40 signal peptide regulates cell surface expression of the NK cell ligands HLA-E and gpUL18. *J Immunol* 188(6), pp. 2794-2804. doi: 10.4049/jimmunol.1102068

Pruessmeyer, J. and Ludwig, A. 2009. The good, the bad and the ugly substrates for ADAM10 and ADAM17 in brain pathology, inflammation and cancer. *Semin Cell Dev Biol* 20(2), pp. 164-174. doi: 10.1016/j.semcdb.2008.09.005

Pérez-Carmona, N., Martínez-Vicente, P., Farré, D., Gabaev, I., Messerle, M., Engel, P. and Angulo, A. 2018. A Prominent Role of the Human Cytomegalovirus UL8 Glycoprotein in Restraining Proinflammatory Cytokine Production by Myeloid Cells at Late Times during Infection. *J Virol* 92(9), doi: 10.1128/JVI.02229-17

Qu, Y., Zhao, G. and Li, H. 2017. Forward and Reverse Signaling Mediated by Transmembrane Tumor Necrosis Factor-Alpha and TNF Receptor 2: Potential Roles in an Immunosuppressive Tumor Microenvironment. *Front Immunol* 8, p. 1675. doi: 10.3389/fimmu.2017.01675

Quinnan, G. V. et al. 1984. Comparative virulence and immunogenicity of the Towne strain and a nonattenuated strain of cytomegalovirus. *Ann Intern Med* 101(4), pp. 478-483. doi: 10.7326/0003-4819-101-4-478

Reeves, M. B. 2011. Chromatin-mediated regulation of cytomegalovirus gene expression. *Virus Res* 157(2), pp. 134-143. doi: 10.1016/j.virusres.2010.09.019

Reeves, M. B., MacAry, P. A., Lehner, P. J., Sissons, J. G. and Sinclair, J. H. 2005. Latency, chromatin remodeling, and reactivation of human cytomegalovirus in the dendritic cells of healthy carriers. *Proc Natl Acad Sci U S A* 102(11), pp. 4140-4145. doi: 10.1073/pnas.0408994102

Reeves, M. B. and Sinclair, J. H. 2013. Circulating dendritic cells isolated from healthy seropositive donors are sites of human cytomegalovirus

reactivation in vivo. *J Virol* 87(19), pp. 10660-10667. doi: 10.1128/JVI.01539-13

Revello, M. G., Percivalle, E., Di Matteo, A., Morini, F. and Gerna, G. 1992. Nuclear expression of the lower matrix protein of human cytomegalovirus in peripheral blood leukocytes of immunocompromised viraemic patients. *J Gen Virol* 73 (Pt 2), pp. 437-442. doi: 10.1099/0022-1317-73-2-437

Ribbert, H. 1904. Ueber protozoenartige Zellen in der Niere eines syphilitischen Neugeborenen und in der Parotis von Kindern. *Zbl All Pathol* 15, pp. 945–948.

Richards, F. M., Tape, C. J., Jodrell, D. I. and Murphy, G. 2012. Anti-tumour effects of a specific anti-ADAM17 antibody in an ovarian cancer model in vivo. *PLoS One* 7(7), p. e40597. doi: 10.1371/journal.pone.0040597

Romania, P. et al. 2017. Identification of a Genetic Variation in ERAP1 Aminopeptidase that Prevents Human Cytomegalovirus miR-UL112-5p-Mediated Immunoevasion. *Cell Rep* 20(4), pp. 846-853. doi: 10.1016/j.celrep.2017.06.084

Romee, R. et al. 2013. NK cell CD16 surface expression and function is regulated by a disintegrin and metalloprotease-17 (ADAM17). *Blood* 121(18), pp. 3599-3608. doi: 10.1182/blood-2012-04-425397

Rossello, A., Nuti, E., Ferrini, S. and Fabbi, M. 2016. Targeting ADAM17 Sheddase Activity in Cancer. *Curr Drug Targets* 17(16), pp. 1908-1927. doi: 10.2174/1389450117666160727143618

Rossini, G. et al. 2012. Interplay between human cytomegalovirus and intrinsic/innate host responses: a complex bidirectional relationship. *Mediators Inflamm* 2012, p. 607276. doi: 10.1155/2012/607276

Roux, K. J., Kim, D. I., Raida, M. and Burke, B. 2012. A promiscuous biotin ligase fusion protein identifies proximal and interacting proteins in mammalian cells. *J Cell Biol* 196(6), pp. 801-810. doi: 10.1083/jcb.201112098

Rowe, W. P., Hartley, J. W., Waterman, S., Turner, H. C. and Huebner, R. J. 1956. Cytopathogenic agent resembling human salivary gland virus recovered from tissue cultures of human adenoids. *Proc Soc Exp Biol Med* 92(2), pp. 418-424.

Rozman, B., Nachshon, A., Levi Samia, R., Lavi, M., Schwartz, M. and Stern-Ginossar, N. 2022. Temporal dynamics of HCMV gene expression in lytic and latent infections. *Cell Rep* 39(2), p. 110653. doi: 10.1016/j.celrep.2022.110653

Ryckman, B. J., Jarvis, M. A., Drummond, D. D., Nelson, J. A. and Johnson, D. C. 2006. Human cytomegalovirus entry into epithelial and endothelial cells depends on genes UL128 to UL150 and occurs by endocytosis and low-pH fusion. *J Virol* 80(2), pp. 710-722. doi: 10.1128/JVI.80.2.710-722.2006

Ryckman, B. J., Rainish, B. L., Chase, M. C., Borton, J. A., Nelson, J. A., Jarvis, M. A. and Johnson, D. C. 2008. Characterization of the human cytomegalovirus gH/gL/UL128-131 complex that mediates entry into epithelial and endothelial cells. *J Virol* 82(1), pp. 60-70. doi: 10.1128/JVI.01910-07

Sabbaghi, A., Miri, S. M., Keshavarz, M., Mahooti, M., Zebardast, A. and Ghaemi, A. 2020. Role of γδ T cells in controlling viral infections with a focus on influenza virus: implications for designing novel therapeutic approaches. *Virol J* 17(1), p. 174. doi: 10.1186/s12985-020-01449-0

Saederup, N. and Mocarski, E. S. 2002. Fatal attraction: cytomegalovirus-encoded chemokine homologs. *Curr Top Microbiol Immunol* 269, pp. 235-256. doi: 10.1007/978-3-642-59421-2_14

Saheb Sharif-Askari, N., Saheb Sharif-Askari, F., Alabed, M., Temsah, M. H., Al Heialy, S., Hamid, Q. and Halwani, R. 2020. Airways Expression of SARS-CoV-2 Receptor, ACE2, and TMPRSS2 Is Lower in Children Than Adults and Increases with Smoking and COPD. *Mol Ther Methods Clin Dev* 18, pp. 1-6. doi: 10.1016/j.omtm.2020.05.013

Salsman, J., Zimmerman, N., Chen, T., Domagala, M. and Frappier, L. 2008. Genome-wide screen of three herpesviruses for protein subcellular localization and alteration of PML nuclear bodies. *PLoS Pathog* 4(7), p. e1000100. doi: 10.1371/journal.ppat.1000100

Sanchez-Correa, B. et al. 2019. DNAM-1 and the TIGIT/PVRIG/TACTILE Axis: Novel Immune Checkpoints for Natural Killer Cell-Based Cancer Immunotherapy. *Cancers (Basel)* 11(6), doi: 10.3390/cancers11060877

Santegoets, S. J. et al. 2015. Monitoring regulatory T cells in clinical samples: consensus on an essential marker set and gating strategy for regulatory T cell analysis by flow cytometry. *Cancer Immunol Immunother* 64(10), pp. 1271-1286. doi: 10.1007/s00262-015-1729-x

Scarpini, S., Morigi, F., Betti, L., Dondi, A., Biagi, C. and Lanari, M. 2021. Development of a Vaccine against Human Cytomegalovirus: Advances, Barriers, and Implications for the Clinical Practice. *Vaccines (Basel)* 9(6), doi: 10.3390/vaccines9060551

Scheller, J., Chalaris, A., Garbers, C. and Rose-John, S. 2011. ADAM17: a molecular switch to control inflammation and tissue regeneration. *Trends Immunol* 32(8), pp. 380-387. doi: 10.1016/j.it.2011.05.005

Schleiss, M. R. 2013. Cytomegalovirus in the neonate: immune correlates of infection and protection. *Clin Dev Immunol* 2013, p. 501801. doi: 10.1155/2013/501801

Schlöndorff, J., Becherer, J. D. and Blobel, C. P. 2000. Intracellular maturation and localization of the tumour necrosis factor alpha convertase (TACE). *Biochem J* 347 Pt 1(Pt 1), pp. 131-138.

Scrivano, L., Sinzger, C., Nitschko, H., Koszinowski, U. H. and Adler, B. 2011. HCMV spread and cell tropism are determined by distinct virus populations. *PLoS Pathog* 7(1), p. e1001256. doi: 10.1371/journal.ppat.1001256

Seidel, E., Dassa, L., Schuler, C., Oiknine-Djian, E., Wolf, D. G., Le-Trilling, V. T. K. and Mandelboim, O. 2021. The human cytomegalovirus protein UL147A downregulates the most prevalent MICA allele: MICA*008, to evade NK cell-mediated killing. *PLoS Pathog* 17(5), p. e1008807. doi: 10.1371/journal.ppat.1008807

Seidel, E. et al. 2015. Dynamic Co-evolution of Host and Pathogen: HCMV Downregulates the Prevalent Allele MICA∗008 to Escape Elimination by NK Cells. *Cell Rep* 10(6), pp. 968-982. doi: 10.1016/j.celrep.2015.01.029

Shafer, R. W. and Vuitton, D. A. 1999. Highly active antiretroviral therapy (HAART) for the treatment of infection with human immunodeficiency virus type 1. *Biomed Pharmacother* 53(2), pp. 73-86. doi: 10.1016/s0753-3322(99)80063-8

Sharma, V., Mobeen, F. and Prakash, T. 2016. Comparative Genomics of Herpesviridae Family to Look for Potential Signatures of Human Infecting Strains. *Int J Genomics* 2016, p. 9543274. doi: 10.1155/2016/9543274

Shikhagaie, M. et al. 2012. The human cytomegalovirus-specific UL1 gene encodes a late-phase glycoprotein incorporated in the virion envelope. *J Virol* 86(8), pp. 4091-4101. doi: 10.1128/JVI.06291-11

Shiomi, T., Tschumperlin, D. J., Park, J. A., Sunnarborg, S. W., Horiuchi, K., Blobel, C. P. and Drazen, J. M. 2011. TNF-α-converting enzyme/a disintegrin and metalloprotease-17 mediates mechanotransduction in murine tracheal epithelial cells. *Am J Respir Cell Mol Biol* 45(2), pp. 376-385. doi: 10.1165/rcmb.2010-0234OC

Siddiquey, M. N. A., Zhang, H., Nguyen, C. C., Domma, A. J. and Kamil, J. P. 2018. The Human Cytomegalovirus Endoplasmic Reticulum-Resident Glycoprotein UL148 Activates the Unfolded Protein Response. *J Virol* 92(20), doi: 10.1128/JVI.00896-18

Sijmons, S., Van Ranst, M. and Maes, P. 2014. Genomic and functional characteristics of human cytomegalovirus revealed by next-generation sequencing. *Viruses* 6(3), pp. 1049-1072. doi: 10.3390/v6031049

Silva, M. C., Yu, Q. C., Enquist, L. and Shenk, T. 2003. Human cytomegalovirus UL99-encoded pp28 is required for the cytoplasmic envelopment of tegument-associated capsids. *J Virol* 77(19), pp. 10594-10605. doi: 10.1128/jvi.77.19.10594-10605.2003

Sinclair, J. and Sissons, P. 2006. Latency and reactivation of human cytomegalovirus. *J Gen Virol* 87(Pt 7), pp. 1763-1779. doi: 10.1099/vir.0.81891-0

Sinzger, C., Digel, M. and Jahn, G. 2008. Cytomegalovirus cell tropism. *Curr Top Microbiol Immunol* 325, pp. 63-83. doi: 10.1007/978-3-540-77349-8_4

Sinzger, C., Grefte, A., Plachter, B., Gouw, A. S., The, T. H. and Jahn, G. 1995. Fibroblasts, epithelial cells, endothelial cells and smooth muscle cells are major targets of human cytomegalovirus infection in lung and gastrointestinal tissues. *J Gen Virol* 76 (Pt 4), pp. 741-750. doi: 10.1099/0022-1317-76-4-741

Sinzger, C. et al. 1999. Modification of human cytomegalovirus tropism through propagation in vitro is associated with changes in the viral genome. *J Gen Virol* 80 (Pt 11), pp. 2867-2877. doi: 10.1099/0022-1317-80-11-2867

Skaletskaya, A., Bartle, L. M., Chittenden, T., McCormick, A. L., Mocarski, E. S. and Goldmacher, V. S. 2001. A cytomegalovirus-encoded inhibitor of

apoptosis that suppresses caspase-8 activation. *Proc Natl Acad Sci U S A* 98(14), pp. 7829-7834. doi: 10.1073/pnas.141108798

Slobedman, B. and Mocarski, E. S. 1999. Quantitative analysis of latent human cytomegalovirus. *J Virol* 73(6), pp. 4806-4812. doi: 10.1128/JVI.73.6.4806-4812.1999

Smith, M. G. 1956. Propagation in tissue cultures of a cytopathogenic virus from human salivary gland virus (SGV) disease. *Proc Soc Exp Biol Med* 92(2), pp. 424-430. doi: 10.3181/00379727-92-22498

Smith, W. et al. 2013. Human cytomegalovirus glycoprotein UL141 targets the TRAIL death receptors to thwart host innate antiviral defenses. *Cell Host Microbe* 13(3), pp. 324-335. doi: 10.1016/j.chom.2013.02.003

Sommer, A. et al. 2016. Phosphatidylserine exposure is required for ADAM17 sheddase function. *Nat Commun* 7, p. 11523. doi: 10.1038/ncomms11523

Sordo-Bahamonde, C., Lorenzo-Herrero, S., Gonzalez-Rodriguez, A. P., R Payer, Á., González-García, E., López-Soto, A. and Gonzalez, S. 2021. BTLA/HVEM Axis Induces NK Cell Immunosuppression and Poor Outcome in Chronic Lymphocytic Leukemia. *Cancers (Basel)* 13(8), doi: 10.3390/cancers13081766

Soroceanu, L., Akhavan, A. and Cobbs, C. S. 2008. Platelet-derived growth factor-alpha receptor activation is required for human cytomegalovirus infection. *Nature* 455(7211), pp. 391-395. doi: 10.1038/nature07209

Sparer, T. E., Gosling, J., Schall, T. J. and Mocarski, E. S. 2004. Expression of human CXCR2 in murine neutrophils as a model for assessing cytomegalovirus chemokine vCXCL-1 function in vivo. *J Interferon Cytokine Res* 24(10), pp. 611-620. doi: 10.1089/jir.2004.24.611

Spencer, J. V., Lockridge, K. M., Barry, P. A., Lin, G., Tsang, M., Penfold, M. E. and Schall, T. J. 2002. Potent immunosuppressive activities of cytomegalovirus-encoded interleukin-10. *J Virol* 76(3), pp. 1285-1292. doi: 10.1128/jvi.76.3.1285-1292.2002

Springer, K. L. and Weinberg, A. 2004. Cytomegalovirus infection in the era of HAART: fewer reactivations and more immunity. *J Antimicrob Chemother* 54(3), pp. 582-586. doi: 10.1093/jac/dkh396

Stanton, R. J. et al. 2010. Reconstruction of the complete human cytomegalovirus genome in a BAC reveals RL13 to be a potent inhibitor of replication. *J Clin Invest* 120(9), pp. 3191-3208. doi: 10.1172/JCI42955

Staras, S. A., Dollard, S. C., Radford, K. W., Flanders, W. D., Pass, R. F. and Cannon, M. J. 2006. Seroprevalence of cytomegalovirus infection in the United States, 1988-1994. *Clin Infect Dis* 43(9), pp. 1143-1151. doi: 10.1086/508173

Stephens, G. J. and Cottrell, G. S. 2019. CACHD1: A new activity-modifying protein for voltage-gated calcium channels. *Channels (Austin)* 13(1), pp. 120-123. doi: 10.1080/19336950.2019.1600968

Stern-Ginossar, N. et al. 2008. Human microRNAs regulate stress-induced immune responses mediated by the receptor NKG2D. *Nat Immunol* 9(9), pp. 1065-1073. doi: 10.1038/ni.1642

Sun, G. et al. 2020. Modeling Human Cytomegalovirus-Induced Microcephaly in Human iPSC-Derived Brain Organoids. *Cell Rep Med* 1(1), p. 100002. doi: 10.1016/j.xcrm.2020.100002

Sylwester, A. W. et al. 2005. Broadly targeted human cytomegalovirus-specific CD4+ and CD8+ T cells dominate the memory compartments of exposed subjects. *J Exp Med* 202(5), pp. 673-685. doi: 10.1084/jem.20050882

Takahashi, S. 2018. Molecular functions of SIRPα and its role in cancer. *Biomed Rep* 9(1), pp. 3-7. doi: 10.3892/br.2018.1102

Takeda, S., Igarashi, T., Mori, H. and Araki, S. 2006. Crystal structures of VAP1 reveal ADAMs' MDC domain architecture and its unique C-shaped scaffold. *EMBO J* 25(11), pp. 2388-2396. doi: 10.1038/sj.emboj.7601131

Takeuchi, O. and Akira, S. 2001. Toll-like receptors; their physiological role and signal transduction system. *Int Immunopharmacol* 1(4), pp. 625-635. doi: 10.1016/s1567-5769(01)00010-8

Tamazato Longhi, M., Magalhães, M., Reina, J., Morais Freitas, V. and Cella, N. 2016. EGFR Signaling Regulates Maspin/SerpinB5 Phosphorylation and Nuclear Localization in Mammary Epithelial Cells. *PLoS One* 11(7), p. e0159856. doi: 10.1371/journal.pone.0159856

Tandon, R. and Mocarski, E. S. 2012. Viral and host control of cytomegalovirus maturation. *Trends Microbiol* 20(8), pp. 392-401. doi: 10.1016/j.tim.2012.04.008

Tandon, R., Mocarski, E. S. and Conway, J. F. 2015. The A, B, Cs of herpesvirus capsids. *Viruses* 7(3), pp. 899-914. doi: 10.3390/v7030899

Tape, C. J. et al. 2011. Cross-domain inhibition of TACE ectodomain. *Proc Natl Acad Sci U S A* 108(14), pp. 5578-5583. doi: 10.1073/pnas.1017067108

Taylor-Wiedeman, J., Sissons, J. G., Borysiewicz, L. K. and Sinclair, J. H. 1991. Monocytes are a major site of persistence of human cytomegalovirus in peripheral blood mononuclear cells. *J Gen Virol* 72 (Pt 9), pp. 2059-2064. doi: 10.1099/0022-1317-72-9-2059

Tian, L. et al. 2007. Activation of NMDA receptors promotes dendritic spine development through MMP-mediated ICAM-5 cleavage. *J Cell Biol* 178(4), pp. 687-700. doi: 10.1083/jcb.200612097

Tian, Y. et al. 2017. Unique phenotypes and clonal expansions of human CD4 effector memory T cells re-expressing CD45RA. *Nat Commun* 8(1), p. 1473. doi: 10.1038/s41467-017-01728-5

Tirabassi, R. S. and Ploegh, H. L. 2002. The human cytomegalovirus US8 glycoprotein binds to major histocompatibility complex class I products. *J Virol* 76(13), pp. 6832-6835. doi: 10.1128/jvi.76.13.6832-6835.2002

Tirosh, B., Iwakoshi, N. N., Lilley, B. N., Lee, A. H., Glimcher, L. H. and Ploegh, H. L. 2005. Human cytomegalovirus protein US11 provokes an unfolded protein response that may facilitate the degradation of class I major histocompatibility complex products. *J Virol* 79(5), pp. 2768-2779. doi: 10.1128/JVI.79.5.2768-2779.2005

Tischer, B. K., Smith, G. A. and Osterrieder, N. 2010. En passant mutagenesis: a two step markerless red recombination system. *Methods Mol Biol* 634, pp. 421-430. doi: 10.1007/978-1-60761-652-8_30

Tomasec, P. et al. 2000. Surface expression of HLA-E, an inhibitor of natural killer cells, enhanced by human cytomegalovirus gpUL40. *Science* 287(5455), p. 1031. doi: 10.1126/science.287.5455.1031

Tomasec, P. et al. 2005. Downregulation of natural killer cell-activating ligand CD155 by human cytomegalovirus UL141. *Nat Immunol* 6(2), pp. 181-188. doi: 10.1038/ni1156

Tomtishen, J. P. 2012. Human cytomegalovirus tegument proteins (pp65, pp71, pp150, pp28). *Virol J* 9, p. 22. doi: 10.1186/1743-422X-9-22

Tovar-Salazar, A., Patterson-Bartlett, J., Jesser, R. and Weinberg, A. 2010. Regulatory function of cytomegalovirus-specific CD4+CD27-CD28- T cells. *Virology* 398(2), pp. 158-167. doi: 10.1016/j.virol.2009.11.038

Tovar-Salazar, A. and Weinberg, A. 2020. Understanding the mechanism of action of cytomegalovirus-induced regulatory T cells. *Virology* 547, pp. 1-6. doi: 10.1016/j.virol.2020.05.001

Tsai, A. P. et al. 2022. PLCG2 is associated with the inflammatory response and is induced by amyloid plaques in Alzheimer's disease. *Genome Med* 14(1), p. 17. doi: 10.1186/s13073-022-01022-0

Van Damme, E. and Van Loock, M. 2014. Functional annotation of human cytomegalovirus gene products: an update. *Front Microbiol* 5, p. 218. doi: 10.3389/fmicb.2014.00218

van Rijckevorsel, G. G., Bovée, L. P., Damen, M., Sonder, G. J., Schim van der Loeff, M. F. and van den Hoek, A. 2012. Increased seroprevalence of IgG-class antibodies against cytomegalovirus, parvovirus B19, and varicella-zoster virus in women working in child day care. *BMC Public Health* 12, p. 475. doi: 10.1186/1471-2458-12-475

Vanarsdall, A. L., Pritchard, S. R., Wisner, T. W., Liu, J., Jardetzky, T. S. and Johnson, D. C. 2018. CD147 Promotes Entry of Pentamer-Expressing Human Cytomegalovirus into Epithelial and Endothelial Cells. *mBio* 9(3), doi: 10.1128/mBio.00781-18

Varnum, S. M. et al. 2004. Identification of proteins in human cytomegalovirus (HCMV) particles: the HCMV proteome. *J Virol* 78(20), pp. 10960-10966. doi: 10.1128/JVI.78.20.10960-10966.2004

Veiga-Parga, T., Sehrawat, S. and Rouse, B. T. 2013. Role of regulatory T cells during virus infection. *Immunol Rev* 255(1), pp. 182-196. doi: 10.1111/imr.12085

Vomaske, J., Nelson, J. A. and Streblow, D. N. 2009. Human Cytomegalovirus US28: a functionally selective chemokine binding receptor. *Infect Disord Drug Targets* 9(5), pp. 548-556. doi: 10.2174/187152609789105696

Wajant, H. and Siegmund, D. 2019. TNFR1 and TNFR2 in the Control of the Life and Death Balance of Macrophages. *Front Cell Dev Biol* 7, p. 91. doi: 10.3389/fcell.2019.00091

Waldman, W. J., Roberts, W. H., Davis, D. H., Williams, M. V., Sedmak, D. D. and Stephens, R. E. 1991. Preservation of natural endothelial cytopathogenicity of cytomegalovirus by propagation in endothelial cells. *Arch Virol* 117(3-4), pp. 143-164. doi: 10.1007/BF01310761

Wan, L., Molloy, S. S., Thomas, L., Liu, G., Xiang, Y., Rybak, S. L. and Thomas, G. 1998. PACS-1 defines a novel gene family of cytosolic sorting proteins required for trans-Golgi network localization. *Cell* 94(2), pp. 205-216. doi: 10.1016/s0092-8674(00)81420-8

Wang, D. and Shenk, T. 2005. Human cytomegalovirus virion protein complex required for epithelial and endothelial cell tropism. *Proc Natl Acad Sci U S A* 102(50), pp. 18153-18158. doi: 10.1073/pnas.0509201102

Wang, E. C. et al. 2002. UL40-mediated NK evasion during productive infection with human cytomegalovirus. *Proc Natl Acad Sci U S A* 99(11), pp. 7570-7575. doi: 10.1073/pnas.112680099

Wang, E. C. Y. et al. 2018. Suppression of costimulation by human cytomegalovirus promotes evasion of cellular immune defenses. *Proc Natl Acad Sci U S A* 115(19), pp. 4998-5003. doi: 10.1073/pnas.1720950115

Wang, F., Song, W., Brancati, G. and Segatori, L. 2011. Inhibition of endoplasmic reticulum-associated degradation rescues native folding in loss of function protein misfolding diseases. *J Biol Chem* 286(50), pp. 43454-43464. doi: 10.1074/jbc.M111.274332

Wang, J., Loveland, A. N., Kattenhorn, L. M., Ploegh, H. L. and Gibson, W. 2006. High-molecular-weight protein (pUL48) of human cytomegalovirus is a competent deubiquitinating protease: mutant viruses altered in its active-site cysteine or histidine are viable. *J Virol* 80(12), pp. 6003-6012. doi: 10.1128/JVI.00401-06

Wang, X., Huong, S. M., Chiu, M. L., Raab-Traub, N. and Huang, E. S. 2003. Epidermal growth factor receptor is a cellular receptor for human cytomegalovirus. *Nature* 424(6947), pp. 456-461. doi: 10.1038/nature01818

Wang, Y. Q. and Zhao, X. Y. 2020. Human Cytomegalovirus Primary Infection and Reactivation: Insights From Virion-Carried Molecules. *Front Microbiol* 11, p. 1511. doi: 10.3389/fmicb.2020.01511

Weber, S. and Saftig, P. 2012. Ectodomain shedding and ADAMs in development. *Development* 139(20), pp. 3693-3709. doi: 10.1242/dev.076398

Weekes, M. P. et al. 2014. Quantitative temporal viromics: an approach to investigate host-pathogen interaction. *Cell* 157(6), pp. 1460-1472. doi: 10.1016/j.cell.2014.04.028

Weir, J. P. 1998. Genomic organization and evolution of the human herpesviruses. *Virus Genes* 16(1), pp. 85-93. doi: 10.1023/a:1007905910939

West, M. A., Prescott, A. R., Chan, K. M., Zhou, Z., Rose-John, S., Scheller, J. and Watts, C. 2008. TLR ligand-induced podosome disassembly in dendritic cells is ADAM17 dependent. *J Cell Biol* 182(5), pp. 993-1005. doi: 10.1083/jcb.200801022

Whitley, R. J. 1996. Herpesviruses. Chapter 68.   In   Baron, S. (ed)   Medical Microbiology. 4th edition. Galveston (TX): University of Texas Medical Branch at Galveston. University of Texas Medical Branch at Galveston.

Wilhelm, M., Kunzmann, V., Eckstein, S., Reimer, P., Weissinger, F., Ruediger, T. and Tony, H. P. 2003. Gammadelta T cells for immune therapy of patients with lymphoid malignancies. *Blood* 102(1), pp. 200-206. doi: 10.1182/blood-2002-12-3665

Wilkinson, G. et al. 2015. Human cytomegalovirus: taking the strain. *Medical Microbiology and Immunology* 204(3), pp. 273-284. doi: 10.1007/s00430-015-0411-4

Wilkinson, G. W., Akrigg, A. and Greenaway, P. J. 1984. Transcription of the immediate early genes of human cytomegalovirus strain AD169. *Virus Res* 1(2), pp. 101-106. doi: 10.1016/0168-1702(84)90067-4

Wilkinson, G. W. et al. 2008. Modulation of natural killer cells by human cytomegalovirus. *J Clin Virol* 41(3), pp. 206-212. doi: 10.1016/j.jcv.2007.10.027

Wilkinson, G. W., Tomasec, P., Stanton, R. J., Armstrong, M., Prod'homme, V., Aicheler, R., McSharry, B. P., Rickards, C. R., Cochrane, D., Llewellyn-Lacey, S., Wang, E. C., Griffin, C. A., & Davison, A. J. 2008. Modulation of natural killer cells by human cytomegalovirus. *Journal of clinical virology : the official publication of the Pan American Society for Clinical Virology*, pp. 41(43), 206–212.

Willcox, C. R. et al. 2012. Cytomegalovirus and tumor stress surveillance by binding of a human γδ T cell antigen receptor to endothelial protein C receptor. *Nat Immunol* 13(9), pp. 872-879. doi: 10.1038/ni.2394

Wille, P. T., Knoche, A. J., Nelson, J. A., Jarvis, M. A. and Johnson, D. C. 2010. A human cytomegalovirus gO-null mutant fails to incorporate gH/gL into the virion envelope and is unable to enter fibroblasts and epithelial and endothelial cells. *J Virol* 84(5), pp. 2585-2596. doi: 10.1128/JVI.02249-09

Wills, M. R., Carmichael, A. J., Mynard, K., Jin, X., Weekes, M. P., Plachter, B. and Sissons, J. G. 1996. The human cytotoxic T-lymphocyte (CTL) response to cytomegalovirus is dominated by structural protein pp65: frequency, specificity, and T-cell receptor usage of pp65-specific CTL. *J Virol* 70(11), pp. 7569-7579. doi: 10.1128/JVI.70.11.7569-7579.1996

Wilson, N. H. and Key, B. 2007. Neogenin: one receptor, many functions. *Int J Biochem Cell Biol* 39(5), pp. 874-878. doi: 10.1016/j.biocel.2006.10.023

Wing, K. and Sakaguchi, S. 2010. Regulatory T cells exert checks and balances on self tolerance and autoimmunity. *Nat Immunol* 11(1), pp. 7-13. doi: 10.1038/ni.1818

Wujcicka, W., Gaj, Z., Wilczyński, J., Sobala, W., Spiewak, E. and Nowakowska, D. 2014. Impact of socioeconomic risk factors on the seroprevalence of cytomegalovirus infections in a cohort of pregnant Polish women between 2010 and 2011. *Eur J Clin Microbiol Infect Dis* 33(11), pp. 1951-1958. doi: 10.1007/s10096-014-2170-3

Wyatt, J. P. and Saxton, J. 1950. Generalized cytomegalic inclusion disease. *J Pediatr* 36(3), pp. 271-294, illust. doi: 10.1016/s0022-3476(50)80097-5

Xu, Y., Colletti, K. S. and Pari, G. S. 2002. Human cytomegalovirus UL84 localizes to the cell nucleus via a nuclear localization signal and is a

component of viral replication compartments. *J Virol* 76(17), pp. 8931-8938. doi: 10.1128/jvi.76.17.8931-8938.2002

Yang, H. 2012. Structure, Expression, and Function of ICAM-5. *Comp Funct Genomics* 2012, p. 368938. doi: 10.1155/2012/368938

Ye, L., Qian, Y., Yu, W., Guo, G., Wang, H. and Xue, X. 2020. Functional Profile of Human Cytomegalovirus Genes and Their Associated Diseases: A Review. *Front Microbiol* 11, p. 2104. doi: 10.3389/fmicb.2020.02104

Yvon, E. S. et al. 2003. Overexpression of the Notch ligand, Jagged-1, induces alloantigen-specific human regulatory T cells. *Blood* 102(10), pp. 3815-3821. doi: 10.1182/blood-2002-12-3826

Zhang, G. et al. 2007. Antisense transcription in the human cytomegalovirus transcriptome. *J Virol* 81(20), pp. 11267-11281. doi: 10.1128/JVI.00007-07

Zhang, K., Sikut, R. and Hansson, G. C. 1997. A MUC1 mucin secreted from a colon carcinoma cell line inhibits target cell lysis by natural killer cells. *Cell Immunol* 176(2), pp. 158-165. doi: 10.1006/cimm.1997.1085

Zhou, M., Lanchy, J. M. and Ryckman, B. J. 2015. Human Cytomegalovirus gH/gL/gO Promotes the Fusion Step of Entry into All Cell Types, whereas gH/gL/UL128-131 Broadens Virus Tropism through a Distinct Mechanism. *J Virol* 89(17), pp. 8999-9009. doi: 10.1128/JVI.01325-15

Zischke, J. et al. 2017. The human cytomegalovirus glycoprotein pUL11 acts via CD45 to induce T cell IL-10 secretion. *PLoS Pathog* 13(6), p. e1006454. doi: 10.1371/journal.ppat.1006454

Zunke, F. and Rose-John, S. 2017. The shedding protease ADAM17: Physiology and pathophysiology. *Biochim Biophys Acta Mol Cell Res* 1864(11 Pt B), pp. 2059-2070. doi: 10.1016/j.bbamcr.2017.07.001

8 Appendix

Table 8.1: A list of all known ADAM17 substrates reported in literature, as well as all potentially novel ADAM17 substrates identified in the PMP proteomics. If a known ADAM17 substrate was also detected in PMP at high significance, a corresponding *p*-value and dKO+D1(A12))/dKO ratio is presented. If no *p*-value or dKO+D1(A12))/dKO ratio presented for known targets, the protein was not detected in PMP or did not pass the significance threshold of *p*<0.05. Proteins presented in blue are HCMV-derived.

Gene symbol	Description	Ratio ((dKO+D1(A12))/dKO)	*p*-value (Significance B)	Known or novel ADAM17 target
TNFRSF1B, TNFBR, TNFR2	Tumour necrosis factor receptor 2	4.56	1.82E-36	Known
NRG1, GGF, HGL, HRGA, NDF, SMDF	Neuregulin 1	3.38	2.16E-25	Known
JAG1, JAGL1	Jagged 1	2.94	1.97E-23	Known
NEO1, IGDCC2, NGN	Neogenin	2.92	4.26E-23	Known
PROCR, EPCR	Endothelial protein C receptor	2.46	4.73E-14	Known

Gene	Protein	Value	P-value	Status
VASN, SLITL2	Vasorin	2.05	2.76E-11	Known
SEMA4D, C9orf164, CD100, SEMAJ	Semaphorin 4D	1.99	1.72E-10	Known
TNFRSF1A, TNFAR, TNFR1	Tumour necrosis factor receptor 1	2.36	7.86E-08	Known
MUC1, PUM	Mucin-1	2.23	5.39E-07	Known
MET	Hepatocyte growth factor receptor	1.60	1.42E-05	Known
VCAM1	Vascular cell adhesion protein 1	1.42	2.42E-02	Known
MERTK, MER	Mer tyrosine kinase	1.26	3.52E-02	Known
PTK7, CCK4	Inactive tyrosine-protein kinase 7	1.23	4.90E-02	Known
GPC1	Glypican-1			Known
SDC1, SDC	Sydecan-1			Known
APP, A4, AD1	Amyloid-beta precursor protein			Known
LYPD3, C4.4A	LY6/PLAUR domain containing 3			Known
THBS4, TSP4	Thrombospondin-4			Known
PTPRF, LAR	Receptor-type tyrosine-protein phosphatase F			Known
NGFR, TNFRSF16	Tumour necrosis factor receptor superfamily member 16			Known

LRP1, A2MR, APR	Prolow-density lipoprotein receptor-related protein 1	Known
NCAM1, NCAM	Neural cell adhesion molecule 1	Known
MICA	MHC class I chain-related protein A	Known
IGF1R	Insulin-like growth factor receptor 1	Known
APLP2, APPL2	Amyloid-like protein 2	Known
F11R, JAM1, JCAM, UNQ264/PRO301	Junctional adhesion molecule A	Known
TLR2, TIL4	Toll-like receptor 2	Known
NRP1, NRP, VEGF165R	Neuropilin-1	Known
PTPRA, PTPA, PTPRL2	Protein tyrosine phosphatase alpha	Known
CD44, LHR, MDU2, MDU3, MIC4	Extracellular matrix receptor III	Known
ICAM1	Intercellular adhesion molecule 1	Known
PRNP, ALTPRP, PRIP, PRP	Major prion protein	Known
SORT1	Sortilin	Known
IGF2R, MPRI	Insulin-like growth factor type 2 receptor	Known
L1CAM CAML1, MIC5	Neural cell adhesion molecule L1	Known

ALCAM, MEMD	Activated leukocyte cell adhesion molecule	Known
EPCAM GA733-2, M1S2, M4S1, MIC18, TACSTD1	Epithelial cell adhesion molecule	Known
SCARB1, CD36L1, CLA1	Scavenger receptor class B member 1	Known
CD274, B7H1, PDCD1L1, PDCD1LG1, PDL1	Programmed cell death 1 ligand 1	Known
TACSTD2, GA733-1, M1S1, TROP2	Tumor-associated calcium signal transducer 2	Known
NOTCH1, TAN1	Notch-1	Known
MICB	MHC class I chain-related protein B	Known
FCGR3B, CD16B, FCG3, FCGR3, IGFR3	Fc-gamma receptor IIIb	Known
HAVCR1, KIM1, TIM1, TIMD1	T-cell immunoglobulin mucin receptor 1	Known
HAVCR2, TIM3, TIMD3	T-cell immunoglobulin mucin receptor 3	Known

TIMD4, TIM4	T-cell immunoglobulin mucin receptor 4	Known
PMEL, D12S53E, PMEL17, SILV	Melanocyte protein PMEL precursor	Known
GHRHR	Growth hormone-releasing hormone receptor	Known
IL23R	IL-23 receptor	Known
IL1R2, IL1RB	IL-1 receptor 2	Known
GP6	Glycoprotein VI	Known
CA9, G250, MN	Carbonic anhydrase IX	Known
LRIG1, LIG1	Leucine-rich repeats and immunoglobulin-like domains 1	Known
TNF, TNFA, TNFSF2	Tumour necrosis factor alpha	Known
CSF1	Macrophage colony-stimulating factor	Known
KL	Klotho	Known
ACE2	Angiotensin-converting enzyme 2	Known
TNFSF11, OPGL, RANKL, TRANCE	Tumour necrosis factor ligand superfamily member 11	Known

CX3CL1, FKN	Fractalkine	Known
LTA, TNFB, TNFSF1	Lymphotoxin alpha	Known
AREG, AREGB, SDGF	Amphiregulin	Known
HBEGF, DTR, DTS, HEGFL	Proheparin-binding EGF-like growth factor	Known
TGFA	Transforming growth factor alpha	Known
EPGN	Epigen	Known
EREG	Epiregulin	Known
LAG3, FDC	Lymphocyte activation gene 3 protein	Known
IL6, IFNB2	IL-6 receptor	Known
DLL1	Delta-like protein 1	Known
ICOSLG, B7H2, B7RP1, ICOSL, KIAA0653	ICOS ligand	Known
IL15	IL15 receptor	Known
AXL	Receptor protein-tyrosine kinase	Known
CD163, M130	Scavenger receptor cysteine-rich type 1 protein M130	Known

TNFRSF8, CD30	Tumour necrosis factor receptor superfamily member 8	Known
TNFRSF9, CD137, ILA	Tumour necrosis factor receptor superfamily member 9	Known
CD40LG, CD40L, TNFSF5, TRAP	Tumour necrosis factor receptor superfamily member 5	Known
FCAR, CD89	Immunoglobulin alpha Fc receptor	Known
ERBB4, HER4	Receptor tyrosine-protein kinase erbB-4	Known
GHR	Growth hormone receptor	Known
CSF1R, FMS	Macrophage colony-stimulating factor 1 receptor	Known
GP1BA	Platelet glycoprotein Ib alpha chain	Known
PTPRZ1, HTPZP2, PTPRZ, PTPRZ2, PTPZ	Receptor-type tyrosine-protein phosphatase zeta	Known
NTRK1, MTC	Neurotrophic Receptor Tyrosine Kinase 1	Known
KDR, FLK1, VEGFR2	Vascular endothelial growth factor receptor 2	Known

SELL LNHR, LYAM1	L-selectin	Known
COL17A1, BP180, BPAG2	Collagen XVII	Known
DSG2 CDHF5	Desmoglein-2	Known
GP5	Platelet glycoprotein V	Known
GP6	Platelet glycoprotein VI	Known
NECTIN4, LNIR, PRR4, PVRL4	Nectin-4	Known
OLR1, CLEC8A, LOX1	Oxidized low-density lipoprotein receptor 1	Known
SORCS1, SORCS	VPS10 domain-containing receptor SorCS1	Known
SORCS3, KIAA1059	VPS10 domain-containing receptor SorCS3	Known
SORL1, C11orf32	Sortilin-related receptor	Known
TREM2	Triggering receptor expressed on myeloid cells 2	Known
NPR1, ANPRA	Atrial natriuretic peptide receptor 1	Known
SDC4	Sydecan-4	Known
PREF-1	Pre-adypocyte factor	Known
TMEFF2 HPP1, TENB2, TPEF	Tomoregulin-2	Known

IGHG1	Ig gamma-1 chain C region	9.97	6.13E-81	Novel
NRG1	Isoform 6 of Pro-neuregulin-1, membrane-bound isoform	5.14	1.68E-51	Novel
IGKC	Ig kappa chain C region	3.54	5.25E-27	Novel
NECTIN1	Nectin-1	2.11	5.01E-12	Novel
PTPRG	Receptor-type tyrosine-protein phosphatase gamma	1.96	4.15E-10	Novel
CACHD1	VWFA and cache domain-containing protein 1	2.08	7.99E-10	Novel
SDC3	Syndecan-3	1.98	3.83E-09	Novel
SIRPA	Tyrosine-protein phosphatase non-receptor type substrate 1	1.93	3.28E-08	Novel
SIRPA	Isoform 2 of Tyrosine-protein phosphatase non-receptor type substrate 1	1.77	1.14E-07	Novel
SEMA7A	Semaphorin-7A	1.64	4.25E-06	Novel
ICAM5	Intercellular adhesion molecule 5	1.62	8.24E-06	Novel
NRCAM	Isoform 5 of Neuronal cell adhesion molecule	1.65	1.73E-05	Novel

Gene	Protein	Ratio	p-value	Status
JAG2	Protein jagged-2	1.63	2.60E-05	Novel
PODXL2	Podocalyxin-like protein 2	1.64	2.70E-05	Novel
NCR3LG1	Natural cytotoxicity triggering receptor 3 ligand 1	1.62	2.82E-05	Novel
LOXL2	Lysyl oxidase homolog 2	1.56	3.62E-05	Novel
AXL	Tyrosine-protein kinase receptor UFO	1.61	4.97E-05	Novel
SLC16A1	Monocarboxylate transporter 1	1.54	6.30E-05	Novel
TIMP1	Metalloproteinase inhibitor 1	1.60	6.51E-05	Novel
GFRA1	GDNF family receptor alpha-1	1.48	2.72E-04	Novel
ROBO1	Isoform 2 of Roundabout homolog 1	1.46	4.50E-04	Novel
HP1BP3	Heterochromatin protein 1-binding protein 3	1.48	8.17E-04	Novel
GNAS	Guanine nucleotide-binding protein G(s) subunit alpha isoforms XLas	1.48	8.24E-04	Novel
ADM	ADM	1.48	8.54E-04	Novel
SPINT1	Kunitz-type protease inhibitor 1	1.40	1.52E-03	Novel
MYOM3	Myomesin-3	1.45	1.59E-03	Novel

PLAU	Urokinase-type plasminogen activator	1.42	2.03E-03	Novel
ZC3H7A	Zinc finger CCCH domain-containing protein 7A	1.43	2.33E-03	Novel
SPINT1	Isoform 2 of Kunitz-type protease inhibitor 1	1.41	2.33E-03	Novel
ACLY	Isoform 2 of ATP-citrate synthase	1.61	2.60E-03	Novel
CUL5	Cullin-5	1.58	3.51E-03	Novel
CCAR2	Cell cycle and apoptosis regulator protein 2	1.40	3.70E-03	Novel
AMIGO2	Amphoterin-induced protein 2	1.40	3.83E-03	Novel
TPST2	Protein-tyrosine sulfotransferase 2	1.39	4.73E-03	Novel
ADAMTS12	A disintegrin and metalloproteinase with thrombospondin motifs 12	1.55	5.22E-03	Novel
EGFR	Epidermal growth factor receptor	1.35	5.36E-03	Novel
CSPG4	Chondroitin sulphate proteoglycan 4	1.35	5.56E-03	Novel
MMP1	Interstitial collagenase	1.38	5.89E-03	Novel
SLC39A6	Zinc transporter ZIP6	1.38	6.08E-03	Novel
SEMA4C	Semaphorin-4C	1.37	6.39E-03	Novel

BRD9	Bromodomain-containing protein 9	1.33	7.62E-03	Novel
SRI	Sorcin	1.36	7.67E-03	Novel
NFKB2	Nuclear factor NF-kappa-B p100 subunit	1.52	7.80E-03	Novel
CD248	Endosialin	1.33	8.18E-03	Novel
POF1B	Isoform 1 of Protein POF1B	1.51	8.29E-03	Novel
KITLG	Kit ligand	1.34	8.37E-03	Novel
MED1	Mediator of RNA polymerase II transcription subunit 1	1.34	8.81E-03	Novel
RPL35A	60S ribosomal protein L35a	1.36	8.82E-03	Novel
SPOCK1	Testican-1	1.49	1.10E-02	Novel
TM2D3	TM2 domain-containing protein 3	1.48	1.12E-02	Novel
MRC2	C-type mannose receptor 2	1.30	1.29E-02	Novel
NID1	Nidogen-1	1.33	1.38E-02	Novel
CPXM2	Inactive carboxypeptidase-like protein X2	1.30	1.42E-02	Novel
CASK	Peripheral plasma membrane protein CASK	1.31	1.69E-02	Novel
BGN	Biglycan	1.30	1.72E-02	Novel

Gene	Protein	Ratio	p-value	Type
GNA13	Guanine nucleotide-binding protein subunit alpha-13	1.31	1.84E-02	Novel
LRRC15	Isoform 2 of Leucine-rich repeat-containing protein 15	1.28	1.96E-02	Novel
CDSN	Corneodesmosin	1.43	2.09E-02	Novel
PELI2	E3 ubiquitin-protein ligase pellino homolog 2	1.29	2.18E-02	Novel
AP3B1	AP-3 complex subunit beta-1	1.43	2.19E-02	Novel
EML4	Echinoderm microtubule-associated protein-like 4	1.42	2.34E-02	Novel
RPL37AP8	Putative 60S ribosomal protein L37a-like protein	1.28	2.49E-02	Novel
KPNA4	Importin subunit alpha-3	1.41	2.54E-02	Novel
NTM	Isoform 4 of Neurotrimin	1.29	2.58E-02	Novel
SAE1	SUMO-activating enzyme subunit 1	1.28	2.62E-02	Novel
GPNMB	Transmembrane glycoprotein NMB	1.29	2.66E-02	Novel
PCDH18	Protocadherin-18	1.29	2.68E-02	Novel
OLFML2A	Olfactomedin-like protein 2A	1.28	2.73E-02	Novel

IARS2	Isoleucine--tRNA ligase, mitochondrial	1.28	2.79E-02	Novel
PCOLCE	Procollagen C-endopeptidase enhancer 1	1.29	2.92E-02	Novel
NOLC1	Isoform Beta of Nucleolar and coiled-body phosphoprotein 1	1.29	2.95E-02	Novel
CCDC88A	Girdin	1.39	3.30E-02	Novel
KIAA2013	Isoform 2 of Uncharacterized protein KIAA2013	1.28	3.43E-02	Novel
GALNT5	Polypeptide N-acetylgalactosaminyltransferase 5	1.26	3.44E-02	Novel
SRSF6	Serine/arginine-rich splicing factor 6	1.28	3.46E-02	Novel
SLC39A10	Zinc transporter ZIP10	1.25	3.52E-02	Novel
SCYL2	SCY1-like protein 2	1.38	3.55E-02	Novel
PLA2R1	Secretory phospholipase A2 receptor	1.26	3.63E-02	Novel
PTPRS	Isoform PTPS-MEA of Receptor-type tyrosine-protein phosphatase S	1.27	3.67E-02	Novel

Gene	Protein	Ratio	p-value	Status
ZC3H18	Zinc finger CCCH domain-containing protein 18	1.37	3.90E-02	Novel
EEF1D	Isoform 2 of Elongation factor 1-delta	1.27	3.94E-02	Novel
GAPDHS	Glyceraldehyde-3-phosphate dehydrogenase, testis-specific	1.27	4.12E-02	Novel
GLCE	D-glucuronyl C5-epimerase	1.36	4.31E-02	Novel
AFP	Alpha-fetoprotein	1.26	4.34E-02	Novel
BIRC6	Baculoviral IAP repeat-containing protein 6	1.25	4.39E-02	Novel
CBR1	Carbonyl reductase [NADPH] 1	1.24	4.40E-02	Novel
RFTN1	Raftlin	1.26	4.50E-02	Novel
RPL8	60S ribosomal protein L8	1.26	4.60E-02	Novel
FAM98A	Protein FAM98A	1.36	4.74E-02	Novel
RPL7A	60S ribosomal protein L7a	1.25	4.76E-02	Novel
RAB10	Ras-related protein Rab-10	1.24	4.81E-02	Novel
HEXA	Beta-hexosaminidase subunit alpha	1.24	4.98E-02	Novel
UL8	Membrane glycoprotein UL8	3.41	9.88E-26	Novel
UL7	Membrane protein UL7 (UL07)	3.37	4.62E-24	Novel

UL144	Membrane glycoprotein UL144	1.80	5.07E-07	Novel
UL40	Protein UL40	1.55	1.26E-04	Novel
UL9	Membrane glycoprotein UL9 (UL09)	1.67	1.20E-03	Novel
RL12	Uncharacterized protein RL12	1.39	2.08E-03	Novel
UL1	Glycoprotein UL1 (UL01)	1.40	3.91E-03	Novel
UL47	Capsid assembly protein UL47 (V120)	1.32	1.78E-02	Novel
US24	Tegument protein US24	1.26	3.82E-02	Novel